Function of NF-κB in human neurons

Dissertation ● Lucia Ruiz ● Bielefeld University

University of Bielefeld, Department of Cell Biology,
AG Molecular Neurobiology

Function of NF-κB in human neurons

Dissertation presented in partial fulfillment of the requirements for the Doctorate degree in Natural Sciences
Doctor rerum naturalis (Dr. rer. nat.)
at the Faculty of Biology, Bielefeld University

by MSc. Lucia M. Ruiz Perera
supervised by Prof. Dr. Barbara Kaltschmidt

Bielefeld, January 2019

Contents

Abstract

Protection of neurons against oxidative stress is crucial during neuronal development, maintenance and for the treatment of neurodegenerative diseases. However, little is known about the molecular mechanisms underlying sex-specific maturation and survival of neurons. In the present study, we demonstrated NF-κB-p65 mediated neuroprotection in human glutamatergic neurons differentiated from inferior turbinate stem cells (ITSCs) in a sex-dependent manner. For this we successfully differentiated ITSCs into $MAP2^+/NF200^+/Synaptophysin^+/vGlut2^+$-glutamatergic neurons *in vitro* and validated their functionality. TNF-α-dependent NF-κB-p65 activation was accompanied by significant neuroprotection against oxidative stress-induced neuronal death, which was unexpectedly higher in neurons from female donors. Accordingly, sex-specific neuroprotection of female neurons was followed by an increased expression of special NF-κB target genes SOD2 and IGF2. Among these, SOD2 is a well known gene protecting cells against oxidative stress resulting in longevity. While, IGF2 is known to promote synapse formation and spine maturation, and it has antioxidant and neuroprotective effects against oxidative damage.

In addition, little is known about the role of NF-κB signaling in the regulation of neuronal differentiation particularly in human neural stem cells. In order to shed light on the understanding of NF-κB mechanisms during neuronal differentiation we efficiently differentiated ITSCs into glutamatergic and dopaminergic neurons as well, and we characterized their NF-κB subunit distribution during early neuronal differentiation, to establish the relevant subunits involved in their regulation. In this work, we demonstrated for the first time a major function of NF-κB during early human neuronal differentiation of ITSCs. We discovered that during glutamatergic differentiation, NF-κB pattern showed a nuclear activation of RelB/p52 heterodimers during an early phase, and a nuclear c-Rel activation peak during a later phase of differentiation. While the classical NF-κB subunits, RelA and p50 had no part during this differentiation. In contrast, during dopaminergic differentiation RelA had an important nuclear activity during an initial phase, whereas c-Rel showed a clear

nuclear peak at a medial phase of differentiation, and RelA and RelB were both strongly increased at a final phase of dopaminergic differentiation. These results confirmed that NF-κB activity is strictly regulated during neuronal differentiation, and thus NF-κB-signalling might have a particular temporal pattern during the differentiation towards different cell fates. Furthermore, our findings revealed that pentoxifylline directly induced a shift from glutamatergic fate towards the oligodendrocyte fate, due to c-Rel nuclear inhibition, and also demonstrated that c-Rel has a key role in cell survival and neuronal fate. These results strongly suggested that NF-κB-c-Rel is essentially necessary for glutamatergic fate commitment during ITSCs differentiation.

Moreover, we further analyzed differences in the ability of female and male-derived ITSCs to differentiate into dopaminergic neurons, and we determined sex-specific differences in the neuronal complexity. In addition, we chemically stimulated dopaminergic neurons using TNF-α, 6-hydroxydopamine (6OHDA) and their combination, to study their functionality. We found out that TNF-α-treatment induced a significant NF-κB-p65 nuclear activation, demonstrating a crucial role of NF-κB in dopaminergic function. Furthermore, stimulation using 6OHDA, exhibited a strong alteration in the neuronal morphology in both sexes, however there was a higher death tendency in male-derived neurons, compared to their female counterparts. Although the death rate differences between female- and male-derived neurons were not significantly different, these trend is in line with gender differences observed in Parkinson's disease, where more men are diagnosed with the disease than women. Also, our results introduce a neuroprotective effect induced by the activation of NF-κB-p65 mediated by TNF-α-pretreatment upon 6-OHDA stimulation of dopaminergic neurons derived from both sexes. Further analysis needs to be done to demonstrate this neuroprotective effect, and also the potential sex-specific differences that might be related to it.

Introduction

1

1.1 Stem cells

Stem cells are undifferentiated cells with the potential to self-renew, which is to produce daughter cells with identical properties, and they also have the capacity to differentiate into highly specialized cell types (Fig. 1-1). Stem cells play an essential role at different stages of development and also within the postnatal organism[5]. There are distinct kinds of stem cells according to their differentiation potential. After fertilization, the zygote is the unique cell to be totipotent, which is to be capable to form all cell lineages of an organism including the extraembryonic tissues like the placenta, this characteristic is present until the stage of 4 blastomeres[6]. Pluripotent stem cells are more specialized cells, being capable to give rise to cells from all three germ layers: endoderm, mesoderm, ectoderm and germ cells, but they do not form extraembryonic tissues. Examples of pluripotent stem cells are the embryonic stem cells (ESCs) and the induced pluripotent stem cells (iPSCs). In contrast, multipotent stem cells are more restricted in their differentiation potential and can develop multiple cell types but only within a specific lineage. Ultimately, unipotent cells can differentiate only into one cell type. Adult stem cells (ASCs), also called somatic stem cells can be either multipotent or unipotent stem cells[5,7].

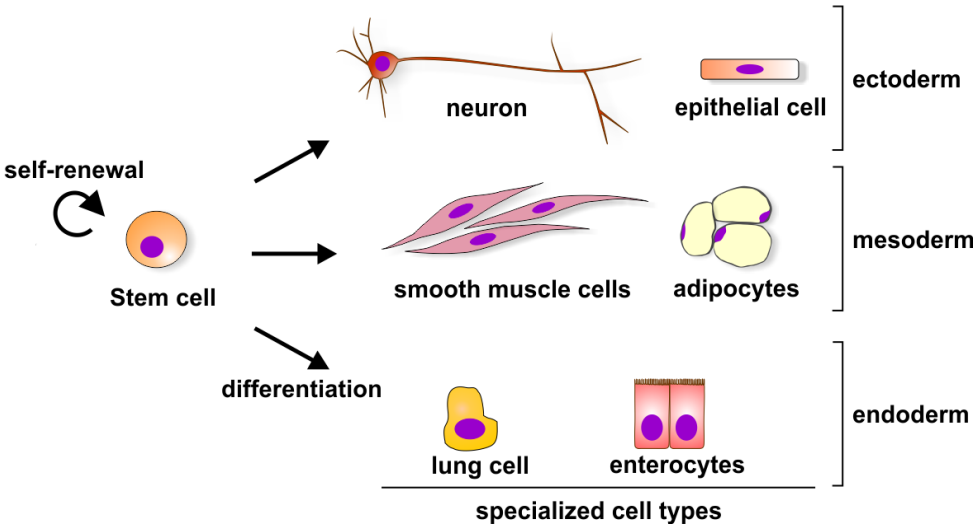

Figure 1-1. Stem cells celf-renew and differentiation. Stem cells have the potential to self-renew and are able to differentiate into highly specialized cell types.

1.1.1 Embryonic stem cells and induced pluripotent stem cells

Embryonic stem cells (ESCs), which are derived from the inner cell mass of the blastocyst, are defined by their capacity for unlimited self-renewal and their ability to differentiate into somatic cells of all three embryonic lineages and germ cells[8-9]. Since the first description of mouse ESCs[10-11], it has been clear that the derivation of human ESCs (hESCs) could provide a unique model to study early human development and differentiation, as well as drug screening for treating multiple diseases[12]. hESCs were established in 1998[13], and were capable of unlimited undifferentiated proliferation *in vitro.* They were also able to give rise to teratomas including cells from all three germ layers *in vivo*, when grafted into immunodeficient mice[12]. hESCs showed normal karyotypes, expressed high levels of telomerase activity, and expressed cell surface markers that characterize primate embryonic stem cells[13]. There are some exclusive surface markers in hESCs such as SSEA-3, SSEA-4, TRA-1-60 and TRA-1-81 and transcription factors like OCT4, SOX2 and NANOG that identify them as pluripotent[8,12,14-16]. These undifferentiated cells also show a high alkaline phosphatase activity, a high nucleus to cytoplasm ratio, prominent nucleoli, as well as a short G1 phase of the cell cycle and form multi-layered colonies[17-20]. There are many differences among mouse and human embryonic stem cells, in particular they respond differently to extrinsic signals and express different markers. Nevertheless, microRNA expression profiles in both revealed that ESCs express a distinctive set of miRNAs and that some of these are conserved among both species[21-22].

Moreover with the arrival of new cellular reprogramming techniques, Yamanaka and Takahashi demonstrated that ectopic expression of four transcription factors normally expressed in ESCs (OCT4, SOX2, KLF4 and c-MYC) was enough to reset a somatic cell like a fibroblast back to an embryonic-like stem cell[23], achieving the derivation of induced pluripotent stem cells (iPSCs). This accomplishment had strong clinical implications, such as the possibility to derive disease-specific and patient-specific iPSCs in order to study them *in vitro*, and to perform genetic and drug screening for patient-specificity treatments. However, the use of human ESCs and IPSCs in clinical applications for cell replacement therapies to treat a variety of diseases remains limited for ethical and practical reasons[13]. Due to the potential tumorigenicity, as well as the risk of the expression of

introduced genes at the genome level in the case of iPSCs[24]. Furthermore the contribution of hESCs or iPSCs to the germ line in chimeras or by tetraploid complementation is not feasible[13]. Thus, demonstration of pluripotency, the capacity to form cell types representing all germ layers had to be determined by teratoma formation and by using protocols for directed differentiation *in vitro* [12,25].

1.1.2 Adult stem cells

Adult stem cells (ACSs) are resident stem cells within different tissues, which persist in the adult organism and whose primary role is to proliferate and differentiate in order to replace damaged or dying cells when necessary, ensuring their own self-renewal[26-27]. Thus, these cells commit to become the functional cells of their tissue of origin depending on the tissue turnover. ASCs have the capability for self-renewal and differentiation, being either multipotent or unipotent[5,7], depending in their differentiation potential. They represent a valuable source for regenerative cell based therapies, being easy to handle in contrast to ESCs or iPSCs, also they do not confer risk for teratomas and they confer low immunogenicity, having no major ethical concerns[28]. These cells can be isolated from different tissues from the same patient, however as they are lineage-restricted and tissue-specific, they do not provide a source for all potential tissue therapies within the adult organism[5,9], having a strong preference for differentiation into specific cell lineages. Nevertheless, only a limited number of cells can be isolated from their tissue of origin.

Most investigated adult stem cells are the neural crest derived stem cells (NCSCs), hematopoietic and mesenchymal stem cells derived from the bone marrow, and neural stem cells derived from the brain[3,7,28]. Other tissue-specific stem cells have limited differentiation potential and they are unipotent, like muscle satellital cells. However, the multipotency or unipotency of ASCs do not impede their therapeutic application, being a rather favourable feature. Nevertheless depending on their potential they should be applied in a tissue specific manner[7]. In the following, this thesis will especially focus in neural crest-derived stem cells and neural stem cells.

1.1.3 Neural crest derived stem cells

During vertebrate development, neural crest (NC) cells migrate from the border between the neural plate and the prospective epidermis and give rise to a wide variety of cell types such as neurons, glial cells, and melanocytes[29] (Fig. 1-2). The induction of early NC territory depends upon the coordinated action of a set of signalling molecules and transcription factors during gastrulation and neurulation stages[30]. The integration of these diffusible signalling molecules: bone morphogenetic proteins (BMPs) produced by the ectoderm, anti-BMPs derived from the neural plate, like chordin, noggin and follistatin (neural inducers), Wnt proteins and retinoic acid (RA) originated from the posterior mesoderm that caudalize the neural tissue, and FGF (fibroblast growth factor) and Notch that originate from the paraxial mesoderm, produce a gradient that initiates the neural crest transcription program at the neural plate border. These transcription factors activate another set of genes that are expressed specifically in the prospective neural crest and play important roles in the establishment and maintenance of the neural crest. As part of NC induction, neural crest cells undergo an epithelial-to-mesenchymal transition and delaminate along almost the entire length of the embryo[31]. Snail, a neural crest specifier, plays a crucial role in this transformation, because it directly represses E-Cadherin, an important cell adhesion molecule promoting delamination[32]. Upon delamination, activation of patterning genes such as Sox10 begins and neural crest cells migrate extensively to colonize their prospective tissue, and they are progressively restricted in their potential as they settle down. The pre-migratory neural crest is subdivided into four distinct axial populations, the cranial, cardiac, vagal and trunk neural crest, each of them migrate along distinct pathways and contribute to different tissues at distinct axial levels[31]. Cranial neural crest cells give rise to cartilage and bone, as well as connective tissue, pigment cells and sensory and parasympathetic ganglia. Cardiac neural crest cells contribute to the aorticopulmonary septum, the aortic arch and parasympathetic cardiac ganglia. Vagal neural crest cells populate the gut and neurons and glia from the enteric nervous system. The trunk neural crest cells differentiate into neurons and glia of the peripheral nervous system, caudal enteric nervous system and pigment cells[31].

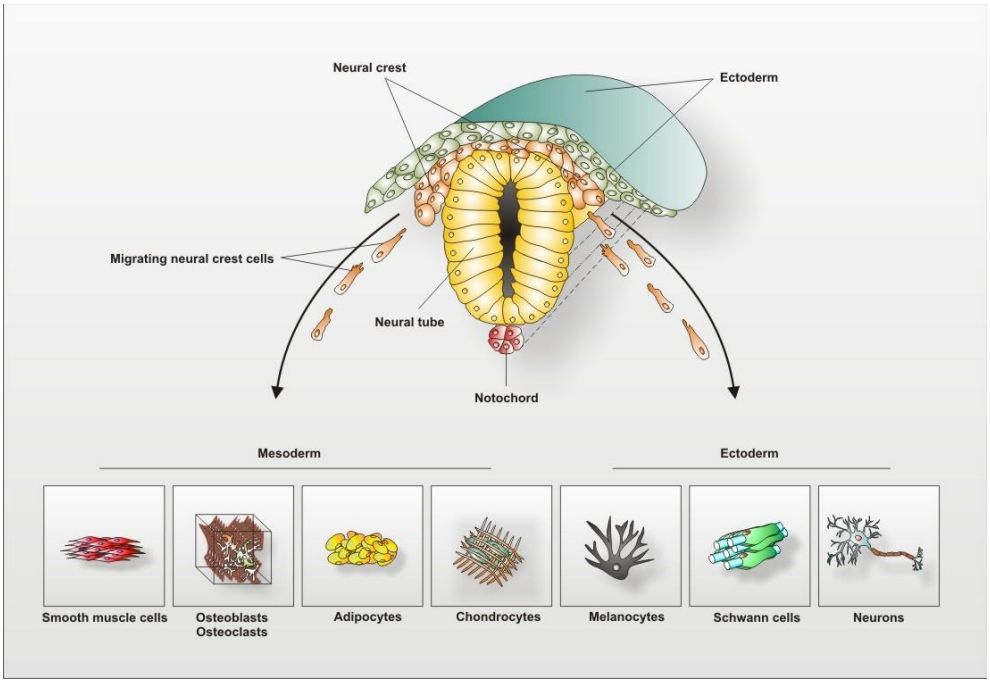

Figure 1-2. Neural crest. Schematic overview showing neural crest formation, delamination and migration, and their ability to differentiate into cells of both mesodermal and ectodermal cell types. NCSCs also persist as uncommitted cells within the adult, Modified from Kaltschmidt et al. 2012[3].

The persistence of these neural crest-derived stem cells (NCSCs) into adulthood was found within various craniofacial tissues, such as the skin, cornea, periodontal ligament, palate, pulp of teeth and nasal turbinates[1,33-38]. Adult NCSCs have the capacity for self-renewal and the ability to differentiate into multiple lineages under appropriate conditions, and they represent a promising stem cell population for cell-based therapies[3]. NCSCs express high levels of nestin, an intermediate filament essential for self-renewal in neural stem cells[39], as well as several additional neural crest markers like the low-affinity nerve growth factor receptor (p75), that vary between different populations of NCSCs.

1.1.4 Inferior turbinate stem cells

Among neural crest-derived stem cells, inferior turbinate stem cells (ITSCs) were localized within the respiratory epithelium of the adult human inferior turbinate (Figure 1-3). Within their endogenous niche, ITSCs are located within the lamina propia, near the nerve fibers between

the glands, and they express NCSCs specific markers Nestin, S100 and $p75^{NTR}$, being glial in nature. When cultured *in vitro*, they also showed high expression levels of Nestin, S100, SLUG and SOX10, and they form spheres under serum-free conditions[1]. Furthermore, ITSCs have a great differentiation capability; they are able to differentiate into diverse mesodermal and neuro-ectodermal cell types such as adipocytes, chondrocytes, osteocytes and glutamatergic and dopaminergic neurons [1,40]. Thus, ITSCs differentiate into neural stem cells, which can give rise to neurons, astrocytes and oligodendrocytes (Fig. 1-4).

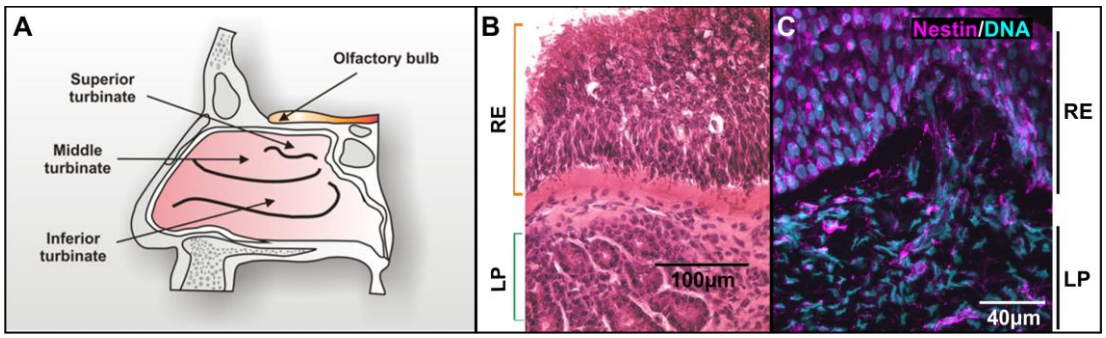

Figure 1-3. Inferior turbinate stem cells localization within the respiratory epithelium of the inferior turbinate of human nose. (A) Schema of the internal structure of the nasal cavity showing the superior, middle and inferior turbinates respectively. (B) hematoxylin-eosin staining of a human inferior turbinate section showing the epithelium and its ciliated surface. C) Inferior turbinate section immunostained against nestin, showing putative stem cells found within the LP and the basal cells of the RE. RE: respiratory epithelium, LP: lamina propria. Modified from Hauser 2012[1].

In addition, these cells do not form teratomas and are a very easily accessible stem cell population, which makes them a promising candidate for the potential clinical use. Considering this, and their capability to efficiently differentiate into functional mature glutamatergic and dopaminergic neurons *in vitro*, ITSCs harbour an immense potential as a model for drug screening and for the treatment of neurodegenerative diseases as well as for other cell-based therapies[1]. Also, as shown by previous findings, transplanted ITSCs functionally improved a parkinsonian rat model, as demonstrated by behavioural tests[40]. After transplantation, cells were able to survive and migrate towards the damaged brain area, and they differentiated into functional neurons. Therefore, ITSCs have a tremendous potential for clinical use. However, little is known about the

molecular mechanisms regulating their fate decisions during differentiation, especially into the neuronal fate.

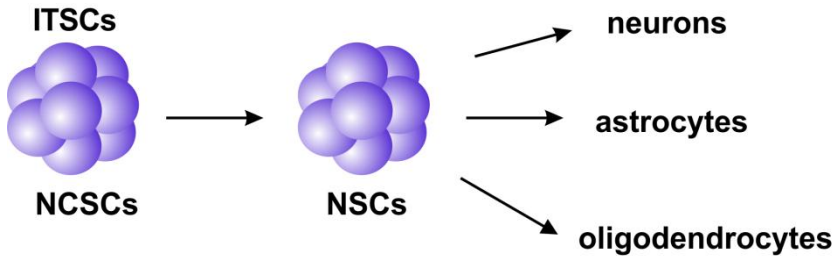

Figure 1-4. Inferior turbinate stem cells differentiation in the neural lineage. ITSC are able to differentiate into neural stem cells (NSCs), which can further differentiate into neurons, astrocytes and oligodendrocytes. NCSCs:neural crest stem cells.

1.1.5 Neural stem cells

Neural stem cells are present in neurogenic niches in discrete regions of the adult brain, in the subventricular zone of the lateral ventricle and in the subgranular zone of the dentate gyrus in the hippocampus[41-42]. Other types of neural stem cells are also found in the peripheral nervous system (PNS), and originate from the neural crest during embryogenesis[43]. NSCs are self-renewing cells capable of differentiating into neurons, astrocytes and oligodendrocytes[44-45], within the embryo they are also known as radial glial cells, and in the adult brain as astrocyte-like stem cells[45]. Both embryonic and adult neural stem cells are glial in nature and share an epithelial morphology essential to their stem cell properties. They had a long process that extends radially from the ventricular apical surface, to the outer pial surface (basal), and expressed high levels of nestin and glial fibrillary acidic protein[42]. Notch signalling maintains their proliferative state, while its withdrawal promotes neural differentiation[46]. NSCs undergo distinct modes of cell division, giving rise to a great diversity of glial and neuronal cell types in the central nervous system (CNS) [41]. As well as they become restricted in their potential to produce specific subtypes of neurons and glial cells, which are defined by their position within the embryo, due to regional specific transcription factors that are expressed in different rostro-caudal and dorso-ventral positions[44,47]. NSCs also generate neuronal and glial intermediate progenitor cells that are capable of generating various

neuronal or glial cell types[41], such as oligodendroglial progenitor cells (OPCs) which can also differentiate into astrocytes, schwann cells, neurons and oligodendrocytes[48].

1.2 Differentiation

1.2.1 Fate specification

The stem cell decision to self-renew or to differentiate is intrinsically controlled by the interplay of specific transcription factors and chromatin regulators[49]. As mentioned before, several key transcription factors are responsible for the self-renewal including OCT4, NANOG and SOX2[50-51]. During development in mammals, the first fate decision occurs during compaction where the cells from the outer layer of the 8-cell embryo develop tight junctions and the cells from the center develop gap junctions, thus the outer cells are specified into the trophectoderm and the central cells into the inner cell mass respectively[52]. Moreover, after blastocoel formation, during gastrulation, cell movements allow the interaction of different cell populations segregated until then, and these interactions together with the expression of genes induce the specification of different cell populations into the three germ layers, endoderm, mesoderm and ectoderm. These extrinsic and intrinsic factors are also used for the specification *in vitro* of embryonic and adult stem cells. Bone morphogenetic proteins (BMPs), WNT and Activin/Nodal pathways which are implied in germ layer development are manipulated to obtain these lineages *in vitro*[53-54]. Both WNT and Activin/Nodal signalling are required for the beginning of gastrulation and favour differentiation into specific derivatives *in vitro*. In particular, high levels of Activin were shown to induce endoderm formation in culture[55], while BMP4 (bone morphogenetic protein 4) signalling is necessary for mesoderm specification. Thus, cell fate decisions occurring *in vitro* resemble those occurring during development.

1.2.2 Neuronal fate specification

Neurons share many features, but they have different phenotypic characteristics that define their function, localization and connectivity. The diversification in different neuronal subtypes in nervous system development involves the integration of extrinsic and intrinsic instructive

signals that result in the expression of distinct regulatory molecules in a spatial and temporal manner. Thus, neuronal induction and differentiation follow a common pattern, of activation and inhibition of various signalling pathways which are strongly regulated epigenetically, in particular by histone modifications and DNA methylation[56]. At the end of gastrulation the prospective neural tissue is already induced and has began to be patterned. The neuronal specification takes place along the rostral-caudal and the dorsal-ventral axes of the neural tube, being coordinated by patterning molecules that confer positional identity. Neural stem cells and other neural progenitor cells (NPCs) respond differently to distinct concentrations of the same molecule, and therefore they differentiate into region-specific progenitors in response to locally positioned/derived signals[42,44,57]. For example, Sonic hedgehog (SHH), is secreted by the notochord and the floor plate of the neural tube (ventralizing activity), whereas WNT proteins and bone morphogenetic proteins (BMPs) are secreted from dorsal regions, by the roof plate and the ectoderm, establishing the dorsal-ventral axis[42]. Thus, treatment with increasing concentrations of SHH promote the ventralization, while retinoic acid (RA), FGF and β-catenin promote specification of more posterior fates[58]. WNT gradient helps to establish the rostral/caudal axis, and its signalling activation produces a dose-dependent effect where increasing levels are patterning the NPCs to forebrain, midbrain, hindbrain and anterior spinal cord identities, respectively[42,58-60]. The resulting morphogen gradient specifies neurons into different subtypes along both dorsal-ventral and anterior-posterior axes, leading to CNS morphogenesis. Neuronal differentiation *in vitro* recapitulates this regional patterning principle from *in vivo* morphogenesis[61].

Moreover, a specific neurotransmitter subtype is usually produced in different parts of the brain at different stages of development, demonstrating that different spatiotemporal signalling molecules converge inducing a similar fate[62]. Then, once specified cells are patterned into specific regional fates, and they finally differentiate into neurons and glia[42]. Cells specified to a neuronal fate express a series of proneural genes either alone or in concert with additional neuronal differentiation genes, which activate Notch signalling pathway, cell cycle withdrawal and pan-neuronal and cell type-specific gene expression[63].

Glutamatergic neuronal fate

Excitatory glutamatergic neurons are found throughout the central nervous system, in the cerebral cortex, in the subcortical regions and within the spinal cord [58,64-65]. Despite the differences in their specification during development, the strategies that have been established to successfully generate glutamatergic neurons are mainly based on the derivation of cortical glutamatergic neurons that originate from the dorsal telencephalic region[66]. Also, forebrain identity is known as a default programme for neuronal differentiation, and existing protocols yield neurons with a glutamatergic identity without the need of a series of patterning molecules[67]. Neural progenitors differentiated from NSCs *in vitro* will adopt a regional identity depending in the morphogens present at the time the precursors are responsive. During development the neuroectoderm at the head region form first, thus neuroepithelial cells initially express forebrain homeobox transcription factors such as OTX1/2 (Orthodenticle homeobox 1 and 2) and brain factor 1 (BF1), but no hox genes that are present in the hindbrain and spinal cord. With the exposure to morphogens like WNTs, RA and FGFs, which caudalize the neuroepithelial cells, less forebrain progenitors are present in neural differentiation cultures. Thus, Neuronal progenitors differentiated by treatment with RA usually display hindbrain and spinal cord identities. RA promotes the expression of Hox genes but suppresses the expression of OTX2 and BF1 in a dose dependent manner. In contrast FGF8 (fibroblast growth factor 8) favours the differentiation of neural progenitors with mid/hindbrain characteristics, while FGF2 (fibroblast growth factor 2) favours differentiation into a mixed population with a range of identities from forebrain to spinal cord phenotypes[47]. Further restriction by dorsal-ventral morphogens limits the differentiating neurons to a specific state in the dorsal-ventral domain of the neural tube. Therefore, glutamatergic neurons are produced by a series of genetically programmed fate choices, applied by developmental transcription factors which are expressed sequentially during glutamatergic neurogenesis, PAX6 (paired box 6), TBR2 (T-box brain protein 2), NEUROD (neuronal differentiation 1), and TBR1 (T-box brain protein 1), which are initially conserved in neocortex, cerebellum, and adult hippocampus. However, subtypes of glutamatergic neurons are further induced by other combinations of transcription factors expressed afterwards in each region[68].

Neurogenin2 (NGN2) regulates glutamatergic differentiation of early-born neurons in the developing forebrain, and expression of TBR1 and TBR2. Whereas MATH1 regulates glutamatergic neuron development and TBR1 expression in the cerebellum. In addition, MATH1 was found to be necessary for TBR2 and PAX6 expression in the cerebellum[68]. Furthermore, molecules that orchestrate neurogenesis not only include transcription factors, but also environmental factors.

Dopaminergic neuronal fate

Dopaminergic neurons are localized in the diencephalon, mesencephalon and the olfactory bulb[69]. Protocols differentiating cells into dopaminergic neurons have focused in particular in the neurons originating from the midbrain[54,70] due to their applicability for the treatment of Parkinson's disease. The molecular patterning and specification of these dopaminergic neurons has been largely studied, over the last decades. Midbrain dopaminergic neurons are specified from the floor plate in the mesencephalon, regulated by WNT, SHH and FGF-8 signalling, essential morphogens for dopaminergic specification[71-72]. Neuronal progenitors in the midbrain are characterized by the expression of LMX1A (LIM homeobox transcription factor 1 alpha), FOXA2 (forkhead box A2), EN1 (Engrailed Homeobox 1) and OTX2 [72]. WNT1 (Wnt family member 1) induces the expression of OTX2, which in turn represses GBX2 (Gastrulation brain homeobox 2) to maintain the mid-hindbrain organizer and also represses NKX2-2 (NK2 homeobox 2), which is a negative regulator that replaces the dopaminergic neurons by serotonergic neurons in the absence of OTX2[73]. OTX2 induces LMX1A expression, which in turn induces the pro-neural gene NGN2 through MSX1 (msh homeobox 1) or represses NKX6-1 (NK6 homeobox 1) to inhibit differentiation into alternative neuronal fates[74-75]. This principle also guides the differentiation of human midbrain dopaminergic neurons *in vitro*, as shown by different protocols based on chemically defined systems. A diversity of this systems that rely on the activation of FGF8 and SHH signalling pathways, have shown the efficient differentiation into the dopaminergic phenotype, of neurons expressing tyrosine hydroxylase (TH)[76-79]. However, the combination of FGF8 and SHH alone was not sufficient to restrict their specification to the midbrain fate[76]. The addition of WNT signalling by using GSK3β inhibitor CHIR99021,

improve the efficiency in the specification into midbrain dopaminergic neurons[4,59,76,80-81]. A short WNT induction with CHIR99021, during early dopaminergic differentiation of human epidermal NCSCs, allowed their restriction into a midbrain dopaminergic neuronal fate, showing a great potential for the use of directed dopaminergic differentiation *in vitro* for modelling neurodegenerative diseases [4,40].

1.3 Nuclear Factor kappa B

1.3.1 NF-κB signalling

NF-κB (nuclear factor kappa-light-chain-enhancer of activated B-cells) is a ubiquitously expressed, inducible transcription factor that regulates the expression of a broad number of genes and is involved in diverse cellular processes such as cell survival, growth, stress, immune and inflammatory responses [82]. Furthermore, within the nervous system NF-κB has special functions, being involved in neuroprotection/degeneration, in neurite growth [83], in dendritic spine formation and functionality [84], in axonal outgrowth [85] and synaptic plasticity [86-87].

In mammalian cells the NF-κB family consists of five subunits, p50/p105, p52/p100, p65 (RelA), c-Rel and RelB, which share an N-terminal domain known as the Rel homology domain (RHD) which allows their dimerization into different NF-κB complexes as homo or heterodimers, as well as DNA binding and nuclear localization [88] (Fig. 1-5). Furthermore, only Rel subfamily members RelA, RelB and c-Rel contain a C-terminal transactivation domain, allowing them to initiate transcription. In most of the cells, NF-κB complexes are sequestered in the cytoplasm by the association with an inhibitory protein of the inhibitor of κB family (IκB). Activation of NF-κB is triggered by multiple stimuli (cytokines, neurotransmitters, mitogens and growth factors) and involves the activation of a kinase cascade, which ends in the activation of the IκB kinase complex (IKKα & IKKβ), which in turn phosphorylates specific serines within the inhibitory IκB-alpha subunit (IκBα), leading to its ubiquitination and

proteosomal degradation. Upon release, NF-κB dimers can translocate to the nucleus and regulate the expression of their target genes [88-90].

Considering that NF-κB has multiple roles in very diverse cellular processes and also within the nervous system, we hypothesized that NF-κB may have a role during the differentiation of ITSCs, especially into the neuronal phenotype. Therefore in the present work, we explored the distribution of NF-κB family members during early stages of neuronal glutamatergic differentiation in ITSCs.

1.3.2 NF-κB signalling in nervous system

Acute and chronic nervous system damage in response to an insult such as oxidative stress is directly associated to neuronal death and degeneration [91]. Thus, appropriate neuroprotection remains as a crucial parameter for effective treatment of neurodegenerative diseases. Interestingly, increasing evidences point towards sex-specific differences in risk, severity and progression of neurodegenerative diseases such as Parkinson's (PD) or Alzheimer's disease (AD) or in case of Ischemic stroke [92-94]. In particular, female AD patients were reported to not only have an increased risk of developing AD compared to age-matched men [95], but also showed a significantly elevated age-related faster decline of cognition [93,96]. On the contrary, PD was shown to have a greater prevalence and occurs in an earlier age in men compared to woman [92]. Although neurodegenerative diseases and preventive neuroprotective mechanisms [97] seem to be subjected to sex-dependent differences, little is known about the underlying molecular mechanisms particularly regarding maturation and survival of neurons differentiated from human stem cells.

The transcription factor NF-κB is involved in a broad range of cellular processes such as cell survival, growth, stress, immune and inflammatory responses [82]. Within the murine nervous system, the NF-κB heterodimers cRel/p65 and p50/p65, and p50 homodimers play an important role during development [98], while the activity of p50/p65 was shown to be predominant in the adult brain[99].

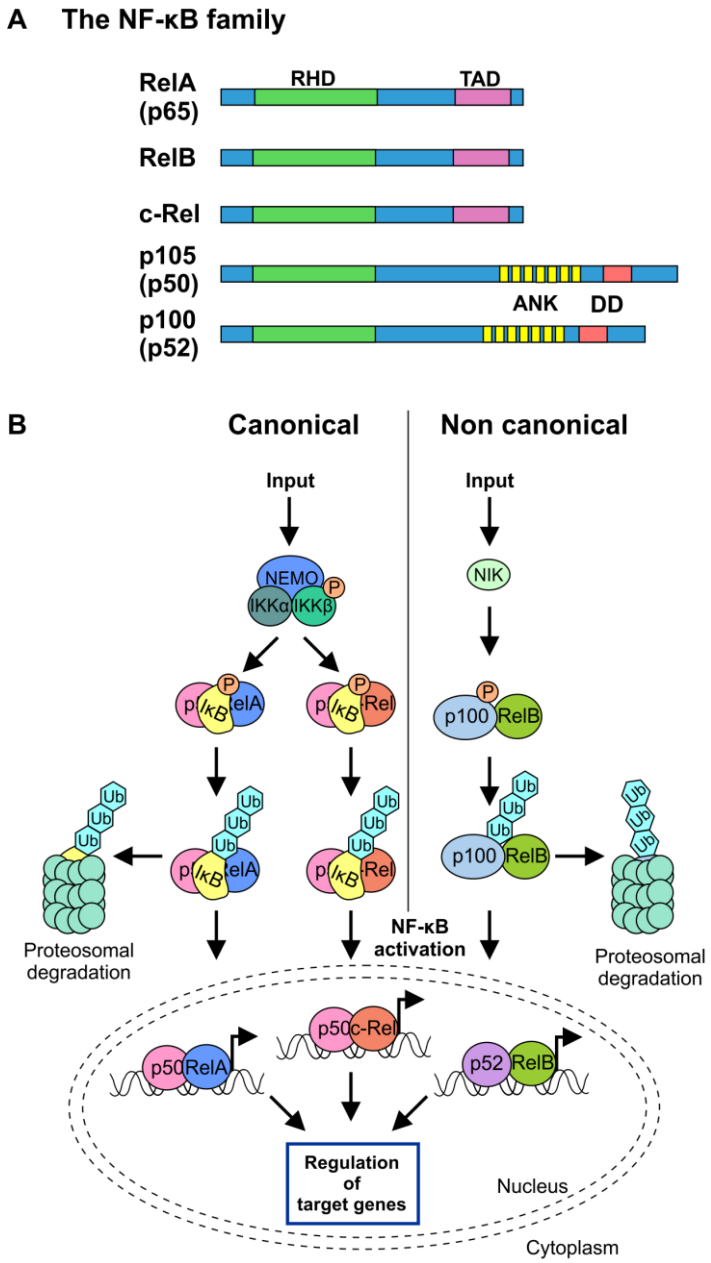

Figure 1-5. NF-κB members and signaling cascades. A) Schematic view of the NF-κB family members. Relevant domains are indicated and alternative nomenclatures are provided in parenthesis. RHD, rel homology domain; TAD, transactivation domain; ANK, ankirin repeats; DD, death domain. C) Schema showing simplified NF-κB canonical and non-canonical signaling pathways. NF-κB activation is triggered by multiple stimulus and involves the activation of a kinase cascade that ends in the IκB kinase complex activation, which causes the degradation of an inhibitory protein or the partial degradation of a NF-κB precursor. The resulting NF-κB dimers translocate into the nucleus and regulate the expression of different target genes.

Activation of NF-κB can be triggered by multiple stimuli such as cytokines like tumour necrosis factor-α (TNF-α) or neurotransmitters like AMPA (agonist α-amino-3-hydroxyl-5-methyl-4-isoxazole-propionate) or glutamate in mouse and rat cerebellar granule cells[100-101]. In murine neurons, NF-κB signalling and its target genes are involved in neuroprotection/degeneration [86], neurite growth [83], the formation of dendritic spines and their functionality [84], axonal outgrowth [85] and synaptic plasticity[87-88,102]. Activation of NF-κB in human and murine cells is also known to be caused by oxidative stress, an increase in intracellular reactive oxygen species (ROS) such as hydrogen peroxide (H_2O_2), superoxide (O_2^-), or hydroxyl radical (OH)[103]. Whithin the nervous system, oxidative stress leads to activation of NF-κB with a direct linkage to several neurologic diseases and brain damage[104]. In functional neurons from humans or mice, activation of various glutamate receptors also induces oxidative stress [105]. On the contrary, reactive oxygen intermediate H_2O_2 is known to act as second messenger despite its cytotoxicity [104,106]. In primary rat cerebellar granule cells, the direct exogenous addition of H_2O_2 to culture medium activates NF-κB[107], as well as it was observed previously in different human cell lines[106,108-109]. In human and mouse embryonic stem cells, metabolic oxidation is known to directly regulate embryonic stem cell differentiation[110]. Maintenance of redox balance was further shown to be crucial for stemness and self-renewal of hematopoietic stem cells (HSCs) and neural stem cells (NSCs)[111] from mice and humans. On the other hand, NF-κB signalling is directly linked to proliferation of rat NSCs[112] and early neuronal differentiation of mouse NSCs[113], although its direct role in protection of human stem cell-derived neurons against oxidative stress still remains unclear.

1.3.3 Aim of the study

The central aim of this project was to study the role of NF-κB subunits during the specification of inferior turbinate stem cells into the neuronal fate and during their maturation, in order to provide a better understanding of the molecular mechanisms underlying the regulation of stem cell properties during differentiation and neuronal physiology.

Therefore we initially tried to efficiently reproduce the neuronal differentiation of ITSCs into glutamatergic and dopaminergic neurons using directed differentiation assays. In addition, upon neuronal differentiation and maturation we verified the expression of characteristic neuronal subtype markers to further validate their differentiation. Also, upon their properly differentiation and maturation we analyzed their functionality *in vitro* by chemical stimulation. Afterwards we characterized the differential NF-κB subunit composition during early neuronal differentiation, to elucidate their role during differentiation. After we determined NF-κB distribution, we further studied the cell fates obtained after inhibition of the central subunit involved during glutamatergic differentiation, for this we analyzed a series of specific cellular markers, to recognize distinct cell fates.

2

2.1 Isolation and Cultivation of ITSCs

ITSCs were isolated from adult human inferior turbinate tissue obtained by biopsy during routine surgery after informed consent according to local and international guidelines and cultivated as described previously [1]. The ethics board of the medical faculty of the University of Münster approved all the procedures described in this article (No. 2012-15-fS). All experiments were performed in accordance. For further cultivation of ITSCs within the 3D blood plasma (BP) matrix [114], ITSCs were dissociated using pre-warmed Collagenase I (NB 4; Serva Electrophoresis, Heidelberg, Germany, http://www.serva.de) for 1 h at 37 °C on an orbital shaker (Edmund Bühler, Hechingen, Germany) and harvested by centrifugation at 300 g for 10 min. ITSCs were resuspended in Dulbecco's modified Eagle's medium/Ham F-12 (DMEM/F-12; Biochrom, Berlin, Germany, http://www.biochrom.de) containing 2 mM L-glutamine (Sigma-Aldrich), penicillin/streptomycin (1x, Sigma-Aldrich), and supplemented with basic fibroblast growth factor-2 (FGF2; 40 ng/ml; Miltenyi Biotec), epidermal growth factor (EGF; 20 ng/ml; Miltenyi Biotec) and B27 supplement (Gibco) followed by supplementation with 10% of clinically accredited therapeutic human blood plasma (obtained from Institut für Laboratoriums und Transfusionsmedizin, Bad Oeynhausen, Germany) and cultivated at 37C, 5% O_2 and 5% CO_2.

2.2 Glutamatergic neuronal differentiation

For neuronal differentiation, cells of three to six donors precultivated within the 3D BP matrix were removed from the matrix as described above, and resuspended in DMEM high glucose (Sigma-Aldrich) containing 2 mM L-glutamine (Sigma-Aldrich), penicillin/streptomycin (1x, Sigma-Aldrich) and 10 % FCS (Sigma-Aldrich) an plated at a density of $5x10^4$ cells per 24 well plate followed by cultivation at 37 °C, 5% CO_2 and atmospheric O_2 in a humidified incubator for 2 days. Afterwards, 1µM dexamethasone (Sigma-Aldrich), 2 µM insulin (Sigma-Aldrich), 500 µM 3-isobutyl-1-methylxanthine (Sigma-Aldrich), 200 µM indomethacin (Sigma-Aldrich) and 200 µM ethanol were added to the medium to induce neuronal differentiation (neuronal induction medium, NIM) according to[40]. After 9

days of differentiation cells were induced adding 0.5 μM retinoic acid (Sigma Aldrich) and 1x N-2 supplement (Gibco, Darmstadt, Germany, http://www.invitrogen.com)[115]. Subsequently, the medium was changed by removing half of the volume, followed by addition of fresh pre-warmed NIM containing 1X N-2 supplement[40]. As a control, undifferentiated ITSCs within the 3D blood plasma matrix were used. ITSCs were differentiated for 1 month, and further stimulated using different drugs, or treated for immunocytochemical and RT-PCR analysis (Reverse transcription Polymerase Chain Reaction).

2.3 Neuronal stimulation of mature glutamatergic neurons

After 30 days of differentiation neurons were exposed to the excitatory neurotransmitter glutamate (GLU) or its agonist α-amino-3-hydroxyl-5-methyl-4-isoxazole-propionate (AMPA), the cytokine Tumour Necrosis Factor α (TNF-α, Calbiochemff), hydrogen peroxide (H_2O_2), and the NF-κB inhibitor pyrrolidine dithiocarbamate (PDTC) [107]. Before treatment with glutamate or AMPA, cells were washed three times with buffered control salt solution (CSS)[116] containing 120 mM NaCl, 5.4 mM KCl, 1.8 mM CaCl2, 25 mM Tris HCl (pH 7.4), 15 mM D-glucose. For inhibitor controls cells were preincubated with either 1 μM dibenzocycloheptеneimine (MK-801, Tochris Bioscience, UK)[117] or 50 μM 6-cyano-7-nitroquinoxaline-2,3-dione (CQNX, Tochris Bioscience, UK) [101] for 10 min at 37 flC, before 10 min treatment with glutamate or AMPA respectively. After treatment, with different concentrations, cells were washed with CSS and incubated with complete medium for 45 min at 37 ° C. Control cells received identical incubation times and washing steps with CSS [101]. The pulse with 10 ng/ml TNF-α was performed for 30 min, 1 h, and 24 hours. For oxidative stress induction, 300 μM H_2O_2 were applied during 25 h and to analyze the neuroprotective role of NF-κB during oxidative stress, a pre-treatment with 10 ng/ml TNF-α was performed for 2 hours previous to the treatment with hydrogen peroxide. Untreated control cells received identical incubation times in complete medium. In order to confirm NF-κB activation due to TNF-α, a pre-treatment using 100 μM PDTC for one hour was performed and afterwards samples were directly used or further treated with TNF-α

for at least one hour. For Indirect immunofluorescence assay cells were fixed for 15 min in phosphate-buffered 4% paraformaldehyde (PFA; 4% pH 7.4). For Smart-seq2, cells were directly used after treatment and treatment duration was slightly longer, PDTC and TNF-α treatment took 3h as well as the combination treatments.

2.4 PTXF treatment - oligodendrocyte differentiation

In order to inhibit c-Rel nuclear translocation during differentiation, cells were treated using pentoxifylline (PTXF), a known inhibitor of c-Rel[2]. For this, 500µg of PTXF per ml were added to the media, in parallel to the differentiation procedure. PTXF was refreshed every 1-2 days. For evaluating the stimulation of ITSCs using PTXF, differentiated ITSCs in the absence of PTXF were used as control. ITSCs were differentiated for a maximum of 1 month, and further treated for immunocytochemical and PCR analysis.

2.5 Classical oligodendrocyte differentiation

For classical oligodendrocyte differentiation, ITSCs were harvested and resuspended in DMEM high glucose (Sigma-Aldrich) containing 2 mM L-glutamine (Sigma-Aldrich), penicillin/streptomycin (1X, Sigma-Aldrich) and 10% FCS (Sigma-Aldrich) an plated at a density of $25x10^4$ cells per 6 well plate followed by cultivation at 37 °C, 5% CO_2 and atmospheric O_2 in a humidified incubator. The next day, after attachment of the cells to the culture surface, medium was switched to oligodendrocyte enrichment medium (Millipore, OEM: DMEM/F12 with 1X NEAA, 2 mM glutamine, N21 medium supplement, a cocktail of growth factors recombinant human PDGF-AA (SRP3268), recombinant human neurotrophin-3 (N1905), and recombinant human basic FGF2 (F0291) to differentiate into olygodendrocyte progenitor cells (OPCs). Media was changed every 2-3 days.

2.6 *In vitro* myelination assay

For *in vitro* myelination, olygodendrocytes derived from ITSCs cultured in oligodendrocyte enrichment medium (Millipore) and those derived from PTXF-treated differentiated ITSCs (cultured in neuronal induction media)

were transplanted after 20 days of differentiation and co-culture with ITSC-derived neurons which were previously differentiated for 20 days. Cells were co-cultured for 10 days in NIM with N2 at 37 ° C in a 5% CO2 incubator. Medium was changed every 2 to 3 days by replacing half of the media with fresh media. Afterwards cells were treated for immunocytochemical and RT-PCR analysis.

2.7 Dopaminergic neuronal differentiation

For dopaminergic differentiation, cells of six donors were expanded within the 3D BP matrix and further dissociated using collagenase, as described above. ITSCs were directly differentiated as previously reported[40] slightly modified from Sieber-Blum et al.[4]. Cells were seeded at a density of $5x10^4$ cells per 24 well plate and cultivated for 18 hours in DMEM high glucose containing 2 mM L-glutamine, penicillin/streptomycin and 10 % FCS. For neuronal induction (Fig. 2-2), cells were exposed to DMEM high glucose supplemented with 1% FCS, penicillin/streptomycin, β-mercaptoethanol (10 µM), B27 without retinoic acid (1X; Life Technologies), purmorphamine (10 µM; Sigma-Aldrich), FGF8 (100 ng/ml; Peprotech), recombinant human glial cell line-derived neurotrophic factor (GDNF; 5 ng/ml; Peprotech), recombinant human brain-derived neurotrophic factor (BDNF; 20 ng/ml; Peprotech), nerve growth factor (NGF; 20 ng/ml; Peprotech), dibutyryl cAMP (1 mM; Sigma- Aldrich), ascorbic acid (200 µM; Sigma-Aldrich), SB-431542 (10µM; Sigma-Aldrich), LDN193189 (100 nM; Abcam, Cambridge, U.K., http://www.abcam.com), and CHIR99021 (0.5µM; Abcam). CHIR99021 was removed after 24 hours. On day 4 of differentiation, the WNT inhibitor IWP-4 (Miltenyi Biotec, Bergisch Gladbach, Germany, http://www.miltenyibiotec.com) was added to the media at a concentration of 100 nM, which was increased to 1 µM at day 6 of differentiation, followed by withdrawal of FCS at day 7. At day 9, the concentration of purmorphamine was decreased to 5 µM. Medium was replaced with prewarmed fresh medium daily.

2.8 Chemical stimulation of dopaminergic differentiated neurons

After 20 days of differentiation, dopaminergic neurons were exposed to 6-hydroxydopamine (6-OHDA), a neurotoxic synthetic organic compound used to selectively destroy dopaminergic neurons, the cytokine Tumour Necrosis Factor α (TNF-α, Calbiochem), as well as their combination. For the each treatment, drugs were applied in the differentiation media. The pulse with 10 ng/ml TNF-α was performed for 2 hours. For neurotoxic induction, 100 µM 6-OHDA were applied during 24 h and to analyze the neuroprotective role of NF-κB during it, a pre-treatment with 10 ng/ml TNF-α was performed for 2 hours previously. Untreated control cells received identical incubation times in complete medium. After treatment, cells were washed and directly fixated for immunocytochemical analysis.

2.9 Immunocytochemistry

Differentiated ITSCs were fixed in phosphate-buffered 4% paraformaldehyde (PFA; 4% pH 7.4) for 15 minutes at room temperature (RT) followed by 3 wash steps in phosphate-buffered saline (1xPBS). The cells were permeabilized with 0.02% Triton X-100 and blocked using 5% of appropriate serum or 3% BSA for 30 minutes at RT, followed by incubation with primary antibodies for 1 hour at RT. Primary antibodies used are listed in Table 1.

Table 1: List of primary antibodies.

Antibody	Origin	Dilution	Company	Code
anti-c-Rel	Rabbit polyclonal	1:100	Santa Cruz Biotechnology	sc-70x
anti-c-Rel	Rabbit monoclonal	1:400	Cell Signaling	#4727
anti-RelB	Rabbit polyclonal	1:100	Santa Cruz Biotechnology	sc-226
anti-RelB	Rabbit monoclonal	1:1600	Cell Signaling	#10544,
anti-p65	Mouse monoclonal	1:100	Santa Cruz Biotechnology	sc-8008

anti-NF-kappaB p65	Rabbit monoclonal	1:200	Cell Signaling	D14E12
anti-p50	Mouse monoclonal	1:100	Santa Cruz Biotechnology	sc-8414
anti p52	Rabbit polyclonal	1:100	Santa Cruz Biotechnology	sc-298
anti-IκBα	Rabbit polyclonal	1:100	Santa Cruz Biotechnology	sc-371
anti-MAP-2 (Microtubule-associated protein 2)	Rabbit polyclonal	1:100	Santa Cruz Biotechnology	Sc-20172
Anti- Synaptophysin	Rabbit monoclonal	1:250	Merck Millipore	MAB5258
anti-vGlut2	Mouse monoclonal	1:200	Millipore	MAB5504
anti-Olig2	Goat polyclonal	1:250	R&D Systems	AF2418
anti-Nestin	Mouse monoclonal	1:200	Millipore	MAB5326
anti-β-III-tubulin	Mouse monoclonal	1:300	Promega	G7121
anti-neurofilament 200 (NF200)	Rabbit polyclonal	1:200	Sigma-Aldrich	N4142
Calretinin	Mouse monoclonal	1:200	Swant	6B3
GFAP	Rabbit polyclonal	1:500	Dako	Z0334
anti-αSMA	Mouse monoclonal	1:200	Sigma	A5691
anti-O4	Mouse monoclonal IgM	1:100	R&D Systems	MAB1326
NGFRp75 (c-20)	Goat polyclonal	1:100	Santa Cruz Biotechnology	sc-6188
anti-clived caspase 3 (Asp 175)	Rabbit monoclonal	1:300	Cell Signaling	#9664
anti-MOG (Myelin oligodendrocyte glycoprotein)	Mouse monoclonal	1:50	Millipore	MAB5680
anti-TH (tyrosine	Rabbit	1:100	Santa Cruz	SC-14007

hydroxylase)	polyclonal			
anti-DA	Rabbit polyclonal	1:100	Millipore	AB1225
anti-PitX3	Rabbit polyclonal	1:100	Millipore	AB5722

The secondary fluorochrome-conjugated antibodies (1:300; goat anti-mouse or goat anti-rabbit Alexa 555, donkey anti goat Alexa 555; and donkey anti-mouse or anti-rabbit Alexa 488; Life Technologies) were incubated for 1 hour at RT. Nuclear counterstaining was performed with 49,6-diamidino-2-phenylindole (DAPI; 1 µg/ml; Sigma-Aldrich) for 15 min at RT. Fluorescence imaging was performed using a confocal laser scanning microscopy (LSM 780; Carl Zeiss, Jena, Germany) and analyzed using ZEN software from the same provider or ImageJ [118].

2.10 Reverse transcription Polymerase Chain Reaction

Total RNA was isolated using the TRI Reagent (Sigma-Aldrich) or the NucleoSpin Kit (Macherey-Nagel) according to the manufacture's guidelines. Quality and concentration of isolated RNA were assessed via Nanodrop ultraviolet spectrophotometry. cDNAs were synthesized by reverse transcription using the First Strand cDNA Synthesis Kit (Fermentas Life Sciences). PCR was performed using the GoTaq (Promega) according to the manufacturer's guidelines and 10 µM primers (Sigma-Aldrich). The cycling conditions comprised an initial denaturation of 1 min at 94 ° C and 35–38 cycles of 15 s at 94 ° C, 15 s at 60 ° C, and 20 s at 72 ° C followed by a final elongation for 1 min at 72 ° C. For primer sequences see Table 2.

Table 2: Primer sequences for RT-PCR.

Target	Sequence 5'-3'
Nestin	CAGCGTTGGAACAGAGGTTG
Rev-Nestin	GCTGGCACAGGTGTCTCAAG
MAP-2	GAGGATGAAGAGGGTGCCTT
Rev-MAP-2	AGCTCTCCGTTGATCCCATTC
Synaptophysin	TGTAGTCTGGTCAGTGAAGCC
Rev- Synaptophysin	GCAGGGCTCAGACAGATAA
AMPA receptor subunit 1	GGGCGATAATTCAAGTGTTCA
Rev-AMPA receptor subunit 1	GGCTCCGTATTTTCCATCAC
NMDA Receptor subunit 1	GCTCCTCGAGAAGGAGAACA
Rev- NMDA Receptor subunit 1	GCCATTGTAGATGCCCACTT
Vesicular glutamate transporter 1	CACAAGACTCGGGAGGAGTG
Rev- Vesicular glutamate transporter 1	GCCTCATCCTCCATTTCGCT
Glutamate metabotropic receptor 1	AGCTGCTGATTTCTCAGCCAA
Rev- Glutamate metabotropic receptor 1	GCCTCCAACATTGGAATGGA
Tyrosine Hydroxylase	CCGTGCTAAACCTGCTCTTC
Rev- Tyrosine Hydroxylase	CGCACGAAGTACTCCAGGT
Choline Transporter	GGCACAGCTGAAGCAGTTTA
Rev- Choline Transporter	CCCATGCGTTTTCCATAGAT
GABA transporter	CAGTGGGATGTGCCTTCTCT
Rev- GABA transporter	CAGGGGTCATGATCATCCAG
Serotonin transporter	CTCCGAGGACAACATCACCT
Rev- Serotonin transporter	CAGAGGTCTTGACGCCTTTC
RPLP0 (Ribosomal Protein Lateral Stalk Subunit P0)	TGGGCAAGAACACCATGATG
Rev-RPLP0	AGTTTCTCCAGAGCTGGGTTGT

2.11 SMART-Seq2

For full-length cDNA generation, the protocol recently described by Picelli et al[119] slightly modified was applied. Approximately 20000 cells/treatment of differently treated ITSC-derived glutamatergic neurons were used. Cells were harvested by centrifugation (5000 g for 5 min at RT) and directly lysed with an adjusted amount of lysis buffer (RNase inhibitor, 0.2% Triton X-100). Afterwards the annealing mix containing AccuStart Taq Polymerase HiFi (Quanta bio), oligo-dT primer, dNTP-mix, was added to the cell lysate. Probes were incubated 3 min at 72 ° C, and the reverse transcription-mix containing SuperScript II reverse transcriptase (Thermo Fisher Scientific) was added. Reverse transcription, relying on template-switching reaction was performed. The cycling program comprised a initial denaturation of 90 min at 42flC, following by 9 cycles of 2 min at 50 ° C and 2 min at 42 ° C followed by a final elongation for 15 min at 70 ° C. The PCR pre-amplification mix was added to the first-strand reaction. PCR pre-amplification-cycling-program used comprised an initial denaturation of 3 min at 98 ° C and 21 cycles of 20 s at 98 ° C, 15 s at 67 ° C, and 6 min at 72 ° C followed by a final elongation for 5 min at 72 ° C.

2.12 Real-time PCR

All Quantitative polymerase chain reaction (qPCR) reactions were performed in triplicate using PerfeCTa SYBR Green qPCR Super-Mix (Quantabio), according to the manufacturer's guidelines, and assayed with a Rotor Gene 6000 (Qiagen). Primers used are listed in Table 3.

Table 3. List of primer sequences used for qPCR.

Target	Sequence 5'-3'
IGF1 (Insulin-like growth factor 1)	GAAGATGCACACCATGTCCT
Rev- IGF1	TAAAAGCCCCTGTCTCCACA
IGF2 (Insulin-like growth factor 2)	TGGACTTGAGTCCCTGAACC
Rev- IGF2	GATGGCCAGTTTACCCTGAA

PKAcatα (c-AMP-dependent protein kinase catalytic subunit α)	TACAACAAGGCCGTGGACTG
Rev- PKAcatα	AGATCTGGATGGGCTGGTCT
SOD2 (Superoxide dismutase 2)	TGGAAGCCATCAAACGTGACT
Rev- SOD2	TTGAAACCAAGCCAACCCCA
cIAP1 (Cellular inhibitor of apoptosis protein 1)	CCA CTG GAG AAG AAA ATG CTG
Rev- c-IAP1	CCA AGG CAG ATT TAA CCA CA
c-IAP2 (Cellular inhibitor of apoptosis protein 2)	GAC AGC CCA GGA GAT GAA AA
Rev- c-IAP2	CAC GGC AGC ATT AAT CAC AG
Fw-NG2 (transmembrane proteoglycan nerve-glia antigen 2*)	CATCCCACTAGAGGCGCAAA
Rev-NG2	CCCAGGAGAGTGGGGAAGTA
Fw-MBP (Myelin basic protein)	GCGTCACAGAAGAGACCCTC
Rev-MBP	CTCTGTGCCTTGGGAGGAAG
Fw-PDGFRA (Platelet derived growth factor receptor alpha)	GAAGAAAACAACAGCGGCCTT
Rev-PDGFRA	TGTACAACCCTGTGTGGGC
Fw-RPLP0 (Ribosomal Protein Lateral Stalk Subunit P0)	TGGGCAAGAACACCATGATG
Rev-RPLP0	AGTTTCTCCAGAGCTGGGTTGT
Fw-GAPDH (Glyceraldehyde-3-phosphate dehydrogenase)	CATGAGAAGTATGACAACAGCCT
Rev-GAPDH	AGTCCTTCCACGATACCAAAGT

* also known as Chondroitin sulfate proteoglycan 4 (CSPG4)

2.13 Cell Counting and Statistics

For nuclear NF-κB analysis, quantification of indirect immunofluorescence was performed for a minimum of 3 different donors. For each time point 6-12 pictures were analyzed per donor, where the mean of the nuclear integrated density was measured by defining the region of interest (ROI) with the nuclear counterstaining (DNA channel) using ImageJ [118]. For analysis of neuronal survival the same channel was used to study the nuclear chromatin morphology. Nonviable neurons were recognized by nuclear condensation and/or fragmented chromatin. In phase contrast images, those neurons were irregularly shaped with shrunken cell bodies and/or disrupted neurites, and in immunocytochemistry analyses they were shown to be positive for clived-caspase 3. The number of viable and nonviable neurons was counted in four to five field pictures and death rate was calculated.

For analysis of positive cells for different markers, 3-4 pictures were analyzed per donor and per marker; positive cells were counted and plotted as the percentage of positive cells. For quantifying the level of intensity within the positive cells, the integrated density was measured by defining the ROI as the cellular contour, manually using ImageJ. The Mean integrated density for each cell was plotted normalized to the highest value of the data set compared (Highest value set to 100%) to better illustrate the differences.

Data was further analyzed for statistics with Past3 [120] and/or GraphPad Prism 5 (GraphPad software, La Jolla, CA, http:// www.graphpad.com). Normality of the data sets was refuted after analysis using Kolmogorov-Smirnov and/or Shapiro-Wilk normality tests. Homogeneity of variance was tested using Levene's test and non-parametric Kruskal-Wallis test was used to compare the medians between the different data sets for the different donors (***$p \leq 0.001$). Bonferroni corrected post-test served to identify the significance of the differences between the groups, by comparing the population means (*$p \leq 0.05$, **$p \leq 0.01$; ***$p \leq 0.001$). Non-parametric Mann-Whitney test was used to compare two pair of groups (***$p \leq 0.001$). Further differences were studied using Tukey's test (*$p \leq 0.05$, **$p \leq 0.01$, ***$p \leq 0.001$).

2.14 Promoter analysis

Sequence of promoter regions (3000 bp downstream and 100 bp upstream the ATG) of genes of interest were taken from Eukaryotic Promoter Database (epd.vital-ti.ch) for *Homo sapiens*. Binding sites for gene of interest in chosen promoter sequence were looked up using JASPAR Tool (jaspar.genereg.net). A relative score threshold of 85% was used. *RELA, RELB* and *REL* binding sites were compared in the promoter regions of target genes of interest.

Sex-specific neuroprotective role of NF-κB-p65 in human stem cell-derived neurons

3

A version of this chapter has been published:

Ruiz-Perera, L. M., Schneider, L., Windmöller, B. A., Müller, J., Greiner, J.F.W., Kaltschmidt, C., Kaltschmidt, B. NF-κB p65 directs sex-specific neuroprotection in human neurons. Manuscript ID: SREP-18-25729A.

3.1 Results

3.1.1 Inferior turbinate stem cells efficiently differentiate into glutamatergic neurons in vitro

In order to gain an appropriate model system for studying the role of NF-κB in neuroprotection during maturation of human NCSC-derived neurons, ITSCs were cultivated following a directed neuronal differentiation procedure for 30 days (Fig. 3-1A) [1,40]. Exposure of ITSCs to a neuronal induction medium for 28 days resulted in a neuronal-like morphology indicated by retraction of the cytoplasm towards the nucleus, extended cellular processes resulting in neurite outgrowth (Fig. 3-1B-D). Immunocytochemical analyzes confirmed the presence of the mature neuronal markers Neurofilament 200 (Fig. 3-1E, H; 92,28% ± 1,45%), MAP-2 (92,28% ± 4,20%; Fig. 3-1F, H) and Synaptophysin (75,77% ± 11,55%; Fig. 3-1I, H). Interestingly, 19,77% ± 6,85% of ITSC-derived neurons were positive for Calretinin (Fig. 3-1G, H), while a small subpopulation of 13,70% ± 8,74% differentiated ITSCs expressed the glial marker (Olig-2 Fig. 3-1H). Further validating their successful differentiation, only 20,96% ± 0,63% of ITSCs showed co-expression of Nestin (Fig. 3-1J) after directed differentiation. Accordingly, RT-PCR analyses depicted a decrease in expression of Nestin as well as an increased expression of MAP-2 and Synaptophysin in NCSC-derived neurons (Fig. 3-1I). Characterizing these neurons in more detail, we observed a low expression of GABA and serotonin transporter, whereas the AMPA receptor subunit 1, NMDA receptor subunit 1, glutamate metabotropic receptor 1 (GRM1) as well as the vesicular glutamate transporter 1 (VGLUT1) were robustly expressed (Fig. 3-1K). Immunocytochemistry further confirmed the glutamatergic phenotype of ITSC-derived neurons by revealing vGlut2-expression on the protein level (Fig. 3-1L, M). In addition to their efficient neuronal differentiation in vitro, ITSCs were able to integrate and differentiate within a neural environment by transplanting undifferentiated stem cells into murine organotypic hippocampal slices[121].

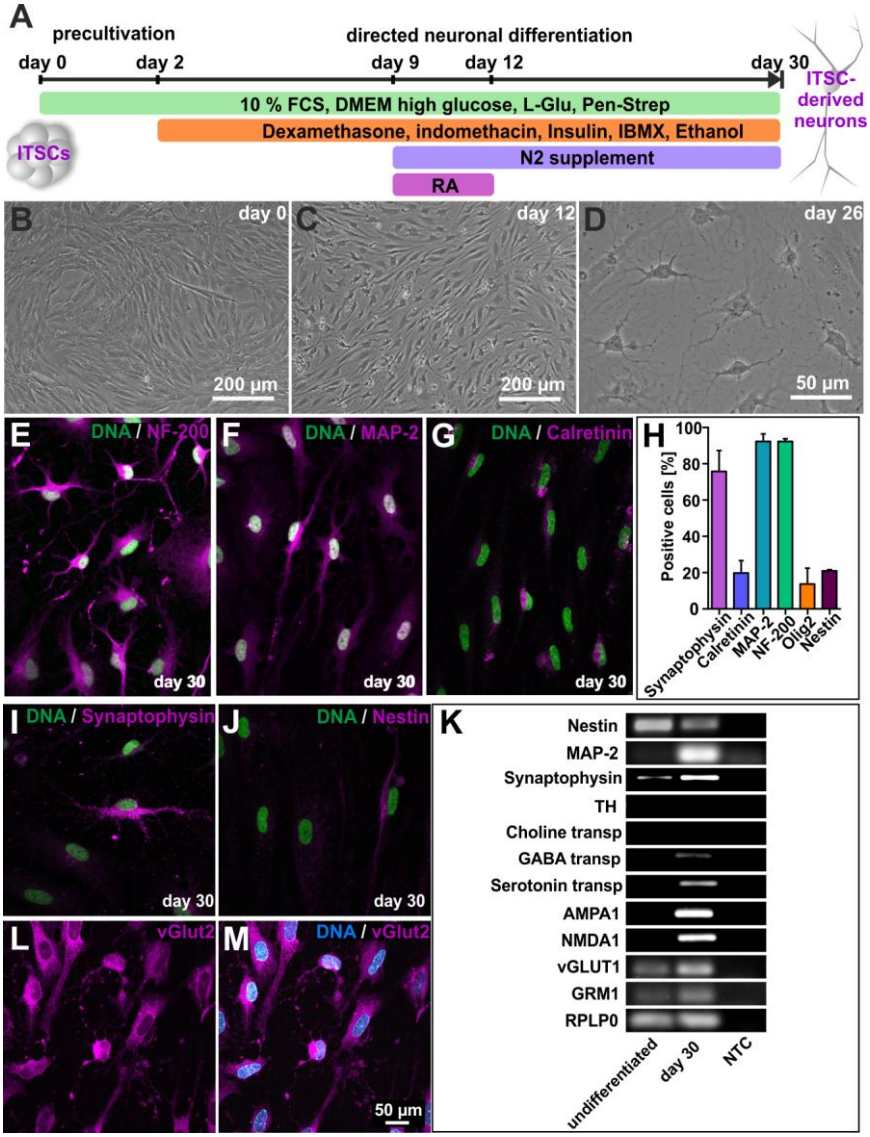

Figure 3-1. Adult human neural crest-derived stem cells from the inferior turbinate (ITSCs) are able to efficiently differentiate into glutamatergic neurons. A: Schematic view of the neuronal differentiation procedure. B-D: ITSCs changed their morphology towards a neuronal phenotype during directed neuronal differentiation. D-G: Immunocytochemistry of ITSCs after 30 days of differentiation depicting the presence of NF200. MAP-2, and calretinin positive. H: Quantification of immunocytochemical analyses showing the percentage of Synaptophysin$^+$ (75,77%±11,55%), Calretinin$^+$ (19,77%±6,85%), MAP-2$^+$ (92,28%±4,20%), NF-200$^+$ (92,28%±1,45%), Olig 2$^+$ (13,70%±8,74%) and Nestin$^+$ (13,70%±0,63%) ITSC-derived neurons after 30 days of differentiation (Mean ± SEM, n=3). I-J: Differentiated ITSCs were positive for Synaptophysin, while small population of cells remained Nestin-positive. K: RT-PCR of differentiated ITSCs showing the down-regulation of Nestin, the up-regulation of MAP-2, Synaptophysin, AMPA receptor subunit 1, NMDA Receptor subunit 1, vesicular glutamate transporter 1, and glutamate metabotropic receptor 1 after neuronal differentiation, and the low expression of GABA and serotonin transporter. RPLP0 served as housekeeping gene. NTC: non-template-control. L-M: Differentiated ITSCs positive for vGlut2, and merge with DNA staining.

3.1.2 ITSCs-derived glutamatergic neurons show AMPA or glutamate-dependent activation of NF-κB-p65

We next investigated the capability of ITSC-derived neurons to respond to the excitatory neurotransmitter glutamate (GLU) or its agonist α-amino-3-hydroxyl-5-methyl-4-isoxazole-propionate (AMPA). Stimulation with GLU or AMPA resulted in a significant increase in nuclear translocation of NF-κB-p65 in a dose-dependent manner (5 μM - 10 μM) in comparison to untreated neurons. On the contrary, treatment with 50 μM GLU or AMPA led to a significant decline in NF-κB-p65 nuclear translocation compared to 10 μM-treatment (Fig. 3-2A-D). We also observed high levels of basal NF-κB-activity (Fig. 3-2A-D), in accordance to the already described constitutive activation of NF-κB particularly in glutamatergic neurons [122]. Treatment of ITSC-derived neurons with their respective inhibitors 6-cyano-7-nitroquinoxaline-2,3-dione (CQNX) or dibenzocycloheptenеimine (MK-801) prior to application of GLU (10 μM) or AMPA (10 μM) resulted in a significantly reduced translocation of NF-κB-p65 into the nucleus compared to the stimulation approaches (Fig. 3-2E-F). These findings provide pharmacological evidence that both kinds of receptors were expressed in human ITSC-derived glutamatergic neurons, which in turn were observed to be fully functional after 30 days of differentiation.

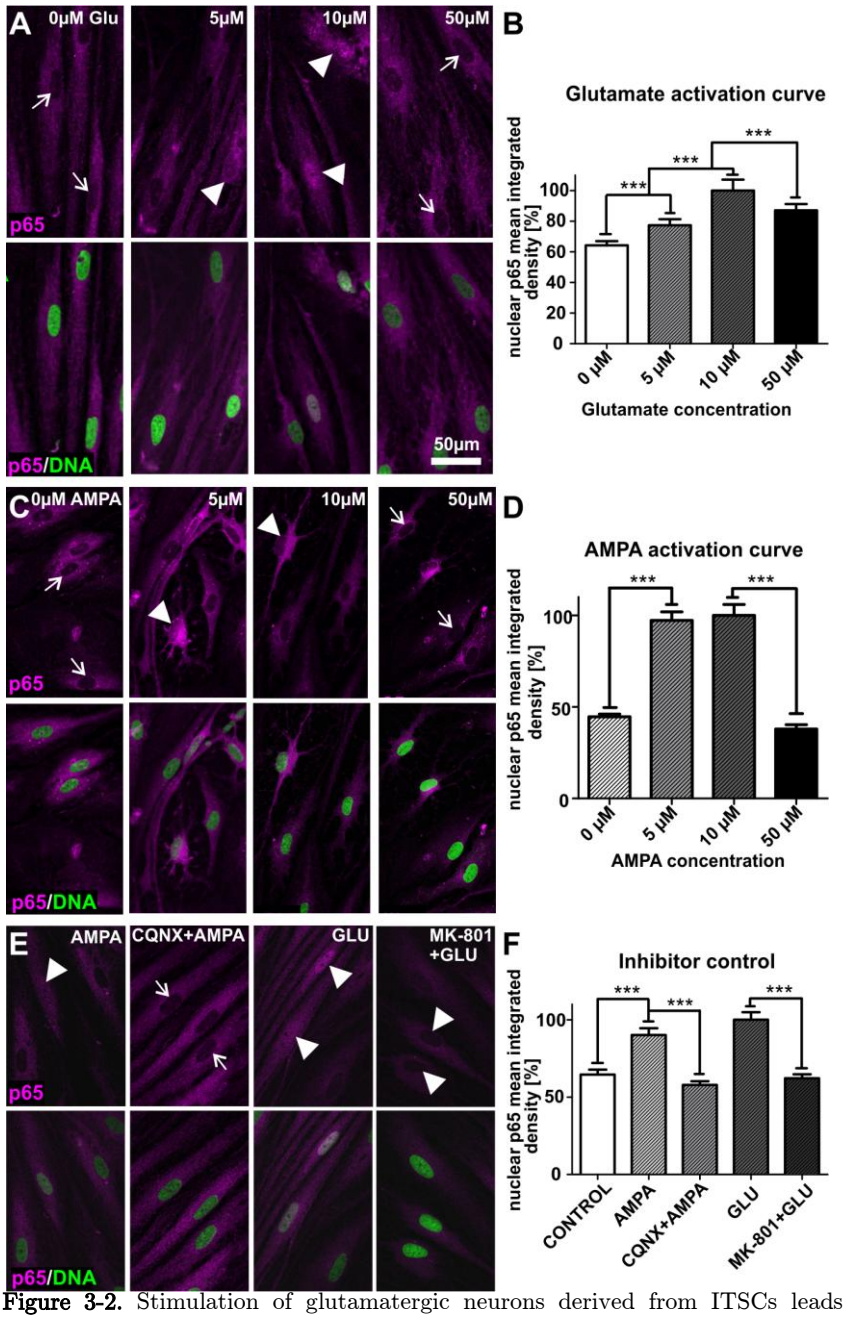

Figure 3-2. Stimulation of glutamatergic neurons derived from ITSCs leads to significantly increased nuclear translocation of NF-κB-p65. A-B: Immunocytochemistry and respective quantification of nuclear mean integrated density of NF-κB-p65 revealed significantly increased nuclear translocation of NF-κB-p65 in ITSC-derived neurons after glutamate (GLU)-dependent stimulation (arrowheads) compared to control (arrows). Mean values were normalized to the highest value. C-D: AMPA-dependent stimulation resulted in significantly increased nuclear translocation of NF-κB-p65 in ITSC-derived neurons (arrowheads) compared to control (arrows). Mean values were normalized to the highest value. E-F: Pre-treatment of ITSC-derived neurons with MK-801 or CQNX prior to GLU or AMPA-treatment led a significant decrease in nuclear translocation of NF-κB-p65 (arrows) compared to GLU or AMPA-dependent stimulation (arrowheads). Mean values were normalized to the highest value. Statistical analysis was performed using Graph Pad Prism 5. Normality of the data sets was refuted after analysis using Kolmogorov-Smirnov and Shapiro-Wilk normality tests. Non-parametric Mann-Whitney test was further used (***$p \leq 0.001$), error bars indicate the standard error of the mean (SEM).

3.1.3 Stimulation with TNF-α leads to significantly increased nuclear translocation of NF-κB-p65 in ITSC-derived glutamatergic neurons

After validating human NCSC-derived neurons as a model system for studying the role of NF-κB during maturation, we investigated the potential of TNF-α to stimulate NF-κB in these neurons. Stimulation of ITSC-derived neurons with TNF-α for 30 minutes or 1 hour resulted in nuclear translocation of NF-κB-p65 subunit (Fig. 3-3A, arrowheads) in comparison to untreated neurons or 24 h of TNF-α-treatment (Fig. 3-3A, arrows). Quantification of the NF-κB-p65 nuclear mean integrated density clearly validated these dynamics by showing a highly significant increase in nuclear NF-κB-p65 fluorescence after 30 minutes (93,96% ± 6,04%) and 1 hour (88,00% ± 12,00%) of TNF-α-treatment compared to untreated controls (≤20%) (Fig. 3-3B). Accordingly, stimulation of ITSC-derived neurons with TNF- α for 24 hours did not result in a significantly different nuclear NF-κB-p65 fluorescence intensity compared to control (Fig. 3-3B). Furthermore we analyzed the activation of the other two Rel members RelB and c-Rel and we clearly evidenced that TNF-α stimulation for 30 minutes activated nuclear c-Rel translocation in addition to p65, but not RelB, emphasizing their role in TNF-α stimulation.

3.1.4 TNF-α-pre-treatment of human ITSC-derived glutamatergic neurons leads to increased NF-κB-activity upon oxidative stress insult

We further analyzed the effect of H_2O_2-mediated oxidative stress insult on the activity of NF-κB-p65 in ITSC-derived neurons. Application of H_2O_2 for 25 h on human glutamatergic neurons differentiated for 30 days led to significantly increased nuclear translocation of NF-κB-p65 in comparison to control. In order to analyze a potential neuroprotective role of NF-κB, we

performed a pre-treatment using 10 ng/ml TNF-α during 2 hours prior to oxidative stress insult.

Notably, TNF-α-pre-treatment of ITSC-derived glutamatergic neurons followed by H_2O_2-mediated oxidative stress resulted in a significant increase in nuclear translocation of NF-κB-p65 compared to the H_2O_2 alone or control (Fig. 3-4A-B, arrowheads). We further applied pyrrolidine dithiocarbamate (PDTC) as a control for guided inhibition of NF-κB. Pre-treatment of the cultivated neurons with PDTC for 1 hour followed by application of TNF-α or sole PDTC-treatment did not result in changes of nuclear translocation of NF-κB-p65 (Fig. 3-4A-B, arrows). Quantification of the nuclear mean integrated density for p65 indicated a small but significant increase in nuclear NF-κB-p65 in both treatments compared to the untreated negative control (Fig. 3-4B).

3.1.5 ITSC-derived glutamatergic neurons are protected from oxidative stress-mediated cell death via TNF-α-dependent activation of NF-κB-p65

Determining the physiological consequences of TNF-α-dependent activation of NF-κB-p65 during oxidative stress, we analyzed the death rate of ITSC-derived neurons after treatment with H_2O_2 or H_2O_2 after TNF-α-pre-treatment. H_2O_2-mediated oxidative stress led to robust and significant apoptosis of glutamatergic neurons compared to untreated control (Fig. 3-4C). Notably, this H_2O_2-mediated increase in apoptosis was significantly reduced down to a level similar to control upon TNF-α-pre-treatment prior to the oxidative stress insult (Fig. 3-4C). Application of TNF-α alone did not affect the survival of ITSC-derived neurons nor did the PDTC treatment, or the PDTC treatment followed by TNF-α in comparison to control (Fig. 3-4C).

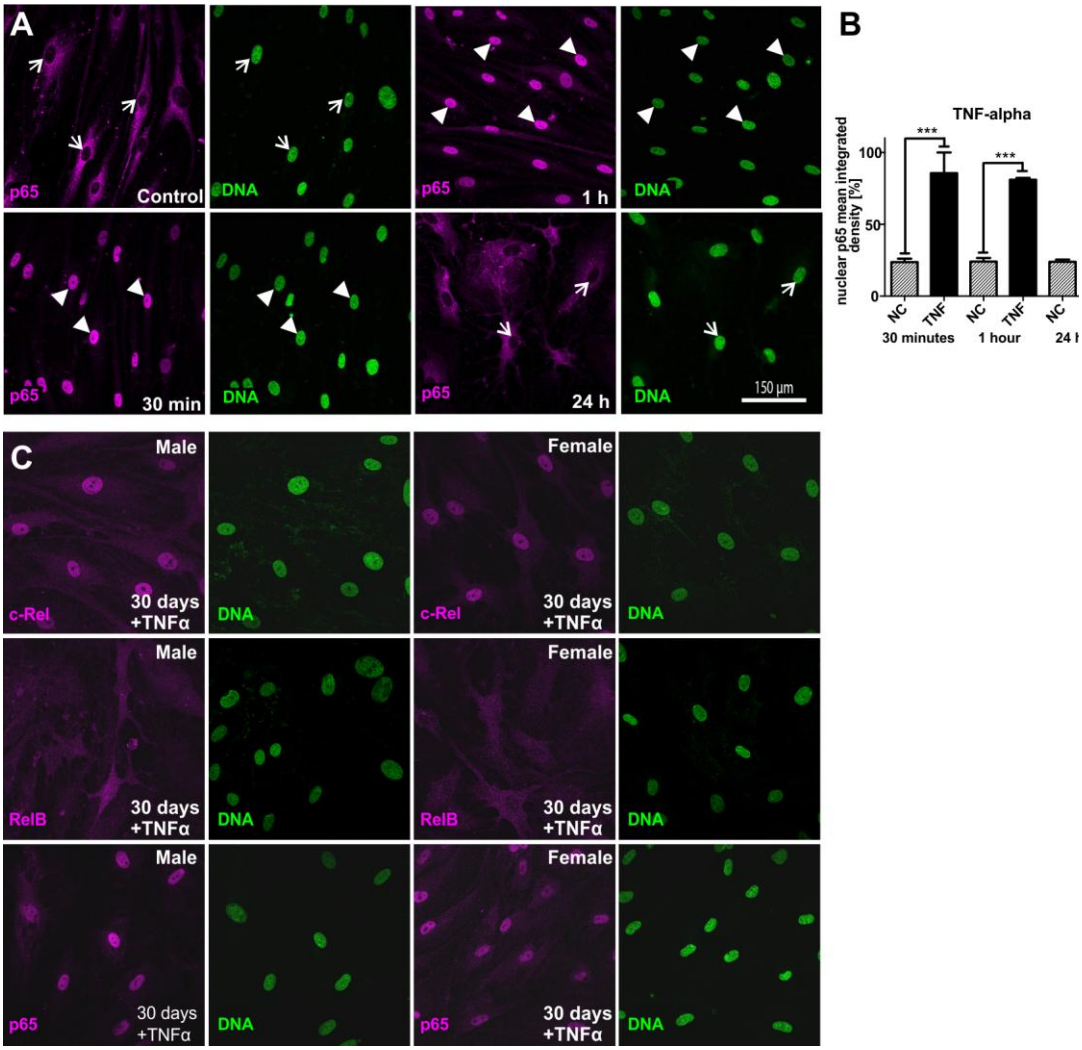

Figure 3-3. TNF-α-dependent stimulation of glutamatergic neurons derived from ITSCs leads to nuclear transloaction of NF-κB-p65. A: Immunocytochemistry of ITSC-derived neurons (30 days of differentiation) showed nuclear translocation of NF-κB-p65 after treatment with TNF-α for 30 min or 1 h (arrowheads), whereas control and 24 h-TNF-α-treatment did not result in nuclear translocation of NF-κB-p65 (arrows). B: Quantification of nuclear mean integrated density of NF-κB-p65 confirmed the significant increase in nuclear NF-κB-p65 after TNF-α-treatment of ITSC-derived neurons for 30 min or 1h compared to 24h and untreated control. Mean values were normalized to the highest value. Statistical analysis was performed using GraphPad Prism 5. Normality of the data sets was refuted after analysis using Kolmogorov-Smirnov and Shapiro-Wilk normality tests. Non-parametric Mann-Whitney test was further used. ***$p \leq 0.001$, error bars indicate the standard error of the mean (SEM). C: Immunocytochemistry of ITSC-derived neurons (30 days of differentiation) showing nuclear translocation of NF-κB-p65 and c-Rel after treatment with TNF-α for 30 minutes, but no nuclear translocation of NF-κB-RelB, for a male and a female donor, and DNA staining.

3.1.6 Sensitivity of glutamatergic neurons to ROS-mediated cell death and neuroprotection via NF-κB-p65 is dependent on the sex of the ITSC-donor

Investigating the effects of TNF-α-treatment on H_2O_2-mediated death of ITSC-derived neurons in more detail, we analyzed the amount of apoptotic cells after oxidative stress and TNF-α-dependent neuroprotection in dependence to the sex of the ITSC-donor. We observed a significant increase in cell death of neurons differentiated from female ITSC-donors compared to their male counterparts, indicating an elevated sensitivity of human female glutamatergic neurons to oxidative stress (Fig. 3-4D). Pre-treatment of ITSC-derived neurons from female donors with TNF-α led to a significant and complete neuroprotection against H_2O_2-mediated cell death. Although neurons from male ITSC-donors were likewise protected against cell death via exposure to TNF-α, we observed a 2-fold increase in TNF-α-dependent neuroprotection in female ITSCs-derived neurons compared to those differentiated from male ITSCs. These findings not only demonstrate a NF-κB-dependent neuroprotection of ITSC-derived neurons against oxidative stress-mediated cell death, but emphazise the dependence on its sensitivity to the sex of the ITSC-donor.

3.1.7 TNF-α-mediated neuroprotection of ITSC-derived neurons is accompanied by sex-specific expression of NF-κB target genes

To investigate the role NF-κB-p65 in protection of ITSC-derived neurons from H_2O_2-mediated death in more detail, expression of NF-κB target genes was assessed by qPCR. Treatment of ITSC-derived neurons with H_2O_2 or TNF-α followed by H_2O_2 led to significantly increased expression levels of cAMP-dependent protein kinase catalytic subunit alpha (PKAcatα) compared to control. We further observed a significant increase in PKAcatα expression levels in male ITSCs-derived neurons compared to those differentiated from female ITSCs after TNF-α/H_2O_2-treatment (Fig. 3-5A). On the contrary, we observed a significant increase in manganese superoxide dismutase (Mn-SOD, SOD2) mRNA levels only in female

ITSCs-derived neurons upon exposure to TNF-α, H_2O_2 and TNF-α/H_2O_2 compared to control (Fig. 3-5B). Expression levels of cellular inhibitor of apoptosis protein-1 and 2 (c-IAP1 and c-IAP2) showed the tendency to be elevated in male ITSCs-derived neurons after TNF-α/H_2O_2-treatment compared to their female counterparts (Fig. 3-5C, D). Treatment with TNF-α, H_2O_2 and TNF-α/H_2O_2 further resulted in significantly increased expression levels of insulin-like growth factor 1 (IGF1) in ITSCs-derived neurons compared to control, although no significant sex-dependent differences were observable. Female ITSCs-derived neurons showed significantly increased expression levels of IGF2 after H_2O_2 and TNF-α/H_2O_2-treatment compared to control, while no expression was detectable in male counterparts. However, sole treatment with TNF-α resulted in significantly increased expression levels of IGF2 in neurons from male and female donors compared to control. These findings strongly suggest a sex-specific NF-κB-p65 target gene expression in dependence to TNF-α-mediated neuroprotection during oxidative stress.

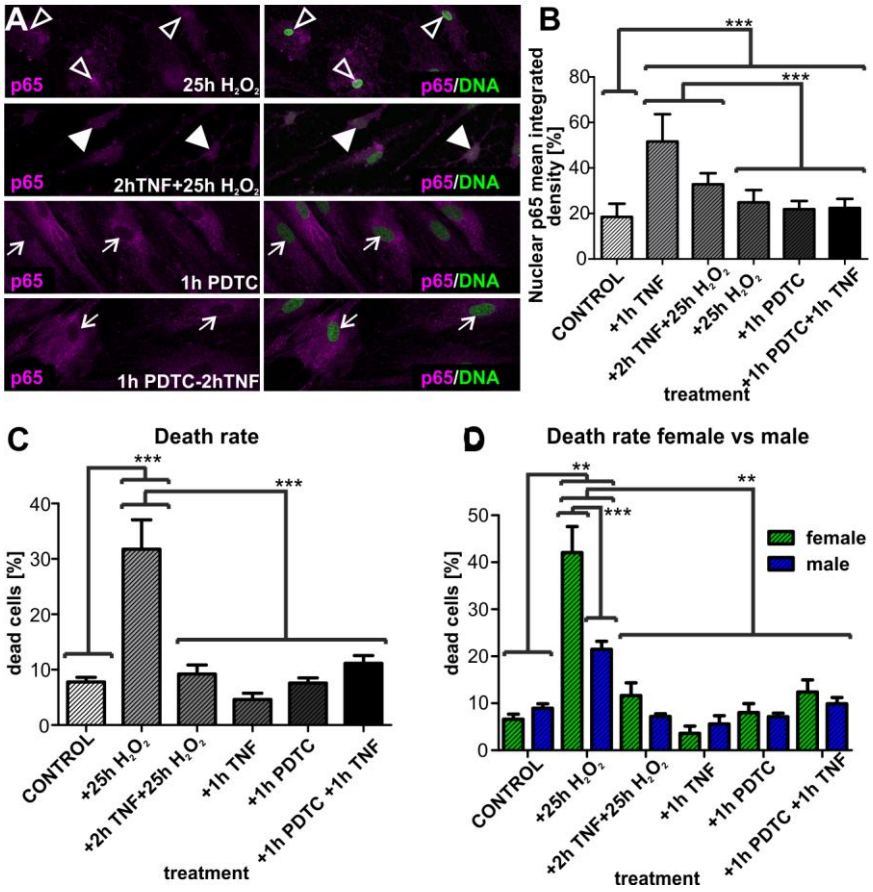

Figure 3-4. Treatment ITSC-derived glutamatergic neurons with TNFα prevents from oxidative stress-mediated cell death in a sex-dependent manner. A: Immunocytochemistry of ITSCs-derived neurons after 30 days of differentiation, after treatment with H_2O_2 alone, TNF-α-pretreatment prior to H_2O_2 and PDTC alone and PDTC followed by TNF-α against NF-κB-p65 B: Quantification of immunocytochemical assays showed significantly increased nuclear translocation of NF-κB-p65 after treatment with TNF-α alone and TNF-α prior to H_2O_2 compared to H_2O_2 alone and untreated control. Pretreatment of ITSC-derived neurons with PDTC for one hour followed by TNF-α-treatment did not result in significantly different amounts of nuclear NF-κB-p65 compared to PDTC alone. Mean values were normalized to the highest value. C: Quantification of neuronal cell death showed significant death after oxidative stress insult (H_2O_2) compared to TNF-α/ H_2O_2, TNF-α, PDTC, PDTC/ TNF-α and untreated control (n=6). D: Quantification of neuronal cell death after oxidative stress (H_2O_2), TNF-α-pretreatment TNF-α, PDTC, PDTC/ TNF-α and untreated control comparing sex differences (n=3 males, n=3 females). Data were showed not to be normally distributed using Kolmogorov-Smirnov and Shapiro-Wilk normality tests. Non-parametric Kruskal-Wallis test was further used ($p \leq 0.001$), and Tukey's post-hoc test (**$p \leq 0.01$, ***$p \leq 0.001$). Mean ± SEM (standard error of the mean).

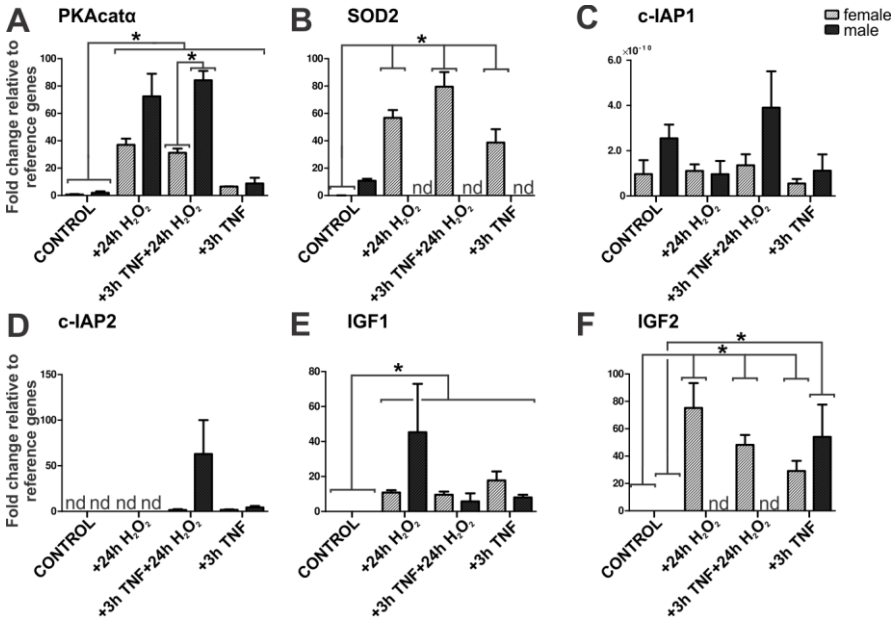

Figure 3-5. Quantitative polymerase chain reaction revealed sex-specific NF-κB-p65 target gene expression after TNFα-dependent neuroprotection upon oxidative stress-insult. A: QPCR analysis revealed increased PKAcatα mRNA levels after H_2O_2 alone, TNF-α-pretreatment prior to H_2O_2 and TNF-α alone compared to untreated control, with a stronger effect for TNFα/H_2O_2 in male compared to female ITSCs-derived neurons. B: SOD2 mRNA levels significantly increased in female ITSCs-derived neurons compared to control and compared to their male counterparts. C: qPCR analysis showing c-IAP1 mRNA levels in male and female ITSCs-derived neurons. D: qPCR analysis showing c-IAP2 mRNA levels in male and female ITSCs-derived neurons. E: qPCR analysis showing significant increased IGF1 mRNA levels compared to control in male and female ITSCs-derived neurons. F: IGF2 mRNA levels were significantly elevated only in female-derived neurons compared to control. Non-parametric Mann Whitney test (*p≤0.05), mean ffi SEM (standard error of the mean). Nd: Not detectable. G: Promotor analysis using the JASPAR Tool (jaspar.genereg.net) validated SOD2, PRKACA and IGF2 to be direct RELA, RELB and REL target genes. RELA binding sites are shown in red, RELB binding sites in green, and REL binding sites in brown. Common RELA and REL binding sites are shown in blue. One promoter is shown for each gene, for more detail see supplementary material.

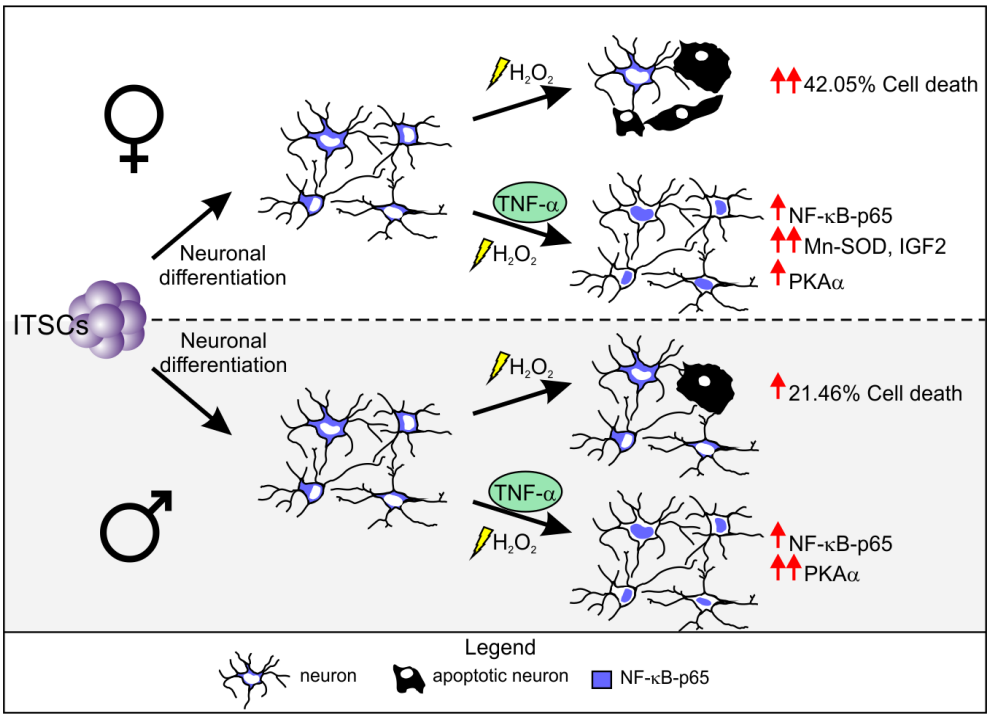

Figure 3-6. Sex-specific response to oxidative stress insult and NF-κB-mediated neuroprotection in human NCSC-derived neurons. Female ITSCs-derived neurons responded with a higher sensitivity to oxidative stress-induced neuronal death, and TNF-α-mediated neuroprotection compared to their male counterparts. TNF-α-mediated neuroprotection led to an increase in NF-κB-p65 nuclear translocation, triggering differential expression of sex-specific NF-κB target genes.

3.2 Discussion

The present study describes for the first time a neuroprotective role of NF-κB-p65 in human NCSC-derived glutamatergic neurons after oxidative stress insult.

We successfully differentiated human neural crest-derived inferior turbinate stem cells into MAP-2$^+$/NF200$^+$/Synaptophysin$^+$/vGlut2$^+$-glutamatergic neurons by application of a directed differentiation assay or via transplantation into organotypic mouse hippocampal slice cultures[121]. Extending our previous findings depicting vesicle recycling and calcium spiking of ITSC-derived neurons[40], we validated their functionality by showing an increased NF-κB-activity upon stimulation with the excitatory neurotransmitter glutamate or its agonist AMPA. Accordingly, ITSC-derived neurons showed expression of NMDA1- and AMPA1-receptors, which were shown to require an appropriate neuronal differentiation in neural stem cells[123]. Inhibitor controls using CQNX and MK-801 led to a decrease in glutamate or AMPA-dependent stimulation of NF-κB-activity, further validating the specificity of the respective receptors. In accordance to our findings, stimulation of ionotropic glutamate receptors was shown to activate NF-κB in primary rat cerebellar granule neurons[100-101]. Given the pivotal role of NF-κB signalling in key elements for neuronal morphology like neurite growth[83], dendritic spine formation[84], axonal outgrowth[85] and synaptic plasticity[87-88,102], our data suggest the participation of NF-κB in the normal physiology of the human nervous system.

In addition to its AMPA- and glutamate-dependent stimulation, we also observed a significant increase in NF-κB-activity in ITSC-derived neurons after treatment with TNF-α. In canonical NF-κB-signalling, recognition of stimuli like cytokines or neurotransmitters leads to phosphorylation of IκB kinases[124-125], in turn resulting in phosphorylation, polyubiquitylation and 26S-proteasome-mediated degradation of IκBs. Demasking of the nuclear translocation signal region of p50/p65 by degradation of IκBs is subsequently followed by translocation of p50/p65 into the nucleus and activation of target gene expression by binding to κB elements[88-90,126-127].

TNF-α is one of the best characterized cytokines inducing this pathway, and its receptors TNFR1 and TNFR2 are widely expressed in the nervous system both in neurons and glia [128-130]. Besides its modulatory effects of neuronal responses to excitotoxic and hypoxic insults in the nervous system[131], the absence of TNFR was shown to result in an increased neuronal damage following either ischemic or kainic acid induced excitotoxic damage[132]. In mouse NSCs, TNF-α-mediated NF-κB signalling was reported to be required for initial neuronal differentiation[113]. Extending these findings, ITSC-derived human glutamatergic neurons revealed a significantly increased nuclear translocation of NF-κB-p65, indicating the crucial role of NF-κB-signalling during stem cell-based neuronal differentiation. We further demonstrated, in the present study that TNF-α stimulation for 30 minutes activated not only NF-κB-p65, but also NF-κB-c-Rel nuclear translocation, emphasizing their role in TNF-α stimulation in neuronal glutamatergic physiology.

Being a major cause of several neurologic diseases and brain damage[104], oxidative stress is known to be directly caused by Alzheimer's disease via amyloid A beta peptide-dependent production of hydrogen peroxide through metal ion reduction[133-134]. In Parkinson's disease, free radicals accumulate in the *substantia nigra pars compacta*, resulting in the formation of 6-hydroxydopamine, in turn leading to the generation of superoxide[135-136]. In the present study, H_2O_2-mediated oxidative stress led to cell death of human NCSC-derived glutamatergic neurons. Although NF-κB is known to be activated by oxidative stress in the nervous system[104], several studies indicated its neuroprotective role in murine cells. Here, Heck and colleagues demonstrated an Insulin-like growth factor-1-mediated neuroprotection of rat primary cerebellar neurons against oxidative stress directly associated to activation of NF-κB[137]. Erythropoietin-mediated neuroprotection of rat cerebrocortical cultures from oxidative stress was also shown to occur in an NF-κB-dependent manner[138]. On the contrary, Zou and colleagues demonstrated TNF-α-treatment of rat hippocampal-entorhinal cortex slice cultures to result in increased neurotoxicity to both glutamate and oxidative stress[139]. In the present study, TNF-α-pre-

treatment led to a significant decrease in H_2O_2-mediated cell death of NCSC-derived human neurons accompanied by a significantly increased nuclear translocation of NF-κB-p65. Our data therefore demonstrate a key role of NF-κB-p65 in protection of human stem cell-derived neurons from oxidative stress, further emphasizing the importance of NF-κB-signalling in neuroprotection[104,137-138].

Interestingly, we further observed a significantly elevated sensitivity of ITSCs-derived neurons from female donors to oxidative stress-induced cell death and to NF-κB-dependent neuroprotection compared to neurons from male donors. These findings were substantiated by a differential expression of NF-κB target genes in a sex-dependent manner. Here, increased Mn-SOD mRNA levels observed in female but not in male ITSCs-derived neurons indicated a NF-κB-dependent induction of Mn-SOD protecting against oxidative stress-induced neuronal apoptosis. Accordingly, Mn-SOD expression was described to be inducible by TNF-α, having an anti-apoptotic role by directly reducing cellular ROS levels[140]. Next to -Mn-SOD, expression levels of IGF2 were significantly elevated only in female neurons after TNF-α/H_2O_2-treatment compared to control. IGF2 is known to promote synapse formation and spine maturation in the mouse brain[141]. Within a mouse model of Alzheimer's disease, IGF2 administration rescued spine formation and synaptic transmission in the hippocampus[142]. In accordance to the present findings, IGF2 was reported to have an antioxidant and neuroprotective effect on oxidative damage and mitochondrial function in cultured adult rat cortical neurons[143-144]. In contrast to their female counterparts, male ITSCs-derived neurons showed a significant increase in the expression level of PKAcatα after TNF-α/H_2O_2-treatment. Interestingly, we observed no significantly altered expression levels of the antiapoptotic proteins c-IAP1 and c-IAP2, known mediators of TNF-α-dependent neuroprotection[145]. With PKAcatα being an essential regulator in learning and memory by transducing synaptic responses through CREB signaling[102,146] and controlling synaptic incorporation of AMPA receptors[147], PKA-activity may directly contribute to the neuroprotective effects observed here. Although being a matter of debate,

sex-dependencies in stem cell biology have already been shown in terms of autosomal gene expression[148] and proliferation[149], particularly regarding mouse NSCs[150-151]. Compared to their male counterparts, female muscle-derived stem cells were reported to have higher muscle regeneration efficiency in mice[152]. In terms of neuroinflammation and neuroprotection, sex-dependent differences between patients have been likewise reported in ischemic stroke[94], PD[92], or AD[93]. While female AD patients were described to have an increased risk of developing AD[93,96], PD was shown to have a greater prevalence in male patients[92]. In line with these findings, our data indicate for the first time a direct sex-dependent difference in neuroprotection of human stem cell-derived neurons against oxidative stress mediated by NF-κB-signalling.

In summary, the present study reveals NF-κB-p65 as a key player in neuroprotection of NCSC-derived neurons against oxidative stress in a sex-dependent manner. We demonstrate a sex-dependent difference of stress response and TNF-α-mediated neuroprotection, with a strong increase of both H_2O_2-mediated cell death as well as neuroprotection against cell death in female NCSC-derived neurons (Fig. 3-6). These differences were emphasized by the sex-specific differential expression of NF-κB-p65 target genes SOD2 and IGF2. In line with our findings, increasing evidences pointing towards sex-specific differences in risk and severity of neurodegenerative diseases, such as Alzheimer's disease. Since oxidative stress is directly associated to neurodegenerative diseases, but little is known about the underlying molecular mechanisms of neuroprotection, NF-κB-signalling may be a crucial parameter for treatment strategies and NCSC-based neuronal regeneration *in vivo*.

Role of NF-κB subunits in the glutamatergic differentiation of adult human stem cells

4

A version of this chapter is in preparation to be published:

Ruiz-Perera, L. M., Greiner, J.F.W., Kaltschmidt, C., Kaltschmidt, B. in prep. Role of NF-κB subunits in the glutamatergic differentiation of adult human stem cells.

4.1 Results

4.1.1 NF-κB subunit distribution in early stages of glutamatergic differentiation of ITSCs

In order to elucidate the possible role of NF-κB during glutamatergic differentiation, we first evaluated the NF-κB subunit composition during early stages of differentiation. For this, ITSCs were cultivated following a directed neuronal differentiation protocol (Fig. 4-1A), samples were taken at different time points (0, 1, 2, 5, 9.5, and 10 days of differentiation) and were analyzed by immunocytochemistry. Furthermore, as the NF-κB family is composed by five subunits, and among them three contain a transactivation domain (Fig. 4-1B) allowing DNA binding and gene expression, we focused specially on these to determine the predominating subunits involved within this process (Fig. 4-1C).

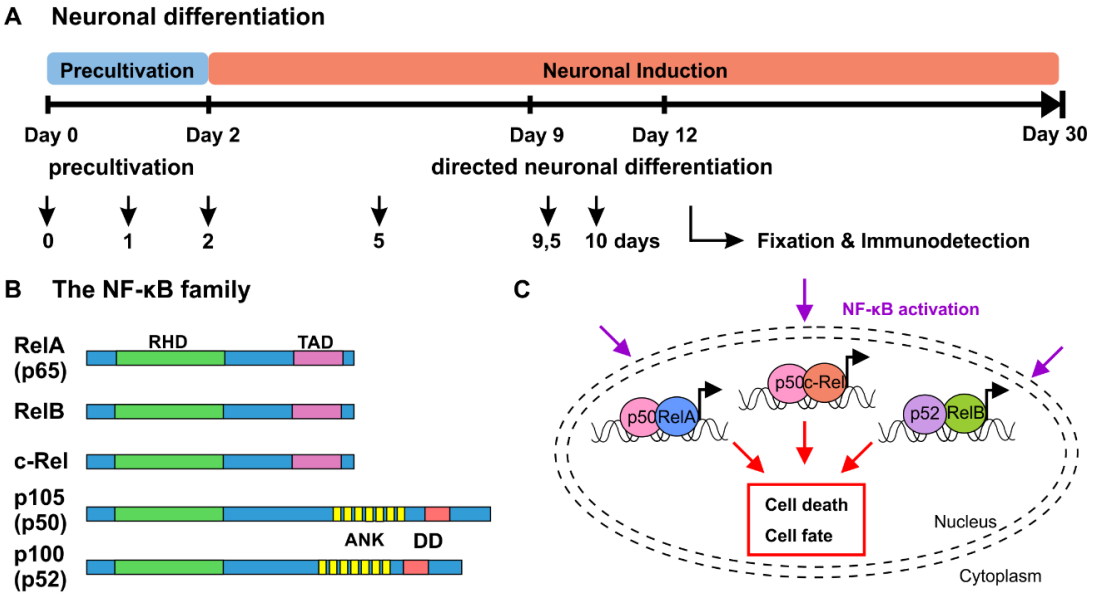

Figure 4-1. Diagrams showing glutamatergic differentiation protocol and NF-κB family members and their potential effects. A: Schematic representation of neuronal differentiation of ITSCs. Adult human inferior turbinate stem cells were differentiated into glutamatergic neurons as previously described[1] and samples were taken at different time points to analyze the NF-κB subunit composition during early differentiation. B: Schematic view of the NF-κB family members. Relevant domains are indicated and alternative nomenclatures are provided in parenthesis. RHD, rel homology domain; TAD, transactivation domain; ANK, ankirin repeats; DD, death domain. C) Schema showing The NF-κB activation triggered during differentiation allowing nuclear translocation of a predominant NF-κB dimmer or a particular combination of NF-κB dimmers which would induce the gene expression program of a distinct cell fate or otherwise it could result in cell death.

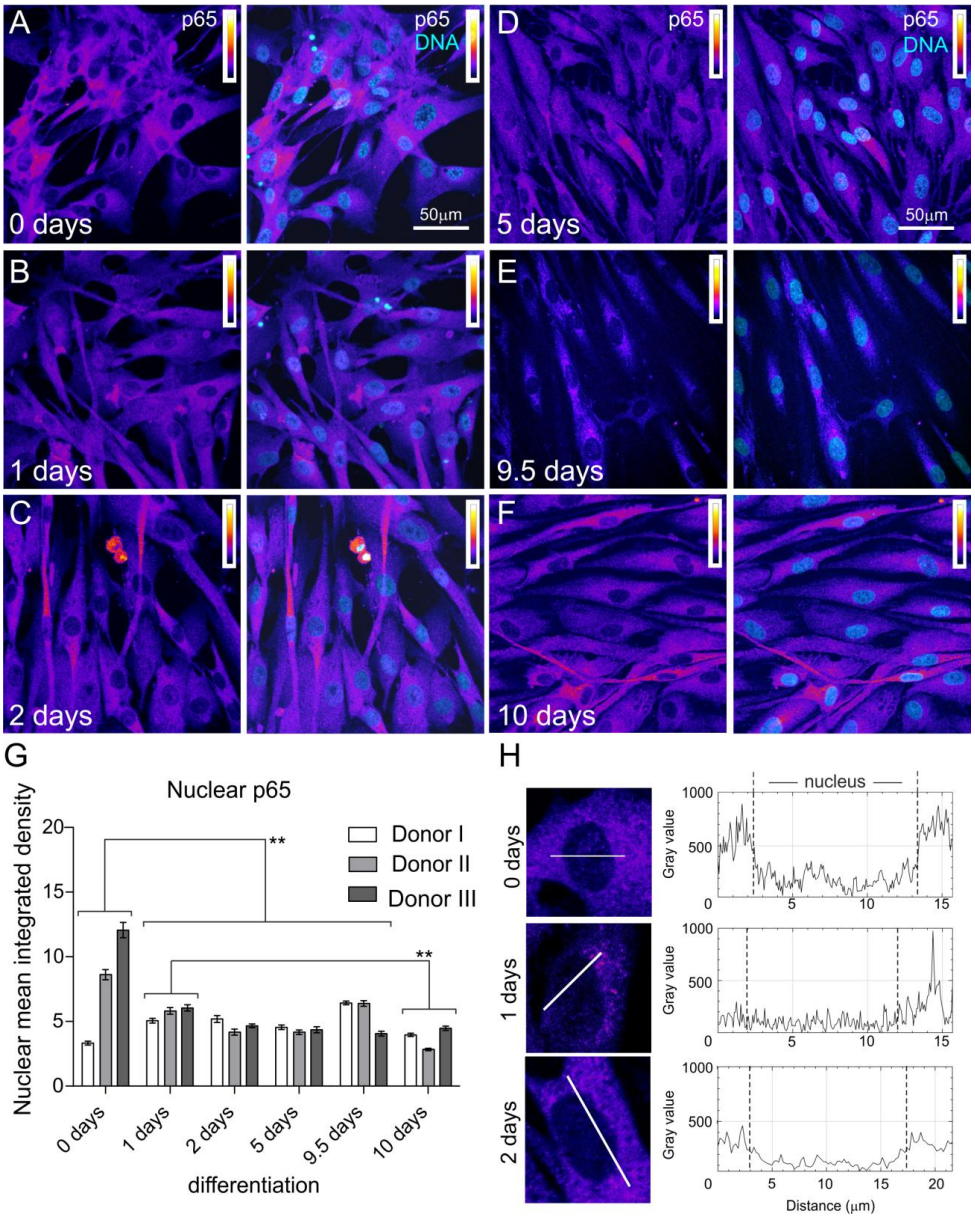

Figure 4-2. Immunocytochemical analysis of NF-κB-p65 (RelA). A-F: ITSCs labeled against RelA after 0, 1, 2, 5, 9.5 and 10 days of glutamatergic differentiation respectively. Each panel shows RelA protein on the left-side and co-localization with DNA staining on the right-side. Intensity scale indicates white as highest intensity level and black as lowest intensity level. G: Quantification of immunocytochemical analyses showing nuclear mean integrated density of RelA/p65 during early differentiation (n=3, mean ± standard error of the mean (SEM)). Normality of the data was refuted using Shapiro-Wilk normality test. Non-parametric Kruskal-Wallis (***p≤0.001) and Bonferroni corrected post-test (**p≤0.01) revealed a significant nuclear translocation of NF-κB-p65 at day 0. H: Fluorescence intensity profiles measured at three different time points (0, 1, 2 days of differentiation), for different cells following transects as shown, to clearly reveal the difference between the nuclear and cytoplasmic fluorescence.

4.1.2 RelA distribution during early glutamatergic differentiation

Immunocytochemistry against NF-κB-p65 (RelA), revealed a strong marked cytoplasmic signal and a faint p65 nuclear level during early differentiation (Fig. 4-2A-C). Little variation was observed on the intensity range for the later time points (Fig. 4-2D-F). Due to the slight nuclear activation observed, we quantified nuclear fluorescence using the nuclear mean integrated density (Fig. 4-2G). Statistical analysis clearly demonstrated significant differences for nuclear RelA between day 0 and all later time points (Non parametric Kruskal-Wallis test, ***$p \leq 0.001$, n=3), which might be due to the role of p65 in cell attachment; and also between day 1 and day 10 (Bonferroni corrected post-test, **$p \leq 0.01$, n=3). These differences were further analyzed with the fluorescence intensity profile, to discriminate fluctuations in p65 subcellular localization comparing cells during early differentiation (at 0, 1, and 2 days, Fig. 4-2H). No changes on nuclear fluorescence intensity were determined, but cytoplasmic level was clearly higher than nuclear level, indicating that RelA might have a role during cell attachment at day 0, but little or no role during early differentiation.

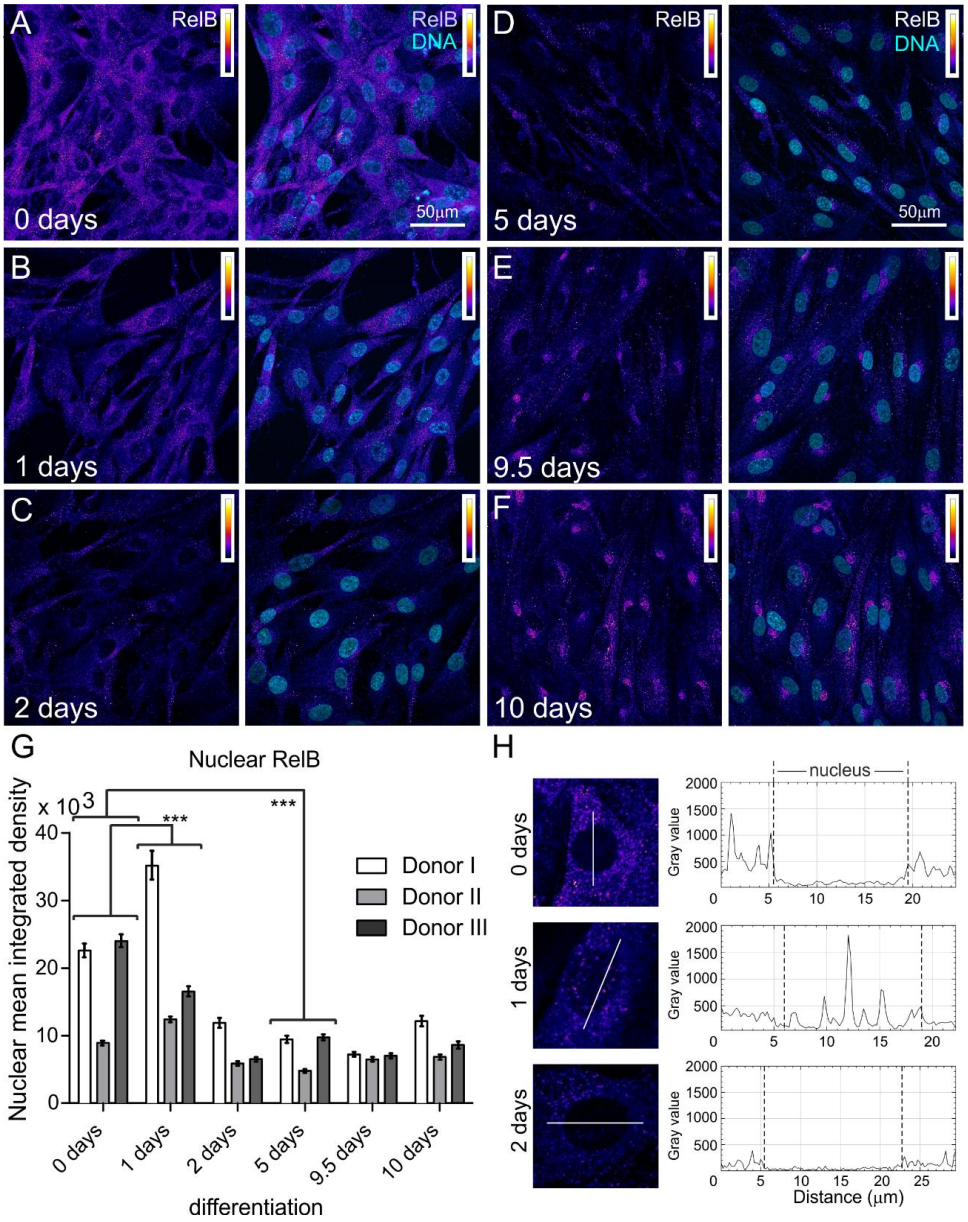

Figure 4-3. Immunocytochemical analysis of RelB. A-F: ITSCs labeled against RelB after 0, 1, 2, 5, 9.5 and 10 days of glutamatergic differentiation respectively. Each panel shows RelB protein on the left-side and co-localization with DNA staining on the right-side. Intensity scale indicates white as highest intensity level and black as lowest intensity level. G: Quantification of immunocytochemical analyses showing nuclear mean integrated density of RelB during early differentiation (n=3, mean ± SEM). Normality of the data was refuted using Shapiro-Wilk normality test. Non-parametric Kruskal-Wallis (***$p \leq 0.001$) and Bonferroni corrected post-test (***$p \leq 0.001$) revealed a significant peak in nuclear translocation of NF-κB-RelB at day 0. H: Fluorescence intensity profiles measured at three different time points (0, 1 and 2 days of differentiation), for different cells following transects as shown, to clearly reveal the difference between the nuclear and cytoplasmic fluorescence.

4.1.3 RelB distribution during early glutamatergic differentiation

Immunostaining analyses also confirmed that RelB had a gradual decrease during early stages of differentiation (Fig. 4-3A-F). ITSCs were strongly positive at day 0, with a robustly labeled cytoplasm; however nuclear RelB was not evident (Fig. 4-3A). At day 1 a slight increase in nuclear RelB was observed (Fig. 4-3B), which was remarkably reduced in the later time points (Fig. 4-3C-F). In these, cytoplasmic RelB was also reduced and gradually concentrated in the perinuclear region (Fig. 4-3F). To detect nuclear intensity changes we quantified nuclear mean integrated density (Fig. 4-3G). Statistical analysis demonstrated significant differences between day 0 and day 1 (Non parametric Kruskal-Wallis test, ***$p \leq 0.001$, n=3), and also between day 0 and day 5 (Bonferroni corrected post-test, ***$p \leq 0.001$, n=3), indicating there was a short NF-κB-RelB activation peak between days 0 and 1. These differences are further illustrated with the fluorescence intensity profile (Fig. 4-3H). In these cells we directly distinguish the intensity fluctuations between nucleus and cytoplasm. At day 0, fluorescence intensity was especially high in the cytoplasm, and was completely negative in the nucleus; while at day 1 we observe exactly the opposite, cytoplasmic intensity was markedly reduced and nuclear RelB was increased. Finally, after 2 days, both cytoplasmic and nuclear fluorescence intensity levels were totally reduced. These findings suggested that RelB has a short function during early glutamatergic differentiation, being strongly inactivated afterwards and sequestered in the perinuclear region.

4.1.4 c-Rel distribution during early glutamatergic differentiation

We further analyzed NF-κB-c-Rel by immunocytochemistry, which determined a low c-Rel level at nuclear and cytoplasmic localization during early time points (Fig. 4-4A-B), and at day 2 experienced a strong increase especially at the nuclear level (Fig. 4-4C), which was maintained after 5 days showing a clear nuclear activation (Fig. 4-4D). This strong c-Rel activation peak was remarkably reduced at later time points at nuclear and cytoplasmic level (Fig. 4-4E-F). Quantification of nuclear mean integrated

density for c-Rel confirmed this nuclear activation, which was statistically relevant (non parametric Kruskal-Wallis test ***p≤0.001, n=3, Fig. 4-4G) indicating that NF-κB-c-Rel activation peak occurred at day 2 (Bonferroni corrected post-test, ***p≤0.001, n=3). Furthermore, the differences in c-Rel expression were illustrated by measuring the fluorescence intensity profile of different cells at the relevant time points (Fig. 4-4H) where the fluorescence fluctuations are particularly apparent. At day 1, fluorescence intensity is extremely low at both cytoplasmic and nuclear level, while at day 2, nuclear and cytoplasmic c-Rel is strongly increased, and finally at day 5, total c-Rel was decreased and concentrated at the nuclear level. These results strongly support the existence of a nuclear c-Rel peak during early differentiation, suggesting that NF-κB-c-Rel might have a predominant role in the neuronal differentiation towards a glutamatergic fate.

4.1.5 p50 and p52 distribution during early glutamatergic differentiation

Similarly, immunostaining analysis of p50 (Fig. 4-5A-F) and p52 (Fig. 4-6A-F), established that p50 had no particular role during early differentiation due to its very little variation, while p52 might have an important role due to a strong nuclear activation at day 1. ITSCs were p50 positive during early time points, however the intensity range was strongly reduced from blue to black (Fig. 4-5C, E-F) and even if quantified differences were significant (Non parametric Kruskal-Wallis test ***p≤0.001; Bonferroni corrected post-test *p≤0.05, n=3; Fig. 4-5G), it was not possible to determine a direct correlation between these and the intensity range, as well as with the differences illustrated by fluorescence intensity profile analyzed (Fig. 4-5H), thus discarding a possible role for p50 during this differentiation. In contrast, p52 showed a robust increase in nuclear translocation after 1 day of differentiation, which was markedly reduced at day 2 (Fig. 4-6A-C), and was dramatically reduced in later time points (Fig. 4-6D-F). Quantification of nuclear mean integrated density and statistical analysis revealed a relevant significant difference between nuclear p52 peak at day 1 and all later time points (Kruskal-Wallis ***p≤0.001, Bonferroni corrected post-hoc ***p≤0.001), suggesting the importance of

p52 during early glutamatergic differentiation. This observation is further illustrated by the fluorescence intensity profile of three cells (Fig. 4-6H). Intensity fluctuations showed a key increase in nuclear p52, while cytoplasmic increase was not so remarkable. These findings further support that NF-κB-p52 subunit might have a central role during neuronal glutamatergic differentiation of ITSCs, suggesting the existence of p52/RelB heterodimers.

4.1.6 IκBα distribution during early glutamatergic differentiation

Furthermore analysis of IκBα, a negative regulator of NF-κB subunits, showed a similar distribution pattern to NF-κB-c-Rel. Cells were negative for IκBα at day 0 but protein levels were raised at day 1 (Fig. 4-7A, B), continuing to increase at day 2 especially within the nucleus (Fig. 4-7C). At day 5 nuclear IκBα was really concentrated (Fig. 4-7D), and was strongly decreased at later stages (Fig. 4-7E, F). Quantification and statistical analysis for IκBα, confirmed a strong significant increase of nuclear mean integrated density at 2 and 5 days (non parametric Kruskal-Wallis test, ***$p \leq 0.001$, n=3), compared to earlier and later time points (Bonferroni corrected post-test, ***$p \leq 0.001$, n=3). Also a significant increase at day 2 compared to day 5 was determined (Bonferroni corrected post-test, ***$p \leq 0.001$, n=3), which demonstrated IκBα peak at day 2. IκBα differences were further exemplified for three cells at few patent time points to see the evident changes in fluorescence intensity (Fig. 4-7H). At day 2, intensity was extremely high at both cytoplasmic and nuclear level, while at day 5, it was kept strictly circumvented to the nucleus; lastly at day 9.5 the intensity was completely decreased. These findings confirmed IκBα distribution resembled that of NF-κB-c-Rel, having a strong peak at day 2 which was gradually decreased, suggesting a strong regulatory mechanism modulated by IκBα.

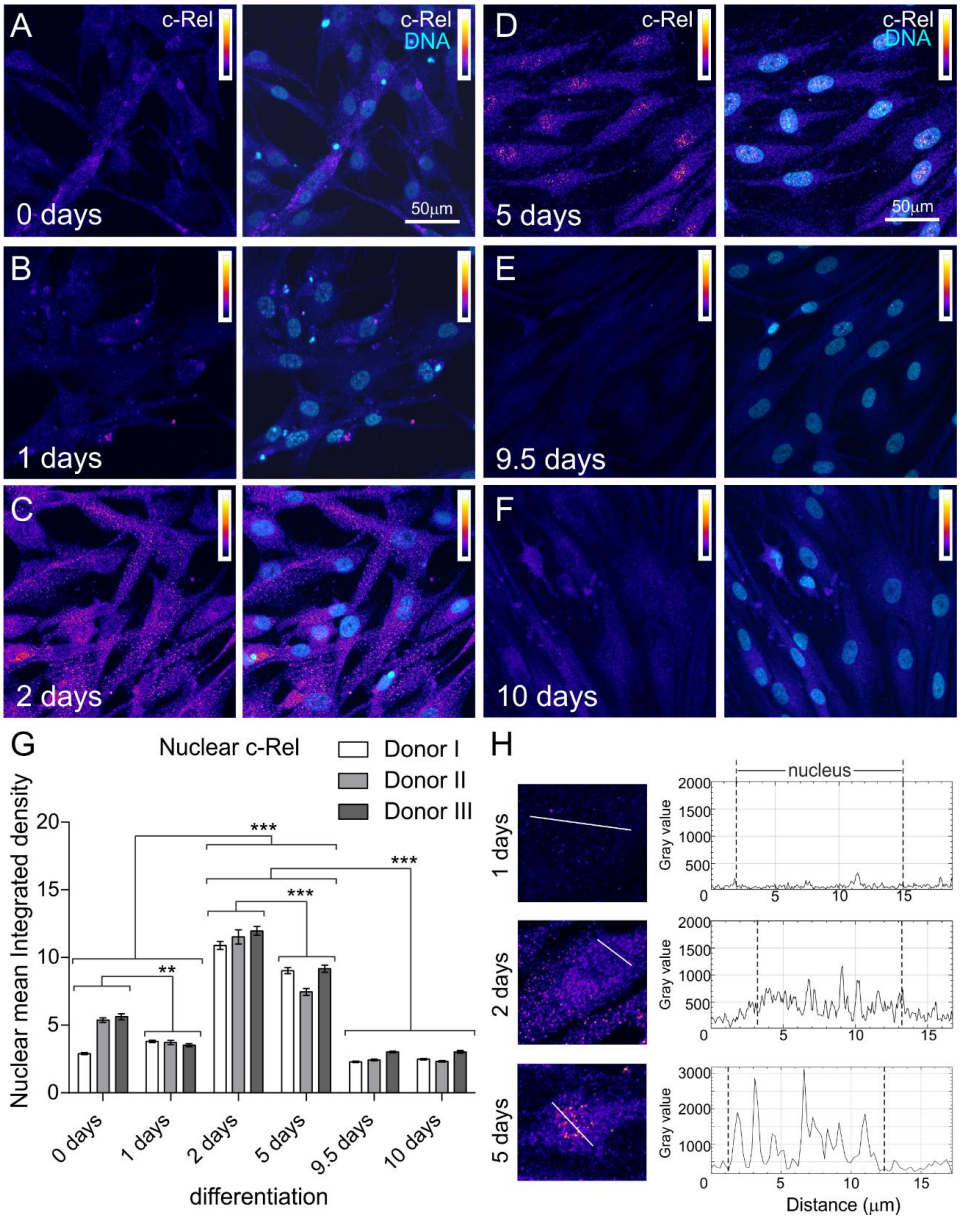

Figure 4-4. Immunocytochemical analysis of c-Rel. A-F: ITSCs labeled against c-Rel after 0, 1, 2, 5, 9.5 and 10 days of glutamatergic differentiation respectively. Each panel shows on the left c-Rel and co-localization with DNA on the right. Intensity scale indicates white as highest intensity level and black as lowest. G: Quantification of immunocytochemical analyses showing nuclear mean integrated density for c-Rel during early differentiation (n=3, mean ± SEM). Normality of the data was refuted using Shapiro-Wilk normality test. Non-parametric Kruskal-Wallis (***$p \leq 0.001$) and Bonferroni corrected post-test (***$p \leq 0.001$) revealed significantly increased nuclear translocation of NF-κB-c-Rel at day 2 and day 5. H: Fluorescence intensity profiles measured at three different time points (1, 2 and 5 days of differentiation), for different cells following transects as shown, in order to clearly reveal the difference between the nuclear and cytoplasmic fluorescence.

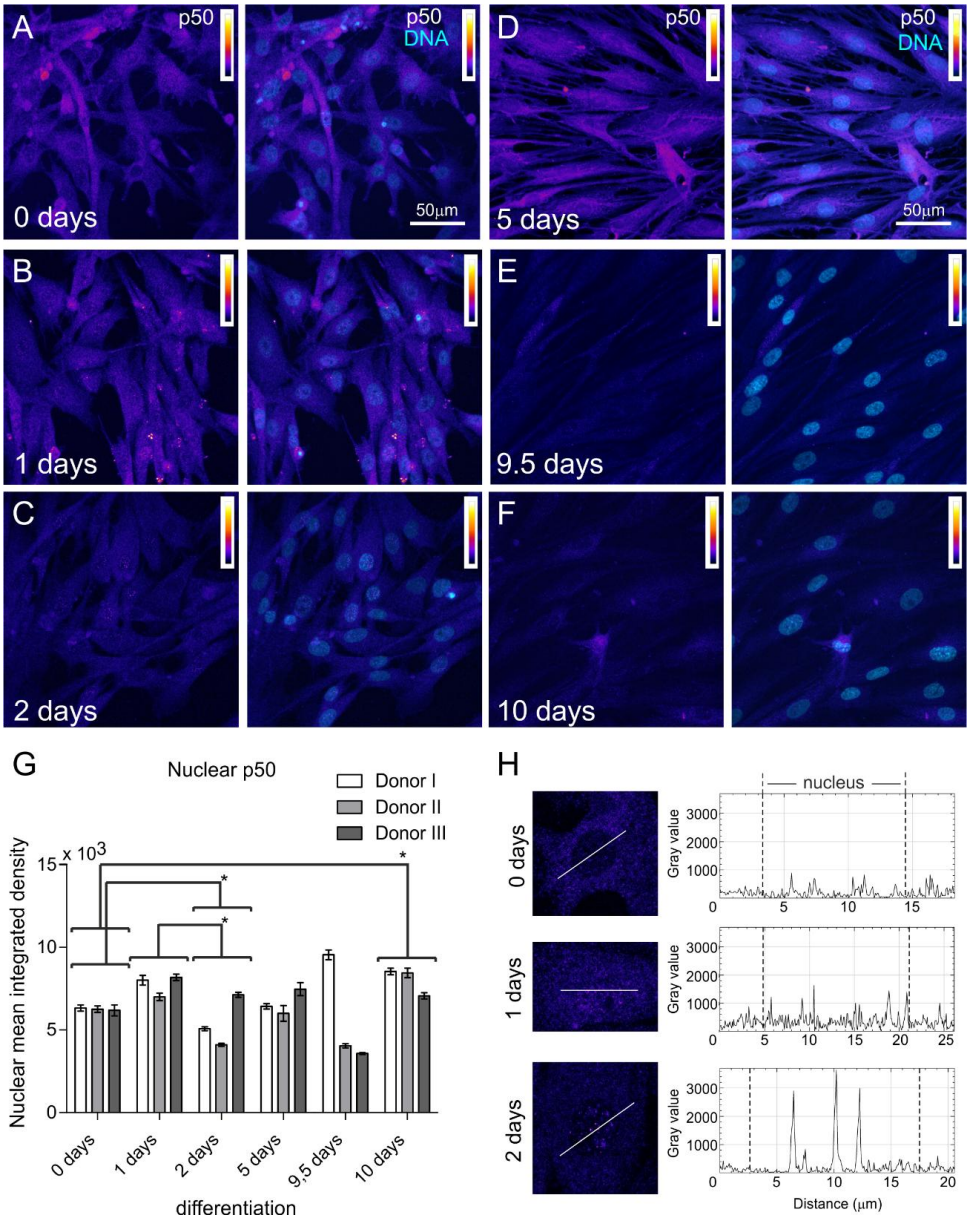

Figure 4-5. Immunocytochemical analysis of p50. A-F: ITSCs labeled against p50 after 0, 1, 2, 5, 9.5 and 10 days of glutamatergic differentiation respectively. Each panel shows p50 protein on the left-side and the co-localization with DNA staining on the right-side. Intensity scale indicates white as highest intensity level and black as lowest intensity level. G: Quantification of immunocytochemical analyses showing nuclear mean integrated density of p50 during early differentiation (n=3, mean ± SEM). Normality of the data was refuted using Shapiro-Wilk normality test. Non-parametric Kruskal-Wallis (***$p \leq 0.001$) and Bonferroni corrected post-test (*$p \leq 0.05$) showed some significant differences between day 0 and 2 and 10 days, and between day 1 and day 2. H: Fluorescence intensity profiles measured at different time points (0, 1 and 2 days of differentiation), for different cells following transects as shown, to clearly expose the difference between nuclear and cytoplasmic fluorescence.

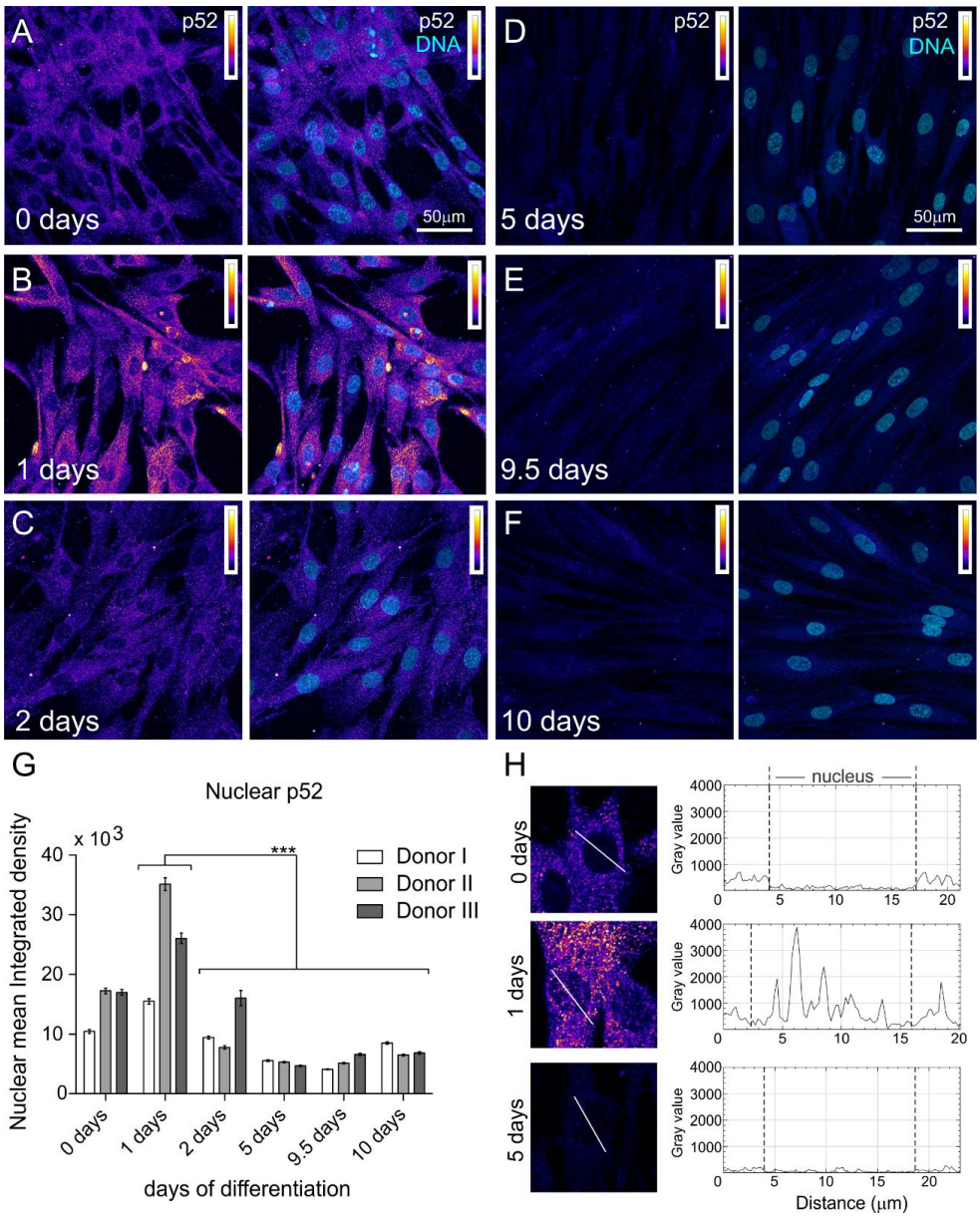

Figure 4-6. Immunocytochemical analysis of p52. A-F: ITSCs labeled against p52 after 0, 1, 2, 5, 9.5 and 10 days of glutamatergic differentiation respectively. Each panel shows p52 subunit on the left-side and the co-localization with DNA on the right-side. Intensity scale indicates white as highest intensity level and black as lowest intensity level. G: Quantification of immunocytochemical analyses showing nuclear mean integrated density of p52 during early differentiation (n=3, mean ± SEM). Normality of the data was refuted using Shapiro-Wilk normality test. Non-parametric Kruskal-Wallis (***$p \leq 0.001$) and Bonferroni corrected post-test (***$p \leq 0.001$) showed a significant peak of p52 at day 1 significantly different to all later time points (2-10 days). H: Fluorescence intensity profiles measured at different time points (0, 1 and 5 days of differentiation), for different cells following transects as shown, to clearly expose the difference between nuclear and cytoplasmic fluorescence.

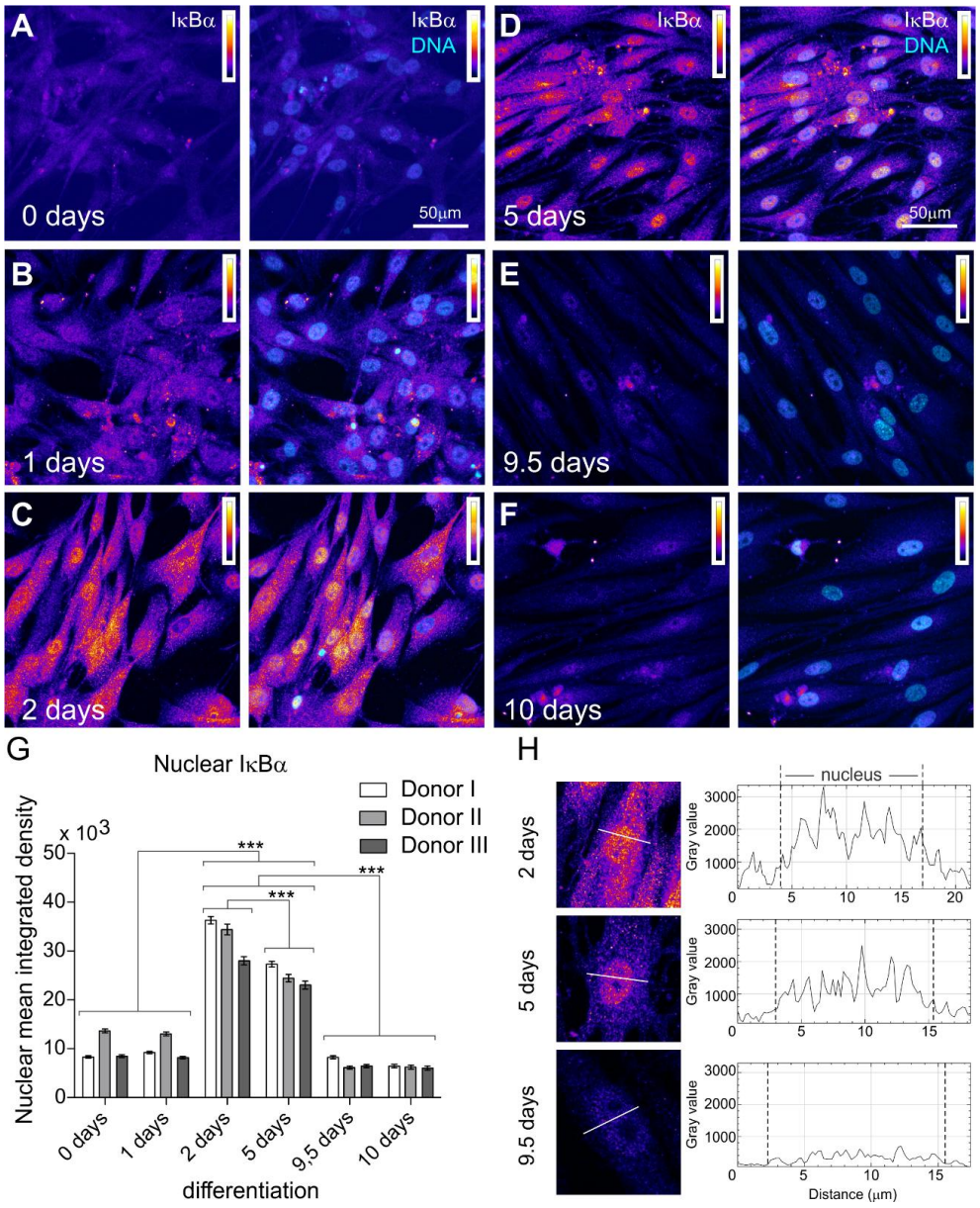

Figure 4-7. Immunocytochemical analysis of IκBα. A-F: ITSCs labeled against IκBα after 0, 1, 2, 5, 9.5 and 10 days of neuronal glutamatergic differentiation respectively. Each panel shows on the left c-Rel and co-localization with DNA on the right. Intensity scale indicates white as highest intensity level and black as lowest. G: Quantification of immunocytochemical analyses showing nuclear mean integrated density for IκBα during early differentiation (n=3, mean ± SEM). Normality of the data was refuted using Shapiro-Wilk normality test. Non-parametric Kruskal-Wallis (***$p \leq 0.001$) and Bonferroni corrected post-test (***$p \leq 0.001$) revealed a significantly increased nuclear translocation of IκBα at days 2 and 5. H: Fluorescence intensity profiles measured at three different time points (2, 5 and 9.5 days of differentiation), for different cells following transects as shown, in order to clearly reveal the difference between the nuclear and cytoplasmic fluorescence.

4.1.7 NF-κB subunit composition in early stages of glutamatergic differentiation of ITSCs

In summary, we characterized the distribution pattern of all NF-κB subunits upon glutamatergic differentiation (Fig. 4-8A), and we found out that each subunit had a particular curve/activity. Among these, RelB and p52 appeared to have a similar behavior during the first days of differentiation, suggesting the presence of p52/RelB heterodimers at the initial time points. Shortly afterwards, c-Rel and IκBα presented a strong peak with a very similar temporary pattern, indicating that after RelB/p52 dimers are inactivated, probably by IκBα up-regulation, c-Rel had a main role during the ongoing differentiation, being down-regulated immediately afterwards and also accompanied by IκBα down-regulation which could imply the inactivation of the pathway for a restoration of the internal balance. In contrast, the classical subunits RelA (p65) and p50 presented an extremely low level with almost no variation, indicating they have no role during this process. These data further indicated that glutamatergic differentiation is driven by the NF-κB subunits c-Rel and RelB.

4.1.8 NF-κB subunit c-Rel is important for cell survival during glutamatergic differentiation of ITSCs

In order to establish the relevance of NF-κB-c-Rel during neuronal glutamatergic differentiation of inferior turbinate stem cells, we further analyzed what happened when we directly blocked c-Rel during differentiation. Thus, we initially confirmed that pentoxifylline (PTXF) was really inhibiting NF-κB-c-Rel[2], by investigating whether PTXF induced a decrease in nuclear translocation of c-Rel during the peak of c-Rel at day 5 of glutamatergic differentiation (Fig. 4-8C- D). Quantification of nuclear mean integrated density of c-Rel confirmed a significant decrease in nuclear c-Rel upon PTXF treatment (non-parametric Mann Whitney test, ***$p \leq 0.0001$), compared to untreated cells (Fig. 4-8G). Thus we tested the hypothesis, that neural stem cells (NSCs) undergo an increase in nuclear NF-κB-c-Rel during early time points, which triggers differentiation towards a glutamatergic neuronal fate (Fig. 4-8H). For this, we treated ITSCs using PTXF during differentiation to block c-Rel nuclear activation, which should result in a shift in the cell fate or otherwise in the cell death (Fig. 4-8H). After 30 days of differentiation we first analyzed cell survival. Nonviable neurons were recognized by an increase in clived-caspase3, together with the nuclear condensation or fragmented chromatin observed (Fig. 4-8E,F). Quantification analyses confirmed a significant decrease in the survival of the treated differentiated-ITSCs, compared to untreated ones (Fig. 4-8B). These findings further suggested that NF-κB-c-Rel has an important role in cell survival during normal differentiation into this neuronal fate.

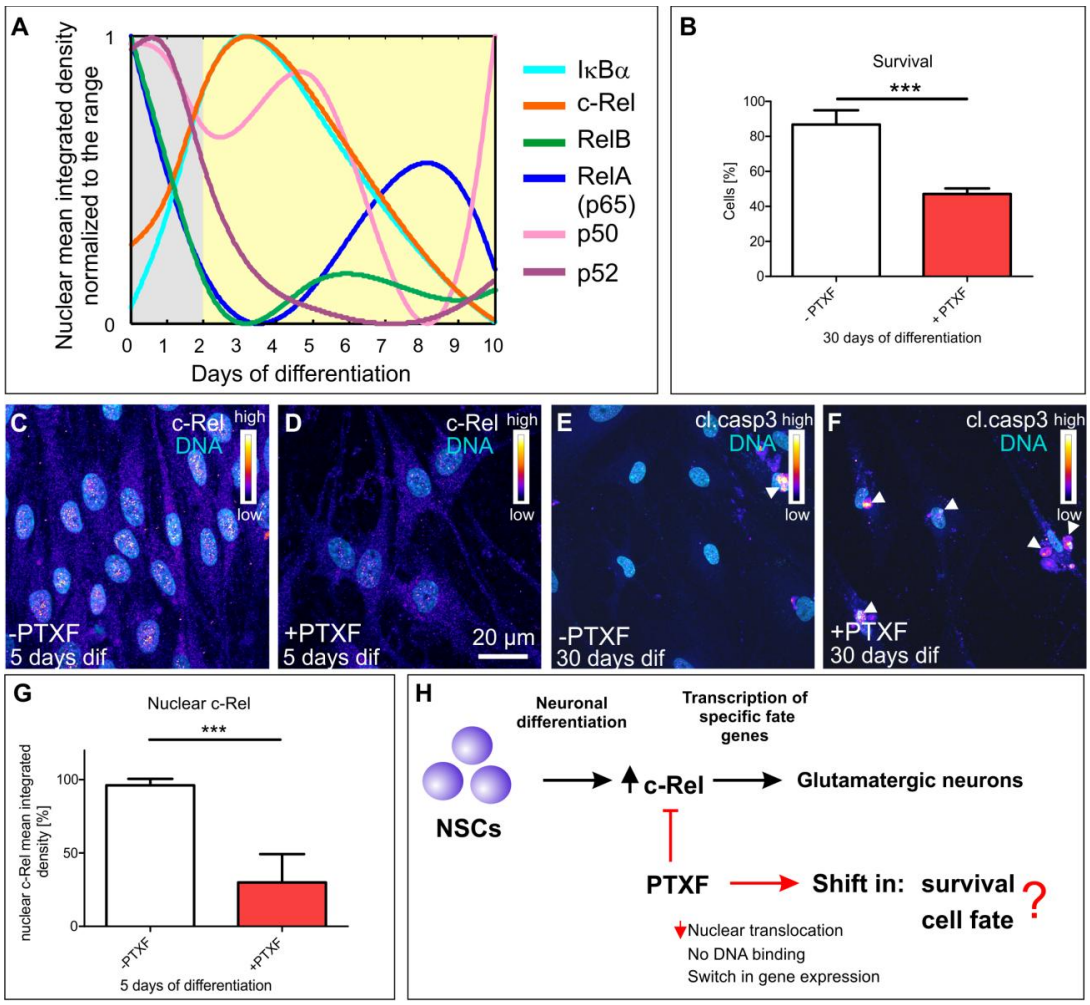

Figure 4-8. NF-κB subunit composition in early gluatamatergic differentiation and c-Rel potential function. A: Diagram summarizing NF-κB subunit distribution during early stages of glutamatergic differentiation. Nuclear mean integrated density shown as the median normalized to the range from 0 to 1, showing the curve for each NF-κB subunit as indicated. B: Quantification of survival of neuronal differentiated-ITSCs for 30 days in the presence or absence of pentoxifylline (PTXF; n=3, mean ± SEM). Non-parametric Mann Whitney test confirmed a significant decrease in survival of PTXF-treated differentiated cells (***p≤0.001), compared to untreated differentiated neurons. C-D: ITSCs differentiated for 5 days in the absence and presence of PTXF respectively, labeled against c-Rel shown with an intensity scale, merged with DNA staining. E-F: ITSCs differentiated for 30 days without and with PTXF, labeled against clived-caspase-3 (cl.casp-3), merged with nuclear counterstaining. G: Quantification of immunocytochemical assay for c-Rel showing nuclear mean integrated density, after 5 days of differentiation with or without PTXF (n=3, mean ± SEM). Non-parametric Mann Whitney test confirmed a significant decrease in nuclear c-Rel after 5 days of differentiation with PTXF (***p≤0.0001), a known c-Rel inhibitor [2]. F: Diagram showing neuronal differentiation mechanism and PTXF mode of action. Neural stem cells differentiating into neurons undergo an increase in nuclear NF-κB-c-Rel, which further induces differentiation into the glutamatergic neuronal fate. The treatment using PTXF during the early neuronal differentiation diminishes c-Rel activation leading to a decrease in the gene expression towards the neuronal fate resulting in a cell fate shift or in cell death. Intensity scale: White as highest intensity level, black as lowest intensity level.

4.1.9 c-Rel inhibition by pentoxifylline provokes a differentiation shift into the oligodendrocyte fate

Furthermore, we investigated the cell fate by immunocytochemistry, which confirmed the presence of mature neuronal markers Neurofilament 200 (41,44% ± 6.31%; Fig. 4-9A-C) and vGlut2 (47,97% ± 2,72%; Fig. 4-9D-F) upon treatment with PTXF, showing however a strong decrease on the percentage of positive cells in comparison to the untreated-differentiated neurons (84,68% ± 7,70% $NF200^+$ neurons; 85,37% ± 5,34% $vGlut2^+$ neurons; Non-parametric Kruskal-Wallis test ***$p \leq 0.0005$). Further analysis revealed that differentiated-ITSCs treated with PTXF were robustly positive for different oligodendrocyte markers such as Olig2 (86,67% ± 6,67%, Fig. 4-9J-L) and O4 (100%, Fig. 4-9M-O) an early and an intermediate marker respectively. Both differences were confirmed to be significantly relevant by non-parametric Kruskal-Wallis test (***$p \leq 0.001$, *$p \leq 0.05$ respectively) which indicated there was a shift of the cell fate into the oligodendrocyte fate. In addition, PDGFRA (Platelet derived growth factor receptor alpha) and NG2 (chondroitin sulfate proteoglycan type 4, CSPG4), two early oligodendrocyte markers, and MBP (Myelin basic protein) a mature marker of myelinating oligodendrocytes were also present at the mRNA level, which were completely absent in the untreated neurons (Fig. 7A-C). These findings also evidenced the clear shift into the oligodendrocyte lineage. Interestingly, differentiated-ITSCs treated with PTXF were totally negative for GFAP (0%, Fig. 6G-I), suggesting no astrocytes were present in the treated differentiated-ITSCs. Besides, differentiated-ITSCs treated with PTXF showed a slight tendency to express Nestin (stemness marker), compared to the untreated cells (Suppl. fig. 3A-C, $p \leq 0.10$). And a similar trend was observed for p75 (Neural crest marker, Suppl. fig. 3D-F, $p \leq 0.10$), suggesting that PTXF treated differentiated-ITSCs might be somewhat less differentiated compared to normal ITSC-derived neurons. In addition, treated and untreated differentiated-ITSCs were negative for αSMA (alpha smooth muscle), indicating the absence of mesodermal-derived cells (Suppl. fig. 3G-I). These

findings discarded a possible switch in the cell fate towards a non neuro-ectodermal lineage.

4.1.10 NF-κB-c-Rel drives neuronal glutamatergic differentiation of ITSCs

Taken together our findings suggested that ITSCs undergo a high increase of nuclear c-Rel during early glutamatergic differentiation, which might induce the expression of a specific gene program towards the neuronal fate. That was evidenced by the enhanced expression of mature neuronal proteins such as NF200 and vGlut2, as well as a strong decrease in oligodendroglial marker proteins like O4 and Olig2, as well as an extremely low level of GFAP. In addition, neuronal differentiation was accompanied by a strong survival (87%, Fig. 4-10). However, when nuclear c-Rel activation was abolished using pentoxifylline, this strong inhibition produced a remarkable shift of the cell fate shift into the oligodendrocyte lineage. This shift was determined by an elevated increase in oligodendrocyte markers like Olig2 and O4 by imunodetection, as well as PDGFRA, NG2 and MBP at the mRNA level (Fig. 4-10A-C). Followed by a significant decrease in the neuronal protein markers NF200 and vGlut2, and also a strong reduction in cell survival (47%). Moreover, the switch in the differentiation program further produced a prominent change in the morphology of the treated-differentiated-ITSCs (Fig. 4-9, 4-10); cells acquired a polygonal-like shape, with an extension of the cell surface, and a reduction of the cellular processes, indicating that cells were unable to produce such cellular processes; further supporting the shift in the cell fate. These changes at the protein and mRNA levels together with the modification of the cellular morphology and the cell survival further demonstrate that the differentiation of neural stem cells into the neuronal phenotype is driven by NF-κB-c-Rel as previously suggested (Fig. 4-8F).

Furthermore, myelination assay results showed that O4 expression was similar in female derived co-cultures of both ITSC-derived neurons and ITSC-derived OPCs, and of ITSC-derived neurons and ITSC-differentiated cells in the presence of PTXF, which were co-cultivated for 10 days, after 20 days of differentiation (Suppl. fig 4I,J). Also, the expression of this oligodendrocyte marker was similar for these co-cultures and the ITSCs

differentiated in OPCs (Oligodendrocyte progenitor cells) and the neuronal-differentiated ITSCs with PTXF, further supporting the shift into the oligodendrocyte fate (Suppl. fig. 4F-J). In addition, both male- and female-derived co-cultures were positive for NF200, indicating neuron progenitors were present in the co-cultures, however these were also slightly positive for Myelin oligodendrocyte glycoprotein further indicating cells were differentiating into mature oligodendrocytes as well (Suppl. fig. 5D-E, I-J). These Findings strongly suggest that both co-culture systems had a mixture of neural progenitors that could further differentiate into neurons or oligodendrocytes, while co-differentiating together.

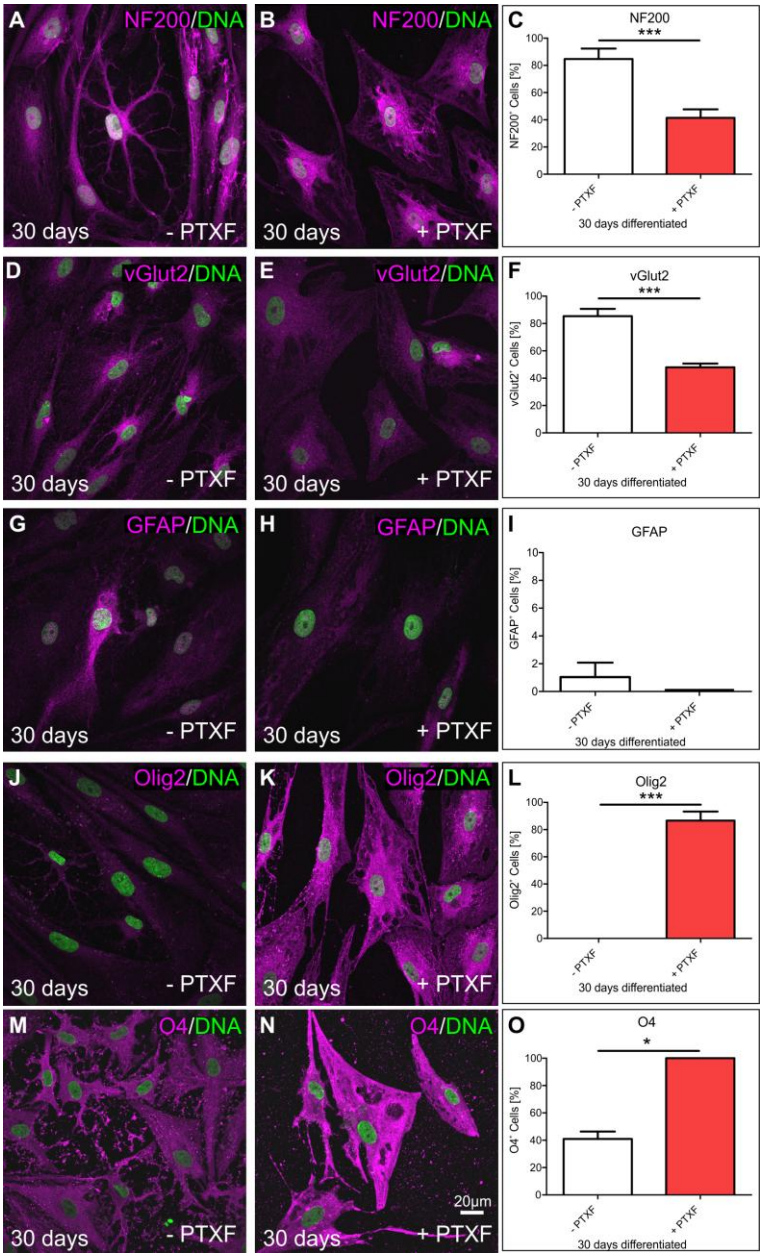

Figure 4-9. Immunocytochemistry against neuronal and glial markers, after glutamatergic differentation in the presence and absence of pentoxifylline (PTXF) and quantification. A-B: Neuronal differentiated-ITSCs labeled against Neurofilament 200 (NF200). C: Quantification showing percentage of $NF200^+$ neurons. Non-parametric Kruskal-Wallis test (***$p \leq 0.0005$) revealed a significant decrease of $NF200^+$ neurons with PTXF, compared to untreated neurons. D-E: Neuronal differentiated-ITSCs labeled against vGlut2. F: Quantification showing percentage of $vGlut2^+$ neurons. Non-parametric Kruskal-Wallis test (***$p \leq 0.0005$) showed a significant decrease of $vGlut2^+$ neurons in the differentiated-ITSCs treated with PTXF, compared to untreated neurons. G-H: Differentiated-ITSCs labeled against GFAP, an astrocyte marker. I: Quantification showing percentage of $GFAP^+$ cells indicates a very low number of astrocytes in the untreated neurons and none in the PTXF-treated differentiated-ITSCs. No significant difference was observed. J-K: Neuronal differentiated-ITSCs labeled against Olig2, an early oligodendrocyte marker. L: Quantification of $Olig2^+$ cells in percentage, no positive cells were present in the untreated neurons, while in the PTXF-treated differentiated-ITSCs almost all cells were $Olig2^+$. Non-parametric Kruskal-Wallis test (***$p \leq 0.001$) confirmed a significant increase of $Olig2^+$ cells upon PTXF treatment, indicating a shift into the oligodendrocyte fate. M-N: Neuronal differentiated-ITSCs labeled against O4, an intermediate oligodendrocyte marker. O: Quantification of $O4^+$ cells, showed a clear increase of $O4^+$ cells in the neuronal PTXF-treated differentiated-ITSCs, confirmed by statistical non-parametric Kruskal-Wallis test (*$p \leq 0.05$).

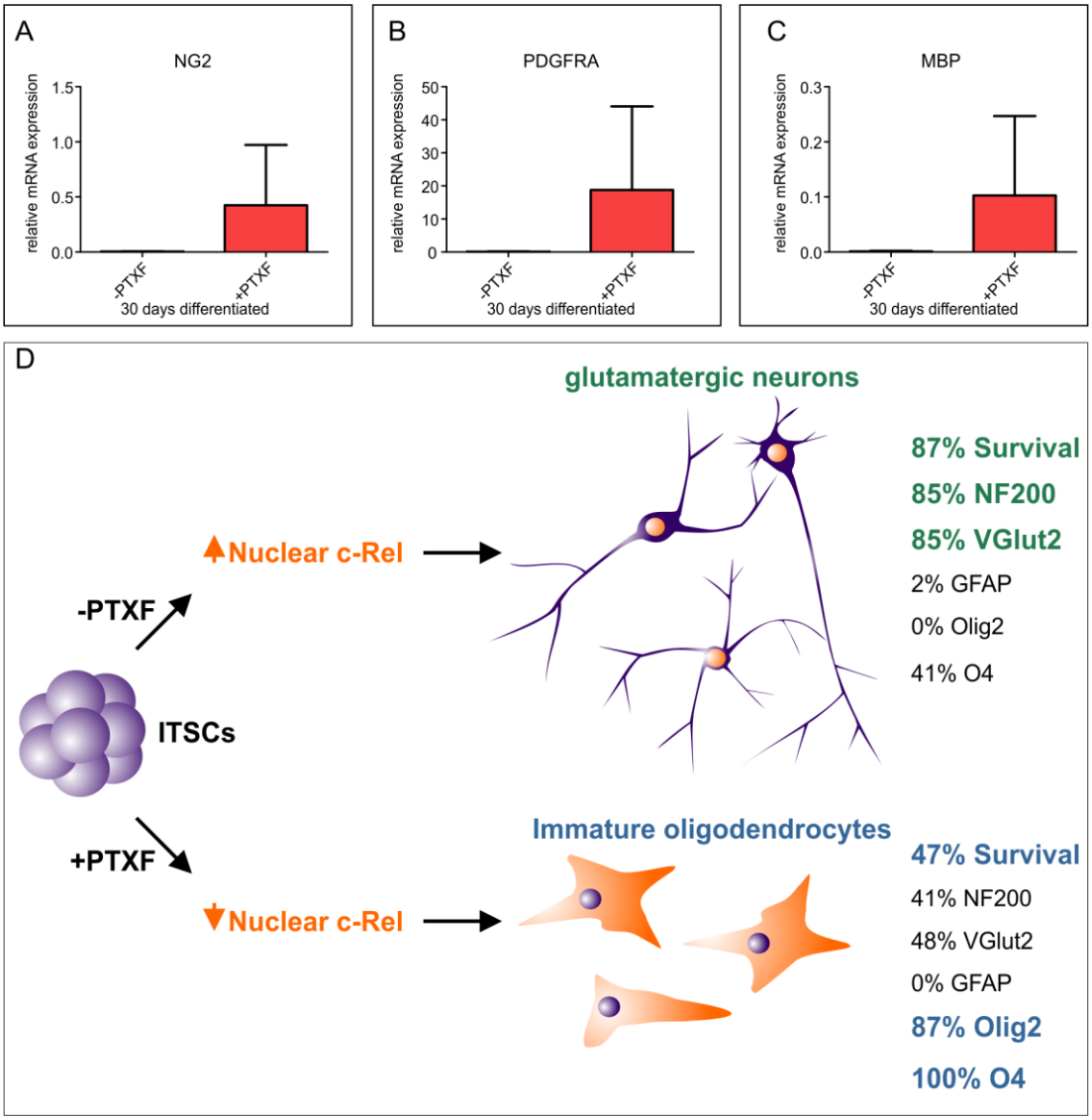

Figure 4-10. Cell fate shift towards the oligodendrocyte phenotype due to c-Rel early inhibition. A-C: Real time polymerase chain reaction showing relative mRNA levels of Oligodendrocyte markers NG2, PDGFRA and MBP respectively. Levels for these Intermediate (NG2, PDGFRA) and mature markers (MBP) are only present in the differentiated-ITSCs treated with PTXF, indicating a shift into the oligodendrocytic lineage (n=2, mean ± SD). D: Summarizing scheme showing outstanding results obtained in this investigation. During neuronal differentiation of ITSCs into glutamatergic neurons, cells undergo a strong increase of c-Rel activation during early time points, which further induces the expression of a specific gene program towards the neuronal fate, which was confirmed by the increased expression of mature neuronal proteins NF200 and vGlut2, and a clear decrease in O4, as well as almost no GFAP and Olig2 accompanied by a strong survival. When ITSCs differentiating were treated in parallel with pentoxifylline, the increase of nuclear c-Rel was almost completely abolished, leading to a shift in the cell fate into the oligodendrocyte lineage, which was confirmed by a strong increase in oligodendrocyte markers Olig2 and O4 and a clear decrease in the neuronal markers NF200 and vGlut2, which was also accompanied by a strong reduction in cell survival.

4.2 Discussion

The present study describes for the first time the main role of NF-κB-Rel-B and c-Rel during glutamatergic neuronal differentiation of human inferior turbinate stem cells. Here, we successfully characterized the NF-κB subunit composition during early stages of differentiation, and we found out that RelB and p52 were activated during an early phase, suggesting RelB/p52 heterodimers had a part at the initial steps of differentiation. Interestingly, their inactivation was opposed to the increase observed for IκBα and c-Rel shortly afterwards, indicating their negative regulation was mediated by IκBα, while in parallel c-Rel was being highly activated, suggesting that c-Rel takes over afterwards. Furthermore c-Rel inactivation might also be mediated by IκBα, which was down-regulated with the restoration of the internal balance (Fig. 4-8A), indicating NF-κB activity is strictly regulated during differentiation. On the contrary, RelA and p50, the classical NF-κB subunits had no part during differentiation, although RelA had an early short significant nuclear increase immediately after seeding, and might be important for the attachment of the cells. In accordance to our findings, previous studies showed that NF-κB-p65 decreased upon differentiation of human embryonic stem cells (hESCs), and was involved in the maintenance of the undifferentiated state [153-154]. Similarly during early differentiation of hESCs, upon inhibition of IKK using IKK small-inhibitor or p65 knockdown, p65 activity was high only during the initial days of differentiation and decreased shortly afterwards, together with the up-regulation of endodermal and mesodermal markers which resulted in MSCs specification [155]. Interestingly, in other hESCs a peak of RelB/p52 was characterized in the undifferentiated cells, and a strong decrease was observed upon 10 days of differentiation, which was further implicated in pluripotency maintenance and proliferation[156]. Whereas p65/p50 were increased upon differentiation and were required for the maintenance of viability and differentiation [156]. These findings are in line with the initial activation of RelB/p52 dimers that we observed, which might be necessary for early neuronal differentiation.

Data presented here further confirmed that c-Rel has an important function in cell survival during neuronal differentiation. Initially we intended to use CRISPR/Cas9-mediated genome editing to delete c-Rel subunit, however it is difficult to apply this strategy in primary cells such as ITSCs, which are not easily transfected in comparison to HEK293 cells[157]. Therefore, as shown by c-Rel inhibition using chronic pentoxifylline (PTXF) treatment, PTXF induced a significant decrease in nuclear c-Rel after 5 days of differentiation, as also observed in PTXF-treated T lymphocytes[158]; and extended treatment produced a strong decrease in cell survival as illustrated by an increase in clived-caspase-3^{+} cells and respective nuclear condensation and/or fragmentation after 30 days of differentiation. These results are in agreement with the known anti-apoptotic effects of c-Rel in different cell types, such as neurons, keratinocytes, and B cells [159-161]. Besides, NF-κB is known to regulate cell proliferation, being involved in the G2/M phase in certain cell types [112,162-163]. Furthermore, c-Rel inhibition generated a strong shift into the oligodendrocyte fate, evidenced by the increase in $Olig2^{+}/O4^{+}$-differentiated-ITSCs after 30 days, suggesting the presence of immature pre-myelinating oligodendrocytes [164-165]. The oligodendrocytes are cells responsible for the production of myelin in the central nervous system (CNS), which is required for the saltatory conduction of electrical impulses across axons. These cells extend multiple cellular processes that individually ensheath different segments of axons. Thus, myelin consists of loops of the oligodendroglial plasma membrane tightly wrapped around the axon. During early embryonic development oligodendrocytes are differentiated from oligodendrocyte progenitor cells, proliferative cells, which migrate and undergo differentiation into mature oligodendrocytes [48]. However, immature oligodendrocytes differentiated from ITSCs also expressed NG2 (CSPG4) and PDGFRα at the mRNA level, known markers of oligodendrocyte progenitors, but they also expressed MBP, a mature marker of myelinating oligodendrocytes [48,166]. Hence, our results suggest that in the absence of c-Rel, ITSCs undergo the differentiation into the oligodendrocyte lineage, resulting in a mixed population of cells with different levels of maturity, from immature pre-myelinating to mature myelinating oligodendrocytes. Furthermore, these findings demonstrated that c-Rel is a key player in the

differentiation of ITSCs, being directly involved in the regulation of neuronal differentiation and survival.

Demyelinating diseases including Multiple sclerosis (MS) are caused by loss of oligodendrocytes and concomitant loss of myelin [166-167]. MS is a chronic inflammatory disease of the CNS acquired in young adults, due to an enhanced autoimmune response against myelin antigens that result in demyelinating lesions in the brain and spinal cord followed by axonal injury [168-169]. Treatments to ameliorate MS are based on decreasing the reactive autoimmune response, an example is Pentoxifylline, a methylxanthine derivative and phosphodiesterase inhibitor, which was used for the treatment of MS alone [170] or accompanying IFN-β1b (Interferon beta-1b) [171]. Treatment using PTXF was shown to deviate the immune response in MS patients, by decreasing pro-inflammatory cytokines like TNF-α and interleukin-2, suggesting a modulation towards a Th2-like response instead of a Th1-like T cell response[170]. Moreover, when patients were treated with both IFN-β1b and PTXF, TNF-α and IFN-α (interferon alpha) were not detected, compared to patients treated with only IFN-β1b, which had an increase in both cytokines [171]. However, during these studies only the inflammatory response was analyzed in detail, thus no relevant changes within the cellular populations within the CNS were analyzed. Nevertheless, new insights suggest that fibrinogen enters the brain when the blood-brain-barrier is damaged due to MS and inhibits OPC differentiation into oligodendrocytes, while inducing their differentiation into astrocytes, further decreasing the oligodendrocyte population and therefore the remyelination[172]. In this work, our results confirmed that PTXF is directly inducing a shift towards the oligodendrocyte fate *in vitro*, due to the inhibition of nuclear c-Rel. Therefore, c-Rel might also have an important function *in vivo* during PTXF-treatment of demyelinating diseases such as multiple sclerosis. Further studies analyzing the modifications induced within the central nervous system upon treatment using pentoxifylline against these neurodegenerative diseases will be needed to elucidate a role in the remyelinating process within the adult ageing human brain.

Role of NF-κB in dopaminergic differentiation and functionality.

5

A version of this chapter is in preparation to be published:
Ruiz-Perera, L. M., Kaltschmidt, C., Kaltschmidt, B. in prep.

5.1 Results

5.1.1 NF-κB subunit distribution in early stages of dopaminergic differentiation of ITSCs

In order to study the role of NF-κB during dopaminergic differentiation, we characterized the NF-κB subunit composition during early stages of differentiation. ITSCs were cultivated following a directed dopaminergic differentiation procedure (Fig. 5-1A)[40]. Samples were taken at different time points (0, 2, 6, and 9 days of differentiation) and analysed by immunocytochemistry for NF-κB-p65 (RelA), RelB and c-Rel (Fig. 5-2, 5-3, 5-4), and we further verified their ability to differentiate into the dopaminergic lineage, demonstrated by morphological changes into a neuronal phenotype (Fig. 5-1B) and by immunostaining analyses showing dopamine (DA) and tyrosine hydroxylase (TH) expression after 21 days of differentiation (Fig. 5-1C-D), further validating that ITSCs efficiently differentiate into mature dopaminergic neurons.

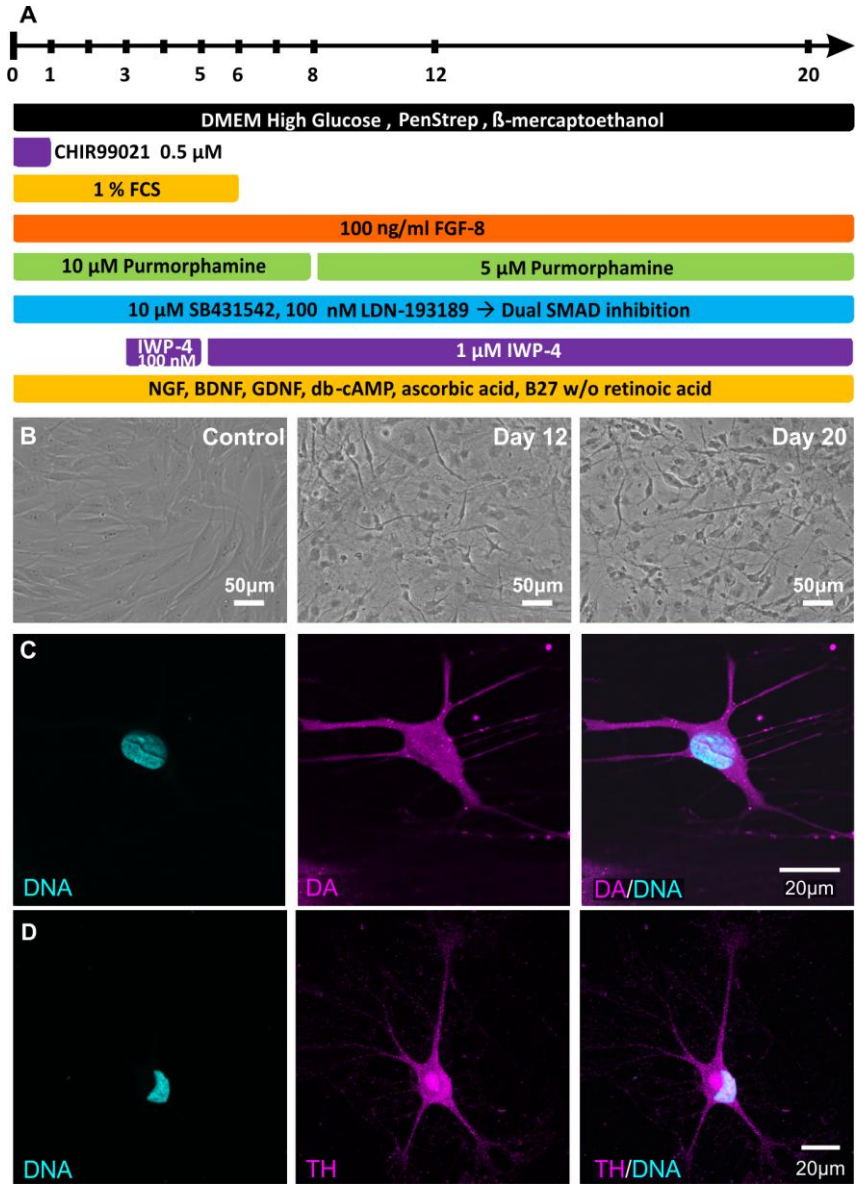

Figure 5-1. ITSCs effieciently differentiate into dopaminergic neurons. A: Diagram showing dopaminergic differentiation procedure. ITSCs were cultivated for at least 12 hours in DMEM high glucose supplemented with 10% FCS. For neuronal induction, media was changed to DMEM high glucose supplemented with 1% FCS, penicillin/streptomycin, β-mercaptoethanol (10 µM), B27 without retinoic acid, purmorphamine (10 µM), FGF8 (100 ng/ml), GDNF (5 ng/ml), BDNF (20 ng/ml), NGF (20 ng/ml), dibutyryl cAMP (1 mM), ascorbic acid (200 µM), SB-431542 (10µM), LDN193189 (100 nM), and CHIR99021 (0.5µM). Afterwards media was modified as indicated in the scheme. Medium was replaced with prewarmed fresh medium daily. Modified from Nartnyk et al., 2014[4]. B: ITSCs changed their morphology towards a neuronal phenotype during directed neuronal differentiation. C-D: Immunocytochemical analysis showing dopamine (DA) and tyrosine hydroxylase (TH) expression after 21 days of differentiation, indicating mature dopaminergic neurons derived from ITSCs.

5.1.2 RelA distribution during early dopaminergic differentiation

Immunocytochemistry against RelA revealed that during the first days of differentiation there is a strong marked cytoplasmic signal and a lower nuclear level in most cells, being strong in some cells (Fig. 5-2A, arrowheads). During the first 4 days of differentiation both cytoplasmic and nuclear RelA decreased (Fig. 5-2A-C), while at day 6 both were slightly increased, having a faint nuclear intensity with a punctuated pattern (Fig. 5-2D). Later, cytoplasmic and nuclear RelA intensity was further increased for donor 1 (Fig. 5-2E), while it decreased for the other two donors, keeping the punctuated pattern observed. Thus, due to the slight changes in nuclear activation observed, we further analyzed the fluorescence intensity profile (Fig. 5-2F), to discriminate the fluctuations in RelA subcellular localization for cells at the different timepoints analyzed. We also quantified nuclear fluorescence using the nuclear mean integrated density for the three female donors analyzed (Fig. 5-2G), that allowed us to determine the changes in nuclear RelA during early dopaminergic differentiation. Statistical analysis clearly demonstrated significant differences for nuclear RelA which had a higher level between day 0 and day 2 compared to day 4 (Non parametric Kruskal-Wallis test, ***$p \leq 0.001$, Tukey's test, ***$p \leq 0.001$, n=3), this could be due to cell attachment, that might be consolidated after day 4. Also there was a significant difference between day 4 and day 6, indicating that RelA increased afterwards, and that it might be important for the differentiation process during later timepoints.

5.1.3 RelB distribution during early dopaminergic differentiation

Immunostaining analyses also confirmed that RelB had a higher level in the cytoplasm than in the nucleus, although the intensity level observed was relatively low (Fig. 5-3A-E). Initially, RelB had a lower intensity level at the beginning of the differentiation and gradually increased over time (Fig. 5-3A-E), showing a peak at day 9, which could be maintained or increased later. However, for female donor 1 RelB level was slightly higher at the beginning and decreased gradually during differentiation. These differences were further analyzed with the fluorescence intensity profile (Fig. 5-3F), were a clear change in the nuclear intensity fluctuations is observed, among cells at different timepoints. In addition, to detect these

nuclear intensity changes, we quantified the nuclear mean integrated density (Fig. 5-3G). As shown by the range of the intensity scale (Fig. 5-3A-E), both cytoplasmic and nuclear RelB levels are very low during the first 4 days of differentiation, however after day 6 there is a clear increase in RelB at both cytoplasmic and nuclear levels. Statistical analysis demonstrated a significant difference between day 0 and day 6 and 9 (Fig. 5-3G, Non-parametric Kruskal-Wallis ***$p \leq 0.001$, Tukey's post hoc test ***$p \leq 0.001$), suggesting that RelB has an important role during this later stage of early dopaminergic differentiation. Although there is a clear increase of nuclear RelB, as the peak observed is not too prominent, it is possible that RelB has an even stronger activation peak at later timepoints. In that case, later timepoints should be analyzed to determine whether RelB has a role during late dopaminergic differentiation.

5.1.4 c-Rel distribution during early dopaminergic differentiation

We further analyzed NF-κB-c-Rel by immunostaining, and determined that c-Rel is highly expressed at day 0 for two female donors (D1 and 2), especially at the cytoplasmic level, however it is highly expressed at the nuclear level (Fig. 5-4A, arrowheads). At day 2 both cytoplasmic and nuclear c-Rel remarkably decreased, however some nuclear activation remained in a lower degree (Fig. 5-4B). In the following timepoints a slight increase at both subcellular localizations was observed (Fig. 5-4C-E). Furthermore, the differences in c-Rel expression were illustrated by measuring the fluorescence intensity profile of cells at the different timepoints studied (Fig. 5-4F), showing a clear nuclear c-Rel increase between days 4 and 9. Quantification of nuclear mean integrated density for c-Rel confirmed this NF-κB-c-Rel activating peak, which was statistically relevant (Fig. 5-4G, non-parametric Kruskal-Wallis ***$p \leq 0.001$ and Tukey's test ***$p \leq 0.001$). As shown in the figure, there was a significant increase of nuclear c-Rel between days 4 and 6 compared to day 2, and also a clear decrease afterwards when comparing days 4 and 6 to day 9 (Fig. 5-4G, Non-parametric Kruskal-Wallis ***$p \leq 0.001$ and Tukey's test ***$p \leq 0.001$). Further, a significant difference was shown between day 0 and all later time points, which could be related to the cell attachment during the beginning

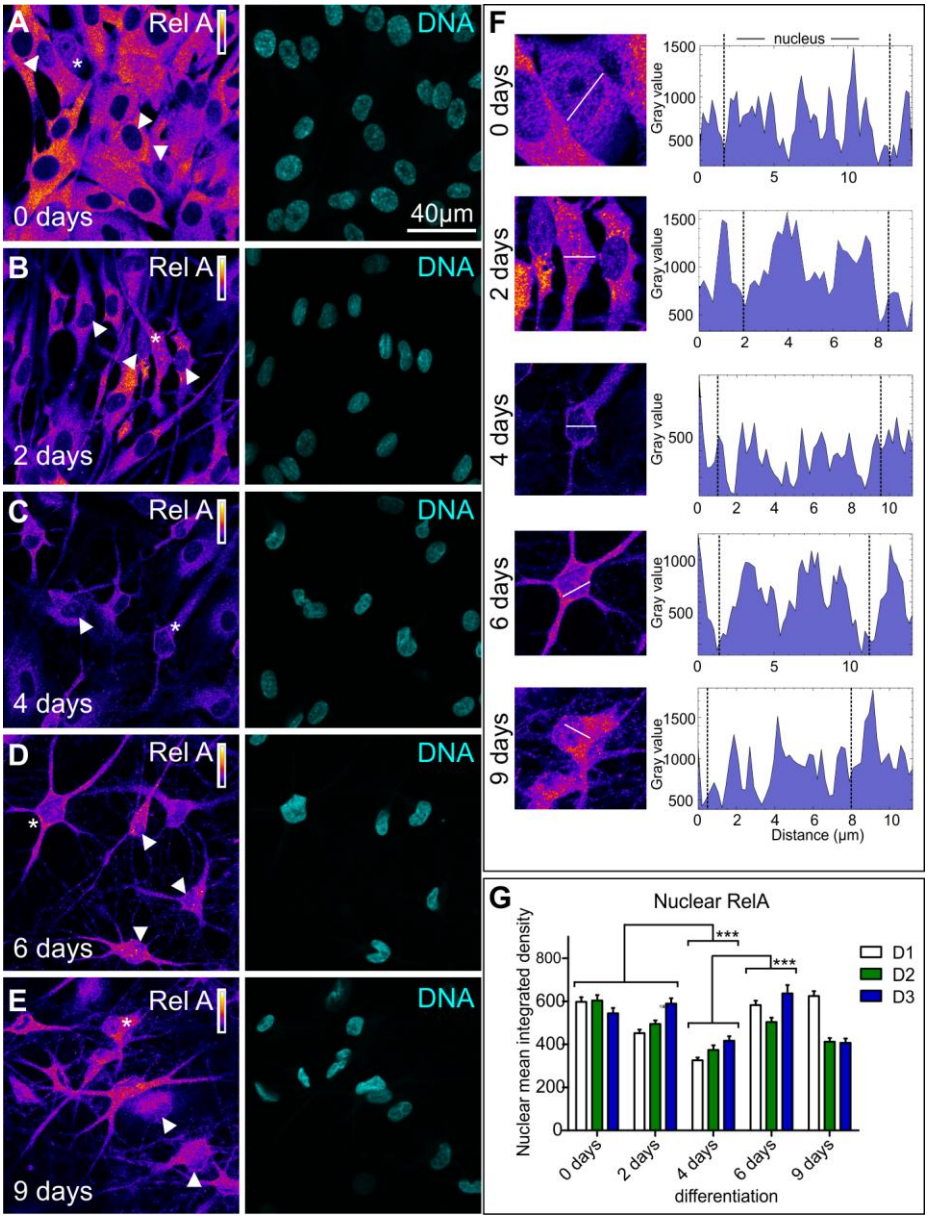

Figure 5-2. Immunocytochemical analysis of RelA (NF-κB-p65) during early dopaminergic diferentiation. A-E: ITSCs labeled against RelA after 0, 2, 4, 6 and 9 days of dopaminergic diferentiation. Each panel shows RelA on the left-side and DNA staining on the right-side. Intensity scale: white highest intensity level and black lowest intensity level. Arrowheads show high RelA nuclear activity, asterisks indicate cells further analyzed in F. F: Fluorescence intensity profiles measured at all time points analyzed, for the cells shown in A-E with asterisks, following transects as shown. Here the difference between the nuclear and cytoplasmic fluorescence is exposed. G: Quantification showing nuclear mean integrated density of RelA for all female donors analyzed (n=3, mean ± SEM) and the Statisic analysis performed. Normality was refuted using Shapiro-Wilk normality test. Non-parametric Kruskal-Wallis (***p≤0.001) and Tukey's test (***p≤0.001) revealed significant differences in nuclear translocation of NF-κB-p65 as indicated.

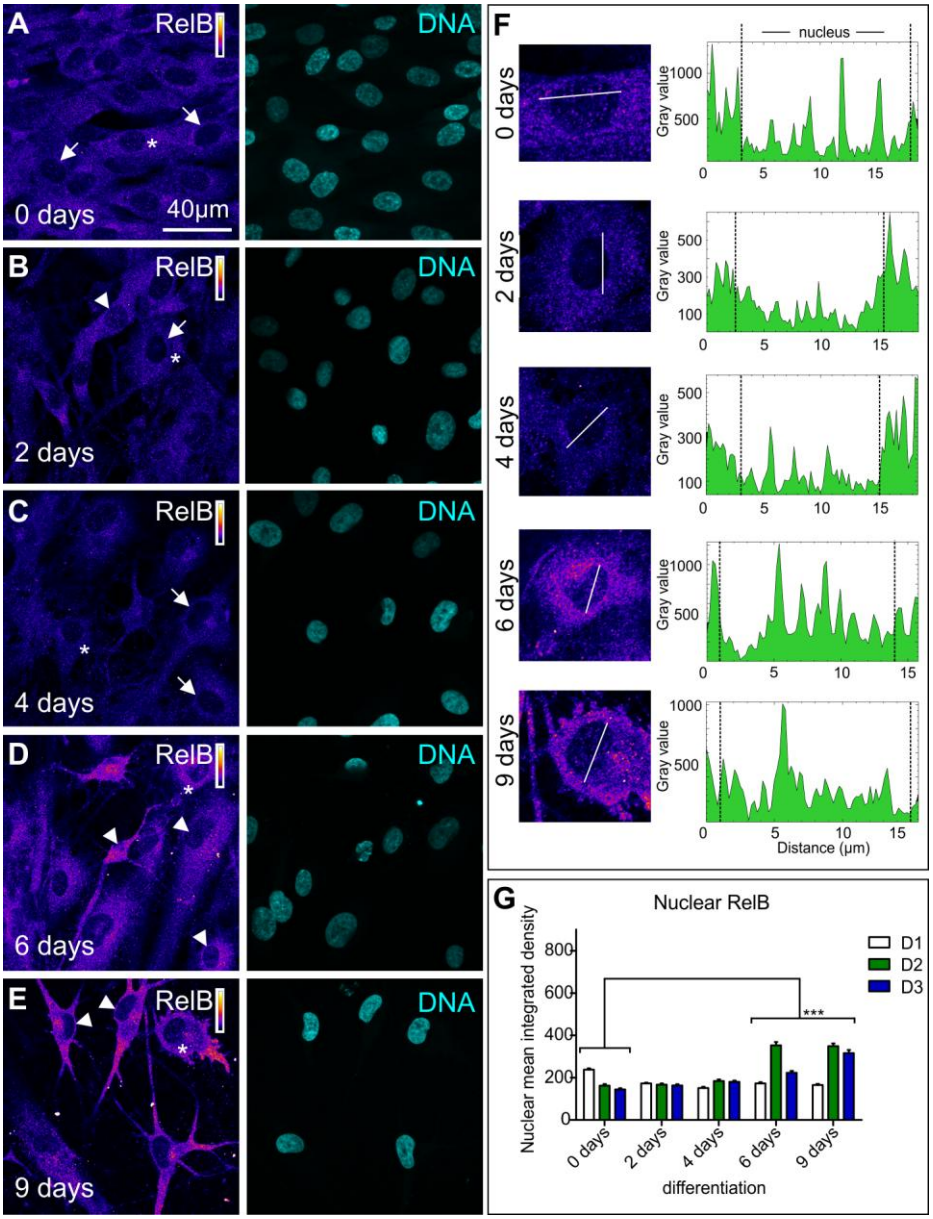

Figure 5-3. Immunocytochemical analysis of RelB during early dopaminergic differentiation. A-E: ITSCs labeled against RelB after 0, 2, 4, 6 and 9 days of dopaminergic diferentiation. Each panel shows RelB on the left-side and DNA staining on the right-side. Intensity scale: white highest intensity level and black lowest intensity level. Arrows indicate cells with low RelB activity, Arrowheads show high RelB nuclear activity, asterisks indicate cells further analyzed in F. F: Fluorescence intensity profiles measured at all time points analyzed, for the cells shown in A-E with asterisks, following transects as shown. Here the difference between the nuclear and cytoplasmic fluorescence is exposed. G: Quantification showing nuclear mean integrated density of RelB for all female donor analyzed (n=3, mean ± SEM) and the statisic analysis performed. Normality of the data set was refuted using Shapiro-Wilk normality test. Non-parametric Kruskal-Wallis (***$p \leq 0.001$) and Tukey's test (***$p \leq 0.001$) revealed significant difference in nuclear RelB between day 0 and day 6 and 9.

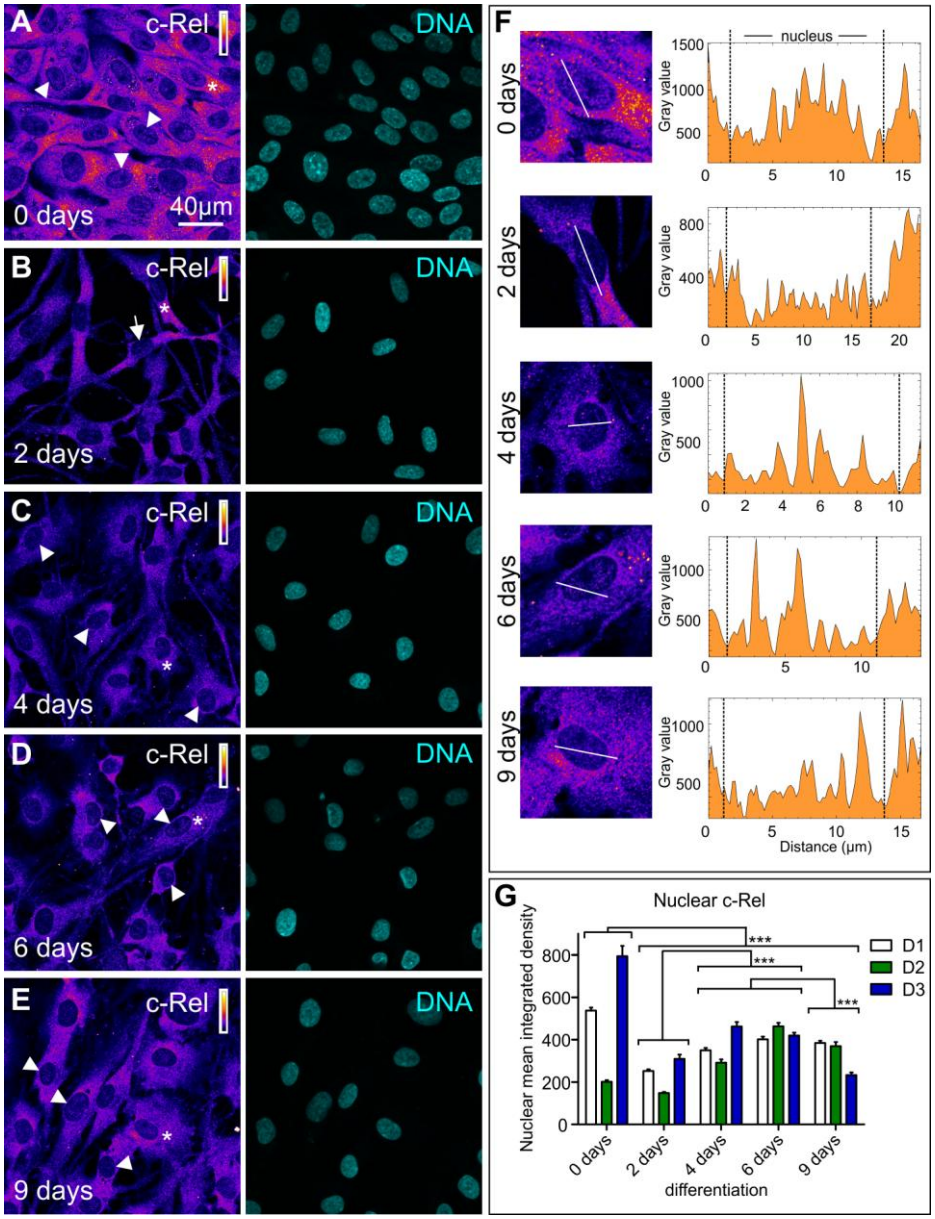

Figure 5-4. Immunocytochemical analysis of c-Rel during early dopaminergic differentiation. A-E: ITSCs labeled against c-Rel after 0, 2, 4, 6 and 9 days of dopaminergic diferentiation. Each panel shows c-Rel on the left-side and DNA staining on the right-side. Intensity scale: white highest intensity level and black lowest intensity level. Arrows indicate cells with low c-Rel nuclear activity, Arrowheads show high c-Rel nuclear activity, asterisks indicate cells further analyzed in F. F: Fluorescence intensity profiles measured at all time points analyzed, for the cells shown in A-E with asterisks, following transects as shown. Here the difference between the nuclear and cytoplasmic fluorescence is exposed. G: Quantification showing nuclear mean integrated density of c-Rel for all female donors analyzed (n=3, mean ± SEM) and the statisical analysis performed. Normality of the data set was refuted using Shapiro-Wilk normality test. Non-parametric Kruskal-Wallis (***$p \leq 0.001$) and Tukey's post hoc test (***$p \leq 0.001$) revealed significant differences in nuclear c-Rel as indicated.

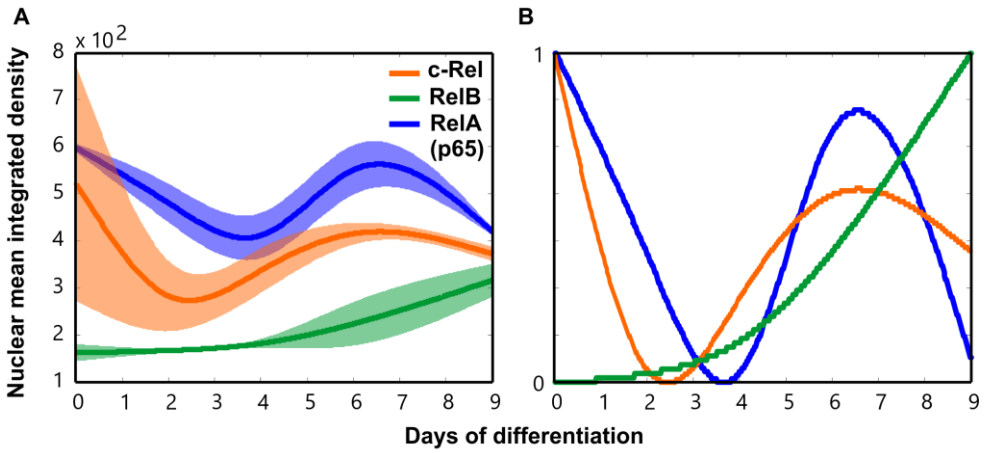

Figure 5-5. NF-κB subunit composition in early dopaminergic differentiation. A: Overview of the NF-κB-Rel subunit distribution showing the nuclear mean integrated density plotted as the median with the median absolute deviation as the variance range. B: Diagram showing NF-κB subunit distribution during early stages of dopaminergic differentiation. Nuclear mean integrated density shown as the median normalized to the range from 0 to 1. The curve for each subunit is represented as indicated.

of differentiation in the early phase (Non-parametric Kruskal-Wallis ***$p \leq 0.001$ and Tukey's post hoc test ***$p \leq 0.001$). These results strongly suggest the presence of a nuclear c-Rel peak during dopaminergic differentiation, indicating that c-Rel might have an essential function during early stages of dopaminergic differentiation.

5.1.5 Dopaminergic differentiation capability of female and male-derived ITSCs

We further analyzed the ability of female and male-derived ITSCs to differentiate into dopaminergic neurons (Fig. 5-6), and we observed that female-derived neurons had a multipolar neuronal morphology, exhibiting a higher amount of neurites, similar to the dopaminergic neuronal mature shape (Fig. 5-6A-C). However male-derived neurons possessed a less complex morphology with a smaller amount of neurites, being most cells bipolar and few of them multipolar. Also male-derived neurons had not a much defined soma, possibly corresponding to a different neuronal subtype or to an immature dopaminergic phenotype. This was supported by the low expression of tyrosine hydroxylase in male-derived neurons, as well as a higher number of cells with a remarkably smaller nucleus, indicating a

higher amount of cell death (Fig. 5-6E-F). These results further indicated the strong capability of female-derived ITSCs to efficiently differentiate into dopaminergic neurons, which was not so evident in male-derived neurons, indicating the existence of a sex-specific difference in dopaminergic differentiation of ITSCs.

5.1.6 Stimulation of dopaminergic differentiated neurons of female and male-derived ITSCs

Furthermore we studied the capability of the dopaminergic neurons to respond to chemical stimulation, specially focusing in the female ITSC-derived neurons, which were shown to differentiate better into this neuronal subtype (Fig. 5-6). We stimulated dopaminergic neurons using TNF-α, 6-hydroxydopamine (6-OHDA), and their combination, and compared to untreated neurons (Fig. 5-7A-F). Subsequently, we analyzed whether the stimulation resulted in the nuclear translocation of the NF-κB-p65 (RelA) by indirect immunodetection, to determine a possible role of p65 in dopaminergic neuronal functionality *in vitro*.

Upon 24h of 100 μM 6-OHDA stimulation, we observed a clear change in neuronal morphology, the cells exhibited an extended soma with a flattened cytoplasm, and enlarged neurites compared to control (Fig. 5-7A, C). We also observed an increase in nuclear NF-κB-p65 activation (Fig. 5-7C, arrowheads) and in neuronal death, after treatment with 6-OHDA. These morphological changes were similar to the alterations observed after treatment with 10 ng/ml TNF-α for 2h (Fig. 5-7B), however in this case, no increase in neuronal death was observed. In contrast, when neurons were pre-treated with TNF-α for 2h upon 6-OHDA stimulation, some neurons maintained their multipolar morphology which was very similar to the one observed in untreated neurons (Fig. 5-7D, arrow), suggesting there was neuroprotection of some cells, although there was still a reduction of neurons observed per area that imply some level of neuronal death.

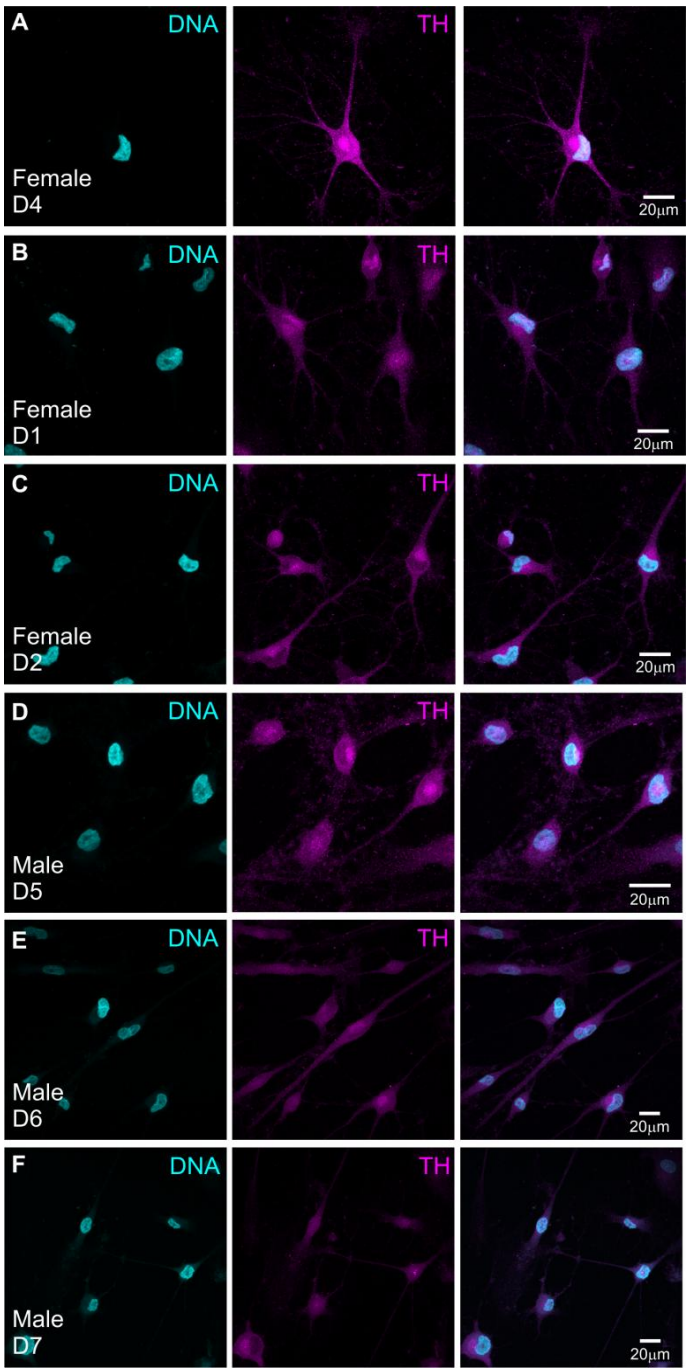

Figure 5-6. Immunocytochemical analysis against tyrosine hydroxylase (TH) performed after 21 days of dopaminergic differentiation of female and male ITSCs. A-C: Dopaminergic neurons differentiated from female ITSC-donors strongly positive for TH, showing multiple neurites. D-F: Dopaminergic neurons differentiated from male ITSC-donors less positive for TH. Male neurons show a lower number of neurites, being most cells bipolar in shape and few of them multipolar.

Due to the nuclear NF-κB-p65 activation observed after the stimulation of dopaminergic neurons, we quantified the nuclear fluorescence using the nuclear mean integrated density (Fig. 5-7E-H), where each female donor showed a particular nuclear p65 curve for the different treatments. Statistical analysis demonstrated that only TNF-α-stimulation showed a clear significant increase in nuclear RelA activation, compared to the untreated control, and it also showed a significant increase compared to 6-OHDA stimulation alone and upon TNF-α-pretreatment (Fig. 5-7H, non-parametric Kruskal-Wallis test, ***$p \leq 0.001$, Tukey's post hoc test ***$p \leq 0.001$, n=3). In particular, this might be due to the high variance on the basal level of p65 observed between the different donors, and also to the variance of nuclear-p65 within 6-OHDA treatment. Thus, these results show that the basal activation of p65 is similar to its activation after treatment with 6-OHDA and TNF-α/6-OHDA. Thus, NF-κB-p65 function upon 6-OHDA stimulation or TNF-α/24h 6-OHDA remains to be determined due to their similarity on p65 level to the untreated control.

Due to the changes in neuronal morphology and death observed in the immunocytochemical assays, the death rate of female-derived dopaminergic neurons after the different stimulations were calculated (Fig. 5-8A), although there was a clear trend in the death rate to increase in neurons treated with 6-OHDA, no significant differences were observed between the treatments and the untreated neurons. Furthermore, in the case of male-differentiated ITSCs, statistical analysis showed similar significant differences, as the ones obtained for female-differentiated dopaminergic neurons (Suppl. fig. 6H, non-parametric Kruskal-Wallis test, ***$p \leq 0.001$, Tukey's post hoc test ***$p \leq 0.001$, n=3). Therefore we analyzed the death rate for the different treatments of the male-derived neurons and compared to the female death rate (Fig. 5-8B). In this manner, we observed that male-derived neurons had a higher tendency to die in most treatments, compared to female dopaminergic neurons, with the exception of TNF-α treatment, however these differences were not statistically relevant. Male-derived neurons showed a similar trend in the death rate of 6-OHDA treated and control neurons, in comparison to female neurons, and both female- and male-derived neurons showed some reduction in death rate

after pre-treatment with TNF-α before 6-OHDA treatment. These preliminary findings propose a possible neuroprotection induced by the activation of NF-κB-p65 mediated by TNF-α-pretreatment in both sexes. Nevertheless, more experiments need to be done to further prove this neuroprotection effect, and the sex-specific differences that might be related.

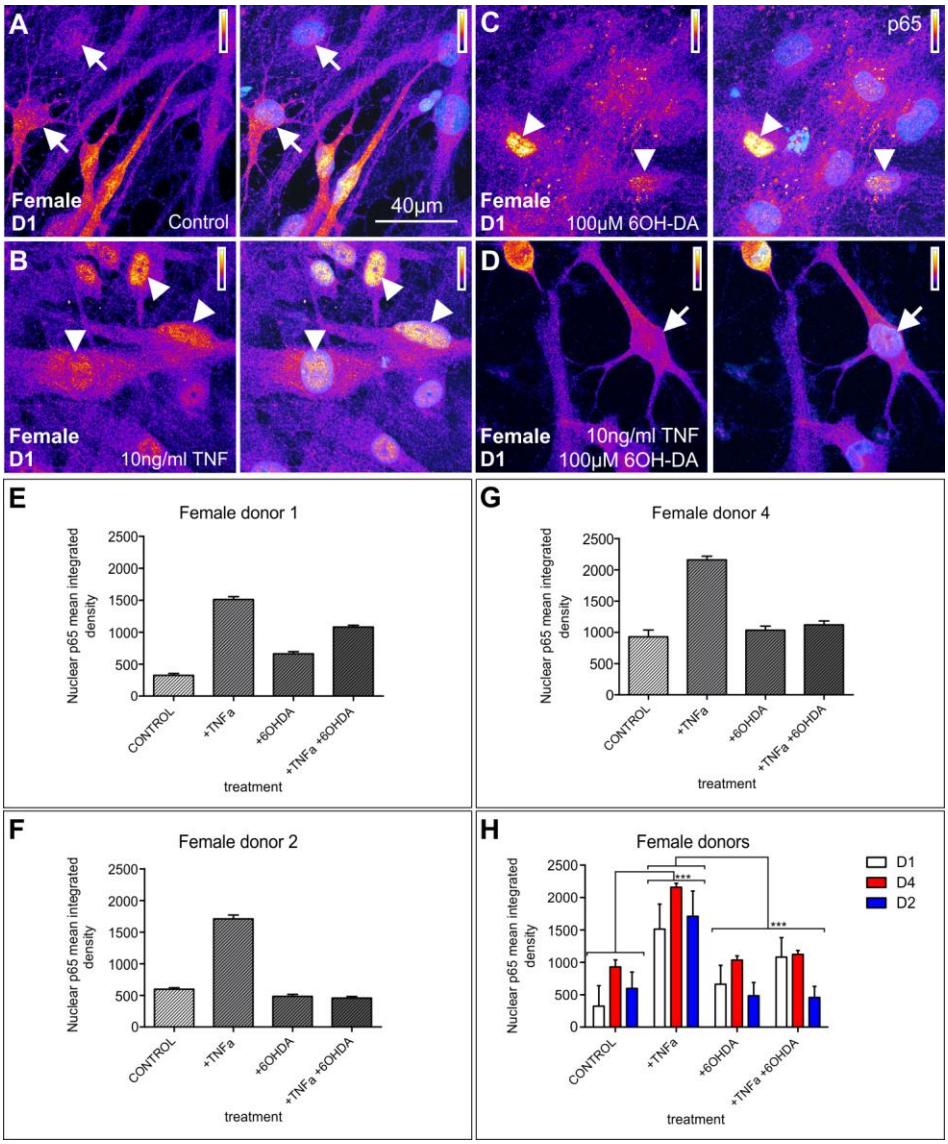

Figure 5-7. Stimulation of dopaminergic differentiated neurons of female-derived ITSCs. A-D: Immunocytochemical assays labeling p65 of female-derived dopaminergic neurons, after treatment with TNF-α, 6-hydroxydopamine (6OHDA), and their combination. Arrows: low endogenous p65 nuclear activity, arrowheads: strong p65 activity. E-G: Quantification analysis of nuclear mean integrated density of p65 after stimulation of dopaminergic differentiated ITSCs shown for the three female donors analyzed. H: Quantiication showing nuclear mean integrated density of p65 after treatment of dopaminergic neurons shown for all female donors (n=3, mean ± SEM) and the statisical analysis performed. Normality was refuted using Shapiro-Wilk normality test. Non-parametric Kruskal-Wallis (***p≤0.001) and Tukey's test (***p≤0.001) revealed significant differences in nuclear p65 as indicated.

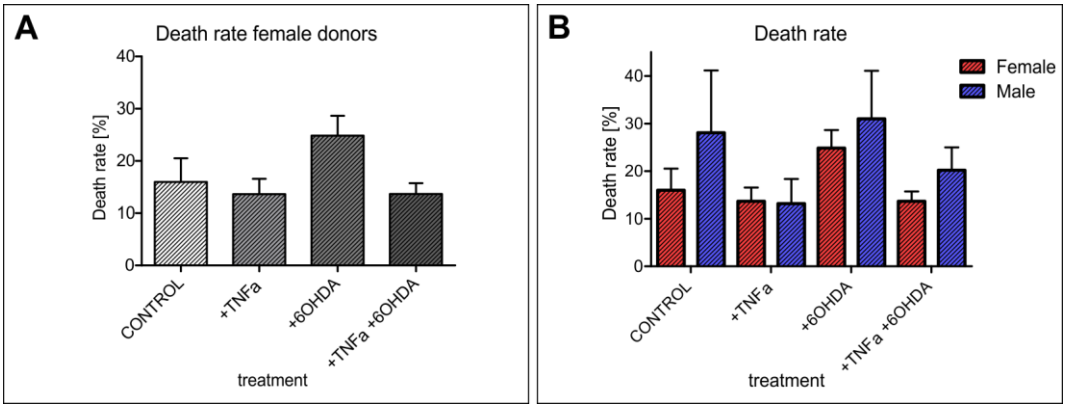

Figure 5-8. Death rate of dopaminergic differentiated ITSCs upon drug treatment. A: Death rate of female-derived dopaminergic neurons. B: Death rate of female versus male-derived dopaminergic-differentiated ITSCs. Statistic analysis using non parametric Kruskal-Wallis test showed no significant differences in neuronal death between the

5.2 Discussion

The present work describes the central function of NF-κB-Rel family members, Rel-A, c-Rel and RelB during dopaminergic neuronal differentiation of human inferior turbinate stem cells. In this work, we efficiently differentiated dopaminergic neurons reproducing and extending previous findings of our lab[40], as verified by the morphological changes into a neuronal phenotype observed and the upregulation of dopamine and tyrosine hydroxylase after 21 days of differentiation. We further characterized the NF-κB subunit composition during early stages of differentiation, and we demonstrated that RelA (p65) was activated during an early phase and gradually decreased, having a strong nuclear increase at day 6. During RelA inactivation, an increase in nuclear c-Rel was observed, showing an activation peak between days 4 and 6. In contrast, RelB had an extremely low nuclear level until day 6, where a significant increase was observed indicating a function at later timepoints. These results strongly suggested that NF-κB activity is strictly regulated during dopaminergic differentiation. In this way, RelA was shown to have an important role during the initial phase that could be related to cell attachment, then, c-Rel seemed to take over during a medial phase of differentiation, showing a clear peak directly afterwards, suggesting a major function during early dopaminergic differentiation. Finally, RelA and RelB significantly increased at day 6, further demonstrating that these subunits are essential at later

timepoints, during a final phase (Fig. 5-5). Furthermore RelB increase at day 6 suggested that it might have an even higher peak at later timepoints, and thus it can have an important function during late differentiation.

Interestingly, we further observed strong differences in the ability of female and male-derived ITSCs to differentiate into dopaminergic neurons. Neurons derived from female donors showed a complex neuronal morphology after 21 days of differentiation, and a higher expression level of tyrosine hydroxylase compared to neurons derived from male donors. In addition, male-derived neurons showed a lower neuronal complexity, evidenced by a minor number of neurites, indicative of the differentiation of these cells into an immature dopaminergic phenotype or into another neuronal subtype. Male-derived neurons also showed an extremely small nuclear size, supporting a higher death rate in comparison to female-derived neurons. This might be due to their lower capacity to differentiate into dopaminergic neurons, thus cells unable to proceed their differentiation undergo apoptosis. These findings confirm the existence of sex-dependent differences in the differentiation of ITSCs into the dopaminergic lineage.

Furthermore, we evaluated the functionality of dopaminergic neurons by chemical stimulation. In the present work, ITSC-derived human dopaminergic neurons revealed a significant increase in nuclear translocation of NF-κB-p65 induced by TNF-α-treatment, indicating a crucial role of NF-κB-signalling in neuronal dopaminergic function, as we also demonstrated for ITSC-derived glutamatergic neurons (see chapter 3). TNF-α is a cytokine mediating the activation of the canonical NF-κB-signalling pathway[124-125], by binding to its receptors TNFR1 and TNFR2 which are broadly expressed in the nervous system [128-130]. TNF-α plays a dual role in neurodegenerative diseases, since stimulation via TNFR1 is predominantly associated with neurodegeneration, and stimulation via TNFR2 is involved in neuroprotection and tissue regeneration[173]. In addition, an *in vitro* model of Parkinson disease showed that induction with a human selective TNFR2 agonist was able to rescue neurons upon induction of cell death by 6-OHDA[174].

Stimulation of dopaminergic neurons using 6-hydroxydopamine, exhibited a strong alteration in the neuronal morphology regardless of the sex of the donor, providing evidence that these neurons respond to the

neurotoxin, however there was a higher tendency to die in male-derived neurons, compared to their female counterpart. Although the differences observed in the death rate between female- and male-derived neurons were not significantly different, our findings indicate a higher tendency in male-derived neurons to die upon 6-OHDA-treatment, in comparison to female-derived neurons. These results are in line with the gender differences observed in PD where more men are diagnosed with the disease than women (by a ratio of 2:1)[175]. Moreover, our results introduce a neuroprotection role induced by the activation of NF-κB-p65 mediated by TNF-α-pretreatment upon 6-OHDA-treatment of dopaminergic neurons derived from donors from both sexes. Indeed, additional analysis needs to be done to further demonstrate this neuroprotective effect, and also the possible sex-specific differences that might be related to it. Additionally, neuronal survival could be promoted using lowered oxygen levels during differentiation, that was shown to enhance proliferation and neuronal survival during dopaminergic differentiation on CNS precursors *in vitro*[176].

Furthermore, as the statistical analysis pointed out 6-OHDA-treated dopaminergic neurons and TNF-α/6-OHDA-treated neurons showed a similar nuclear RelA level compared to the basal state in untreated neurons. This is probably due to the high variance observed in nuclear p65 level in control neurons among the different donors, this elevated heterogeneity might be masking the real differences between the treated and the untreated neurons. Therefore, to determine a real difference we should increase the N, by increasing the number of donors analyzed or the number of replicates used to diminish the variance observed. Besides, the concentration of 6-OHDA used, could have been too low to produce a strong neurotoxic effect, even if the neurons were stressed as shown by the morphological alterations observed. Moreover, these dopaminergic neurons were able to produce dopamine and tyrosine hydroxylase, which are essential for normal neuronal function. It is thus possible that endogenous dopamine masked in part the effect of 6-OHDA stimulation in nuclear-p65 activation, however we used a higher level, probably saturated that makes this unlikely. Nonetheless, this could also be due to the timepoints analyzed and the dynamics in NF-κB-signaling. It is known that NF-κB-p65 nuclear dynamics upon TNF-α stimulation, is initially very high and decreases over

time, thus something similar might be happening upon 6-OHDA stimulation. Thus, if the signaling dynamics vary depending on the stimuli used, NF-κB-p65 peak might have a differential temporal pattern depending on the stimuli used. Therefore, the nuclear-p65 activation induced by TNF-α could be completely different to the one induced by 6-OHDA. Hence, in order to determine a clear difference we should optimize the concentration of 6-OHDA utilized as well as the treatment duration.

Outlook

6

In the presented study, we efficiently differentiated and validated the functionality of glutamatergic neurons derived from inferior turbinate stem cells, and we further demonstrated a key role of NF-κB-p65 in sex-specific neuroprotection during their maturation after oxidative stress insult. In this way, our findings showed a significantly elevated sensitivity of female-derived neurons to oxidative stress-induced neuronal death and to NF-κB-dependent neuroprotection compared to male-derived neurons. These were accompanied by a differential expression of NF-κB-p65 target genes in a sex-dependent manner. In addition, we further revealed TNF-α stimulation of glutamatergic neurons, induced NF-κB-c-Rel nuclear translocation. Thus, an interesting study to be carried on in the near future is the analysis of the function of c-Rel during H_2O_2-mediated oxidative stress and TNF-α-mediated neuroprotection in glutamatergic neurons. It is sensible to think that both subunits RelA and c-Rel are affected during TNF-α-mediated neuroprotection, and thus c-Rel might also induce the expression of a special set of genes that could also be sex-specific and complement the regulatory mechanism observed. Furthermore, as the entire mechanism involved in this process was not completely elucidated, sex-specific investigation is essential. An important point to follow up this research project is to study the mechanisms regulating TNF-α-mediated neuroprotection at the chromatin and DNA level. In this way, epigenetic regulation mechanisms such as DNA methylation, histone deacetylation, or other histone post translational modifications controlling chromatin

remodelling and DNA access by transcription factors should be further analyzed.

In addition, we demonstrated for the first time a key role of NF-κB subunits during neuronal differentiation of human inferior turbinate stem cells. We were able to determine the NF-κB subunit composition present during early stages of glutamatergic and dopaminergic neuronal differentiation. In the case of glutamatergic differentiation, NF-κB subunit pattern showed a nuclear activation of RelB/p52 heterodimers during an early phase, and a c-Rel nuclear activation peak during a later phase of differentiation. While the classical NF-κB subunits, RelA and p50 had no part during this differentiation. In contrast, during dopaminergic differentiation RelA had an important role during the initial phase of differentiation, whereas c-Rel showed a clear activation peak during the medial phase of differentiation, and finally RelA and RelB were significantly increased at a later and final phase of dopaminergic differentiation. These results confirmed that NF-κB activity is strictly regulated during neuronal differentiation, and thus NF-κB-signalling might have a particular temporal pattern during the differentiation towards any cell fate. Therefore, it would be of outmost importance to further determine NF-κB subunit composition during early and late differentiation of inferior turbinate stem cells into different mesodermal lineages, such as osteoblasts, adipocytes and chondrogenic cells, to gain insight in the NF-κB regulatory network involved during human stem cell differentiation.

Furthermore, here we confirmed that modifying the expression of the NF-κB subunits involved in a particular differentiation mechanism, we can shift the differentiation into a completely different cell fate, with the respective potential restrictions in the fate lineage. In this work we were able to switch the cell fate from the glutamatergic phenotype to the oligodendrocyte phenotype by the sole inhibition of c-Rel using pentoxifylline, during the differentiation procedure. These findings further implicate that the NF-κB regulatory network involved during stem cell differentiation is somehow interconnected. Therefore, another approach to continue the study of the role of NF-κB in the regulation during differentiation is the use of CRISPR/Cas9 to eliminate the different NF-κB

subunits and elucidate their role during different directed differentiations. This could be a particularly helpful tool to determine other possible shifts in cell fate during differentiation. However, it is a difficult task to apply this strategy in primary cells, which are not easily transfected especially with huge plasmids (>9Kb), unless the lentivirus approach for transduction is established and performed instead.

Furthermore, the investigation of the mechanisms underlying differentiation could be studied from a different perspective. An interesting way to enlighten the changes observed during differentiation, could be to determine the methylation state of the cells before and after the differentiation. One would expect that DNA methylation has a particular pattern in undifferentiated stem cells and it becomes modified upon differentiation, making certain DNA regions accessible for transcription factors, with the concomitant expression of specific target genes for differentiation and specification into a particular lineage. Thus, this would be a very important hint to determine the mechanisms implicated during differentiation.

Moreover, we further analyzed differences in the ability of female and male-derived ITSCs to differentiate into dopaminergic neurons, and we determined differences in neuronal complexity, in a sex-dependent manner. We also studied their capability to respond to stimulation using TNF-α, 6-hydroxydopamine, and their combination. Hence, stimulation of dopaminergic neurons using 6-hydroxydopamine, evidenced a strong alteration in neuronal morphology, evidencing neurons were able to respond to 6-OHDA, however male-derived neurons had a higher tendency to die, compared to female-derived neurons. Although these differences were not significantly relevant, these results are in line with the gender differences observed in Parkinson's disease. Our results bring in a neuroprotection function, by NF-κB-p65 mediated activation induced by TNF-α-pretreatment upon 6-OHDA-treatment of female- and male-derived dopaminergic neurons. Indeed, additional investigation in this direction needs to be done to demonstrate these preliminary results about this potential neuroprotective effect, and also the possible sex-specific differences that might be related to it. Therefore, insight into this line of investigation would help to improve our understanding about the characteristics of sex-specific differences in neuronal differentiation and neurodegenerative

diseases as well as to further develop appropriate therapies for their treatment.

References

7

1 Hauser, S. *et al.* Isolation of novel multipotent neural crest-derived stem cells from adult human inferior turbinate. *Stem Cells Dev* **21**, 742-756, doi: https://doi.org/10.1089/scd.2011.0419 (2012).

2 Grinberg-Bleyer, Y. *et al.* NF-kappaB c-Rel Is Crucial for the Regulatory T Cell Immune Checkpoint in Cancer. *Cell* **170**, 1096-1108 e1013, doi: https://doi.org/10.1016/j.cell.2017.08.004 (2017).

3 Kaltschmidt, B., Kaltschmidt, C. & Widera, D. Adult craniofacial stem cells: sources and relation to the neural crest. *Stem Cell Rev* **8**, 658-671, doi: https://doi.org/10.1007/s12015-011-9340-9 (2012).

4 Narytnyk, A. *et al.* Differentiation of human epidermal neural crest stem cells (hEPI-NCSC) into virtually homogenous populations of dopaminergic neurons. *Stem Cell Rev* **10**, 316-326, doi:10.1007/s12015-013-9493-9 [doi] (2014).

5 Daley, G. Q. Stem cells and the evolving notion of cellular identity. *Philos Trans R Soc Lond B Biol Sci* **370**, 20140376, doi: https://doi.org/10.1098/rstb.2014.0376 (2015).

6 Van de Velde, H., Cauffman, G., Tournaye, H., Devroey, P. & Liebaers, I. The four blastomeres of a 4-cell stage human embryo are able to develop individually into blastocysts with inner cell mass and trophectoderm. *Hum Reprod* **23**, 1742-1747, doi: https://doi.org/10.1093/humrep/den190 (2008).

7 Dulak, J., Szade, K., Szade, A., Nowak, W. & Jozkowicz, A. Adult stem cells: hopes and hypes of regenerative medicine. *Acta Biochim Pol* **62**, 329-337, doi: https://doi.org/10.18388/abp.2015˙1023 (2015).

8 Koestenbauer, S. *et al.* Embryonic stem cells: similarities and differences between human and murine embryonic stem cells. *Am J Reprod Immunol* **55**, 169-180, doi: https://doi.org/10.1111/j.1600-0897.2005.00354.x (2006).

9 Smith, K. P., Luong, M. X. & Stein, G. S. Pluripotency: toward a gold standard for human ES and iPS cells. *J Cell Physiol* **220**, 21-29, doi:10.1002/jcp.21681 [doi] (2009).

10 Evans, M. J. & Kaufman, M. H. Establishment in culture of pluripotential cells from mouse embryos. *Nature* **292**, 154-156 (1981).

11 Martin, G. R. Isolation of a pluripotent cell line from early mouse embryos cultured in medium conditioned by teratocarcinoma stem cells. *Proc Natl Acad Sci U S A* **78**, 7634-7638 (1981).

12 Reubinoff, B. E., Pera, M. F., Fong, C. Y., Trounson, A. & Bongso, A. Embryonic stem cell lines from human blastocysts: somatic differentiation in vitro. *Nat Biotechnol* **18**, 399-404, doi: https://doi.org/10.1038/74447 (2000).

13 Thomson, J. A. *et al.* Embryonic stem cell lines derived from human blastocysts. *Science* **282**, 1145-1147 (1998).

14 Nichols, J. *et al.* Formation of pluripotent stem cells in the mammalian embryo depends on the POU transcription factor Oct4. *Cell* **95**, 379-391, doi: https://doi.org/10.1016/S0092-8674(00)81769-9 (1998).

15 Chambers, I. *et al.* Functional expression cloning of Nanog, a pluripotency sustaining factor in embryonic stem cells. *Cell* **113**, 643-655 (2003).

16 Mitsui, K. *et al.* The homeoprotein Nanog is required for maintenance of pluripotency in mouse epiblast and ES cells. *Cell* **113**, 631-642 (2003).

17 Meshorer, E. & Misteli, T. Chromatin in pluripotent embryonic stem cells and differentiation. *Nat Rev Mol Cell Biol* **7**, 540-546, doi: https://doi.org/10.1038/nrm1938 (2006).

18 Becker, K. A. *et al.* Self-renewal of human embryonic stem cells is supported by a shortened G1 cell cycle phase. *J Cell Physiol* **209**, 883-893, doi: https://doi.org/10.1002/jcp.20776 (2006).

19 Ghule, P. N. *et al.* Cell cycle dependent phosphorylation and subnuclear organization of the histone gene regulator p220(NPAT) in human embryonic stem cells. *J Cell Physiol* **213**, 9-17, doi: https://doi.org/10.1002/jcp.21119 (2007).

20 Ghule, P. N. *et al.* Staged assembly of histone gene expression machinery at subnuclear foci in the abbreviated cell cycle of human embryonic stem cells. *Proc Natl Acad Sci U S A* **105**, 16964-16969, doi: https://doi.org/10.1073/pnas.0809273105 (2008).

21 Houbaviy, H. B., Murray, M. F. & Sharp, P. A. Embryonic stem cell-specific MicroRNAs. *Dev Cell* **5**, 351-358 (2003).

22 Suh, M. R. *et al.* Human embryonic stem cells express a unique set of microRNAs. *Dev Biol* **270**, 488-498, doi: https://doi.org/10.1016/j.ydbio.2004.02.019 (2004).

23 Takahashi, K. & Yamanaka, S. Induction of pluripotent stem cells from mouse embryonic and adult fibroblast cultures by defined factors. *Cell* **126**, 663-676, doi: https://doi.org/10.1016/j.cell.2006.07.024 (2006).

24 Walia, B., Satija, N., Tripathi, R. P. & Gangenahalli, G. U. Induced pluripotent stem cells: fundamentals and applications of the reprogramming process and its ramifications on regenerative medicine. *Stem Cell Rev* **8**, 100-115, doi: https://doi.org/10.1007/s12015-011-9279-x (2012).

25 Trounson, A. The production and directed differentiation of human embryonic stem cells. *Endocr Rev* **27**, 208-219, doi: https://doi.org/10.1210/er.2005-0016 (2006).

26 Avgustinova, A. & Benitah, S. A. Epigenetic control of adult stem cell function. *Nat Rev Mol Cell Biol* **17**, 643-658, doi: https://doi.org/10.1038/nrm.2016.76 (2016).

27 Chiu, R. C. Adult stem cell therapy for heart failure. *Expert Opin Biol Ther* **3**, 215-225, doi: https://doi.org/10.1517/14712598.3.2.215 (2003).

28 Liu, S. *et al.* Strategies to Optimize Adult Stem Cell Therapy for Tissue Regeneration. *Int J Mol Sci* **17**, doi: https://doi.org/10.3390/ijms17060982 (2016).

29 Le Douarin, N. M., Calloni, G. W. & Dupin, E. The stem cells of the neural crest. *Cell Cycle* **7**, 1013-1019, doi: https://doi.org/10.4161/cc.7.8.5641 (2008).

30 Nikitina, N., Sauka-Spengler, T. & Bronner-Fraser, M. Chapter 1. Gene regulatory networks in neural crest development and evolution. *Curr Top Dev Biol* **86**, 1-14, doi: https://doi.org/10.1016/S0070-2153(09)01001-1 (2009).

31 Crane, J. F. & Trainor, P. A. Neural crest stem and progenitor cells. *Annu Rev Cell Dev Biol* **22**, 267-286, doi: https://doi.org/10.1146/annurev.cellbio.22.010305.103814 (2006).

32 Cano, A. *et al.* The transcription factor snail controls epithelial-mesenchymal transitions by repressing E-cadherin expression. *Nat Cell Biol* **2**, 76-83, doi: https://doi.org/10.1038/35000025 (2000).

33 Toma, J. G. *et al.* Isolation of multipotent adult stem cells from the dermis of mammalian skin. *Nat Cell Biol* **3**, 778-784, doi: https://doi.org/10.1038/ncb0901-778 (2001).

34 Brandl, C., Florian, C., Driemel, O., Weber, B. H. & Morsczeck, C. Identification of neural crest-derived stem cell-like cells from the corneal limbus of juvenile mice. *Exp Eye Res* **89**, 209-217, doi: https://doi.org/10.1016/j.exer.2009.03.009 (2009).

35 Widera, D. *et al.* Highly efficient neural differentiation of human somatic stem cells, isolated by minimally invasive periodontal surgery. *Stem Cells Dev* **16**, 447-460, doi: https://doi.org/10.1089/scd.2006.0068 (2007).

36 Techawattanawisal, W. *et al.* Isolation of multipotent stem cells from adult rat periodontal ligament by neurosphere-forming culture system. *Biochem Biophys Res Commun* **357**, 917-923, doi: https://doi.org/10.1016/j.bbrc.2007.04.031 (2007).

37 Waddington, R. J., Youde, S. J., Lee, C. P. & Sloan, A. J. Isolation of distinct progenitor stem cell populations from dental pulp. *Cells Tissues Organs* **189**, 268-274, doi: https://doi.org/10.1159/000151447 (2009).

38 Widera, D. *et al.* Adult palatum as a novel source of neural crest-related stem cells. *Stem Cells* **27**, 1899-1910, doi: https://doi.org/10.1002/stem.104 (2009).

39 Park, D. *et al.* Nestin is required for the proper self-renewal of neural stem cells. *Stem Cells* **28**, 2162-2171, doi: https://doi.org/10.1002/stem.541 (2010).

40 Muller, J. *et al.* Intrastriatal transplantation of adult human neural crest-derived stem cells improves functional outcome in parkinsonian rats. *Stem Cells Transl Med* **4**, 31-43, doi: https://doi.org/10.5966/sctm.2014-0078 (2015).

41 Kriegstein, A. & Alvarez-Buylla, A. The glial nature of embryonic and adult neural stem cells. *Annu Rev Neurosci* **32**, 149-184, doi: https://doi.org/10.1146/annurev.neuro.051508.135600 (2009).

42 Grabel, L. Developmental origin of neural stem cells: the glial cell that could. *Stem Cell Rev* **8**, 577-585, doi: https://doi.org/10.1007/s12015-012-9349-8 (2012).

43 Dupin, E. & Coelho-Aguiar, J. M. Isolation and differentiation properties of neural crest stem cells. *Cytometry A* **83**, 38-47, doi: https://doi.org/10.1002/cyto.a.22098 (2013).

44 Temple, S. The development of neural stem cells. *Nature* **414**, 112-117, doi: https://doi.org/10.1038/35102174 (2001).

45 Doetsch, F. The glial identity of neural stem cells. *Nat Neurosci* **6**, 1127-1134, doi: https://doi.org/10.1038/nn1144 (2003).

46 Gaiano, N. & Fishell, G. The role of notch in promoting glial and neural stem cell fates. *Annu Rev Neurosci* **25**, 471-490, doi: https://doi.org/10.1146/annurev.neuro.25.030702.130823 (2002).

47 Zhang, S. C. Neural subtype specification from embryonic stem cells. *Brain Pathol* **16**, 132-142, doi: https://doi.org/10.1111/j.1750-3639.2006.00008.x (2006).

48 Miron, V. E., Kuhlmann, T. & Antel, J. P. Cells of the oligodendroglial lineage, myelination, and remyelination. *Biochim Biophys Acta* **1812**, 184-193, doi: https://doi.org/10.1016/j.bbadis.2010.09.010 (2011).

49 Sarkar, A. & Hochedlinger, K. The sox family of transcription factors: versatile regulators of stem and progenitor cell fate. *Cell Stem Cell* **12**, 15-30, doi: https://doi.org/10.1016/j.stem.2012.12.007 (2013).

50 Boyer, L. A. *et al.* Core transcriptional regulatory circuitry in human embryonic stem cells. *Cell* **122**, 947-956, doi: https://doi.org/10.1016/j.cell.2005.08.020 (2005).

51 Chambers, I. & Tomlinson, S. R. The transcriptional foundation of pluripotency. *Development* **136**, 2311-2322, doi: https://doi.org/10.1242/dev.024398 (2009).

52 Rossant, J. & Tam, P. P. Blastocyst lineage formation, early embryonic asymmetries and axis patterning in the mouse. *Development* **136**, 701-713, doi: https://doi.org/10.1242/dev.017178 (2009).

53 Murry, C. E. & Keller, G. Differentiation of embryonic stem cells to clinically relevant populations: lessons from embryonic development. *Cell* **132**, 661-680, doi: https://doi.org/10.1016/j.cell.2008.02.008 (2008).

54 Schwartz, P. H., Brick, D. J., Stover, A. E., Loring, J. F. & Muller, F. J. Differentiation of neural lineage cells from human pluripotent stem cells. *Methods* **45**, 142-158, doi: https://doi.org/10.1016/j.ymeth.2008.03.007 (2008).

55 D'Amour, K. A. *et al.* Efficient differentiation of human embryonic stem cells to definitive endoderm. *Nat Biotechnol* **23**, 1534-1541, doi: https://doi.org/10.1038/nbt1163 (2005).

56 Imamura, T., Uesaka, M. & Nakashima, K. Epigenetic setting and reprogramming for neural cell fate determination and differentiation. *Philos Trans R Soc Lond B Biol Sci* **369**, doi: https://doi.org/10.1098/rstb.2013.0511 (2014).

57 Wichterle, H., Lieberam, I., Porter, J. A. & Jessell, T. M. Directed differentiation of embryonic stem cells into motor neurons. *Cell* **110**, 385-397, doi: https://doi.org/10.1016/S0092-8674(02)00835-8 (2002).

58 Davis-Dusenbery, B. N., Williams, L. A., Klim, J. R. & Eggan, K. How to make spinal motor neurons. *Development* **141**, 491-501, doi: https://doi.org/10.1242/dev.097410 (2014).

59 Kirkeby, A. *et al.* Generation of regionally specified neural progenitors and functional neurons from human embryonic stem cells under defined conditions. *Cell Rep* **1**, 703-714, doi: https://doi.org/10.1016/j.celrep.2012.04.009 (2012).

60 Tao, Y. & Zhang, S. C. Neural Subtype Specification from Human Pluripotent Stem Cells. *Cell Stem Cell* **19**, 573-586, doi: https://doi.org/10.1016/j.stem.2016.10.015 (2016).
61 Liu, H. & Zhang, S. C. Specification of neuronal and glial subtypes from human pluripotent stem cells. *Cell Mol Life Sci* **68**, 3995-4008, doi: https://doi.org/10.1007/s00018-011-0770-y (2011).
62 Gabilondo, H. *et al.* Neuronal Cell Fate Specification by the Convergence of Different Spatiotemporal Cues on a Common Terminal Selector Cascade. *PLoS Biol* **14**, e1002450, doi: https://doi.org/10.1371/journal.pbio.1002450 (2016).
63 Howard, M. J. Mechanisms and perspectives on differentiation of autonomic neurons. *Dev Biol* **277**, 271-286, doi: https://doi.org/10.1016/j.ydbio.2004.09.034 (2005).
64 Costa, M. R. & Muller, U. Specification of excitatory neurons in the developing cerebral cortex: progenitor diversity and environmental influences. *Front Cell Neurosci* **8**, 449, doi: https://doi.org/10.3389/fncel.2014.00449 (2014).
65 Song, H. *et al.* Ascl1 and Helt act combinatorially to specify thalamic neuronal identity by repressing Dlxs activation. *Dev Biol* **398**, 280-291, doi: https://doi.org/10.1016/j.ydbio.2014.12.003 (2015).
66 Li, X. J. *et al.* Coordination of sonic hedgehog and Wnt signaling determines ventral and dorsal telencephalic neuron types from human embryonic stem cells. *Development* **136**, 4055-4063, doi: https://doi.org/10.1242/dev.036624 (2009).
67 Kiecker, C. & Lumsden, A. The role of organizers in patterning the nervous system. *Annu Rev Neurosci* **35**, 347-367, doi: https://doi.org/10.1146/annurev-neuro-062111-150543 (2012).
68 Hevner, R. F., Hodge, R. D., Daza, R. A. & Englund, C. Transcription factors in glutamatergic neurogenesis: conserved programs in neocortex, cerebellum, and adult hippocampus. *Neurosci Res* **55**, 223-233, doi: https://doi.org/10.1016/j.neures.2006.03.004 (2006).
69 Chinta, S. J. & Andersen, J. K. Dopaminergic neurons. *Int J Biochem Cell Biol* **37**, 942-946, doi: https://doi.org/10.1016/j.biocel.2004.09.009 (2005).
70 Ono, Y. *et al.* Differences in neurogenic potential in floor plate cells along an anteroposterior location: midbrain dopaminergic neurons originate from mesencephalic floor plate cells. *Development* **134**, 3213-3225, doi: https://doi.org/10.1242/dev.02879 (2007).
71 Placzek, M. & Briscoe, J. The floor plate: multiple cells, multiple signals. *Nat Rev Neurosci* **6**, 230-240, doi: https://doi.org/10.1038/nrn1628 (2005).
72 Abeliovich, A. & Hammond, R. Midbrain dopamine neuron differentiation: factors and fates. *Dev Biol* **304**, 447-454, doi: https://doi.org/10.1016/j.ydbio.2007.01.032 (2007).
73 Prakash, N. *et al.* A Wnt1-regulated genetic network controls the identity and fate of midbrain-dopaminergic progenitors in vivo. *Development* **133**, 89-98, doi: https://doi.org/10.1242/dev.02181 (2006).
74 Andersson, E. *et al.* Identification of intrinsic determinants of midbrain dopamine neurons. *Cell* **124**, 393-405, doi: https://doi.org/10.1016/j.cell.2005.10.037 (2006).

75 Chung, S. *et al.* Wnt1-lmx1a forms a novel autoregulatory loop and controls midbrain dopaminergic differentiation synergistically with the SHH-FoxA2 pathway. *Cell Stem Cell* **5**, 646-658, doi: https://doi.org/10.1016/j.stem.2009.09.015 (2009).
76 Xi, J. *et al.* Specification of midbrain dopamine neurons from primate pluripotent stem cells. *Stem Cells* **30**, 1655-1663, doi: https://doi.org/10.1002/stem.1152 (2012).
77 Cai, J. *et al.* Dopaminergic neurons derived from human induced pluripotent stem cells survive and integrate into 6-OHDA-lesioned rats. *Stem Cells Dev* **19**, 1017-1023, doi: https://doi.org/10.1089/scd.2009.0319 (2010).
78 Swistowski, A. *et al.* Efficient generation of functional dopaminergic neurons from human induced pluripotent stem cells under defined conditions. *Stem Cells* **28**, 1893-1904, doi: https://doi.org/10.1002/stem.499 (2010).
79 Yan, Y. *et al.* Directed differentiation of dopaminergic neuronal subtypes from human embryonic stem cells. *Stem Cells* **23**, 781-790, doi: https://doi.org/10.1634/stemcells.2004-0365 (2005).
80 Kriks, S. *et al.* Dopamine neurons derived from human ES cells efficiently engraft in animal models of Parkinson's disease. *Nature* **480**, 547-551, doi: https://doi.org/10.1038/nature10648 (2011).
81 Doi, D. *et al.* Isolation of human induced pluripotent stem cell-derived dopaminergic progenitors by cell sorting for successful transplantation. *Stem Cell Reports* **2**, 337-350, doi: https://doi.org/10.1016/j.stemcr.2014.01.013 (2014).
82 Karin, M. & Lin, A. NF-kappaB at the crossroads of life and death. *Nat Immunol* **3**, 221-227, doi: https://doi.org/10.1038/ni0302-221 (2002).
83 Gavalda, N., Gutierrez, H. & Davies, A. M. Developmental switch in NF-kappaB signalling required for neurite growth. *Development* **136**, 3405-3412, doi:dev.035295 [pii]
10.1242/dev.035295 [doi] (2009).
84 Boersma, M. C. *et al.* A requirement for nuclear factor-kappaB in developmental and plasticity-associated synaptogenesis. *J Neurosci* **31**, 5414-5425, doi: https://doi.org/10.1523/JNEUROSCI.2456-10.2011 (2011).
85 Imielski, Y. *et al.* Regrowing the adult brain: NF-kappaB controls functional circuit formation and tissue homeostasis in the dentate gyrus. *PLoS One* **7**, e30838, doi: https://doi.org/10.1371/journal.pone.0030838 (2012).
86 Kaltschmidt, B. & Kaltschmidt, C. NF-kappaB in the nervous system. *Cold Spring Harb Perspect Biol* **1**, a001271, doi: https://doi.org/10.1101/cshperspect.a001271 (2009).
87 Mattson, M. P. & Meffert, M. K. Roles for NF-kappaB in nerve cell survival, plasticity, and disease. *Cell Death Differ* **13**, 852-860, doi: https://doi.org/10.1038/sj.cdd.4401837 (2006).
88 Hayden, M. S. & Ghosh, S. Regulation of NF-kappaB by TNF family cytokines. *Semin Immunol* **26**, 253-266, doi: https://doi.org/10.1016/j.smim.2014.05.004 (2014).
89 Perkins, N. D. Integrating cell-signalling pathways with NF-kappaB and IKK function. *Nat Rev Mol Cell Biol* **8**, 49-62, doi: https://doi.org/10.1038/nrm2083 (2007).

90 Harhaj, E. W. & Dixit, V. M. Regulation of NF-kappaB by deubiquitinases. *Immunol Rev* **246**, 107-124, doi: https://doi.org/10.1111/j.1600-065X.2012.01100.x (2012).

91 Vajda, F. J. Neuroprotection and neurodegenerative disease. *Journal of clinical neuroscience : official journal of the Neurosurgical Society of Australasia* **9**, 4-8, doi:10.1054/jocn.2001.1027 (2002).

92 Gillies, G. E., Pienaar, I. S., Vohra, S. & Qamhawi, Z. Sex differences in Parkinson's disease. *Frontiers in neuroendocrinology* **35**, 370-384, doi:10.1016/j.yfrne.2014.02.002 (2014).

93 Li, R. & Singh, M. Sex differences in cognitive impairment and Alzheimer's disease. *Frontiers in neuroendocrinology* **35**, 385-403, doi:10.1016/j.yfrne.2014.01.002 (2014).

94 Spychala, M. S., Honarpisheh, P. & McCullough, L. D. Sex differences in neuroinflammation and neuroprotection in ischemic stroke. *Journal of neuroscience research* **95**, 462-471, doi:10.1002/jnr.23962 (2017).

95 Vina, J. & Lloret, A. Why women have more Alzheimer's disease than men: gender and mitochondrial toxicity of amyloid-beta peptide. *Journal of Alzheimer's disease : JAD* **20 Suppl 2**, S527-533, doi:10.3233/JAD-2010-100501 (2010).

96 Henderson, V. W. & Buckwalter, J. G. Cognitive deficits of men and women with Alzheimer's disease. *Neurology* **44**, 90-96 (1994).

97 Demarest, T. G. & McCarthy, M. M. Sex differences in mitochondrial (dys)function: Implications for neuroprotection. *Journal of bioenergetics and biomembranes* **47**, 173-188, doi:10.1007/s10863-014-9583-7 (2015).

98 Bakalkin, G., Yakovleva, T. & Terenius, L. NF-kappa B-like factors in the murine brain. Developmentally-regulated and tissue-specific expression. *Brain Res Mol Brain Res* **20**, 137-146 (1993).

99 Meffert, M. K., Chang, J. M., Wiltgen, B. J., Fanselow, M. S. & Baltimore, D. NF-kappa B functions in synaptic signaling and behavior. *Nat Neurosci* **6**, 1072-1078, doi: https://doi.org/10.1038/nn1110 (2003).

100 Guerrini, L., Blasi, F. & Denis-Donini, S. Synaptic activation of NF-kappa B by glutamate in cerebellar granule neurons in vitro. *Proceedings of the National Academy of Sciences of the United States of America* **92**, 9077-9081 (1995).

101 Kaltschmidt, C., Kaltschmidt, B. & Baeuerle, P. A. Stimulation of ionotropic glutamate receptors activates transcription factor NF-kappa B in primary neurons. *Proceedings of the National Academy of Sciences of the United States of America* **92**, 9618-9622 (1995).

102 Kaltschmidt, B. *et al.* NF-kappaB regulates spatial memory formation and synaptic plasticity through protein kinase A/CREB signaling. *Mol Cell Biol* **26**, 2936-2946, doi: https://doi.org/10.1128/MCB.26.8.2936-2946.2006 (2006).

103 Bowie, A. & O'Neill, L. A. Oxidative stress and nuclear factor-kappaB activation: a reassessment of the evidence in the light of recent discoveries. *Biochem Pharmacol* **59**, 13-23, doi: https://doi.org/10.1016/S0006-2952(99)00296-8 (2000).

104 Kaltschmidt, B., Sparna, T. & Kaltschmidt, C. Activation of NF-kappa B by reactive oxygen intermediates in the nervous system. *Antioxid Redox Signal* **1**, 129-144, doi: https://doi.org/10.1089/ars.1999.1.2-129 (1999).

105 Coyle, J. T. & Puttfarcken, P. Oxidative stress, glutamate, and neurodegenerative disorders. *Science* **262**, 689-695 (1993).
106 Schmidt, K. N., Amstad, P., Cerutti, P. & Baeuerle, P. A. The roles of hydrogen peroxide and superoxide as messengers in the activation of transcription factor NF-kappa B. *Chem Biol* **2**, 13-22, doi:1074-5521(95)90076-4 [pii] (1995).
107 Kaltschmidt, B., Uherek, M., Volk, B., Baeuerle, P. A. & Kaltschmidt, C. Transcription factor NF-kappaB is activated in primary neurons by amyloid beta peptides and in neurons surrounding early plaques from patients with Alzheimer disease. *Proceedings of the National Academy of Sciences of the United States of America* **94**, 2642-2647 (1997).
108 Schreck, R., Rieber, P. & Baeuerle, P. A. Reactive oxygen intermediates as apparently widely used messengers in the activation of the NF-kappa B transcription factor and HIV-1. *EMBO J* **10**, 2247-2258 (1991).
109 Meyer, M., Schreck, R. & Baeuerle, P. A. H2O2 and antioxidants have opposite effects on activation of NF-kappa B and AP-1 in intact cells: AP-1 as secondary antioxidant-responsive factor. *EMBO J* **12**, 2005-2015 (1993).
110 Yanes, O. *et al.* Metabolic oxidation regulates embryonic stem cell differentiation. *Nat Chem Biol* **6**, 411-417, doi: https://doi.org/10.1038/nchembio.364 (2010).
111 Bigarella, C. L., Liang, R. & Ghaffari, S. Stem cells and the impact of ROS signaling. *Development* **141**, 4206-4218, doi: https://doi.org/10.1242/dev.107086 (2014).
112 Widera, D., Mikenberg, I., Elvers, M., Kaltschmidt, C. & Kaltschmidt, B. Tumor necrosis factor alpha triggers proliferation of adult neural stem cells via IKK/NF-kappaB signaling. *BMC Neurosci* **7**, 64, doi: https://doi.org/10.1186/1471-2202-7-64 (2006).
113 Zhang, Y. *et al.* Nuclear factor kappa B signaling initiates early differentiation of neural stem cells. *Stem Cells* **30**, 510-524, doi: https://doi.org/10.1002/stem.1006 (2012).
114 Greiner, J. F. *et al.* Efficient animal-serum free 3D cultivation method for adult human neural crest-derived stem cell therapeutics. *Eur Cell Mater* **22**, 403-419 (2011).
115 Bibel, M., Richter, J., Lacroix, E. & Barde, Y. A. Generation of a defined and uniform population of CNS progenitors and neurons from mouse embryonic stem cells. *Nat Protoc* **2**, 1034-1043, doi: https://doi.org/10.1038/nprot.2007.147 (2007).
116 Choi, D. W., Maulucci-Gedde, M. & Kriegstein, A. R. Glutamate neurotoxicity in cortical cell culture. *J Neurosci* **7**, 357-368 (1987).
117 Hu, X. J. & Ticku, M. K. Chronic ethanol treatment upregulates the NMDA receptor function and binding in mammalian cortical neurons. *Brain Res Mol Brain Res* **30**, 347-356 (1995).
118 Schneider, C. A., Rasband, W. S. & Eliceiri, K. W. NIH Image to ImageJ: 25 years of image analysis. *Nat Methods* **9**, 671-675 (2012).
119 Picelli, S. *et al.* Full-length RNA-seq from single cells using Smart-seq2. *Nature Protocols* **9**, 171, doi: https://doi.org/10.1038/nprot.2014.006 https://www.nature.com/articles/nprot.2014.006#supplementary-information (2014).

120 Hammer O., H., D.A.T., Ryan, P.D. PAST: Paleontological statistics software package for education and data analysis. *Palaeontologia Electronica* **4**, 9pp (2001.).
121 Ruiz-Perera, L. M. *et al.* NF-kappaB p65 directs sex-specific neuroprotection in human neurons. *Sci Rep* **8**, 16012, doi: https://doi.org/10.1038/s41598-018-34394-8 (2018).
122 Kaltschmidt, C., Kaltschmidt, B., Neumann, H., Wekerle, H. & Baeuerle, P. A. Constitutive NF-kappa B activity in neurons. *Molecular and cellular biology* **14**, 3981-3992 (1994).
123 Muth-Kohne, E., Pachernegg, S., Karus, M., Faissner, A. & Hollmann, M. Expression of NMDA receptors and Ca2+-impermeable AMPA receptors requires neuronal differentiation and allows discrimination between two different types of neural stem cells. *Cell Physiol Biochem* **26**, 935-946, doi: https://doi.org/10.1159/000324002 (2010).
124 Varfolomeev, E. & Vucic, D. Intracellular regulation of TNF activity in health and disease. *Cytokine*, doi: https://doi.org/10.1016/j.cyto.2016.08.035 (2016).
125 Peltzer, N., Darding, M. & Walczak, H. Holding RIPK1 on the Ubiquitin Leash in TNFR1 Signaling. *Trends in cell biology* **26**, 445-461, doi:10.1016/j.tcb.2016.01.006 (2016).
126 Hayden, M. S. & Ghosh, S. Shared principles in NF-kappaB signaling. *Cell* **132**, 344-362, doi: https://doi.org/10.1016/j.cell.2008.01.020 (2008).
127 Ben-Neriah, Y. Regulatory functions of ubiquitination in the immune system. *Nat Immunol* **3**, 20-26, doi: https://doi.org/10.1038/ni0102-20 (2002).
128 Kinouchi, K., Brown, G., Pasternak, G. & Donner, D. B. Identification and characterization of receptors for tumor necrosis factor-alpha in the brain. *Biochem Biophys Res Commun* **181**, 1532-1538 (1991).
129 Tchelingerian, J. L., Monge, M., Le Saux, F., Zalc, B. & Jacque, C. Differential oligodendroglial expression of the tumor necrosis factor receptors in vivo and in vitro. *Journal of neurochemistry* **65**, 2377-2380 (1995).
130 Dopp, J. M., Mackenzie-Graham, A., Otero, G. C. & Merrill, J. E. Differential expression, cytokine modulation, and specific functions of type-1 and type-2 tumor necrosis factor receptors in rat glia. *Journal of neuroimmunology* **75**, 104-112 (1997).
131 Cheng, B., Christakos, S. & Mattson, M. P. Tumor necrosis factors protect neurons against metabolic-excitotoxic insults and promote maintenance of calcium homeostasis. *Neuron* **12**, 139-153 (1994).
132 Bruce, A. J. *et al.* Altered neuronal and microglial responses to excitotoxic and ischemic brain injury in mice lacking TNF receptors. *Nat Med* **2**, 788-794 (1996).
133 Huang, X. *et al.* The A beta peptide of Alzheimer's disease directly produces hydrogen peroxide through metal ion reduction. *Biochemistry* **38**, 7609-7616, doi: https://doi.org/10.1021/bi990438f (1999).
134 Jang, J. H. & Surh, Y. J. beta-Amyloid induces oxidative DNA damage and cell death through activation of c-Jun N terminal kinase. *Annals of the New York Academy of Sciences* **973**, 228-236 (2002).

135 Heikkila, R. E. & Cohen, G. 6-Hydroxydopamine: evidence for superoxide radical as an oxidative intermediate. *Science* **181**, 456-457 (1973).
136 Wang, X. & Michaelis, E. K. Selective neuronal vulnerability to oxidative stress in the brain. *Front Aging Neurosci* **2**, 12, doi: https://doi.org/10.3389/fnagi.2010.00012 (2010).
137 Heck, S., Lezoualc'h, F., Engert, S. & Behl, C. Insulin-like growth factor-1-mediated neuroprotection against oxidative stress is associated with activation of nuclear factor kappaB. *The Journal of biological chemistry* **274**, 9828-9835 (1999).
138 Digicaylioglu, M. & Lipton, S. A. Erythropoietin-mediated neuroprotection involves cross-talk between Jak2 and NF-kappaB signalling cascades. *Nature* **412**, 641-647, doi: https://doi.org/10.1038/35088074 (2001).
139 Zou, J. & Crews, F. CREB and NF-kappaB transcription factors regulate sensitivity to excitotoxic and oxidative stress induced neuronal cell death. *Cell Mol Neurobiol* **26**, 385-405, doi: https://doi.org/10.1007/s10571-006-9045-9 (2006).
140 Circu, M. L. & Aw, T. Y. Reactive oxygen species, cellular redox systems, and apoptosis. *Free Radic Biol Med* **48**, 749-762, doi: https://doi.org/10.1016/j.freeradbiomed.2009.12.022 (2010).
141 Schmeisser, M. J. *et al.* IkappaB kinase/nuclear factor kappaB-dependent insulin-like growth factor 2 (Igf2) expression regulates synapse formation and spine maturation via Igf2 receptor signaling. *J Neurosci* **32**, 5688-5703, doi: https://doi.org/10.1523/JNEUROSCI.0111-12.2012 (2012).
142 Pascual-Lucas, M. *et al.* Insulin-like growth factor 2 reverses memory and synaptic deficits in APP transgenic mice. *EMBO Mol Med* **6**, 1246-1262, doi: https://doi.org/10.15252/emmm.201404228 (2014).
143 Martin-Montanez, E. *et al.* Involvement of IGF-II receptors in the antioxidant and neuroprotective effects of IGF-II on adult cortical neuronal cultures. *Biochim Biophys Acta* **1842**, 1041-1051, doi: https://doi.org/10.1016/j.bbadis.2014.03.010 (2014).
144 Martin-Montanez, E. *et al.* IGF-II promotes neuroprotection and neuroplasticity recovery in a long-lasting model of oxidative damage induced by glucocorticoids. *Redox Biol* **13**, 69-81, doi: https://doi.org/10.1016/j.redox.2017.05.012 (2017).
145 Wang, C. Y., Mayo, M. W., Korneluk, R. G., Goeddel, D. V. & Baldwin, A. S., Jr. NF-kappaB antiapoptosis: induction of TRAF1 and TRAF2 and c-IAP1 and c-IAP2 to suppress caspase-8 activation. *Science* **281**, 1680-1683 (1998).
146 Abel, T. *et al.* Genetic demonstration of a role for PKA in the late phase of LTP and in hippocampus-based long-term memory. *Cell* **88**, 615-626 (1997).
147 Esteban, J. A. *et al.* PKA phosphorylation of AMPA receptor subunits controls synaptic trafficking underlying plasticity. *Nat Neurosci* **6**, 136-143, doi: https://doi.org/10.1038/nn997 (2003).
148 Ronen, D. & Benvenisty, N. Sex-dependent gene expression in human pluripotent stem cells. *Cell reports* **8**, 923-932, doi:10.1016/j.celrep.2014.07.013 (2014).
149 Nakada, D. *et al.* Oestrogen increases haematopoietic stem-cell self-renewal in females and during pregnancy. *Nature* **505**, 555-558, doi:10.1038/nature12932 (2014).

150 Pawluski, J. L., Brummelte, S., Barha, C. K., Crozier, T. M. & Galea, L. A. Effects of steroid hormones on neurogenesis in the hippocampus of the adult female rodent during the estrous cycle, pregnancy, lactation and aging. *Frontiers in neuroendocrinology* **30**, 343-357, doi:10.1016/j.yfrne.2009.03.007 (2009).

151 Dulken, B. & Brunet, A. Stem Cell Aging and Sex: Are We Missing Something? *Cell stem cell* **16**, 588-590, doi:10.1016/j.stem.2015.05.006 (2015).

152 Deasy, B. M. *et al.* A role for cell sex in stem cell-mediated skeletal muscle regeneration: female cells have higher muscle regeneration efficiency. *The Journal of cell biology* **177**, 73-86, doi:10.1083/jcb.200612094 (2007).

153 Armstrong, L. *et al.* The role of PI3K/AKT, MAPK/ERK and NFkappabeta signalling in the maintenance of human embryonic stem cell pluripotency and viability highlighted by transcriptional profiling and functional analysis. *Hum Mol Genet* **15**, 1894-1913, doi: https://doi.org/10.1093/hmg/ddl112 (2006).

154 Takase, O. *et al.* The role of NF-kappaB signaling in the maintenance of pluripotency of human induced pluripotent stem cells. *PLoS One* **8**, e56399, doi: https://doi.org/10.1371/journal.pone.0056399 (2013).

155 Deng, P., Zhou, C., Alvarez, R., Hong, C. & Wang, C. Y. Inhibition of IKK/NF-kappaB Signaling Enhances Differentiation of Mesenchymal Stromal Cells from Human Embryonic Stem Cells. *Stem Cell Reports* **6**, 456-465, doi: https://doi.org/10.1016/j.stemcr.2016.02.006 (2016).

156 Yang, C. *et al.* Opposing putative roles for canonical and noncanonical NFkappaB signaling on the survival, proliferation, and differentiation potential of human embryonic stem cells. *Stem Cells* **28**, 1970-1980, doi: https://doi.org/10.1002/stem.528 (2010).

157 Slotta, C. *et al.* CRISPR/Cas9-mediated knockout of c-REL in HeLa cells results in profound defects of the cell cycle. *PLoS One* **12**, e0182373, doi: https://doi.org/10.1371/journal.pone.0182373 (2017).

158 Wang, W., Tam, W. F., Hughes, C. C., Rath, S. & Sen, R. c-Rel is a target of pentoxifylline-mediated inhibition of T lymphocyte activation. *Immunity* **6**, 165-174 (1997).

159 Pizzi, M. *et al.* Opposing roles for NF-kappa B/Rel factors p65 and c-Rel in the modulation of neuron survival elicited by glutamate and interleukin-1beta. *J Biol Chem* **277**, 20717-20723, doi: https://doi.org/10.1074/jbc.M201014200 (2002).

160 Lorenz, V. N., Schon, M. P. & Seitz, C. S. c-Rel downregulation affects cell cycle progression of human keratinocytes. *J Invest Dermatol* **134**, 415-422, doi: https://doi.org/10.1038/jid.2013.315 (2014).

161 Grumont, R. J. *et al.* B lymphocytes differentially use the Rel and nuclear factor kappaB1 (NF-kappaB1) transcription factors to regulate cell cycle progression and apoptosis in quiescent and mitogen-activated cells. *J Exp Med* **187**, 663-674 (1998).

162 Guttridge, D. C., Albanese, C., Reuther, J. Y., Pestell, R. G. & Baldwin, A. S., Jr. NF-kappaB controls cell growth and differentiation through transcriptional regulation of cyclin D1. *Mol Cell Biol* **19**, 5785-5799 (1999).

163 Ledoux, A. C. & Perkins, N. D. NF-kappaB and the cell cycle. *Biochem Soc Trans* **42**, 76-81, doi: https://doi.org/10.1042/BST20130156 (2014).

164 Sommer, I. & Schachner, M. Monoclonal antibodies (O1 to O4) to oligodendrocyte cell surfaces: an immunocytological study in the central nervous system. *Dev Biol* **83**, 311-327, doi:0012-1606(81)90477-2 [pii] (1981).

165 Bansal, R., Stefansson, K. & Pfeiffer, S. E. Proligodendroblast antigen (POA), a developmental antigen expressed by A007/O4-positive oligodendrocyte progenitors prior to the appearance of sulfatide and galactocerebroside. *J Neurochem* **58**, 2221-2229, doi: https://doi.org/10.1111/j.1471-4159.1992.tb10967.x (1992).

166 Goldman, S. A. & Kuypers, N. J. How to make an oligodendrocyte. *Development* **142**, 3983-3995, doi: https://doi.org/10.1242/dev.126409 (2015).

167 Domingues, H. S., Portugal, C. C., Socodato, R. & Relvas, J. B. Oligodendrocyte, Astrocyte, and Microglia Crosstalk in Myelin Development, Damage, and Repair. *Front Cell Dev Biol* **4**, 71, doi: https://doi.org/10.3389/fcell.2016.00071 (2016).

168 Noseworthy, J. H., Lucchinetti, C., Rodriguez, M. & Weinshenker, B. G. Multiple sclerosis. *N Engl J Med* **343**, 938-952, doi: https://doi.org/10.1056/NEJM200009283431307 (2000).

169 Olsen, J. A. & Akirav, E. M. Remyelination in multiple sclerosis: cellular mechanisms and novel therapeutic approaches. *J Neurosci Res* **93**, 687-696, doi: https://doi.org/10.1002/jnr.23493 (2015).

170 Rieckmann, P. *et al.* Pentoxifylline, a phosphodiesterase inhibitor, induces immune deviation in patients with multiple sclerosis. *J Neuroimmunol* **64**, 193-200 (1996).

171 Weber, F. *et al.* Synergistic immunomodulatory effects of interferon-beta1b and the phosphodiesterase inhibitor pentoxifylline in patients with relapsing-remitting multiple sclerosis. *Ann Neurol* **44**, 27-34, doi: https://doi.org/10.1002/ana.410440109 (1998).

172 Petersen, M. A. *et al.* Fibrinogen Activates BMP Signaling in Oligodendrocyte Progenitor Cells and Inhibits Remyelination after Vascular Damage. *Neuron* **96**, 1003-1012 e1007, doi: https://doi.org/10.1016/j.neuron.2017.10.008 (2017).

173 Fischer, R. & Maier, O. Interrelation of oxidative stress and inflammation in neurodegenerative disease: role of TNF. *Oxid Med Cell Longev* **2015**, 610813, doi: https://doi.org/10.1155/2015/610813 (2015).

174 Fischer, R. *et al.* A TNF receptor 2 selective agonist rescues human neurons from oxidative stress-induced cell death. *PLoS One* **6**, e27621, doi: https://doi.org/10.1371/journal.pone.0027621 (2011).

175 Miller, I. N. & Cronin-Golomb, A. Gender differences in Parkinson's disease: clinical characteristics and cognition. *Mov Disord* **25**, 2695-2703, doi: https://doi.org/10.1002/mds.23388 (2010).

176 Studer, L. *et al.* Enhanced proliferation, survival, and dopaminergic differentiation of CNS precursors in lowered oxygen. *J Neurosci* **20**, 7377-7383 (2000).

Supplementary Material

8

8.1 Supplementary Figures

Supplementary figure 1. Promotor analysis using the JASPAR Tool (jaspar.genereg.net) validated SOD2, PRKACA to be direct RELA, RELB and REL target genes. RELA binding sites are shown in red, RELB binding sites in green, and REL binding sites in brown. Common RELA and REL binding sites are shown in blue. One promoter is shown for each gene, for more detail see supplementary material.

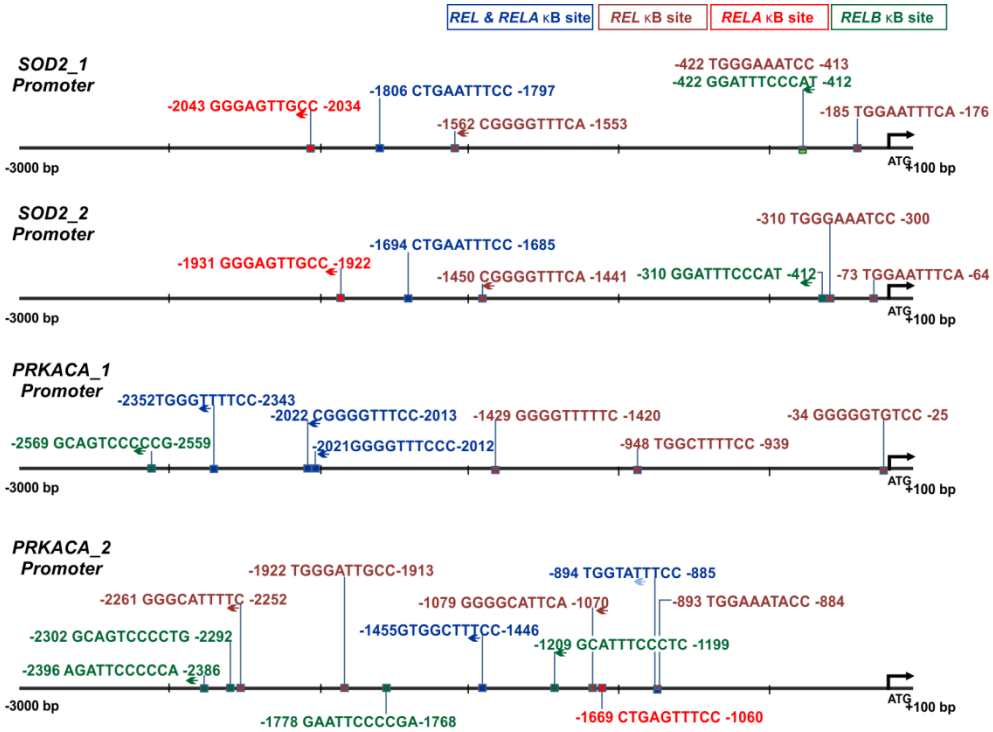

Supplementary figure 2: Promotor analysis using the JASPAR Tool (jaspar.genereg.net) validated IGF2 to be direct RELA, RELB and REL target genes. Six promoters are shown for IGF2. RELA binding sites are shown in red, RELB binding sites in green, and REL binding sites in brown. Common RELA and REL binding sites are shown in blue. Sequences in the antisense strand are indicated with an arrow.

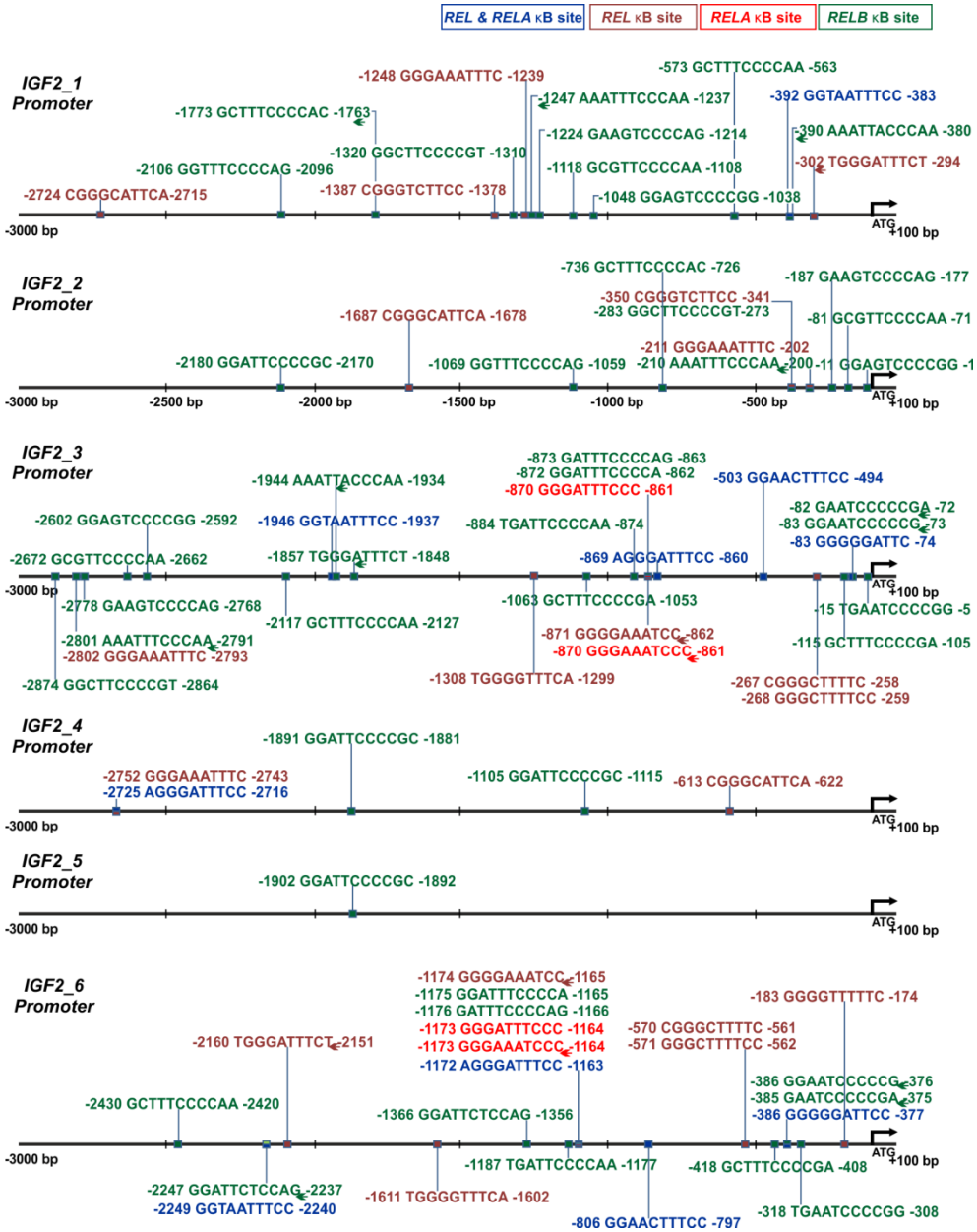

Supplementary figure 3. Immunocytochemistry assays showing different cell markers after 30 days of glutamatergic neuronal differentation in the absence or presence of pentoxifylline (PTXF) and their respective quantifications. A-B) Neuronal differentiated- ITSCs labeled against Nestin, a stemness marker. C) Quantification of the percentage of Nestin^{+} cells shows a higher tendency on Nestin for the differentiated-ITSCs treated with PTXF, compared to the untreated differentiated-ITSCs. However it is not significantly relevant difference. D-E) Neuronal differentiated- ITSCs labeled against alpha smooth muscle actin (αSMA). F) Quantification showing the percentage of αSMA^{+} cells which is cero for the differentiated-ITSCs treated with PTXF and it is 1% in untreated differentiated-ITSCs. No significant difference was observed. G-H) Differentiated-ITSCs labeled against p75, a neural crest marker. I) Quantification of the percentage of p75^{+} cells indicates a lower ammount of p75^{+} cells (10%), present in the untreated neuronal differentiated-ITSCs and a higher tendency of positive cells in the differentiated-ITSCs treated with PTXF (40%). However it was not a significant difference. Non-parametric Kruskal-Wallis test ($p \leq 0.10$), no significant differences observed.

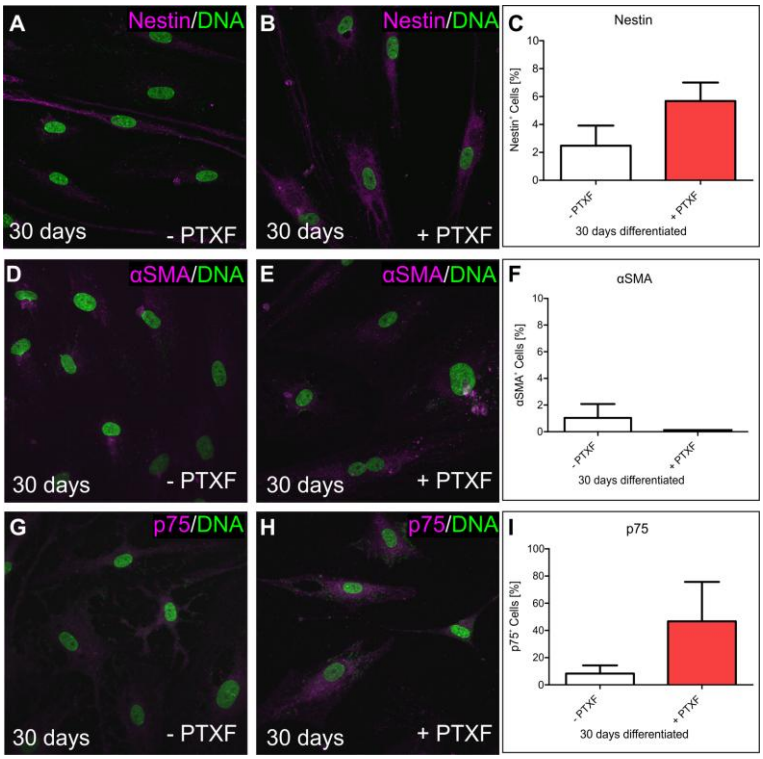

Supplementary figure 4. Myelination assay showing immunostainings against O4 and NF200, an oligodendrogilal and neuronal marker respectively. A-E: immunocytochemical assays showing male-derived differentiated inferior turbinate stem cells (ITSCs), F-J: immunocytochemical assays showing female-derived differentiated ITSCs. A, F: ITSC-derived oligodendrocyte progenitor cells (ITSC-OPCs), B, G: Neuronal differentiated ITSCs in the presence of pentoxifylline (PTXF). C, H: Neurons differentiated from ITSCs. D, I: Co-cultures of ITSC-derived neurons and ITSC-derived OPCs co-cultivated after 20 days of neuronal and oligodedrocyte differentiation. E, J: Co-cultures of ITSC-derived neurons and ITSC-differentiated cells in the presence of PTXF, co-cultivated after 20 days of neuronal differentiation. Whithin both co-cultivation assays, cells were co-cultured for 10 days in neuronal induction media supplemented with N2 at 37 ° C in a 5% CO2 incubator.

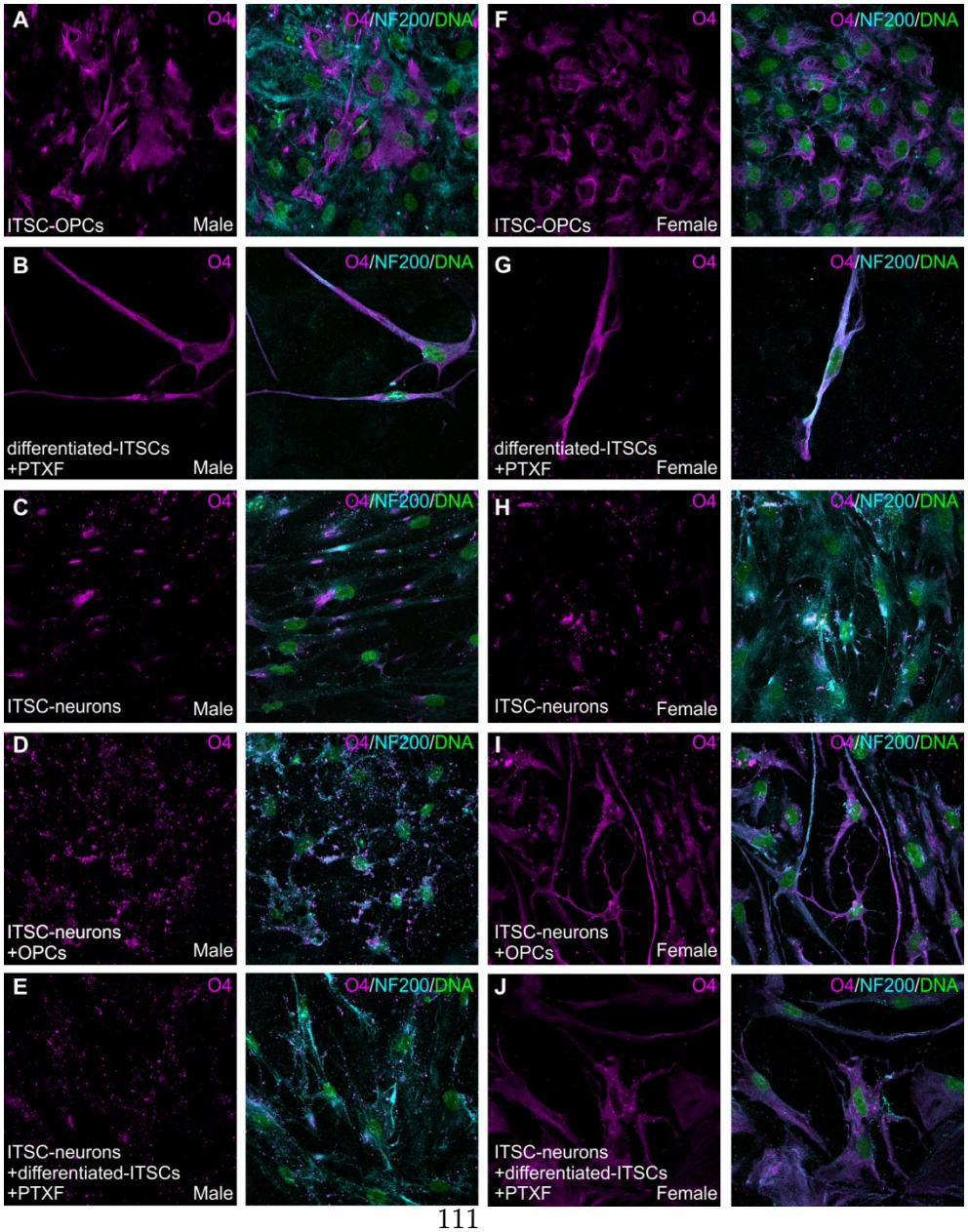

Supplementary figure 5. Myelination assay. Myelination assay showing immunostainings against MOG (Myelin oligodendrocyte glycoprotein) and MAP-2 (Microtubule-associated protein 2), an oligodendrogilal and neuronal marker respectively. A-E: immunocytochemical assays showing male-derived differentiated inferior turbinate stem cells (ITSCs), F-J: immunocytochemical assays showing female-derived differentiated ITSCs. A, F: ITSC-derived oligodendrocyte progenitor cells (ITSC-OPCs), B, G: Neuronal differentiated ITSCs in the presence of pentoxifylline (PTXF). C, H: Neurons differentiated from ITSCs. D, I: Co-cultures of ITSC-derived neurons and ITSC-derived OPCs co-cultivated after 20 days of neuronal and oligodedrocyte differentiation. E, J: Co-cultures of ITSC-derived neurons and ITSC-differentiated cells in the presence of PTXF, co-cultivated after 20 days of neuronal differentiation. Whithin both co-cultivation assays, cells were co-cultured for 10 days in neuronal induction media supplemented with N2 at 37 ˚ C in a 5% CO2 incubator.

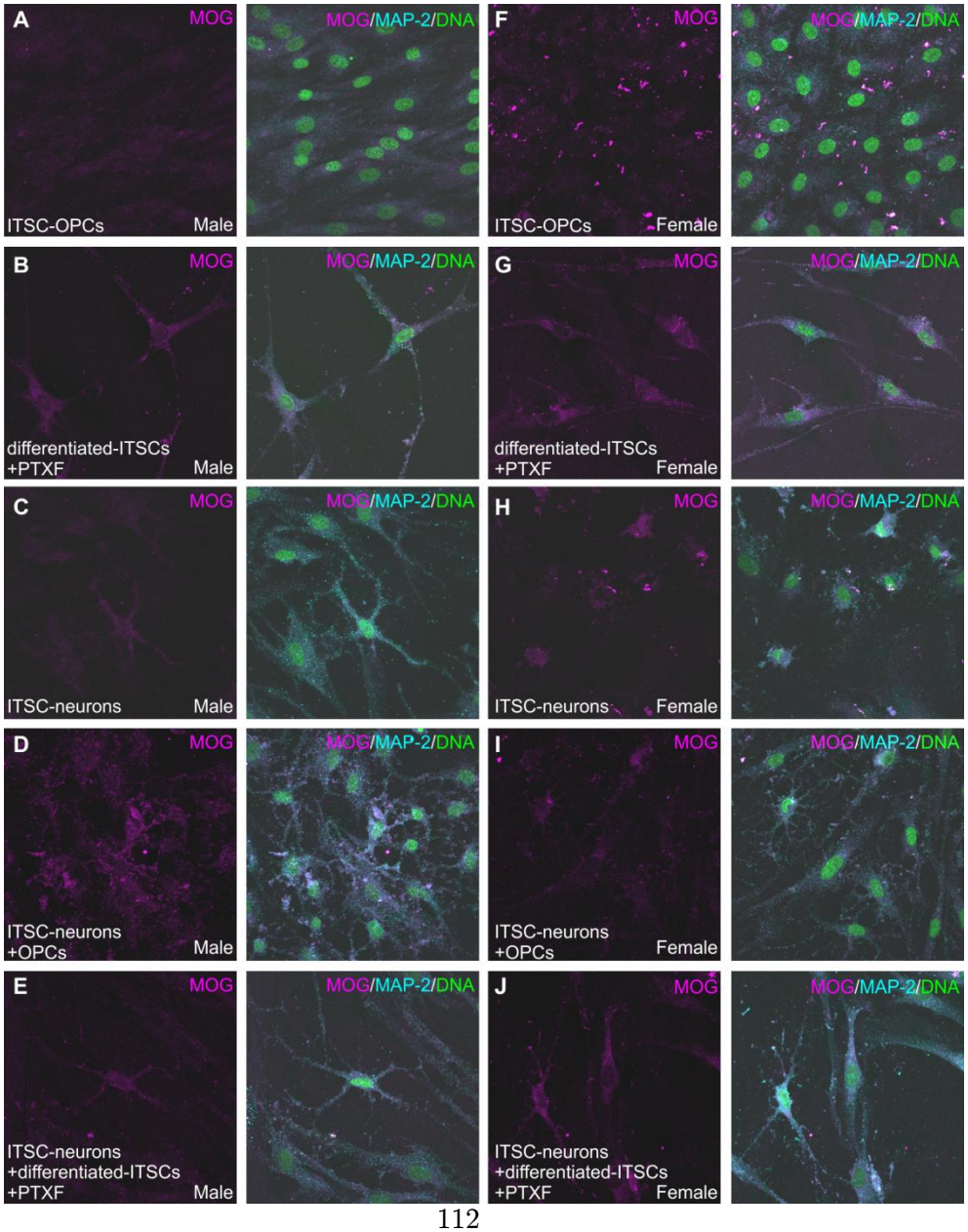

Supplementary figure 6. Stimulation of dopaminergic differentiated neurons of male-derived ITSCs. A-D: Immunocytochemical assays labeling p65 of male-derived dopaminergic neurons, after treatment with TNF-α, 6-hydroxydopamine (6OHDA), and their combination. Arrows: low endogenous p65 nuclear activity, arrowheads: strong p65 activity. E-G: Quantification analysis of nuclear mean integrated density of p65, after treatment of dopaminergic neurons shown for the three male donors analyzed. H: Quantification showing nuclear mean integrated density of p65 (n=3, mean ± SEM) and the statisical analysis performed. Normality of the data set was refuted using Shapiro-Wilk test. Non-parametric Kruskal-Wallis (***p≤0.001) and Tukey's test (***p≤0.001) revealed significant difference in nuclear p65 as indicated.

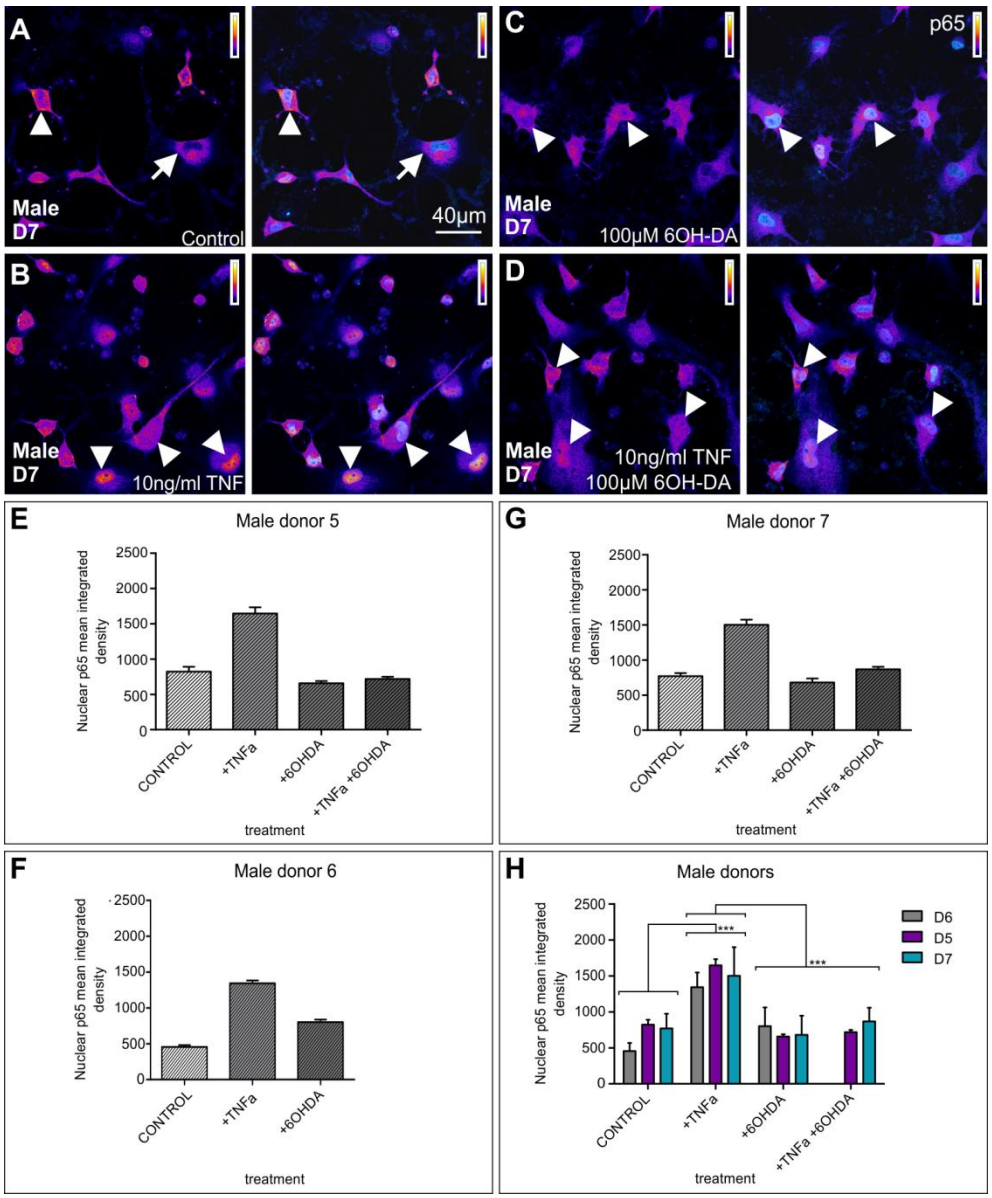

8.2 Supplementary tables

Supplementary table 1: ITSCs donors differentiated into dopaminergic neurons.

Donor	Internal code	Gender	Age
1	K278N	Female	20
2	K325N	Female	68
3	K395N	Female	61
4	K272N	Female	26
5	K284N	Male	23
6	K243N	Male	53
7	NM4	Male	50

8.3 List of Abreviations

ESCs	embyonic stem cells
iPSCs	induced pluripotent stem cells
ASCs	Adult stem cells
SSEA-3	stage specific embryonic antigen 3, cell surface antigen used to recognize human embryonic stem cells
SSEA-4	stage specific embryonic antigen 4, cell surface antigen used to recognize human embryonic stem cells
TRA-1-60	keratan sulfate antigen from human embryonic stem cells used as specific surface marker
TRA-1-81	keratan sulfate antigen from human embryonic stem cells used as specific surface marker
OCT4	octamer-binding transcription factor 4, also known as POU class 5 homeobox 1
SOX2	SRY(sex determining region Y) -box 2
NANOG	homeobox protein NANOG

KLF4	Kruppel like factor 4
C-MYC	MYC proto-oncogene, bHLH transcription factor
NCSCs	neural crest derived stem cells
NC	neural crest
BMPs	bone morphogenetic proteins
RA	retinoic acid
FGF	fibroblast growth factor
ITSCs	inferior turbinate stem cells
S100	S100 calcium binding protein
p75NTR	low-affinity neurotrophin receptor, nerve growth factor receptor p75
SOX10	SRY(sex determining region Y) -box 10
NSCs	neural stem cells
PNS	peripheral nervous system
CNS	central nervous system
OPCs	oligodendroglial progenitor cells
NPCs	neural progenitor cells
BMP4	bone morphogenetic protein 4
SHH	sonic hedgehog
OTX1	Orthodenticle homeobox 1
OTX2	Orthodenticle homeobox 2
BF1	brain factor 1
FGF8	fibroblast growth factor 8
FGF2	fibroblast growth factor 2
PAX6	paired box 6
TBR2	T-box brain protein 2
NEUROD	neuronal differentiation 1
TBR1	T-box brain protein 1
NGN2	Neurogenin2
LMX1A	LIM homeobox transcription factor 1 alpha
FOXA2	forkhead box A2

EN1	Engrailed Homeobox 1
WNT1	Wnt family member 1
GBX2	Gastrulation brain homeobox 2
NKX2-2	NK2 homeobox 2
MSX1	msh homeobox 1
NKX6-1	NK6 homeobox 1
TH	tyrosine hydroxylase
NF-κB	nuclear factor kappa-light-chain-enhancer of activated B-cells
RHD	Rel homology domain
IκB	inhibitor of κB family
IκBα	IκB-alpha subunit
PD	Parkinson's disease
AD	Alzheimer's disease
TNF-α	tumor necrosis factor alpha
AMPA	agonist α-amino-3-hydroxyl-5-methyl-4-isoxazole-propionate
ROS	reactive oxygen species
H_2O_2	hydrogen peroxide
O_2^-	superoxide
OH	hydroxyl radical
HSCs	hematopoietic stem cells
NSCs	neural stem cells
BP	blood plasma
EGF	epidermal growth factor
NIM	neuronal induction medium
RT-PCR	reverse transcription polymerase chain reaction
GLU	glutamate
CSS	buffered control salt solution
CQNX	6-cyano-7-nitroquinoxaline-2,3-dione
PFA	paraformaldehyde
PTXF	pentoxifylline, a known inhibitor of c-Rel

OEM	oligodendrocyte enrichment medium
GDNF	glial cell line-derived neurotrophic factor
BDNF	brain-derived neurotrophic factor
NGF	nerve growth factor
6-OHDA	6-hydroxydopamine
NF200	anti-neurofilament 200
RPLP0	Ribosomal Protein Lateral Stalk Subunit P0
qPCR	Quantitative polymerase chain reaction
IGF1	Insulin-like growth factor 1
IGF2	Insulin-like growth factor 2
PKAcatα	c-AMP-dependent protein kinase catalytic subunit alpha
SOD2	Superoxide dismutase 2, also known as manganese superoxide dismutase , Mn-SOD
cIAP1	Cellular inhibitor of apoptosis protein 1
cIAP2	Cellular inhibitor of apoptosis protein 2
NG2	transmembrane proteoglycan nerve-glia antigen 2, also known as Chondroitin sulfate proteoglycan 4, CSPG4
PDGFRA	Platelet derived growth factor receptor alpha
GAPDH	Glyceraldehyde-3-phosphate dehydrogenase
ROI	region of interest
GLU	glutamate
AMPA	3-hydroxyl-5-methyl-4-isoxazole-propionate
CQNX	6-cyano-7-nitroquinoxaline-2,3-dione
MK-801	dibenzocycloheptenеimine
TNFR1	tumor necrosis factor receptor 1
TNFR2	tumor necrosis factor receptor 2
IFN-β1b	Interferon beta-1b
IFN-α	interferon alpha

8.4 List of Figures

Documentation

9

9.1 Acknowledgements

I would like to acknowledge all the people who helped and supported me throughout my PhD and that in some way contributed to this work.

First I would like to express my sincere deep gratitude to my supervisor Prof. Dr. Barbara Kaltschmidt for her support and guidance over the past years, and for giving me the opportunity to work in this project. I would like to thank Dr. Prof. Christian Kaltschmidt for his interesting ideas, helpful discussions, and support. Both always provided me with great advice concerning my research projects and supported me in every question.

I would like to thank Angela Kralemann-Köhler for her excellent technical assistance, and her support in the lab.

I would like to thank Dr. Johannes Greiner who was always willing to give good advice regarding all my questions.

I am very grateful to Beatrice Windmöller, Lennart Schneider and Ronja Ossenbrink, for their contribution in this wonderful project.

I thank all the co-authors of the papers published and the manuscripts that hopefully will be published soon for their great contributions.

I am very grateful to all former and current members of the Department of Cell Biology for nice coffee- and lunchbreaks and the supportive friendly atmosphere. I would like to thank Hussam and Carsten, with whom I shared this path from the very beginning. I specially thank Madlen for having such nice atmosphere in our office. I want to thank Anna, Bea and Kaya for their help and the nice time. I would like to thank Peter, Elke, Doris and Chris which were always there to help me.

I would like to thank my colleagues from next door lab: Anna, Marco, Mohaned and Tania, for the fun time shared, the exchanged support, and many non-scientific discussions.

I had equally amazing time at the active sensing group, and enjoyed discussions during breakfast and lunch times as well as the nice activities regarding Indian and German cooking.

Most importantly, I am deeply indebted to my family and friends for their continuous love and support across the distance. I would like to dedicate this thesis to my nephew Teo, the new family member.

This work would not have been possible without the constant patience and support of my boyfriend Federico to whom I am deeply owe a debt of gratitude.

9.2 Curriculum Vitae

Personal Data

Name: Lucia Mercedes

Surname: Ruiz Perera

Gender: Female

Nationality: Uruguayan/Spanish

Date of birth: 02/01/1986

Address: Große-Kurfürsten-Straße 32, 33615 Bielefeld, Germany

Phone number: (+49) 17656981033

E-mail: lucia.ruiz@uni-bielefeld.de

Institutional address: University of Bielefeld, Faculty of Biology,

Universitätsstraße 25, 33615, Bielefeld, Germany

Phone: (+49) 521 106 00 5620

Academic degrees.

2015 - Present. PhD Student in Biology. Molecular Neurobiology, Department of Cell Biology, Faculty of Biology, University of Bielefeld, Germany. Supervisor: Prof. Dr. Barbara Kaltschmidt. Scholarships: DAAD-ROU and Gender Stipend, from the Equality Commission of the Faculty of Biology, University of Bielefeld.

2010 - 2013. Masters Degree in Biological Sciences (option Neurosciences). PEDECIBA. Faculty of Science, University of the Republic, Uruguay.
Title: Searching proteins responsible of plasticity reactivation in the visual cortex of adult mouse. Supervisor: Dr. Francesco M. Rossi. Grade: 8.29 (83% according to scale grade). Scholarship from Agencia Nacional de Investigación e Innovación (ANII), Uruguay.

2004 - 2009. Bachelors Degree in Biological Sciences (option Cell Biology). Faculty of Science, University of the Republic, Uruguay.
Title: Studying the presence of S25p-MARCKS in neural crest derived cells in the chick embryo. Supervisor: Dr. Flavio R. Zolessi. Grade: 7.68 (80% according to scale grade).

Publications

Ruiz-Perera LM, Greiner JFW, Kaltschmidt C, Kaltschmidt B. Role of NF-κB subunits in glutamatergic differentiation of adult human nasal stem cells. Manuscript in preparation.

Ruiz-Perera LM, Schneider L, Windmöller BA, Müller J, Greiner JFW, Kaltschmidt C, Kaltschmidt B. NF-kB p65 directs sex-specific

neuroprotection in human neurons. Sci Rep. 2018 Oct 30 ;8(1):16012. https://doi.org/10.1038/s41598-018-34394-8.

Slotta C, Storm J, Pfisterer N, Henkel E, Kleinwächter S, Pieper M, **Ruiz-Perera LM**, Greiner JFW, Kaltschmidt B, Kaltschmidt C. IKK1/2 protect human cells from TNF-mediated RIPK1-dependent apoptosis in an NF-κB-independent manner. BBA-Molecular Cell Research. 2018 Aug. 1865 (8): 1025-1033.

Slotta C, Schlüter T, **Ruiz-Perera LM**, Kadhim HM, Tertel T, Henkel E, Hübner W, Greiner JFW, Huser T, Kaltschmidt B, Kaltschmidt C. CRISPR/Cas9-mediated knockout of c-REL in HeLa cells results in profound defects of the cell cycle. PLoS ONE. 2017 Aug. 12(8): e0182373. https://doi.org/10.1371/journal.pone.0182373.

Ruiz-Perera LM, Muniz M, Vierci G, Bornia N, Baroncelli L, Sale A, Rossi FM Fluoxetine increases plasticity and modulates the proteomic profile in the adult mouse visual cortex. Sci Rep. 2015 Jul. DOI: 10.1038/srep12517

Ruiz-Perera LM, Arruti C, Zolessi, FR. Early phosphorylation of MARCKS at Ser25 in migrating precursor cells and differentiating peripheral neurons. Neurosci Lett. 2013 Jun 7;544:5-9. doi: 10.1016/j.neulet.2013.02.042.

Vierci G, Oliveira CS, **Ruiz-Perera LM**, Bornia N, Leal RB, Rossi FM. Creb is modulated in the mouse superior colliculus in developmental and experimentally-induced models of plasticity. Int J Dev Neurosci. 2013 Feb; 31(1):46-52. doi: 10.1016/j.ijdevneu.2012.10.003.

Conference Proceedings

Ruiz-Perera LM, Kaltschmidt C., Kaltschmidt, B. Involvement of transcription factor NF-kappaB during glutamatergic differentiation of adult human stem cells. 9th International Meeting Stem Cell Network North Rhine Westphalia. Münster, Germany, 2017. **Poster.**

Ruiz-Perera LM, Kaltschmidt C., Kaltschmidt, B. NF-kB dependent cell fate determination in the specification of human stem cells into glutamatergic neurons. 8th Westerberger Herbsttagung 2016 together with GBM study group meeting. Perspectives of Molecular Neurobiology: from single molecules to systems. Osnabrück, Germany, 2016. **Poster.**

Rossi FM, **Ruiz-Perera LM,** Muniz M, Vierci G, Bornia N, Baroncelli L, Sale A. Analysis of proteins restoring plasticity in the adult mouse visual cortex: a proteomic approach. 9th FENS Forum of Neuroscience. Milan, Italy, 2014. **Poster.**

Ruiz-Perera LM. Searching proteins responsible of plasticity reactivation in the adult mouse visual cortex. 8th Conference of the Sociedad de Bioquímica y Biología Molecular (SBBM, Society for Biochemistry and Molecular Biology). Montevideo, Uruguay, 2013. **Talk.**

Ruiz-Perera LM, Vierci G, Bornia N, and Rossi FM. A search for proteins restoring plasticity in the adult mouse visual cortex. XXVIII Annual Congress of the Argentinean Society of Research in Neurosciences. Córdoba, Argentina, 2013. **Poster.**

Ruiz-Perera LM, Bornia N, and Rossi FM. Molecular mechanisms underlying neuronal plasticity in the visual cortex of mice a proteomic approach. First FALAN Congress, Cancún, México, 2012. **Poster.**

Ruiz-Perera LM, Bornia N, Vierci G, and Rossi FM. Study of the molecular mechanismsof neuronal plasticity in the visual cortex: a proteomic aproximation. 7th Conference of the Society for Biochemistry and Molecular Biology (SBBM), Montevideo, Uruguay, 2011. **Poster.**

Ruiz-Perera LM, Zolessi FR, and Arruti C. S25p-MARCKS in neural crest derived cells in the chick embryo. XIII Conference of the Sociedad Uruguaya de Biociencias. Piriápolis, Uruguay, 2010. **Poster.** Prize distinction.

Research projects

2015-Present: NF-κB in differentiation and maturation of human nasal stem cells. Responsible: Prof. Dr. Barbara Kaltshmidt

2010-2014: Search of proteins involved in the regulation of visual cortical plasticity. Responsible: Dr. Francesco Rossi. ANII.

2006-2010: Functions of the MARCKS family of proteins in the development of the vertebrate nervous system. Responsible: Dr. Flavio R. Zolessi. CSIC (Comisión Sectorial de Investigación Científica).

Awards and Memberships

2018 - Gender Equality Stipend to finish the PhD - Equality Commission of the Faculty of Biology, University of Bielefeld.

2014 - German Academic Exchange Service (DAAD) - Educational and Cultural Affairs of the Republic of Uruguay (ROU) scholarship. Awarded to achieve the PhD in Bielefeld, Germany from 2015-2018. Uruguay-Germany.

2012 - National fellowship from the Society for Biochemistry and Molecular Biology (SBBM), awarded to attend the First Congress of the Federation of Latin American and Caribbean Associations of Neuroscience (FALAN) in November 2012. It consisted in financial aid to participate in the international event. Montevideo, Uruguay.

2012 - National fellowship from the CSIC (Sectorial Commission of Scientific Research), awarded to attend the First Congress of the FALAN in November 2012. It consisted in financial aid to participate in the international event. Montevideo, Uruguay.

2011 - National Scholarship from the National Academy for Research and Innovation (ANII), awarded to complete the Masters Degree in Biology from 2011-2012. Montevideo, Uruguay.

Academic contents and Positions

2018- Present. Research Assistant. Institute for Laboratory and Transfusion Medicine at the Heart and Diabetes Center North Rhine-Westphalia, Bad Oeynhausen, Germany.

2010 - 2014. Assistant Grade 1 in Cellular Biology (20 hours/week). Faculty of Science, University of the Republic, Uruguay.

Supervision of Bachelor Students

Jantje Spieker. Bachelor thesis title: Characterization of RELA and REL using the CRISPR-Cas9 system in HEK 293. August 2015. Department of Cell Biology, Faculty of Biology, University of Bielefeld. First supervisor: Prof. Dr. Barbara Kaltschmidt. Second supervisor: M.Sc. Lucia Ruiz

Pascal Segura. Bachelor thesis title: Investigation on IkBa-knockout by CRISPR/Cas9 technology. September 2016. Department of Cell Biology, Faculty of Biology, University of Bielefeld. First Supervisor: Prof. Dr. Christian Kaltschmidt, Second Supervisor: MSc. Lucia Ruiz

Lennart Schneider. Bachelor thesis title: Characterisation of glutamatergic neurons derived from human nasal stem cells. September 2017. Department of Cell Biology, Faculty of Biology, University of Bielefeld. First Supervisor: Prof. Dr. Barbara Kaltschmidt, Second Supervisor: MSc. Lucia Ruiz.

Ronja Ossenbrink. Bachelor thesis: "Analysis of NF-kB subunits during osteogenic differentiation of human nasal stem cells". September 2017. Department of Cell Biology, Faculty of Biology, University of Bielefeld. First Supervisor: Prof. Dr. Barbara Kaltschmidt, Second Supervisor: MSc. Lucia Ruiz.

Teaching in practical courses

Master

2016 - Molecular Biology of the Stem Cells. Master module. Faculty of Biology, Universität Bielefeld, Germany. Assistent.

2010 - Molecular and Celullar Biology. Master module."Neruronal tracing in the visual system". Regional Course "Development and Plasticity of the Nervous System". PEDECIBA, Faculty of Science, University of the Republic, Uruguay. Asistent.

Bachelor

2014 - 2017 -CRISPR/Cas9 genome engineering course. Special Module Molecular Cell Biology. Assistent.

2010 - 2014 - Cell Biology. 3rd Semester. Bach. in Natural Sciences and in Biochemistry. Faculty of Science, University of the Republic, Uruguay.

2010 - 2014 - Developmental Biology. 4th Semester. Bach. in Natural Sciences and in Biochemistry. Faculty of Science, University of the Republic, Uruguay.

2011 - Introduction to General Biology. Seminar: Celullar phenomena in regenerative events. Asistent. 1st Semester. Bach. in Natural Sciences and in Biochemistry.

2008 - Introduction to General Biology. Seminar: "Analysis of the diferential regulation of a protein linked to the cytoskeleton: MARCKS", Asistent. 1st Semester. Bach. in Natural Sciences and in Biochemistry.

Module projects

2014 - 2017 -Students developed a small project using CRISPR/Cas9 gene targeting or differentiating ITSCs, learning cell culture techniques, western blot and immunocytochemistry.

Languages

Spanish: Native speaker
English: Upper intermediate (B2)
French: Proficiency (C2)
German: Intermediate (B1.1)

9.3 List of publications

Parts of the dissertation presented were published:

Ruiz-Perera LM, Schneider L, Windmöller BA, Müller J, Greiner JFW, Kaltschmidt C, Kaltschmidt B. NF-κB p65 directs sex-specific neuroprotection in human neurons. Sci Rep. 2018 Oct 30 ;8(1):16012. https://doi.org/10.1038/s41598-018-34394-8.

Following studies are published but not referred to in this dissertation:

Slotta C, Storm J, Pfisterer N, Henkel E, Kleinwächter S, Pieper M, **Ruiz-Perera LM**, Greiner JFW, Kaltschmidt B, Kaltschmidt C. IKK1/2 protect human cells from TNF-mediated RIPK1-dependent apoptosis in an NF-κB-independent manner. BBA-Molecular Cell Research. 2018 Aug. 1865 (8): 1025-1033.

Slotta C, Schlüter T, **Ruiz-Perera LM**, Kadhim HM, Tertel T, Henkel E, Hübner W, Greiner JFW, Huser T, Kaltschmidt B, Kaltschmidt C. CRISPR/Cas9-mediated knockout of c-REL in HeLa cells results in profound defects of the cell cycle. PLoS ONE. 2017 Aug. 12(8): e0182373. https://doi.org/10.1371/journal.pone.0182373.

9.4 Declaration

This thesis "Function of NF-κB in human neurons" is a presentation of my own original research. I hereby confirm that I have written this thesis on my own and that the only aids used for composing this dissertation are those stated therein. All external resources and intellectual contributions of others have been indicated. Citations have been provided in all cases where the published work of others was consulted.

I have neither acquired nor tried to acquire a PhD or an equal degree at the Faculty of Biology, University of Bielefeld, or anywhere else before.

Bielefeld, 14.01.2019 *Lucia Ruiz*

Appendix

10

SCIENTIFIC REPORTS

OPEN

NF-κB p65 directs sex-specific neuroprotection in human neurons

Lucia M. Ruiz-Perera[1], Lennart Schneider[1], Beatrice A. Windmöller[1], Janine Müller[1], Johannes F. W. Greiner[2], Christian Kaltschmidt[2] & Barbara Kaltschmidt[1,2]

Received: 16 July 2018
Accepted: 15 October 2018
Published online: 30 October 2018

Protection of neurons against oxidative stress is crucial during neuronal development, maintenance and for treating neurodegenerative diseases. However, little is known about the molecular mechanisms underlying sex-specific maturation and survival of neurons. In the present study, we demonstrate NF-κB-p65 mediated neuroprotection in human glutamatergic neurons differentiated from inferior turbinate stem cells (ITSCs) in a sex-dependent manner. We successfully differentiated ITSCs into MAP-2$^+$/NF200$^+$/Synaptophysin$^+$/vGlut2$^+$-glutamatergic neurons *in vitro* and *ex vivo* and validated their functionality. TNF-α-dependent NF-κB-p65 activation was accompanied by significant neuroprotection against oxidative stress-induced neuronal death, which was surprisingly higher in neurons from female donors. Accordingly, sex-specific neuroprotection of female neurons was followed by an increased expression of special NF-κB target genes SOD2 and IGF2. Among these, SOD2 is a well known gene protecting cells against oxidative stress resulting in longevity. In addition, IGF2 is known to promote synapse formation and spine maturation, and it has antioxidant and neuroprotective effects against oxidative damage. In conclusion, we show that NF-κB-p65 is a key player in neuroprotection of human neurons, however the protective gene expression program beneath it differs between sexes. Our findings are in accordance with the increasing evidences pointing towards sex-specific differences in risk and severity of neurodegenerative diseases.

Acute and chronic nervous system damage in response to an insult such as oxidative stress is directly associated to neuronal death and degeneration[1]. Thus, appropriate neuroprotection remains as a crucial parameter for effective treatment of neurodegenerative diseases. Interestingly, increasing evidences point towards sex-specific differences in risk, severity and progression of neurodegenerative diseases such as Parkinson's (PD) or Alzheimer's disease (AD) or in case of Ischemic stroke[2–4]. In particular, female AD patients were reported to not only have an increased risk of developing AD compared to age-matched men[5], but also showed a significantly elevated age-related decline of cognition[3,6]. On the contrary, PD was shown to have a greater prevalence and occurred in an earlier age in men compared to woman[2]. Although neurodegenerative diseases and preventive neuroprotective mechanisms[7] seem to be subjected to sex-dependent differences, little is known about the underlying molecular mechanisms particularly regarding maturation and survival of neurons differentiated from human stem cells.

The transcription factor NF-κB (nuclear factor kappa-light-chain-enhancer of activated B-cells) is involved in a broad range of cellular processes such as cell survival, growth, stress, immune and inflammatory responses[8]. Within the murine nervous system, the NF-κB heterodimers c-Rel/p65 and p50/p65, and p50 homodimers play an important role during development[9], while the activity of p50/p65 was shown to be predominant in the adult brain[10]. Activation of NF-κB can be triggered by multiple stimuli such as cytokines like tumour necrosis factor-α (TNF-α) or neurotransmitters like AMPA or glutamate in mouse and rat cerebellar granule cells[11,12]. In murine neurons, NF-κB signalling and its target genes are involved in neuroprotection/degeneration[13], neurite growth[14], the formation of dendritic spines and their functionality[15], axonal outgrowth[16] and synaptic plasticity[17,18]. Activation of NF-κB in human and murine cells is also known to be caused by oxidative stress, an increase in intracellular reactive oxygen species (ROS) such as H_2O_2, superoxide (O_2^-), or hydroxyl radical (OH)[19]. Whithin the nervous system, oxidative stress leads to activation of NF-κB with a direct linkage to several neurological diseases and brain damage[20]. In functional neurons from humans or mice, activation of various glutamate receptors also induces oxidative stress[21]. On the contrary, reactive oxygen intermediate hydrogen peroxide (H_2O_2) is known to act as a second messenger despite its cytotoxicity[20,22]. In primary rat cerebellar granule cells, the direct exogenous addition of H_2O_2 to culture medium activates NF-κB[23], as well as it was observed previously in different

[1]Molecular Neurobiology, University of Bielefeld, Bielefeld, Germany. [2]Department of Cell Biology, University of Bielefeld, Bielefeld, Germany. Correspondence and requests for materials should be addressed to B.K. (email: barbara.kaltschmidt@uni-bielefeld.de)

human cell lines[22,24,25]. In human and mouse embryonic stem cells, metabolic oxidation is known to directly regulate cell differentiation[26]. Maintenance of redox balance was further shown to be crucial for stemness and self-renewal of hematopoietic stem cells (HSCs) and neural stem cells (NSCs)[27] from mice and humans. On the other hand, NF-κB signalling is directly linked to proliferation of rat NSCs[28] and early neuronal differentiation of mouse NSCs[29], although its direct role in protection of human stem cell-derived neurons against oxidative stress still remains unclear.

In the present study, we demonstrate a neuroprotective role of NF-κB-p65 through maturation of human glutamatergic neurons derived from neural crest-derived stem cells (NCSCs) after oxidative stress insult. During vertebrate development, neural crest cells migrate from the border between neural plate and non-neural ectoderm and give rise to a wide variety of cell types like neurons, glial cells, or melanocytes[30]. Pursuing their role in development, neural crest cells also persist into adulthood as NCSCs within various tissues, including skin[31], cornea[32], periodontal ligament[33], palate[34] and pulp of teeth[35]. A particularly interesting population of NCSCs has been found within the respiratory epithelium in the inferior turbinate of the human nose. Inferior turbinate stem cells (ITSCs) are able to differentiate into a wide variety of cell types from mesodermal and neuro-ectodermal lineages, such as chondrocytes, osteocytes, adipocytes, and glutamatergic as well as dopaminergic neurons[36–38]. Due to their capability to efficiently give rise to neuronal cell types, ITSCs harbor great potential for the treatment of neurodegenerative diseases[38]. Thus, ITSC-derived neurons served as an ideal model system for determining molecular mechanisms regulating maturation and survival of human neurons in the present study. We differentiated ITSCs into $MAP2^+/NF200^+/Synaptophysin^+/vGlut2^+$-glutamatergic neurons, which we successfully stimulated with AMPA or glutamate leading to activation of NF-κB-p65. TNF-α-dependent stimulation of NF-κB-p65 in ITSC-derived neurons resulted in a significant neuroprotective effect against oxidative stress-induced cell death. ITSC-derived neurons from female donors further showed a significantly elevated sensitivity to H_2O_2 as well as a 2-fold increase in TNF-α-dependent neuroprotection compared to neurons from male donors. Our findings reveal NF-κB-p65 as a key player in neuroprotection of NCSC-derived neurons in a sex-dependent manner, indicating the pivotal role of NF-κB-signalling during stem cell-based neuronal differentiation.

Results

Inferior turbinate stem cells efficiently differentiate into glutamatergic neurons *in vitro*. In order to gain an appropriate model system for studying the role of NF-κB in neuroprotection during maturation of human NCSC-derived neurons, ITSCs were cultivated following a directed neuronal differentiation procedure for 30 days (Fig. 1a)[36,38]. Exposure of ITSCs to a neuronal induction medium for 28 days resulted in a neuronal-like morphology indicated by retraction of the cytoplasm towards the nucleus, and extended cellular processes resulting in neurite outgrowth (Fig. 1b–d). Immunocytochemical analyses confirmed the presence of the mature neuronal markers Neurofilament 200 (Fig. 1e,h; 92,28% ± 1,45%), MAP-2 (92,28% ± 4,20%; Fig. 1f,h) and Synaptophysin (75,77% ± 11,55%; Fig. 1i,h). Interestingly, 19,77% ± 6,85% of ITSC-derived neurons were positive for Calretinin (Fig. 1g,h), while a small subpopulation of 13,70% ± 8,74% differentiated ITSCs expressed the glial marker Olig-2 (Fig. 1h). Further validating their successful differentiation, only 20,96% ± 0,63% of ITSCs showed co-expression of Nestin (Fig. 1j) after directed differentiation. Accordingly, RT-PCR analyses depicted a decrease in expression of Nestin as well as an increased expression of MAP-2 and Synaptophysin in ITSC-derived neurons (Fig. 1i). Characterizing these neurons in more detail, we observed AMPA receptor subunit 1, NMDA receptor subunit 1, glutamate metabotropic receptor 1 (GRM1) as well as the vesicular glutamate transporter 1 (VGLUT1) were robustly expressed (Fig. 1k). Immunocytochemistry further confirmed the glutamatergic phenotype of ITSC-derived neurons by revealing vGlut2-expression on the protein level (Fig. 1l,m).

Integration and differentiation of ITSC-derived glutamatergic neurons after transplantation into *ex vivo*-cultivated murine organotypic hippocampal slices. In addition to their efficient neuronal differentiation *in vitro*, we evaluated the ability of ITSCs to integrate and differentiate within a neural environment by transplanting undifferentiated stem cells into murine organotypic hippocampal slices (Fig. 2a). Transplanted human ITSCs were able to integrate in the murine neural tissue and differentiated into $MAP\text{-}2^+$ and $Gat\text{-}1^+$ neurons after 14 days of co-cultivation (Fig. 2b,c). Furthermore, GFP-positive ITSCs integrated particularly into the dentate gyrus of organotypic hippocampal slices, where they exhibited a clear neuronal phenotype accompanied by expression of vGlut2 and Synaptophysin on protein level (Fig. 2d–f). These findings confirmed that ITSCs are also able to give rise to excitatory glutamatergic neurons within the proper neural environment.

ITSC-derived glutamatergic neurons show AMPA or glutamate-dependent activation of NF-κB-p65. We next investigated the capability of ITSC-derived neurons to respond to the excitatory neurotransmitter glutamate (GLU) or its agonist α-amino-3-hydroxyl-5-methyl-4-isoxazole-propionate (AMPA). Stimulation with GLU or AMPA resulted in a significant increase in nuclear translocation of NF-κB-p65 in a dose-dependent manner (5–10 µM) in comparison to untreated neurons. On the contrary, treatment with 50 µM GLU or AMPA led to a significant decline in NF-κB-p65 nuclear translocation compared to 10 µM-treatment (Fig. 3a–d). We also observed high levels of basal NF-κB-activity (Fig. 3a–d), in accordance to the already described constitutive activation of NF-κB particularly in glutamatergic neurons[39]. Treatment of ITSC-derived neurons with their respective inhibitors 6-cyano-7-nitroquinoxaline-2, 3-dione (CQNX) or dibenzocycloheptene-imine (MK-801) prior to application of GLU (10 µM) or AMPA (10 µM) resulted in a significantly reduced translocation of NF-κB-p65 into the nucleus compared to the stimulation approaches (Fig. 3e,f). These findings provide pharmacological evidence that both kinds of receptors were expressed in human ITSC-derived glutamatergic neurons, which in turn were observed to be fully functional after 30 days of differentiation.

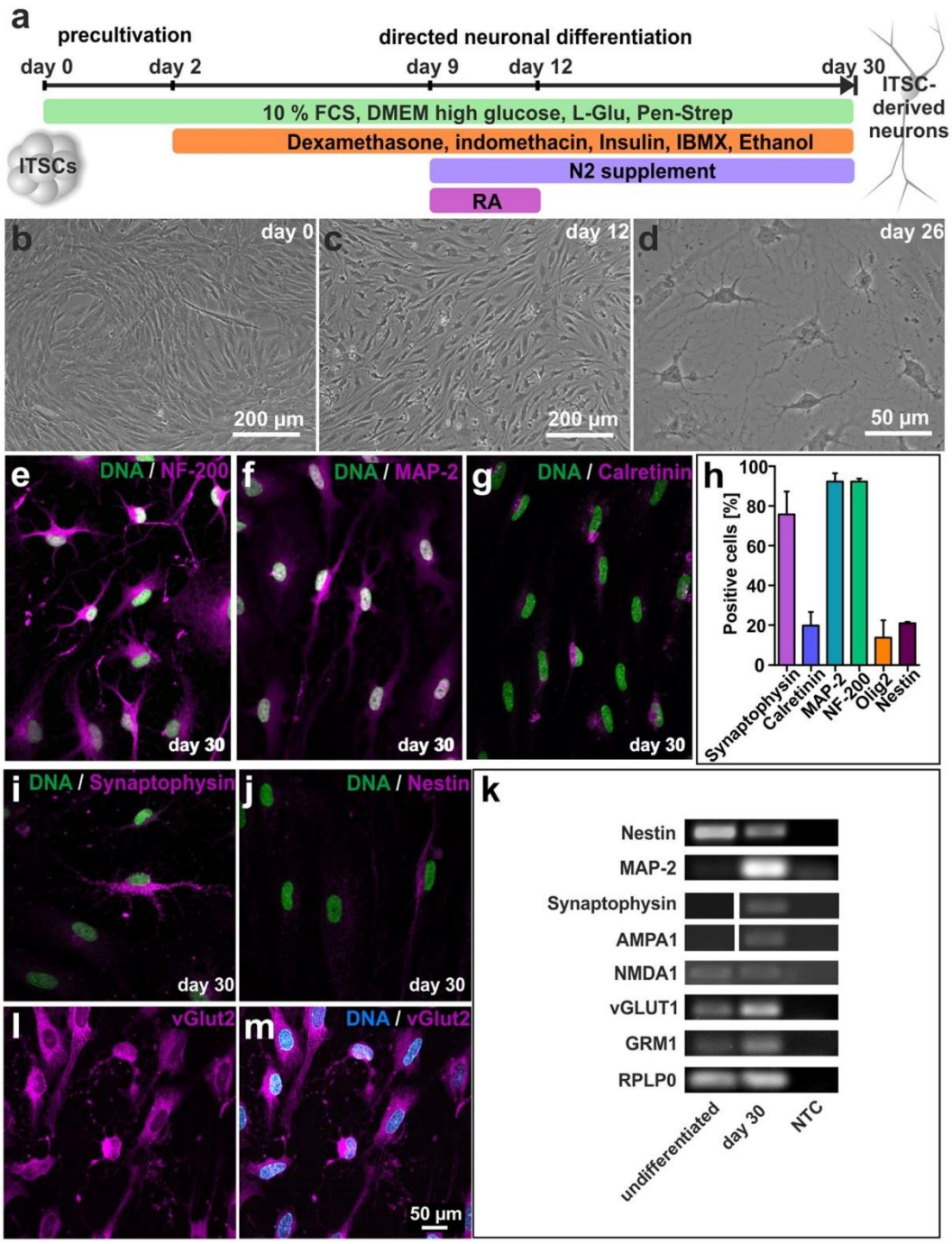

Figure 1. Adult human neural crest-derived stem cells from the inferior turbinate (ITSCs) are able to efficiently differentiate into glutamatergic neurons. (**a**) Schematic view of the neuronal differentiation procedure. (**b**–**d**) ITSCs changed their morphology towards a neuronal phenotype during directed neuronal differentiation. (**e**–**g**) Immunocytochemistry of ITSCs after 30 days of differentiation depicting the presence of positive cells for NF200, MAP-2 and calretinin (perinuclear region). (**h**) Quantification of immunocytochemical analyses showing the percentage of Synaptophysin$^+$ (75,77% ± 11,55%), Calretinin$^+$ (19,77% ± 6,85%), MAP-2$^+$ (92,28% ± 4,20%), NF-200$^+$ (92,28% ± 1,45%), Olig2$^+$ (13,70% ± 8,74%) and Nestin$^+$ (13,70% ± 0,63%) ITSC-derived neurons after 30 days of neuronal differentiation (Mean ± SEM; n = 3). (**I**,**j**) Differentiated ITSCs were positive for Synaptophysin, while small population of cells remained Nestin-positive. (**k**) RT-PCR of differentiated ITSCs showing the down-regulation of Nestin and the up-regulation of MAP-2, Synaptophysin, AMPA receptor subunit 1, NMDA Receptor subunit 1, vesicular glutamate transporter 1, and glutamate metabotropic receptor 1 after neuronal differentiation at the mRNA level. RPLP0 served as housekeeping gene. NTC: non-template-control. The grouped gels were cropped from different parts of the same gel or from different gels, full-length gels are shown in the Supplementary Fig. S1. (**l**,**m**) Most ITSC-derived neurons were vGlut2$^+$.

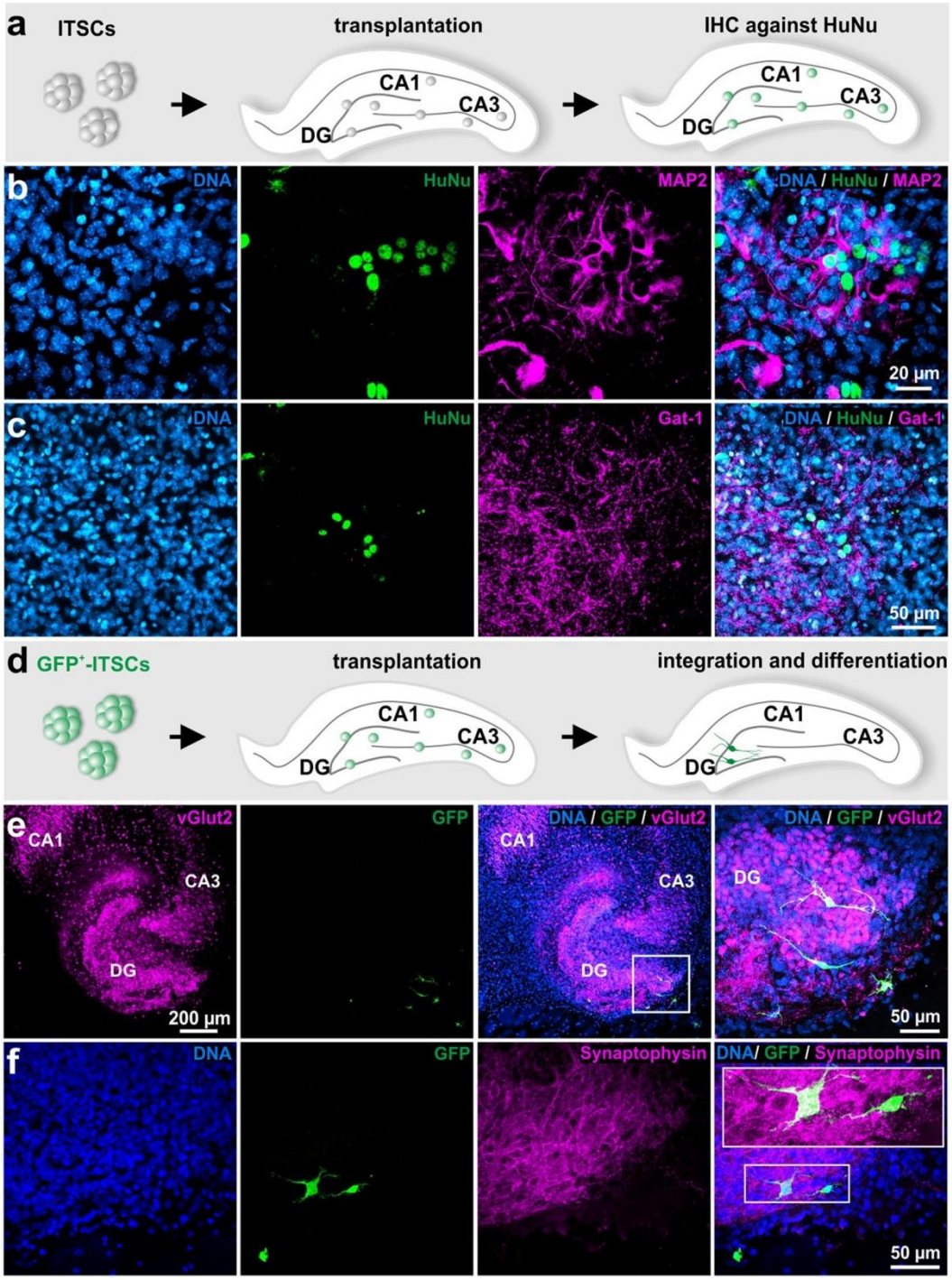

Figure 2. ITSCs differentiate into glutamatergic neurons after transplantation into *ex vivo*-cultivated murine organotypic hippocampal slices. (**a**) Schematic view showing experimental design of ITSC-transplantation into organotypic hippocampal slices. (**b**) Immunocytochemistry showing differentiation of ITSCs into MAP-2 and Gat-1 positive neurons, indicating successful integration of transplanted ITSCs into organotypic hippocampal slices. (**d**) Schematic view showing the transplantation procedure of GFP-positive ITSCs into organotypic hippocampal slices. E: GFP^+-ITSCs integrated within the dentate gyrus of the hippocampus and exhibited a neuronal phenotype accompanied by expression of vGlut2 and Synaptophysin.

Stimulation with TNF-α leads to significantly increased nuclear translocation of NF-κB-p65 in ITSC-derived glutamatergic neurons. After validating human ITSC-derived neurons as a model system for studying the role of NF-κB during maturation, we investigated the potential of TNF-α to stimulate NF-κB in these neurons. Stimulation of ITSC-derived neurons with TNF-α for 30 minutes or 1 hour resulted in nuclear translocation of NF-κB-p65 (Fig. 4a, arrowheads) in comparison to untreated neurons or 24 h of

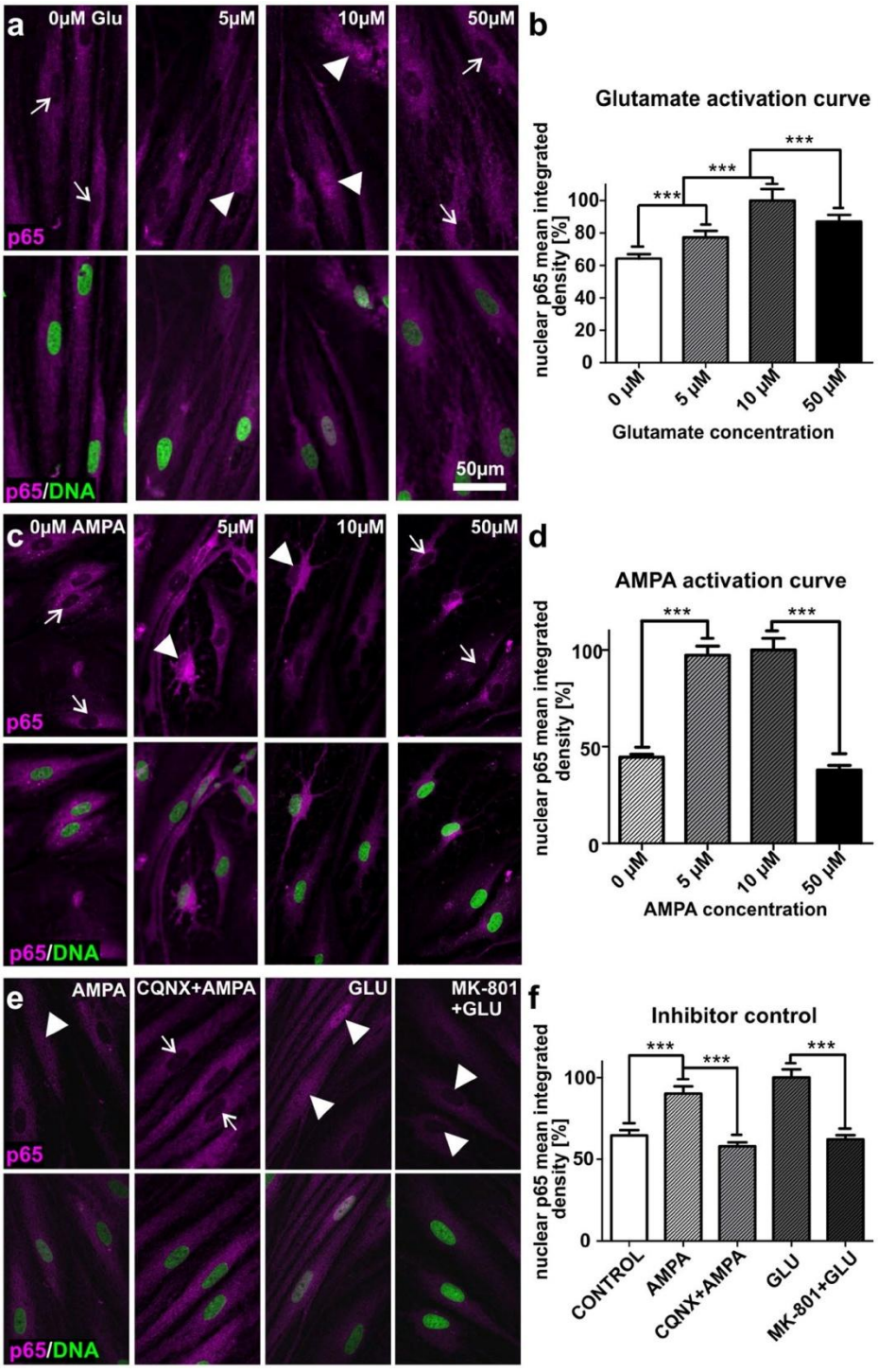

Figure 3. Stimulation of glutamatergic neurons derived from ITSCs leads to significantly increased nuclear translocation of NF-κB-p65. (**a**,**b**) Immunocytochemistry and respective quantification of nuclear mean integrated density of NF-κB-p65 revealed significantly increased nuclear translocation of NF-κB-p65 in ITSC-derived neurons after glutamate (GLU)-dependent stimulation (arrowheads) compared to control (arrows). Mean values were normalized to the highest value. (**c**,**d**) AMPA-dependent stimulation resulted in significantly increased nuclear translocation of NF-κB-p65 in ITSC-derived neurons (arrowheads) compared to control (arrows). Mean values were normalized to the highest value. (**e**,**f**) Pre-treatment of ITSC-derived neurons with dibenzocycloheptenimine (MK-801) or 6-cyano-7-nitroquinoxaline-2, 3-dione (CQNX) prior to GLU or AMPA-treatment led a significant decrease in nuclear translocation of NF-κB-p65 (arrows) compared to GLU or AMPA-dependent stimulation (arrowheads). Mean values were normalized to the highest value. Statistical analysis was performed using Graph Pad Prism 5. Normality of the data sets was refuted after analysis using Kolmogorov-Smirnov and Shapiro-Wilk normality tests. Non-parametric Mann-Whitney test was further used (***$p \leq 0.001$), error bars indicate the standard error of the mean (SEM).

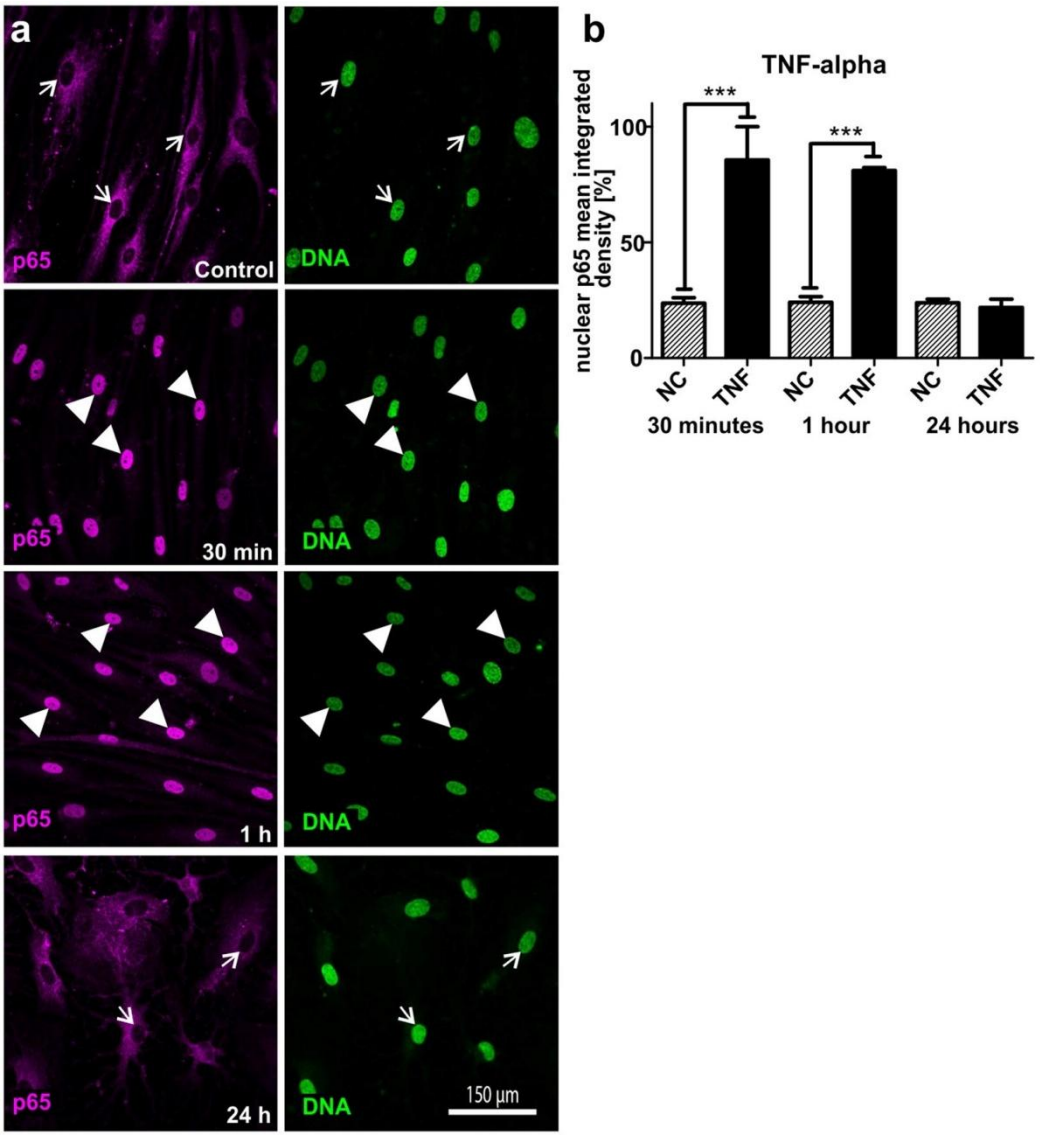

Figure 4. TNF-α-dependent stimulation of glutamatergic neurons derived from ITSCs leads to nuclear transloaction of NF-κB-p65. (**a**) Immunocytochemistry of ITSC-derived neurons (30 days of differentiation) showed nuclear translocation of NF-κB-p65 after treatment with TNF-α for 30 min or 1 h (arrowheads), whereas control and 24 h-TNF-α-treatment did not result in nuclear translocation of NF-κB-p65 (arrows). (**b**) Quantification of nuclear mean integrated density of NF-κB-p65 confirmed the significant increase in nuclear NF-κB-p65 after TNF-α-treatment of ITSC-derived neurons for 30 min or 1 h compared to 24 h and untreated control. Mean values were normalized to the highest value. Statistical analysis was performed using Graph Pad Prism 5. Normality was refuted after analysis using Kolmogorov-Smirnov and Shapiro-Wilk normality tests. Non-parametric Mann-Whitney test was further used. ***$p \leq 0.001$, error bars indicate the standard error of the mean (SEM).

TNF-α-treatment (Fig. 4a, arrows). Quantification of the NF-κB-p65 nuclear mean integrated density clearly validated these dynamics by showing a highly significant increase in nuclear NF-κB-p65 fluorescence after 30 minutes (93,96% ± 6,04%) and 1 hour (88,00% ± 12,00%) of TNF-α-treatment compared to untreated controls (<20%) (Fig. 4b). Accordingly, stimulation of ITSC-derived neurons with TNF-α for 24 hours did not result in a significantly different nuclear NF-κB-p65 fluorescence intensity compared to control (Fig. 4b).

TNF-α-pre-treatment of human ITSC-derived glutamatergic neurons leads to increased NF-κB-p65-activity upon oxidative stress insult. We further analyzed the effect of H_2O_2-mediated oxidative stress insult on the activity of NF-κB-p65 in ITSC-derived neurons. Application of H_2O_2 for 25 h on human glutamatergic neurons differentiated for 30 days led to significantly increased nuclear translocation of NF-κB-p65 in comparison to control. In order to analyze a potential neuroprotective role of NF-κB, we performed a pre-treatment using 10 ng/ml TNF-α during 2 hours prior to oxidative stress insult.

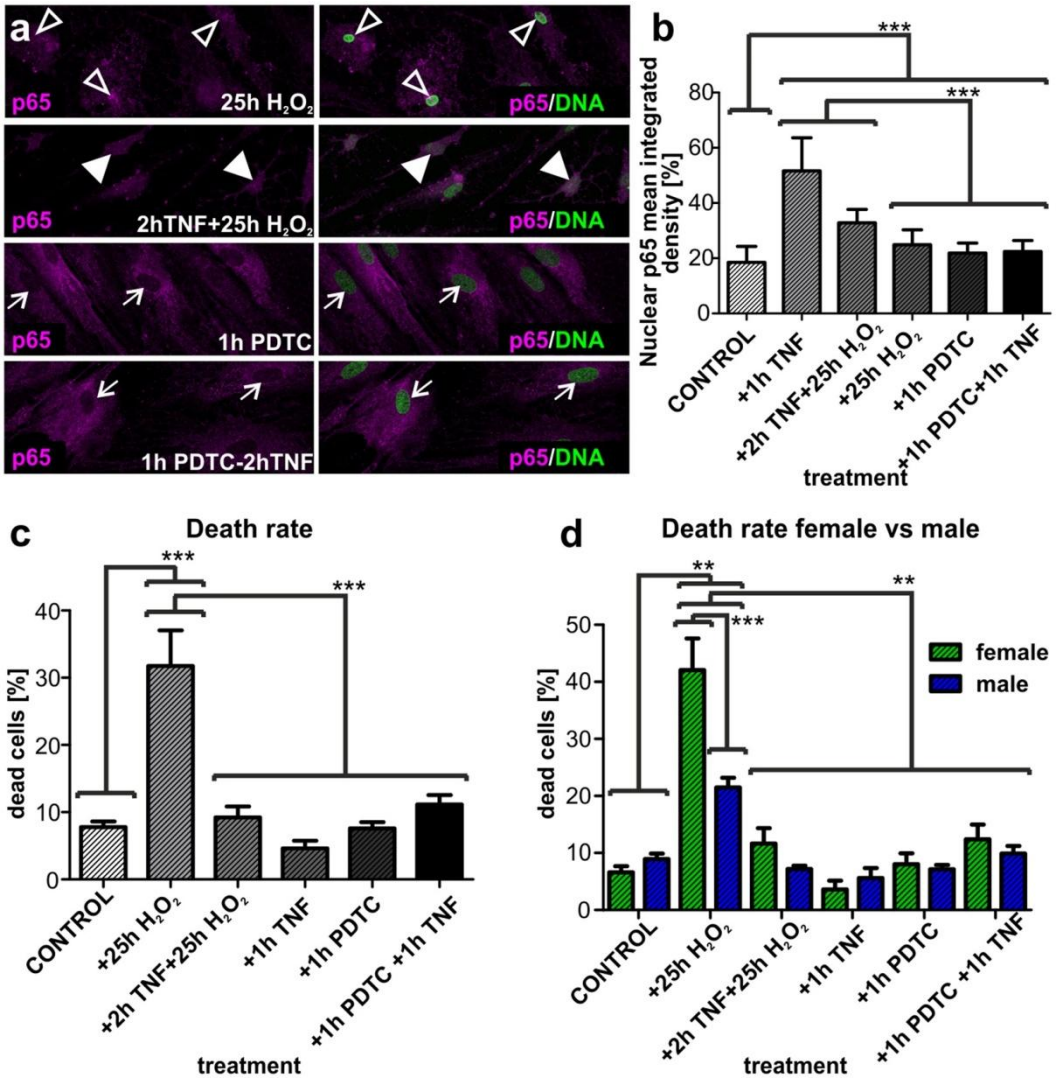

Figure 5. Treatment of ITSC-derived glutamatergic neurons with TNF-α prevents from oxidative stress-mediated cell death in a sex-dependent manner. (**a**) Immunocytochemistry of ITSC-derived neurons after 30 days of differentiation, after treatment with H_2O_2 alone, TNF-α-pre-treatment prior to H_2O_2, PDTC alone and PDTC followed by TNF-α against NF-κB-p65. (**b**) Quantification of immunocytochemical assays showed significantly increased nuclear translocation of NF-κB-p65 after treatment with TNF-α alone and TNF-α prior to H_2O_2 compared to H_2O_2 alone and untreated control. Pre-treatment of ITSC-derived neurons with PDTC for one hour followed by TNF-α-treatment did not result in significantly different amounts of nuclear NF-κB-p65 compared to PDTC alone. Mean values were normalized to the highest value. (**c**) Quantification of neuronal cell death showed significant death after oxidative stress insult (H_2O_2) compared to TNF-α/ H_2O_2, TNF-α, PDTC, PDTC/TNF-α and untreated control (n = 6). (**d**) Quantification of neuronal cell death after oxidative stress (H_2O_2), TNF-α-pre-treatment, TNF-α, PDTC, PDTC/ TNF-α and untreated control comparing sex differences (n = 3 males, n = 3 females). Data were showed not to be normally distributed using Kolmogorov-Smirnov and Shapiro-Wilk normality tests. Non-parametric Kruskal-Wallis test was further used ($p \leq 0.001$), and Tukey's post-hoc test (**$p \leq 0.01$, ***$p \leq 0.001$). Mean ± SEM (standard error of the mean).

Notably, TNF-α-pre-treatment of ITSC-derived glutamatergic neurons followed by H_2O_2-mediated oxidative stress resulted in a significant increase in nuclear translocation of NF-κB-p65 compared to the H_2O_2 alone or control (Fig. 5a,b, arrowheads). We further applied pyrrolidine dithiocarbamate (PDTC) as a control for guided inhibition of NF-κB. Pre-treatment of the cultivated neurons with PDTC for 1 hour followed by application of TNF-α or sole PDTC-treatment did not result in changes of nuclear translocation of NF-κB-p65 (Fig. 5a,b, arrows). Quantification of the nuclear mean integrated density for p65 indicated a small but significant increase in nuclear NF-κB-p65 in both treatments compared to the untreated negative control (Fig. 5b).

ITSC-derived glutamatergic neurons are protected from oxidative stress-mediated cell death via TNF-α-dependent activation of NF-κB-p65. Determining the physiological consequences of TNF-α-dependent activation of NF-κB-p65 during oxidative stress, we analysed the death rate of ITSC-derived

neurons after treatment with H_2O_2 or H_2O_2 after TNF-α-pre-treatment. H_2O_2-mediated oxidative stress led to robust and significant apoptosis of glutamatergic neurons compared to untreated control (Fig. 5c). Notably, this H_2O_2-mediated increase in apoptosis was significantly reduced down to a level similar to control upon TNF-α-pre-treatment prior to the oxidative stress insult (Fig. 5c). Application of TNF-α alone did not affect the survival of ITSC-derived neurons nor did the PDTC treatment, or the PDTC treatment followed by TNF-α in comparison to control (Fig. 5c).

Sensitivity of glutamatergic neurons to ROS-mediated cell death and neuroprotection via NF-κB-p65 is dependent on the sex of the ITSC-donor. Investigating the effects of TNF-α-treatment on H_2O_2-mediated death of ITSC-derived neurons in more detail, we analysed the amount of apoptotic cells after oxidative stress and TNF-α-dependent neuroprotection in dependence to the sex of the ITSC-donor. We observed a significant increase in cell death of neurons differentiated from female ITSC-donors compared to their male counterparts, indicating an elevated sensitivity of human female glutamatergic neurons to oxidative stress (Fig. 5d). Pre-treatment of ITSC-derived neurons from female donors with TNF-α led to a significant and complete neuroprotection against H_2O_2-mediated cell death. Although neurons from male ITSC-donors were likewise protected against cell death via exposure to TNF-α, we observed a 2-fold increase in TNF-α-dependent neuroprotection in female ITSC-derived neurons compared to those differentiated from male ITSCs. These findings not only demonstrate a NF-κB-dependent neuroprotection of ITSC-derived neurons against oxidative stress-mediated cell death, but emphazise the dependence on its sensitivity to the sex of the ITSC-donor.

TNF-α-mediated neuroprotection of ITSC-derived neurons is accompanied by sex-specific expression of NF-κB target genes. To investigate the role of NF-κB-p65 in protection of ITSC-derived neurons from H_2O_2-mediated death in more detail, expression of NF-κB target genes was assessed by qPCR. Treatment of ITSC-derived neurons with H_2O_2 or TNF-α followed by H_2O_2 led to significantly increased expression levels of cAMP-dependent protein kinase catalytic subunit alpha (PKAcatα) compared to control. We further observed a significant increase in PKAcatα expression levels in male ITSCs-derived neurons compared to those differentiated from female ITSCs after TNF-α/H_2O_2-treatment (Fig. 6a). On the contrary, we observed a significant increase in manganese superoxide dismutase (Mn-SOD, SOD2) mRNA levels only in female ITSCs-derived neurons upon exposure to TNF-α, H_2O_2 and TNF-α/H_2O_2 compared to control (Fig. 6b). Expression levels of cellular inhibitor of apoptosis protein-1 and 2 (c-IAP1 and c-IAP2) showed the tendency to be elevated in male ITSCs-derived neurons after TNF-α/H_2O_2-treatment compared to their female counterparts (Fig. 6c,d) however no significant alteration was detectable. Treatment with TNF-α, H_2O_2 and TNF-α/H_2O_2 further resulted in significantly increased expression levels of insulin-like growth factor 1 (IGF1) in ITSCs-derived neurons compared to control (Fig. 6e), although no significant sex-dependent differences were observable. Female ITSCs-derived neurons showed significantly increased expression levels of IGF2 after H_2O_2 and TNF-α/H_2O_2-treatment compared to control (Fig. 6f), while no expression was detectable in male counterparts. However, sole treatment with TNF-α resulted in significantly increased expression levels of IGF2 in neurons from male and female donors compared to control (Fig. 6F). These findings strongly suggest a sex-specific NF-κB-p65 target gene expression in dependence to TNF-α-mediated neuroprotection during oxidative stress.

Discussion

The present study describes for the first time a neuroprotective role of NF-κB-p65 in human ITSC-derived glutamatergic neurons after oxidative stress insult in a sex-specific manner. We successfully differentiated human neural crest-derived inferior turbinate stem cells into MAP-2$^+$/NF200$^+$/Synaptophysin$^+$/vGlut2$^+$-glutamatergic neurons by application of a directed differentiation assay or via transplantation into organotypic mouse hippocampal slice cultures. Extending our previous findings depicting vesicle recycling and calcium spiking of ITSC-derived neurons[38], we validated their functionality by showing increased NF-κB-activity upon stimulation with the excitatory neurotransmitter glutamate or its agonist AMPA. Inhibitor controls using CQNX and MK-801 led to a decrease in glutamate or AMPA-dependent stimulation of NF-κB-activity, further validating the specificity of the respective receptors. In accordance to our findings, stimulation of ionotropic glutamate receptors was shown to activate NF-κB in primary rat cerebellar granule neurons[11,12]. Given the pivotal role of NF-κB signalling in key elements for neuronal morphology like neurite growth[14], dendritic spine formation[15], axonal outgrowth[16] and synaptic plasticity[17,18], our data suggest the participation of NF-κB in the normal physiology of the human nervous system.

In addition to its AMPA- and glutamate-dependent stimulation, we also observed a significant increase in NF-κB-activity in ITSC-derived neurons after treatment with TNF-α. In canonical NF-κB-signalling, recognition of stimuli like cytokines or neurotransmitters leads to phosphorylation of IκB kinases[40,41], in turn resulting in phosphorylation, polyubiquitination and 26S-proteasome-mediated degradation of IκBs. Demasking of the nuclear translocation signal region of p50/p65 by degradation of IκBs is subsequently followed by translocation of p50/p65 into the nucleus and activation of target gene expression by binding to κB elements[18,42–45]. TNF-α is one of the best characterized cytokines inducing this pathway, and its receptors TNFR1 and TNFR2 are widely expressed in the nervous system both in neurons and glia[46–48]. Besides its modulatory effects of neuronal responses to excitotoxic and hypoxic insults in the nervous system[49], the absence of TNFR was shown to result in an increased neuronal damage following either ischemic or kainic acid induced excitotoxic damage[50]. In mouse NSCs, TNF-α-mediated NF-κB signalling was reported to be required for initial neuronal differentiation[29]. In accordance, preliminary data from our lab suggests that NF-κB-c-Rel might be the relevant subunit for glutamatergic differentiation and not NF-κB-p65, having no significant differences with respect to sex (unpublished data). Extending these findings, mature human ITSC-derived glutamatergic neurons revealed a significantly increased

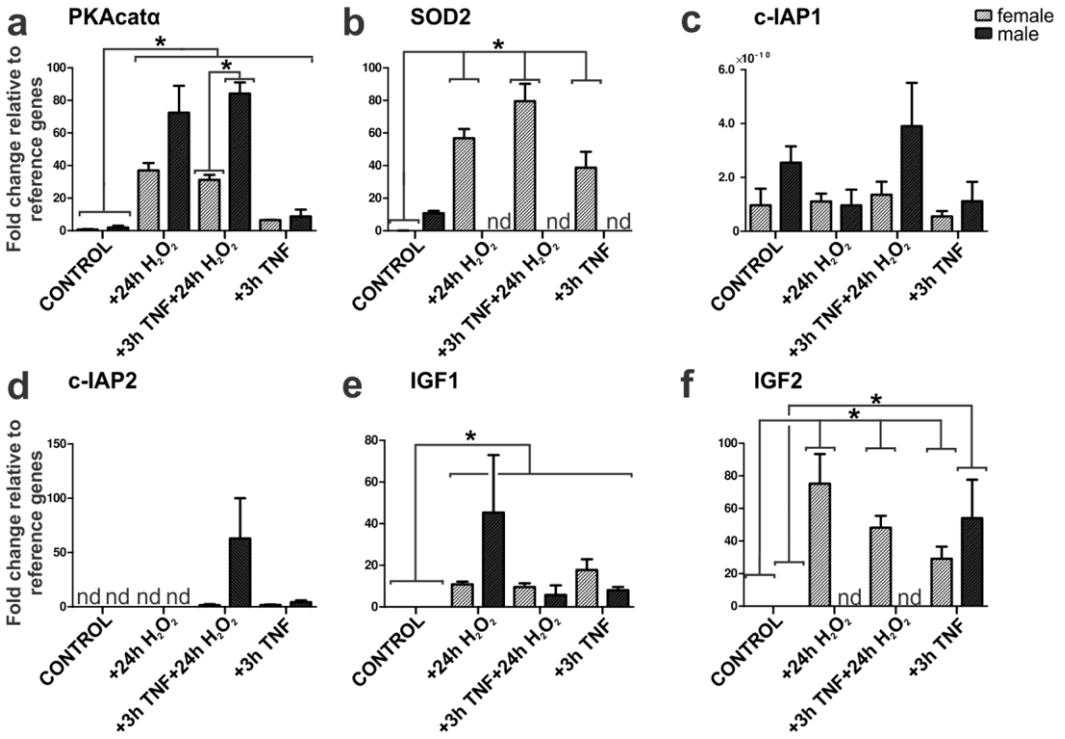

Figure 6. Quantitative polymerase chain reaction revealed sex-specific NF-κB-p65 target gene expression after TNF-α-dependent neuroprotection upon oxidative stress-insult. (**a**) qPCR analysis revealed increased PKAcatα mRNA levels after H_2O_2 alone, TNF-α-pre-treatment prior to H_2O_2 and TNF-α alone compared to untreated control, with a stronger effect for TNF-α/H_2O_2 in male compared to female ITSC-derived neurons. (**b**) SOD2 mRNA levels significantly increased in female ITSC-derived neurons compared to control and compared to their male counterparts. (**c**) qPCR analysis showing c-IAP1 mRNA levels in male and female ITSC-derived neurons. (**d**) qPCR analysis showing c-IAP2 mRNA levels in male and female ITSC-derived neurons. (**e**) qPCR analysis showing significant increased IGF1 mRNA levels compared to control in male and female ITSC-derived neurons. (**f**) IGF2 mRNA levels were significantly elevated only in female-derived neurons compared to control. Non-parametric Mann Whitney test (*$p \leq 0.05$), mean ± SEM (standard error of the mean, n = 3 males, n = 3 females). Nd: Not detectable. Ct values were normalized to reference genes β-actin and RPLP0 (Ribosomal Protein Lateral Stalk Subunit P0).

nuclear translocation of NF-κB-p65 after TNF-α-stimulation in the present study, indicating the crucial role of NF-κB-signalling during stem cell-based neuronal differentiation and neuroprotection in humans.

Being a major cause of several neurologic diseases and brain damage[20], oxidative stress is known to be directly caused by Alzheimer's disease via amyloid beta peptide-dependent production of hydrogen peroxide through metal ion reduction[51,52]. In Parkinson's disease, free radicals accumulate in the *substantia nigra pars compacta*, resulting in the formation of 6-hydroxydopamine, in turn leading to the generation of superoxide[53,54]. In the present study, H_2O_2-mediated oxidative stress led to cell death of human ITSC-derived glutamatergic neurons. Although NF-κB is known to be activated by oxidative stress in the nervous system[20], several studies indicated its neuroprotective role in murine cells. Here, Heck and colleagues demonstrated an Insulin-like growth factor-1-mediated neuroprotection of rat primary cerebellar neurons against oxidative stress directly associated to activation of NF-κB[55]. Erythropoietin-mediated neuroprotection of rat cerebral cortical cell cultures from oxidative stress was also shown to occur in an NF-κB-dependent manner[56]. On the contrary, Zou and colleagues demonstrated TNF-α-treatment of rat hippocampal-entorhinal cortex slice cultures to result in increased neurotoxicity to both glutamate and oxidative stress[57]. In the present study, TNF-α-pre-treatment led to a significant decrease in H_2O_2-mediated cell death of ITSC-derived human neurons accompanied by a significantly increased nuclear translocation of NF-κB-p65. Our data therefore demonstrate a key role of NF-κB-p65 in protection of human stem cell-derived neurons from oxidative stress, further emphasizing the importance of NF-κB-signalling in neuroprotection[20,55,56].

Interestingly, we further observed a significantly elevated sensitivity of ITSC-derived neurons from female donors to oxidative stress-induced cell death and to NF-κB-dependent neuroprotection compared to neurons from male donors. These findings were confirmed by a differential expression of NF-κB target genes in dependence to the sex of the ITSC-donor. Here, increased SOD2 mRNA levels observed in female but not in male ITSC-derived neurons indicated a NF-κB-associated induction of SOD2 protecting against oxidative stress-induced neuronal apoptosis. Accordingly, SOD2 expression was described to be inducible by TNF-α, having an anti-apoptotic role by directly reducing cellular ROS levels[58]. Next to SOD2, expression levels of IGF2 were significantly elevated only in female neurons after TNF-α/H_2O_2-treatment compared to control. IGF2 is known

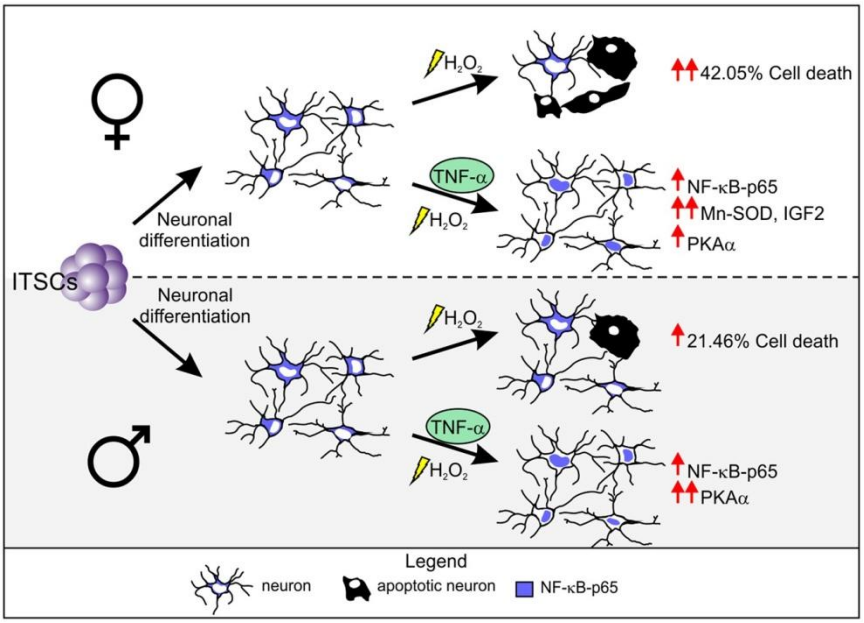

Figure 7. Sex-specific response to oxidative stress insult and NF-κB-mediated neuroprotection in human NCSC-derived neurons. Female ITSC-derived neurons responded with a higher sensitivity to oxidative stress-induced neuronal death, and TNF-α-mediated neuroprotection compared to their male counterparts. TNF-α-mediated neuroprotection led to an increase in NF-κB-p65 nuclear translocation, triggering differential expression of sex-specific NF-κB target genes.

to promote synapse formation and spine maturation in the mouse brain[59]. Within a mouse model of Alzheimer's disease, IGF2 administration rescued spine formation and synaptic transmission in the hippocampus[60]. In accordance to the present findings, IGF2 was reported to have an antioxidant and neuroprotective effect on oxidative damage and mitochondrial function in cultured adult rat cortical neurons[61,62]. In contrast to their female counterparts, male ITSC-derived neurons showed a significant increase in the expression level of PKAcatα after TNF-α/H_2O_2-treatment. Interestingly, we observed no significantly altered expression levels of the antiapoptotic proteins c-IAP1 and c-IAP2, known mediators of TNF-α-dependent neuroprotection[63]. With PKAcatα being an essential regulator in learning and memory by transducing synaptic responses through CREB signalling[64,65] and controlling synaptic incorporation of AMPA receptors[66], PKA-activity may directly contribute to the neuroprotective effects observed here. Although being a matter of debate, sex-dependencies in stem cell biology have already been shown in terms of autosomal gene expression[67] and proliferation[68], particularly regarding mouse NSCs[69,70]. Compared to their male counterparts, female muscle-derived stem cells were reported to have higher muscle regeneration efficiency in mice[71]. In terms of neuroinflammation and neuroprotection, sex-dependent differences between patients have been likewise reported in ischemic stroke[4], PD[2], or AD[3]. While female AD patients were described to have an increased risk of developing AD[3,6], PD was shown to have a greater prevalence in male patients[2]. These data are in agreement with sex-specific differences found in adult murine microglia, where female microglia exhibited a neuroprotective phenotype upon ischemic insult, which was retained after being transferred into male brains[72]. In addition sex-specific differences in the expression of iNOS and NF-κB were previously reported in human polymorphonuclear neutrophils, being higher in female than in male cells[73]. In line with these findings, our data indicate for the first time a direct sex-dependent difference in neuroprotection of human stem cell-derived neurons against oxidative stress mediated by NF-κB-signalling.

In summary, we provide here evidence that NF-κB-p65 is a key player in neuroprotection of human neurons against oxidative stress in a sex-dependent manner. We demonstrate a sex-dependent difference of stress response and TNF-α-mediated neuroprotection, with a strong increase of both H_2O_2-mediated cell death as well as neuroprotection against cell death in female derived neurons compared to their male counterparts (Fig. 7). These differences were emphasized by the sex-specific differential expression of NF-κB-p65 target genes SOD2 and IGF2 in TNF-α-dependent neuroprotection upon oxidative stress-insult. In line with our findings, increasing evidences pointing towards sex-specific differences in risk and severity of neurodegenerative diseases, such as Alzheimer's disease. Since oxidative stress is directly associated to neurodegenerative diseases, but little is known about the underlying molecular mechanisms of neuroprotection, NF-κB-signalling may be a crucial parameter for treatment strategies and neuronal regeneration therapies.

Methods

All methods were performed in accordance to the relevant guidelines and regulations.

Isolation and Cultivation of ITSCs. ITSCs were isolated from adult human inferior turbinate tissue obtained by biopsy during routine surgery after informed consent according to local and international guidelines and cultivated as described previously[36]. The ethics board of the medical faculty of the University of Münster

approved all the procedures described in this article (No. 2012–015-f-S). All experiments and methods were performed in accordance to the relevant guidelines and regulations. ITSCs were cultivated within the 3D blood plasma (BP) matrix[37], and dissociated ITSCs were resuspended in Dulbecco's modified Eagle's medium/Ham F-12 (DMEM/F-12; Biochrom, Berlin, Germany, http://www.biochrom.de) supplemented with basic fibroblast growth factor-2 (FGF2; 40 ng/ml; Miltenyi Biotec), epidermal growth factor (EGF; 20 ng/ml; Miltenyi Biotec) and B27 supplement (Gibco) followed by supplementation with 10% of clinically accredited therapeutic human blood plasma (BP; obtained from Institut für Laboratoriums und Transfusionsmedizin, Bad Oeynhausen, Germany) and cultivated at 37 °C, 5% O_2 and 5% CO_2.

Neuronal differentiation. For neuronal differentiation, cells of six donors were expanded within the 3D BP matrix, were dissociated and resuspended in DMEM high glucose (Sigma-Aldrich) containing 200 mM L-glutamine (Sigma-Aldrich) and 10% foetal calf serum (Sigma-Aldrich) an plated at a density of 5×10^4 cells per 24 well plate followed by cultivation at 37 °C, 5% CO_2 and atmospheric O_2 for 2 days. Afterwards, 1 µM dexamethasone (Sigma-Aldrich), 2 µM insulin (Sigma-Aldrich), 500 µM 3-isobutyl-1-methylxanthine (Sigma-Aldrich), 200 µM indomethacin (Sigma-Aldrich) and 200 µM ethanol were added to the medium to induce neuronal differentiation (neuronal induction medium, NIM). After 9 days of differentiation cells were induced adding 0.5 µM retinoic acid (Sigma Aldrich) and 1x N-2 supplement (Gibco, Darmstadt, Germany, http://www.invitrogen.com). Subsequently, the medium was changed by removing half of the volume, followed by addition of fresh pre-warmed NIM containing 1x N-2 supplement[38]. ITSCs were differentiated for 1 month, and further stimulated using different drugs, or treated for immunocytochemical and RT-PCR analysis.

Neuronal stimulation. After 30 days of differentiation neurons were exposed to the excitatory neurotransmitter glutamate (GLU) or its agonist α-amino-3-hydroxyl-5-methyl-4-isoxazole-propionate (AMPA), the cytokine Tumour Necrosis Factor α (TNF-α, Calbiochem®), hydrogen peroxide (H_2O_2), and the NF-κB inhibitor pyrrolidine dithiocarbamate (PDTC)[23]. Before treatment with glutamate or AMPA, cells were washed three times with buffered control salt solution (CSS)[74] containing 120 mM NaCl, 5.4 mM KCl, 1.8 mM CaCl2, 25 mM Tris HCl (pH 7.4), 15 mM D-glucose. For inhibitor controls cells were pre-incubated with either 1 µM dibenzocycloheptеneimine (MK-801, Tochris Bioscience, UK)[75] or 50 µM 6-cyano-7-nitroquinoxaline-2,3-dione (CQNX, Tochris Bioscience, UK)[12] for 10 min at 37 °C, before 10 min treatment with glutamate or AMPA respectively. After treatment with different concentrations, cells were washed with CSS and incubated with complete medium for 45 min at 37 °C. Control cells received identical incubation times and washing steps with CSS[12]. The pulse with 10 ng/ml TNF-α was performed for 30 min, 1 h, and 24 hours. For oxidative stress induction, 300 µM H_2O_2 were applied during 25 h and to analyse the neuroprotective role of NF-κB during oxidative stress, a pre-treatment with 10 ng/ml TNF-α was performed for 2 hours previous to the treatment with H_2O_2. Untreated control cells received identical incubation times. In order to confirm NF-κB activation due to TNF-α, a pre-treatment using 100 µM PDTC for one hour was performed and samples were directly used or further treated with TNF-α for at least one hour. For Indirect immunofluorescence assay cells were fixed as described below. For Smart-seq. 2, cells were directly used after treatment, whose duration was 3 h for PDTC and TNF-α treatment as well as for the combination treatments.

Immunocytochemistry. Differentiated ITSCs were fixed for 15 min in phosphate-buffered 4% paraformaldehyde (PFA 4% pH 7.4) at room temperature (RT) followed by 3 wash steps in phosphate-buffered saline (1xPBS). The cells were permeabilized with 0.02% Triton X-100 and blocked using 5% of appropriate serum or 3% BSA for 30 minutes at RT, followed by incubation with primary antibodies for 1 hour at RT. Antibodies used were anti-neurofilament NF200 (1:200, N4142, Sigma-Aldrich), anti-MAP-2 (1:100, Sc-20172, Santa Cruz Biotechnology), anti-Synaptophysin (1:250, MAB5258, Merck Millipore), anti-vGlut2 (1:200, MAB5504, Millipore), anti-nestin (1:200, MAB5326, Millipore) anti-olig-2 (1:250, Q13516, R&D Systems), anti-NF-kappa B p65 (D14E12, Cell Signaling). The secondary fluorochrome-conjugated antibodies (1:300; goat anti-mouse Alexa 555, goat anti-rabbit Alexa 555, donkey anti goat Alexa 555; Life Technologies) were incubated for 1 hour at RT. Nuclear counterstaining was performed with 49,6-diamidino-2-phenylindole (DAPI; 1 µg/ml; Sigma-Aldrich) for 15 min at RT. Fluorescence imaging was performed using a confocal laser scanning microscope (LSM 780; Carl Zeiss, Jena, Germany) and analyzed using ZEN software from the same provider or ImageJ[76].

Reverse transcription Polymerase Chain Reaction. Total RNA was isolated using the TRI Reagent (Sigma-Aldrich) according to the manufacture's guidelines. Quality and concentration of RNA were assessed via Nanodrop ultraviolet spectrophotometry. cDNAs were synthesized by reverse transcription using the First Strand cDNA Synthesis Kit (Fermentas Life Sciences). PCR was performed using the GoTaq (Promega) according to the manufacturer's guidelines and 10 µM primers (Sigma-Aldrich). The cycling conditions comprised an initial denaturation of 1 min at 94 °C and 35–38 cycles of 15 s at 94 °C, 15 s at 60 °C, and 20 s at 72 °C followed by a final elongation for 1 min at 72 °C. For primer sequences see Table 1.

SMART-Seq2. For full-length cDNA generation, the protocol recently described by Picelli *et al.*[77] slightly modified was applied. Approximately 20000 cells/treatment ITSC-derived glutamatergic neurons were used. Cells were harvested by centrifugation (5000 g for 5 min at RT) and directly lysed with an adjusted amount of lysis buffer (RNase inhibitor, 0.2% Triton X-100). Afterwards the annealing mix containing AccuStart Taq Polymerase HiFi (Quanta bio), oligo-dT primer, dNTP-mix, was added to the cell lysate. Probes were incubated 3 min at 72 °C, and the reverse transcription-mix containing SuperScript II reverse transcriptase (Thermo Fisher Scientific) was added. Reverse transcription, relying on template-switching reaction was performed. The cycling program comprised an initial denaturation of 90 min at 42 °C, following by 9 cycles of 2 min at 50 °C and 2 min at 42 °C followed

Target	Sequence 5′-3′
Nestin	CAGCGTTGGAACAGAGGTTG
Rev-Nestin	GCTGGCACAGGTGTCTCAAG
MAP-2	GAGGATGAAGAGGGTGCCTT
Rev-MAP-2	AGCTCTCCGTTGATCCCATTC
Synaptophysin	TGTAGTCTGGTCAGTGAAGCC
Rev- Synaptophysin	GCAGGGCTCAGACAGATAA
AMPA receptor subunit 1	GGGCGATAATTCAAGTGTTCA
Rev-AMPA receptor subunit 1	GGCTCCGTATTTTCCATCAC
NMDA Receptor subunit 1	GCTCCTCGAGAAGGAGAACA
Rev- NMDA Receptor subunit 1	GCCATTGTAGATGCCCACTT
Vesicular glutamate transporter 1	CACAAGACTCGGGAGGAGTG
Rev- Vesicular glutamate transporter 1	GCCTCATCCTCCATTTCGCT
Glutamate metabotropic receptor 1	AGCTGCTGATTTCTCAGCCAA
Rev- Glutamate metabotropic receptor 1	GCCTCCAACATTGGAATGGA
Tyrosine Hydroxylase	CCGTGCTAAACCTGCTCTTC
Rev- Tyrosine Hydroxylase	CGCACGAAGTACTCCAGGT
Choline Transporter	GGCACAGCTGAAGCAGTTTA
Rev- Choline Transporter	CCCATGCGTTTTCCATAGAT
Serotonin transporter	CTCCGAGGACAACATCACCT
Rev- Serotonin transporter	CAGAGGTCTTGACGCCTTTC
RPLP0 (Ribosomal Protein Lateral Stalk Subunit P0)	TGGGCAAGAACACCATGATG
Rev-RPLP0	AGTTTCTCCAGAGCTGGGTTGT

Table 1. Primers sequences for reverse transcription polymerase chain reaction.

by a final elongation for 15 min at 70 °C. The PCR pre-amplification mix was added to the first-strand reaction. PCR pre-amplification-cycling-program comprised an initial denaturation of 3 min at 98 °C and 21 cycles of 20 s at 98 °C, 15 s at 67 °C, and 6 min at 72 °C followed by a final elongation for 5 min at 72 °C.

Real-time PCR. All Quantitative polymerase chain reactions (qPCR) were performed in triplicate using Platinum SYBR Green qPCR Super-Mix UDG (Invitrogen), according to the manufacturer's guidelines, and assayed with a Rotor Gene 6000 (Qiagen). Primers used are listed in Supplementary Table S1.

Hippocampal Slice Culture and transplantation of ITSCs on organotypic hippocampal slice cultures and Immunocytochemical analyzes. For organotypic hippocampal slice culture, hippocampi of mice (postnatal day 5) were isolated and rapidly cut perpendicularly to the longitudinal axis into 400 µm thick slices with a McIllwain Tissue Chopper. Slices were cultivated on culture plate inserts according to De Simoni and Yu[78]. In parallel ITSCs were transduced with lentivirus pFUGW containing a constitutively expressed GFP-gene under control of human ubiquitin c promoter. GFP^+-ITSCs and ITSCs were cultivated as neurospheres for 2 days. 7 days after slice preparation, dissociated cells (1×10^4) were dropped onto each slice following by cultivation for 14 days at 37 °C and 5% CO_2. Slices were cut off from the membrane and free-floating fixated in PFA 4% for 1 h at 4 °C on agitation. After 3 washes with PBS, slices were incubated in PBS containing 0.1% Triton X-100 and 5% goat serum for 1 hour at RT. Slices containing transplanted GFP^+-ITSCs were double immuno-labeled with anti-GFP (1:1000, sc-9996, Santa Cruz) combined with anti-synaptophysin (1:200) or anti-vGlut2 (1:200). Slices containing transplanted non transduced ITSCs were free-floating stained with anti-human nuclei (HuNu, 1:200, MAB1281, Millipore) combined with anti-MAP-2 (1:100), or anti-Gat1 (1:200, AB1570, Millipore) for 48 h at 4 °C. Respective secondary fluorochrome-conjugated antibodies (goat anti-mouse Alexa 555, goat anti-rabbit Alexa 555, donkey anti-rabbit Alexa 488, donkey anti-mouse Alexa 488) were applied for 2 h at RT under exclusion of light. Nuclei were stained with TOTO®-3 Iodide (642/660 nm, life technologies).

Cell Counting and Statistics. Quantification of immunofluorescence staining was performed for minimum 3 different donors. For each time point 6–12 pictures were analysed per donor, where the mean of the nuclear integrated density was measured by defining the region of interest with the nuclear DNA channel using ImageJ[76]. For analysis of neuronal survival the same channel was used to analyse the nuclear chromatin morphology. Nonviable neurons were recognized by nuclear condensation and/or fragmented chromatin. In phase contrast images, those neurons were irregularly shaped with shrunken cell body and/or disrupted neurites. The number of viable and nonviable neurons was counted in four to five field pictures and death rate was calculated. Data was further analysed for statistics using Past3[79] and/or GraphPad Prism 5 (GraphPad software, La Jolla, CA, http://www.graphpad.com). Normality of the data sets was refuted after analysis using Kolmogorov-Smirnov and Shapiro-Wilk normality tests. Non-parametric Kruskal-Wallis test was used to compare the medians between the different data sets for the different donors (***$p \leq 0.001$). Non-parametric Mann-Whitney test was used to compare two pair of groups (***$p \leq 0.001$). Further analysis was performed using Tukey's test (*$p \leq 0.05$, **$p \leq 0.01$, ***$p \leq 0.001$).

References

1. Vajda, F. J. Neuroprotection and neurodegenerative disease. *Journal of clinical neuroscience: official journal of the Neurosurgical Society of Australasia* **9**, 4–8, https://doi.org/10.1054/jocn.2001.1027 (2002).
2. Gillies, G. E., Pienaar, I. S., Vohra, S. & Qamhawi, Z. Sex differences in Parkinson's disease. *Frontiers in neuroendocrinology* **35**, 370–384, https://doi.org/10.1016/j.yfrne.2014.02.002 (2014).
3. Li, R. & Singh, M. Sex differences in cognitive impairment and Alzheimer's disease. *Frontiers in neuroendocrinology* **35**, 385–403, https://doi.org/10.1016/j.yfrne.2014.01.002 (2014).
4. Spychala, M. S., Honarpisheh, P. & McCullough, L. D. Sex differences in neuroinflammation and neuroprotection in ischemic stroke. *Journal of neuroscience research* **95**, 462–471, https://doi.org/10.1002/jnr.23962 (2017).
5. Vina, J. & Lloret, A. Why women have more Alzheimer's disease than men: gender and mitochondrial toxicity of amyloid-beta peptide. *Journal of Alzheimer's disease: JAD* **20**(Suppl 2), S527–533, https://doi.org/10.3233/JAD-2010-100501 (2010).
6. Henderson, V. W. & Buckwalter, J. G. Cognitive deficits of men and women with Alzheimer's disease. *Neurology* **44**, 90–96, https://doi.org/10.1212/WNL.44.1.90 (1994).
7. Demarest, T. G. & McCarthy, M. M. Sex differences in mitochondrial (dys)function: Implications for neuroprotection. *Journal of bioenergetics and biomembranes* **47**, 173–188, https://doi.org/10.1007/s10863-014-9583-7 (2015).
8. Karin, M. & Lin, A. NF-kappaB at the crossroads of life and death. *Nat Immunol* **3**, 221–227, https://doi.org/10.1038/ni0302-221 (2002).
9. Bakalkin, G., Yakovleva, T. & Terenius, L. NF-kappa B-like factors in the murine brain. *Developmentally-regulated and tissue-specific expression. Brain Res Mol Brain Res* **20**, 137–146, https://doi.org/10.1016/0169-328X(93)90119-A (1993).
10. Meffert, M. K., Chang, J. M., Wiltgen, B. J., Fanselow, M. S. & Baltimore, D. NF-kappa B functions in synaptic signaling and behavior. *Nat Neurosci* **6**, 1072–1078, https://doi.org/10.1038/nn1110 (2003).
11. Guerrini, L., Blasi, F. & Denis-Donini, S. Synaptic activation of NF-kappa B by glutamate in cerebellar granule neurons *in vitro*. *Proceedings of the National Academy of Sciences of the United States of America* **92**, 9077–9081, https://doi.org/10.1073/pnas.92.20.9077 (1995).
12. Kaltschmidt, C., Kaltschmidt, B. & Baeuerle, P. A. Stimulation of ionotropic glutamate receptors activates transcription factor NF-kappa B in primary neurons. *Proceedings of the National Academy of Sciences of the United States of America* **92**, 9618–9622, https://doi.org/10.1073/pnas.92.21.9618 (1995).
13. Kaltschmidt, B. & Kaltschmidt, C. NF-kappaB in the nervous system. *Cold Spring Harb Perspect Biol* **1**, a001271, https://doi.org/10.1101/cshperspect.a001271 (2009).
14. Gavalda, N., Gutierrez, H. & Davies, A. M. Developmental switch in NF-kappaB signalling required for neurite growth. *Development* **136**, 3405–3412, https://doi.org/10.1242/dev.035295 (2009).
15. Boersma, M. C. *et al*. A requirement for nuclear factor-kappaB in developmental and plasticity-associated synaptogenesis. *J Neurosci* **31**, 5414–5425, https://doi.org/10.1523/JNEUROSCI.2456-10.2011 (2011).
16. Imielski, Y. *et al*. Regrowing the adult brain: NF-kappaB controls functional circuit formation and tissue homeostasis in the dentate gyrus. *PLoS One* **7**, e30838, https://doi.org/10.1371/journal.pone.0030838 (2012).
17. Mattson, M. P. & Meffert, M. K. Roles for NF-kappaB in nerve cell survival, plasticity, and disease. *Cell Death Differ* **13**, 852–860, https://doi.org/10.1038/sj.cdd.4401837 (2006).
18. Hayden, M. S. & Ghosh, S. Regulation of NF-kappaB by TNF family cytokines. *Semin Immunol* **26**, 253–266, https://doi.org/10.1016/j.smim.2014.05.004 (2014).
19. Bowie, A. & O'Neill, L. A. Oxidative stress and nuclear factor-kappaB activation: a reassessment of the evidence in the light of recent discoveries. *Biochem Pharmacol* **59**, 13–23, https://doi.org/10.1016/S0006-2952(99)00296-8 (2000).
20. Kaltschmidt, B., Sparna, T. & Kaltschmidt, C. Activation of NF-kappa B by reactive oxygen intermediates in the nervous system. *Antioxid Redox Signal* **1**, 129–144, https://doi.org/10.1089/ars.1999.1.2-129 (1999).
21. Coyle, J. T. & Puttfarcken, P. Oxidative stress, glutamate, and neurodegenerative disorders. *Science* **262**, 689–695, https://doi.org/10.1126/science.7901908 (1993).
22. Schmidt, K. N., Amstad, P., Cerutti, P. & Baeuerle, P. A. The roles of hydrogen peroxide and superoxide as messengers in the activation of transcription factor NF-kappa B. *Chem Biol* **2**, 13–22, https://doi.org/10.1016/1074-5521(95)90076-4 (1995).
23. Kaltschmidt, B., Uherek, M., Volk, B., Baeuerle, P. A. & Kaltschmidt, C. Transcription factor NF-kappaB is activated in primary neurons by amyloid beta peptides and in neurons surrounding early plaques from patients with Alzheimer disease. *Proceedings of the National Academy of Sciences of the United States of America* **94**, 2642–2647, https://doi.org/10.1073/pnas.94.6.2642 (1997).
24. Schreck, R., Rieber, P. & Baeuerle, P. A. Reactive oxygen intermediates as apparently widely used messengers in the activation of the NF-kappa B transcription factor and HIV-1. *EMBO J* **10**, 2247–2258, https://doi.org/10.1002/j.1460-2075.1991.tb07761.x (1991).
25. Meyer, M., Schreck, R. & Baeuerle, P. A. H2O2 and antioxidants have opposite effects on activation of NF-kappa B and AP-1 in intact cells: AP-1 as secondary antioxidant-responsive factor. *EMBO J* **12**, 2005–2015, https://doi.org/10.1002/j.1460-2075.1993.tb05850.x (1993).
26. Yanes, O. *et al*. Metabolic oxidation regulates embryonic stem cell differentiation. *Nature chemical biology* **6**, 411–417, https://doi.org/10.1038/nchembio.364 (2010).
27. Bigarella, C. L., Liang, R. & Ghaffari, S. Stem cells and the impact of ROS signaling. *Development* **141**, 4206–4218, https://doi.org/10.1242/dev.107086 (2014).
28. Widera, D., Mikenberg, I., Elvers, M., Kaltschmidt, C. & Kaltschmidt, B. Tumor necrosis factor alpha triggers proliferation of adult neural stem cells via IKK/NF-kappaB signaling. *BMC neuroscience* **7**, 64, https://doi.org/10.1186/1471-2202-7-64 (2006).
29. Zhang, Y. *et al*. Nuclear factor kappa B signaling initiates early differentiation of neural stem cells. *Stem Cells* **30**, 510–524, https://doi.org/10.1002/stem.1006 (2012).
30. Le Douarin, N. M., Calloni, G. W. & Dupin, E. The stem cells of the neural crest. *Cell Cycle* **7**, 1013–1019, https://doi.org/10.4161/cc.7.8.5641 (2008).
31. Toma, J. G. *et al*. Isolation of multipotent adult stem cells from the dermis of mammalian skin. *Nat Cell Biol* **3**, 778–784, https://doi.org/10.1038/ncb0901-778 (2001).
32. Brandl, C., Florian, C., Driemel, O., Weber, B. H. & Morsczeck, C. Identification of neural crest-derived stem cell-like cells from the corneal limbus of juvenile mice. *Exp Eye Res* **89**, 209–217, https://doi.org/10.1016/j.exer.2009.03.009 (2009).
33. Techawattanawisal, W. *et al*. Isolation of multipotent stem cells from adult rat periodontal ligament by neurosphere-forming culture system. *Biochem Biophys Res Commun* **357**, 917–923, https://doi.org/10.1016/j.bbrc.2007.04.031 (2007).
34. Widera, D. *et al*. Adult palatum as a novel source of neural crest-related stem cells. *Stem Cells* **27**, 1899–1910, https://doi.org/10.1002/stem.104 (2009).
35. Widera, D. *et al*. Highly efficient neural differentiation of human somatic stem cells, isolated by minimally invasive periodontal surgery. *Stem Cells Dev* **16**, 447–460, https://doi.org/10.1089/scd.2006.0068 (2007).
36. Hauser, S. *et al*. Isolation of novel multipotent neural crest-derived stem cells from adult human inferior turbinate. *Stem Cells Dev* **21**, 742–756, https://doi.org/10.1089/scd.2011.0419 (2012).
37. Greiner, J. F. *et al*. Efficient animal-serum free 3D cultivation method for adult human neural crest-derived stem cell therapeutics. *Eur Cell Mater* **22**, 403–419, https://doi.org/10.22203/eCM.v022a30 (2011).
38. Muller, J. *et al*. Intrastriatal transplantation of adult human neural crest-derived stem cells improves functional outcome in parkinsonian rats. *Stem Cells Transl Med* **4**, 31–43, https://doi.org/10.5966/sctm.2014-0078 (2015).

39. Kaltschmidt, C., Kaltschmidt, B., Neumann, H., Wekerle, H. & Baeuerle, P. A. Constitutive NF-kappa B activity in neurons. *Molecular and cellular biology* **14**, 3981–3992, https://doi.org/10.1128/MCB.14.6.3981 (1994).
40. Varfolomeev, E. & Vucic, D. Intracellular regulation of TNF activity in health and disease. *Cytokine*, https://doi.org/10.1016/j.cyto.2016.08.035 (2016).
41. Peltzer, N., Darding, M. & Walczak, H. Holding RIPK1 on the Ubiquitin Leash in TNFR1 Signaling. *Trends in cell biology* **26**, 445–461, https://doi.org/10.1016/j.tcb.2016.01.006 (2016).
42. Hayden, M. S. & Ghosh, S. Shared principles in NF-kappaB signaling. *Cell* **132**, 344–362, https://doi.org/10.1016/j.cell.2008.01.020 (2008).
43. Ben-Neriah, Y. Regulatory functions of ubiquitination in the immune system. *Nat Immunol* **3**, 20–26, https://doi.org/10.1038/ni0102-20 (2002).
44. Perkins, N. D. Integrating cell-signalling pathways with NF-kappaB and IKK function. *Nat Rev Mol Cell Biol* **8**, 49–62, https://doi.org/10.1038/nrm2083 (2007).
45. Harhaj, E. W. & Dixit, V. M. Regulation of NF-kappaB by deubiquitinases. *Immunol Rev* **246**, 107–124, https://doi.org/10.1111/j.1600-065X.2012.01100.x (2012).
46. Kinouchi, K., Brown, G., Pasternak, G. & Donner, D. B. Identification and characterization of receptors for tumor necrosis factor-alpha in the brain. *Biochem Biophys Res Commun* **181**, 1532–1538, https://doi.org/10.1016/0006-291X(91)92113-X (1991).
47. Tchelingerian, J. L., Monge, M., Le Saux, F., Zalc, B. & Jacque, C. Differential oligodendroglial expression of the tumor necrosis factor receptors *in vivo* and *in vitro*. *Journal of neurochemistry* **65**, 2377–2380, https://doi.org/10.1046/j.1471-4159.1995.65052377.x (1995).
48. Dopp, J. M., Mackenzie-Graham, A., Otero, G. C. & Merrill, J. E. Differential expression, cytokine modulation, and specific functions of type-1 and type-2 tumor necrosis factor receptors in rat glia. *Journal of neuroimmunology* **75**, 104–112, https://doi.org/10.1016/S0165-5728(97)00009-X (1997).
49. Cheng, B., Christakos, S. & Mattson, M. P. Tumor necrosis factors protect neurons against metabolic-excitotoxic insults and promote maintenance of calcium homeostasis. *Neuron* **12**, 139–153, https://doi.org/10.1016/0896-6273(94)90159-7 (1994).
50. Bruce, A. J. *et al*. Altered neuronal and microglial responses to excitotoxic and ischemic brain injury in mice lacking TNF receptors. *Nat Med* **2**, 788–794, https://doi.org/10.1038/nm0796-788 (1996).
51. Huang, X. *et al*. The A beta peptide of Alzheimer's disease directly produces hydrogen peroxide through metal ion reduction. *Biochemistry* **38**, 7609–7616, https://doi.org/10.1021/bi990438f (1999).
52. Jang, J. H. & Surh, Y. J. beta-Amyloid induces oxidative DNA damage and cell death through activation of c-Jun N terminal kinase. *Annals of the New York Academy of Sciences* **973**, 228–236, https://doi.org/10.1111/j.1749-6632.2002.tb04639.x (2002).
53. Heikkila, R. E. & Cohen, G. 6-Hydroxydopamine: evidence for superoxide radical as an oxidative intermediate. *Science* **181**, 456–457, https://doi.org/10.1126/science.181.4098.456 (1973).
54. Wang, X. & Michaelis, E. K. Selective neuronal vulnerability to oxidative stress in the brain. *Frontiers in aging neuroscience* **2**, 12, https://doi.org/10.3389/fnagi.2010.00012 (2010).
55. Heck, S., Lezoualc'h, F., Engert, S. & Behl, C. Insulin-like growth factor-1-mediated neuroprotection against oxidative stress is associated with activation of nuclear factor kappaB. *The Journal of biological chemistry* **274**, 9828–9835, https://doi.org/10.1074/jbc.274.14.9828 (1999).
56. Digicaylioglu, M. & Lipton, S. A. Erythropoietin-mediated neuroprotection involves cross-talk between Jak2 and NF-kappaB signalling cascades. *Nature* **412**, 641–647, https://doi.org/10.1038/35088074 (2001).
57. Zou, J. & Crews, F. CREB and NF-kappaB transcription factors regulate sensitivity to excitotoxic and oxidative stress induced neuronal cell death. *Cellular and molecular neurobiology* **26**, 385–405, https://doi.org/10.1007/s10571-006-9045-9 (2006).
58. Circu, M. L. & Aw, T. Y. Reactive oxygen species, cellular redox systems, and apoptosis. *Free Radic Biol Med* **48**, 749–762, https://doi.org/10.1016/j.freeradbiomed.2009.12.022 (2010).
59. Schmeisser, M. J. *et al*. IkappaB kinase/nuclear factor kappaB-dependent insulin-like growth factor 2 (Igf2) expression regulates synapse formation and spine maturation via Igf2 receptor signaling. *J Neurosci* **32**, 5688–5703, https://doi.org/10.1523/JNEUROSCI.0111-12.2012 (2012).
60. Pascual-Lucas, M. *et al*. Insulin-like growth factor 2 reverses memory and synaptic deficits in APP transgenic mice. *EMBO Mol Med* **6**, 1246–1262, https://doi.org/10.15252/emmm.201404228 (2014).
61. Martin-Montanez, E. *et al*. Involvement of IGF-II receptors in the antioxidant and neuroprotective effects of IGF-II on adult cortical neuronal cultures. *Biochim Biophys Acta* **1842**, 1041–1051, https://doi.org/10.1016/j.bbadis.2014.03.010 (2014).
62. Martin-Montanez, E. *et al*. IGF-II promotes neuroprotection and neuroplasticity recovery in a long-lasting model of oxidative damage induced by glucocorticoids. *Redox Biol* **13**, 69–81, https://doi.org/10.1016/j.redox.2017.05.012 (2017).
63. Wang, C.-Y., Mayo, M. W., Korneluk, R. G., Goeddel, D. V. & Baldwin, A. S. NF-κB Antiapoptosis: Induction of TRAF1 and TRAF2 and c-IAP1 and c-IAP2 to Suppress Caspase-8 Activation. *Science* **281**, 1680–1683, https://doi.org/10.1126/science.281.5383.1680 (1998).
64. Abel, T. *et al*. Genetic demonstration of a role for PKA in the late phase of LTP and in hippocampus-based long-term memory. *Cell* **88**, 615–626, https://doi.org/10.1016/S0092-8674(00)81904-2 (1997).
65. Kaltschmidt, B. *et al*. NF-kappaB regulates spatial memory formation and synaptic plasticity through protein kinase A/CREB signaling. *Molecular and cellular biology* **26**, 2936–2946, https://doi.org/10.1128/MCB.26.8.2936-2946.2006 (2006).
66. Esteban, J. A. *et al*. PKA phosphorylation of AMPA receptor subunits controls synaptic trafficking underlying plasticity. *Nat Neurosci* **6**, 136–143, https://doi.org/10.1038/nn997 (2003).
67. Ronen, D. & Benvenisty, N. Sex-dependent gene expression in human pluripotent stem cells. *Cell reports* **8**, 923–932, https://doi.org/10.1016/j.celrep.2014.07.013 (2014).
68. Nakada, D. *et al*. Oestrogen increases haematopoietic stem-cell self-renewal in females and during pregnancy. *Nature* **505**, 555–558, https://doi.org/10.1038/nature12932 (2014).
69. Pawluski, J. L., Brummelte, S., Barha, C. K., Crozier, T. M. & Galea, L. A. Effects of steroid hormones on neurogenesis in the hippocampus of the adult female rodent during the estrous cycle, pregnancy, lactation and aging. *Frontiers in neuroendocrinology* **30**, 343–357, https://doi.org/10.1016/j.yfrne.2009.03.007 (2009).
70. Dulken, B. & Brunet, A. Stem Cell Aging and Sex: Are We Missing Something? *Cell stem cell* **16**, 588–590, https://doi.org/10.1016/j.stem.2015.05.006 (2015).
71. Deasy, B. M. *et al*. A role for cell sex in stem cell-mediated skeletal muscle regeneration: female cells have higher muscle regeneration efficiency. *The Journal of cell biology* **177**, 73–86, https://doi.org/10.1083/jcb.200612094 (2007).
72. Villa, A. *et al*. Sex-Specific Features of Microglia from Adult Mice. *Cell reports* **23**, 3501–3511, https://doi.org/10.1016/j.celrep.2018.05.048 (2018).
73. Ratajczak-Wrona, W., Nowak, K., Garley, M., Tynecka, M. & Jablonska, E. Sex-specific differences in the regulation of inducible nitric oxide synthase by bisphenol A in neutrophils. *Hum Exp Toxicol*, 960327118793188, https://doi.org/10.1177/0960327118793188 (2018).
74. Choi, D. W., Maulucci-Gedde, M. & Kriegstein, A. R. Glutamate neurotoxicity in cortical cell culture. *J Neurosci* **7**, 357–368, https://doi.org/10.1523/JNEUROSCI.07-02-00357.1987 (1987).
75. Hu, X. J. & Ticku, M. K. Chronic ethanol treatment upregulates the NMDA receptor function and binding in mammalian cortical neurons. *Brain Res Mol Brain Res* **30**, 347–356, https://doi.org/10.1016/0169-328X(95)00019-O (1995).

76. Schneider, C. A., Rasband, W. S. & Eliceiri, K. W. NIH Image to ImageJ: 25 years of image analysis. *Nat Methods* **9**, 671–675, https://doi.org/10.1038/nmeth.2089 (2012).
77. Picelli, S. *et al.* Full-length RNA-seq from single cells using Smart-seq2. *Nature Protocols* **9**, 171, https://doi.org/10.1038/nprot.2014.006 https://www.nature.com/articles/nprot.2014.006#supplementary-information (2014).
78. De Simoni, A. & Yu, L. M. Preparation of organotypic hippocampal slice cultures: interface method. *Nat Protoc* **1**, 1439–1445, https://doi.org/10.1038/nprot.2006.228 (2006).
79. Hammer O., Harper, D. A. T., Ryan, P. D. PAST: Paleontological statistics software package for education and data analysis. *Palaeontologia Electronica* **4**, 9pp (2001).

Acknowledgements

The excellent technical help of Angela Kralemann-Köhler is gratefully acknowledged. This work was funded by the University of Bielefeld. Lucia M Ruiz-Perera was funded by a DAAD Regierungsstipendien -Uruguay -ANII scholarship (91554135, POS_EXT_2013_1_13498).

Author Contributions

L.M.R.-P. Collection and assembly of data, data analysis and interpretation, conception and design, manuscript writing, final approval of manuscript. L.S. Collection and assembly of data, data analysis and interpretation, final approval of manuscript. B.A.W. Collection and assembly of data, data analysis and interpretation, final approval of manuscript. J.M. Collection and assembly of data, final approval of manuscript. J.F.W.G. Data analysis and interpretation, manuscript writing, final approval of manuscript. C.K. Conception and design, financial support, data analysis and interpretation, final approval of manuscript. B.K. Conception and design, financial support, data analysis and interpretation, manuscript writing, final approval of manuscript.

Additional Information

Supplementary information accompanies this paper at https://doi.org/10.1038/s41598-018-34394-8.

Competing Interests: The authors declare no competing interests.

Publisher's note: Springer Nature remains neutral with regard to jurisdictional claims in published maps and institutional affiliations.

PLOS ONE

RESEARCH ARTICLE

CRISPR/Cas9-mediated knockout of *c-REL* in HeLa cells results in profound defects of the cell cycle

Carsten Slotta[1☯], Thomas Schlüter[1☯], Lucia M. Ruiz-Perera[2], Hussamadin M. Kadhim[1], Tobias Tertel[1], Elena Henkel[1], Wolfgang Hübner[3], Johannes F. W. Greiner[1], Thomas Huser[3], Barbara Kaltschmidt[1,2], Christian Kaltschmidt[1]*

1 Department of Cell Biology, University of Bielefeld, Bielefeld, Germany, **2** AG Molecular Neurobiology, University of Bielefeld, Bielefeld, Germany, **3** Biomolecular Photonics, University of Bielefeld, Bielefeld, Germany

☯ These authors contributed equally to this work.
*c.kaltschmidt@uni-bielefeld.de

Citation: Slotta C, Schlüter T, Ruiz-Perera LM, Kadhim HM, Tertel T, Henkel E, et al. (2017) CRISPR/Cas9-mediated knockout of *c-REL* in HeLa cells results in profound defects of the cell cycle. PLoS ONE 12(8): e0182373. https://doi.org/10.1371/journal.pone.0182373

Editor: Maria Fiammetta Romano, Universita degli Studi di Napoli Federico II, ITALY

Received: March 21, 2017

Accepted: July 17, 2017

Published: August 2, 2017

Data Availability Statement: All relevant data are within the paper and its Supporting Information files.

Funding: The authors received no specific funding for this work.

Competing interests: The authors have declared that no competing interests exist.

Abstract

Cervical cancer is the fourth common cancer in women resulting worldwide in 266,000 deaths per year. Belonging to the carcinomas, new insights into cervical cancer biology may also have great implications for finding new treatment strategies for other kinds of epithelial cancers. Although the transcription factor NF-κB is known as a key player in tumor formation, the relevance of its particular subunits is still underestimated. Here, we applied CRISPR/Cas9n-mediated genome editing to successfully knockout the NF-κB subunit *c-REL* in HeLa Kyoto cells as a model system for cervical cancers. We successfully generated a homozygous deletion in the *c-REL* gene, which we validated using sequencing, qPCR, immunocytochemistry, western blot analysis, EMSA and analysis of off-target effects. On the functional level, we observed the deletion of *c-REL* to result in a significantly decreased cell proliferation in comparison to wildtype (wt) without affecting apoptosis. The impaired proliferative behavior of *c-REL*$^{-/-}$ cells was accompanied by a strongly decreased amount of the H2B protein as well as a significant delay in the prometaphase of mitosis compared to *c-REL*$^{+/+}$ HeLa Kyoto cells. *c-REL*$^{-/-}$ cells further showed significantly decreased expression levels of *c-REL* target genes in comparison to wt. In accordance to our proliferation data, we observed the *c-REL* knockout to result in a significantly increased resistance against the chemotherapeutic agents 5-Fluoro-2'-deoxyuridine (5-FUDR) and cisplatin. In summary, our findings emphasize the importance of c-REL signaling in a cellular model of cervical cancer with direct clinical implications for the development of new treatment strategies.

Introduction

Cervical cancer is an epithelial cancer, also called carcinoma, and the fourth common cancer in women worldwide with an estimated 5-year survival rate of 70% following diagnosis [1, 2]. Based on the degenerated cell type in the uterus, cervical cancer can be classified into

squamous cell cancer and adenocarcinoma [1]. The most common reason for cervical cancer is an infection by the human papilloma virus (HPV), namely by HPV 16 and HPV 18 causing malignant transformations or carcinogenesis in 85% of the diagnosed cases [3, 4]. Treatment strategies of cervical cancer highly depend on the stage of progression and range from radio- therapy and surgery [5] to chemotherapy with cisplatin or 5-fluorouracil (5-FU) [6, 7].

Discovered in 1986 [8, 9], the transcription factor nuclear factor kappa-light-chain-enhancer of activated B-cells (NF-κB) has been shown to play a key role in various cellular pro- cesses as cell growth, differentiation, apoptosis, inflammation, learning and memory as well as immunity [10, 11]. Given the importance of NF-κB in these processes, deregulation of its sig- naling is directly associated to the formation of tumors and cancer progression [12–14], partic- ularly regarding breast cancer [15] and cervical carcinomas [1]. In 2003, Nair and coworkers showed a constitutive activation of the NF-κB subunit p65 during human cervical cancer pro- gression. Here, NF-κB p65 was demonstrated to be particularly activated in high-grade squa- mous intraepithelial lesions and squamous cell carcinomas of the human uterine cervix [16]. Next to NF-κB p65, the subunit c-REL was shown to possess a key role in tumor formation. Initial studies demonstrated severe B-cell lymphomas in chickens infected with avian reticu- loendotheliosis comprising V-REL [17]. Expression of wildtype human *c-REL* in primary chicken spleen cell cultures was likewise shown to result in malignant transformation events [18], although respective mutations increasing the oncogenicity of the c-REL protein in the avian system were not observable in human cancers (reviewed in [19]). However, amplifica- tion of *c-REL* was observed in a broad range of human B-cell lymphomas [20, 21]. In terms of human cervical cancer, Shehata and coworkers demonstrated a 6-fold slowed cell growth in cultivated cervical cancer cells by expression of the *c-REL* homolog Xrel3 from *Xenopus laevi* [22]. Accordingly, downregulation of *c-REL* by small interfering RNA was shown to result in reduced proliferation of human keratinocytes [23], directly correlating *c-REL* signaling to impaired cell cycle progression in a non-cancerous environment. Expression of the *c-REL* homolog Xrel3 in human cervical cancer cells was further shown to lead to anti- or pro-apo- ptotic effects during cisplatin-treatment in a concentration-dependent manner. These findings emphasize the importance of *c-REL*-signaling in resistance of cervical carcinoma to chemo- therapeutic agents [24].

The present study further extends these promising findings by showing a profound overexpression of *c-REL* in cancers located in human ovary, cervix and endometrium using database mining. To investigate the role of *c-REL* in human cervical cancers in more detail, we applied CRISPR/Cas9n-mediated genome editing in a multiplex way to delete *c-REL* in HeLa Kyoto cells. Initially discovered as a part of adaptive immune system of bacteria and archaea [25], the clustered regularly interspaced short palindromic repeats (CRISPR) system has been developed to a state-of-the-art technique for editing the human genome [26, 27]. Applications of the CRISPR/Cas9-system particularly include cancer modeling [28] or knockout studies using human cancer cell lines [27, 29]. In the present study, we applied a Cas9 nickase mutant (Cas9n) inducing single-strand breaks to minimize the possibility of off-target cleavage in turn increasing the specificity of genome editing [30].

Using the CRISPR/Cas9n approach, we successfully deleted the *c-REL* gene on chromo- somes 2 of HeLa Kyoto cells (*c-REL*$^{-/-}$). In comparison to wildtype, *c-REL*$^{-/-}$ HeLa Kyoto cells showed a significantly decreased proliferation accompanied by strongly reduced amounts of histone H2B, a delay in the prometaphase of mitosis and decreased expression levels of *c-REL* target genes. We further observed a significantly increased resistance against the chemothera- peutic agents 5-Fluoro-2'-deoxyuridine (5-FUDR) and cisplatin in HeLa Kyoto cells with *c- REL* deletion compared to wildtype (wt). Our findings emphasize the importance of *c-REL*

signaling in a cellular model of cervical cancer with direct clinical implications concerning the resistance of cervical carcinoma to chemotherapeutic agents.

Materials and methods

Target design and cloning

The design of the sgRNAs was done using the CRISPR/Cas9n Target Online Predictor from University of Heidelberg (crispr.cos.uni-heidelberg.de). The gene sequence was taken from Ensembl Genome Browser (ensembl.org). Two nicking pairs were designed resulting in two double strand breaks creating a deletion. Nicking pairs were chosen according to the criteria described by Ran and coworkers [30]. All oligos designed were cloned into one vector essen- tially as described [31].

Cell culture and transfection

HeLa Kyoto cells [32] were cultured in Dulbecco's Modified Eagle's Medium (DMEM) (Sigma Aldrich, Taufkirchen, Germany) containing high glucose (25 mM), and sodium pyruvate (1 mM). This medium was supplemented with 10% (v/v) heat-inactivated fetal calf serum (FCS) (VWR, Darmstadt, Germany), 2 mM L-glutamine (Sigma Aldrich), 100 U/ml Penicillin/Strep- tomycin (P/S) (Sigma Aldrich), and 0.5 mg/ml geneticin (G418) (Sigma Aldrich). Cells were cultivated at 37˚C with 5% CO_2 at saturated humidity.

Transfection of HeLa Kyoto cells (3 x 10^5 cells / transfection) was performed by electroporation using Amaxa Cell Line Nucleofector Kit R (Lonza, Basel, Schweiz) according to the manufacturer's protocol. 48 hours after transfection knockout generation was checked by genomic PCR and cells were used for limiting dilution to obtain clonal *c-REL* knockout cells.

Genomic PCR and Native PAGE

For cell lysis, cells were harvested at 300 g for 5 min and resuspended in cell lysis buffer (0.1 μg/mL gelatine, 50 mM KCl, 1.5 mM $MgCl_2$, 0.45% NP40, 10 mM TRIS pH 8.3, 0.45% TWEEN 20). Proteinase K (20 mg/ml, Serva Electrophoresis, Heidelberg, Germany) was added followed by incubation of the cell lysate for at least 1 h at 55˚C and 5 min at 95˚C. 2 μL were used for PCR (*c-REL* primers: Fw 5´-TGCATTTTCATTTTCAGTGAATGGT-3´, Rev 5´-ACCTGTGGAGATGACTGTGAAG-3´). Resulting bands on agarose gels were extracted using NucleoSpin Gel and PCR Clean up Kit (Macherey Nagel) according to manufacturer's guidelines and subsequently analyzed by sequencing.

For Native PAGE, DNA of the PCR product was denaturized and re-annealed (5 min at 95˚C, -2˚C/s from 95˚C to 85˚C and 0.1˚C/s from 85˚C to 25˚C). PCR product was separated on a 10% native Polyacrylamide-gel for 2 h at 150 V. Gene Ruler DNA Ladder Mix (Thermo Fisher Scientific, Waltham, MA, USA) served as marker, gel was immersed in 0.05% ethidium bromide (Carl Roth GmbH, Karlsruhe, Germany) for 5 min prior to visualization.

Quantitative real-time PCR

RNA isolation was done with NucleoSpin ^{1} RNA Kit (Macherey-Nagel) according to manufacturer's guidelines. 500 ng RNA were used for cDNA synthesis. Quantitative real-time PCR (qPCR) was performed using SYBR Green Master Mix (Thermo Fisher Scientific). cDNA was diluted 1:50 and 2 μL/reaction were used as template. Primer sequences were 5´-CTCCTGACTGACTGACTGCG-3´ (Fw *c-REL* target deletion), 5´-TACGGGTTATACGCACCGGA-3´ (Rev *c-REL* target deletion), 5´-CCTGGAGCAGGCTATCAGTC-3´ (Fw *RELA*), 5´-CACTGTCACCTGGAAGCAGA-3´

(Rev *RELA*), 5´-ACATCAAGGAGAACGGCTTCG-3´(Fw *RELB*), 5´-GACACTAGTCG GCCCAGG-3´ (Rev *RELB*), 5´-GCACCCTGACCTTGCCTATT-3´ (Fw *NFKB1*), 5´-GCT CTTTTTCCCGATCTCCCA-3´ (Rev NFKB1), 5´-CAACCCAG GTCTGGATGGTA-3´ (Fw *NFKB2*), 5´-CTGCTTAGGCTGTTCCACGA -3´ (Rev NFKB2), 5´-TGACAGTGA GCCCTGAAAGC-3´ (Fw *IKBKE*),5´-CCGGATTTCCCACACTCTGA-3´ (Rev *IKBKE*), 5´-CGGAGACCCGGCTGGTATAA-3´ (Fw *TBK1*), 5´-ATCCACTGGACGAAGGAAGC-3´ (Rev *TBK1*), 5´-CTGAAAACGAACGGTGACGG-3´ (Fw *A20*), 5´-TCCAGTTGCCAG CGGAATTT-3´ (Rev *A20*), 5´-CAGGATAACGGAGGCTGGGATG-3´ (Fw *BCL2*), 5´-TTCACTTGTGGCCCAGATAGG -3´ (Rev *BCL2*), 5´-GCTTGGATGGCCACTTACCT-3´ (Fw*BCL-XL*), 5´-ACAAAAGTATCCCAGCCGCC-3´ (Rev *BCL-XL*), 5´-GCAAGTGGAC ATCAACGGGT-3´ (Fw *TGFB1*), 5´- TCCGTGGAGCTGAAGCAATA-3´ (Rev *TGFB1*), 5´-GTAGTGGAAAACCAGCAGCC-3´ (Fw *MYC*), 5´-AGAAATACGGCTGCACCGAG-3´ (Rev *MYC*),5´-ATGGCAACGACTCCTTCTCG-3´ (Fw *ICAM-1*), 5´-GCCGGAAAGCTGTA GATGGT-3´(Rev *ICAM-1*). Ct values were normalized to reference genes *GAPDH* (Fw 5´-CATGAGAAGTATGACAACAGCCT-3´, Rev 5´-AGTCCTTCCACGATACCAAAGT-3´), *RPLP0* (Fw 5´–TGGGCAAGAACACCATGATG-3´, Rev 5´-AGTTTCTCCAGAGCTGGG TTGT-3´) and *eEF2* (Fw 5´-AGGTCGGTTCTACGCCTTTG-3´, 5´-TTCCCACAAGG CACATCCTC-3´).

Western blotting

For analysis of RELA and A20, *c-REL*$^{-/-}$ and *c-REL*$^{+/+}$ cells were treated with human recombi- nant TNFα (10ng/ml, Calbiochem, Merck, Darmstadt, Germany) for 24h prior to protein iso- lation. Protein extracts were made using cell lysis buffer (0.01 M TRIS, 3 mM EDTA, 1% SDS) and equal amounts of protein were separated by SDS-PAGE and transferred to a PVDF mem- brane. Membranes were blocked using PBS containing 0.05% Tween 20 and 5% milk powder and probed with primary antibodies (rabbit anti-c-REL (#4727), Cell Signaling Technology, Danvers, MA, USA); rabbit anti-p65 (#8242), Cell Signaling; mouse anti-A20 (sc-166692), Santa Cruz Biotechnology, Heidelberg, Germany) overnight at 4˚C. Horseradish peroxidase- conjugated secondary antibodies were applied for 1h at room temperature and blots were sub- sequently developed using enhanced chemiluminescence.

Electrophoretic mobility shift assay

Electrophoretic Mobility Shift Assay was performed using DIG Gel Shift Kit, 2nd generation (Deutschland Holding GmbH, Grenzach-Wyhlen, Germany) according to manufacturer's guidelines. For *c-REL* probe sequence (5´-TCGAGGGCTCGGGCTTTCC ATCTCTCGA-3´), *c-REL* binding site CGGGCTTTCC was assessed using the JASPAR Tool (jaspar.genereg.net). Protein isolation procedure and unspecific competitor sequence were applied as described by Tokunaga and coworkers [33]. PAGE was performed as described above.

Immunocytochemistry and fluorescence imaging of H2B-mcherry

For immunostaining and imaging of H2B-mCherry cells were seeded and cultivated on cover- slips. Fixation was done by adding 4% paraformaldehyde (PFA) for 10 min. After repetitive washing using phosphate-buffered saline (PBS), cells were either directly mounted with Mowiol/DABCO or carried over to immunostaining. For immunocytochemistry, cells were blocked and permeabilized using 0.02% PBST (PBS with Triton X-100) containing 5% goat serum for 30 min at RT. Primary antibody (rabbit anti-c-REL (#4727), Cell Signaling; mouse anti-CD54/ICAM MAB1379, Chemicon, Merck) was applied for 1 h at RT. After washing, cells were incubated with secondary antibody (goat anti-rabbit Alexa Fluor 647, Thermo Fisher Sci- entific) for 1 h at RT under exclusion of

light. Finally, coverslips were mounted with Mowiol/ DABCO. Imaging was done by confocal laser scanning microscopy (LSM 780, Carl Zeiss, Oberkochen, Germany) and image processing was done using Fiji) and Adobe Photoshop CS6 (Adobe Systems, San Jos´, USA) or Corel Draw (Corel Corporation, Ottawa, Canada).

Proliferation & survival assay

Proliferation was analyzed with Orangu Cell Proliferation Assay Kit (Cell Guidance Systems, Cambridge, UK) used following the manufacturer's protocol. Cells were counted with Cell- ometer Auto T4 Cell Viability Counter (Nexcelom, Lawrence, USA). For a calibrating curve 1000, 2500, 5000, 7500, 10000 and 15000 wildtype cells were seeded and incubated for 24 h at 37˚C. For correct cell number determination after one day, one well of each condition was recounted.

For survival assay 5000 cells in 100 μl were seeded one day before treatment. Cells were incubated with chemotherapeutic agents cisplatin (CDDP) (P4394, Sigma Aldrich) and 5-Fluoro-2´-deoxyuridine (5-FUDR) (Sigma Aldrich) for 21 h and subsequently Orangu Cell Proliferation Assay Kit was applied.

Flow cytometric analysis of the cell cycle, apoptosis and histone H2B- mCherry

DNA content measurement for analyzing cell cycle parameters was performed according to Kaltschmidt and colleagues [34] by harvesting 1 x 10^6 cells at 300 g for 5 min followed by fixa- tion with 70% (v/v) ethanol. After centrifugation at 300 x g for 10 minutes, staining solution (PBS containing 1 mg/ml glucose (Carl Roth GmbH), 4´,6-diamidino-2-phenylindole (DAPI; 0.5 mg/ml; Sigma-Aldrich), and 100 Kunitz units RNaseA (Thermo Fisher Scientific) was applied for 60 min under exclusion of light.

For apoptosis measurement, 1 x 106 cells were labeled with Annexin V-PE (Miltenyi Biotec, Bergisch Gladbach, Germany) according to the manufacturer's instructions. For analysis of H2B-mCherry, 1 x 106 c-REL+/+ and c-REL-/- cells were harvested and directly applied for flow cytometric analysis without additional staining procedures. DAPI or Annexin V-PE-labeled cells as well as unstained cells (H2B-mCherry) were analyzed using a Gallios™ 10/3 flow cytometer (Beckman Coulter, Brea, CA, USA). Data analysis was performed using FlowJo Software (TreeStar, Olten, Switzerland), doublet discrimination for cell cycle analysis was assured by appropriate gating strategies.

Live cell imaging

We imaged H2B-mCherry alpha-tubulin-eGFP expressing HeLa Kyoto c-REL+/+ and c-REL-/- cells in growth conditions at 37 degrees for more than 20 hours with a DeltaVision Elite imaging system (GE Healthcare). At 20x magnification (Olympus UPlanSApo 20x 0.75), we recorded on a CoolSNAP HQ2 (Photometrics, USA) CCD camera 15 different lateral positions with 3 axial position with 1μm spacing for each c-REL+/+ and c-REL-/- cells respectively every 10 minutes for each fluorescent emission channels (LED excitation source 461-489nm, 553- 597nm and emission filtered at 501-549nm, 603-647nm respectively). A DIC image was recorded for reference at each timepoint. The fluorescent images were deconvolved with the appropriate OTF in SoftWoRx (version 6.1.3, GE Healthcare), analysed with Fiji and figures were prepared with Omero.

Promoter analysis

Sequence of promoter regions (1500 bp downstream and 100 bp upstream to respective ATG, 5000 bp downstream for c-Myc promoter) of interest were taken from Eukaryotic Promoter

Database (epd.vital-ti.ch) for *Homo sapiens*. Binding sites for gene of interest in chosen pro- moter sequence were looked up using JASPAR Tool (jaspar.genereg.net). A relative score threshold of 85% was used. *RELA* and *c-REL* binding sites were compared in promoter regions of selected target genes.

Statistics

All statistical tests were performed with PrismGraph Pad 5 (GraphPad Software, La Jolla, USA). Statistical significance of qPCR results and fluorescence intensity quantification was analyzed using unpaired t-test. Welch correction was performed, if variances were significantly different. Data of proliferation and survival assays were shown to be not normally distributed (Shapiro-Wilk test) and analyzed using Kruskal-Wallis test with Dunn post-hoc test.

Results

c-REL is overexpressed in human cervical cancers

To assess the clinical implications of a *c-REL* knockout, we assessed levels of *c-REL* overexpression in human cancers by database mining using COSMIC [35]. We found *c-REL* to be profoundly overexpressed in human cancers, particularly within those located in human ovary, cervix and endometrium in comparison to oesophagus (Fig 1A, cancer.sanger.ac.uk; 02-14-2017 16:00; 02-21-2017 15:10). Due to their human cervix origin, we decided to apply HeLa Kyoto cells for the CRISPR/Cas9n-mediated *c-REL* knockout.

Successful knockout of *c-REL* in HeLa Kyoto cells using CRISPR/Cas9n

To generate a *c-REL* knockout in HeLa Kyoto cells, we designed a target deletion around 450 bp between intron 1 and exon 2 of chromosome 2 using the CRISPR/Cas9 Target Online Pre- dictor tool (Fig 1B, [36], crispr.cos.uni-heidelberg.de). All designed oligonucleotides were cloned into an all-in-one vector according to Golden Gate Assembly method (mCRISPR, [31]) allowing easier generation of knockouts. Genomic PCR depicted

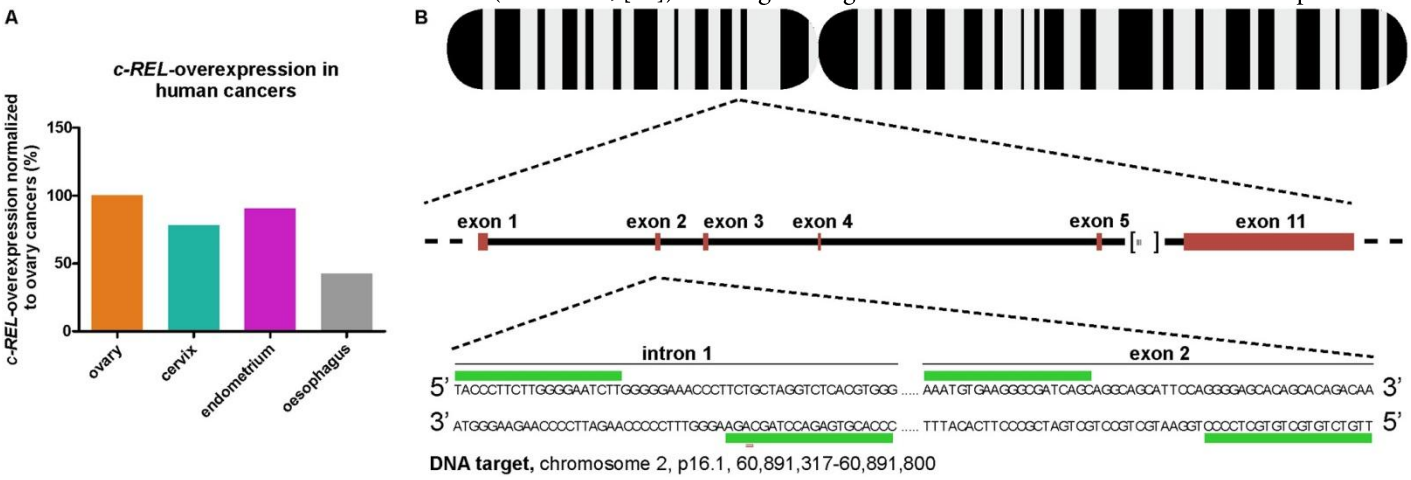

Fig 1. Assessment of *c-REL* overexpression in human cancers and target design of CRISPR/Cas9n-mediated *c-REL* knockout. A: Database mining revealed more profound overexpression of ***c-REL*** in cancers from human ovary, cervix and endometrium compared to oesophagus ([35], sancer. sanger.ac.uk; 02-14-2017 16:00; 02-21-2017 15:10). **B**: Target design showing the proposed ***c-REL*** knockout with an expected deletion around 450 bp targeting the intron 1-exon 2-boundary of the ***c-REL*** gene. The design was done with the CRISPR/Cas9n Target Online Predictor from the University of Heidelberg [36], crispr.cos.uni-heidelberg.de) and the gene sequence was taken from Ensembl Genome Browser (ensembl.org).

https://doi.org/10.1371/journal.pone.0182373.g001

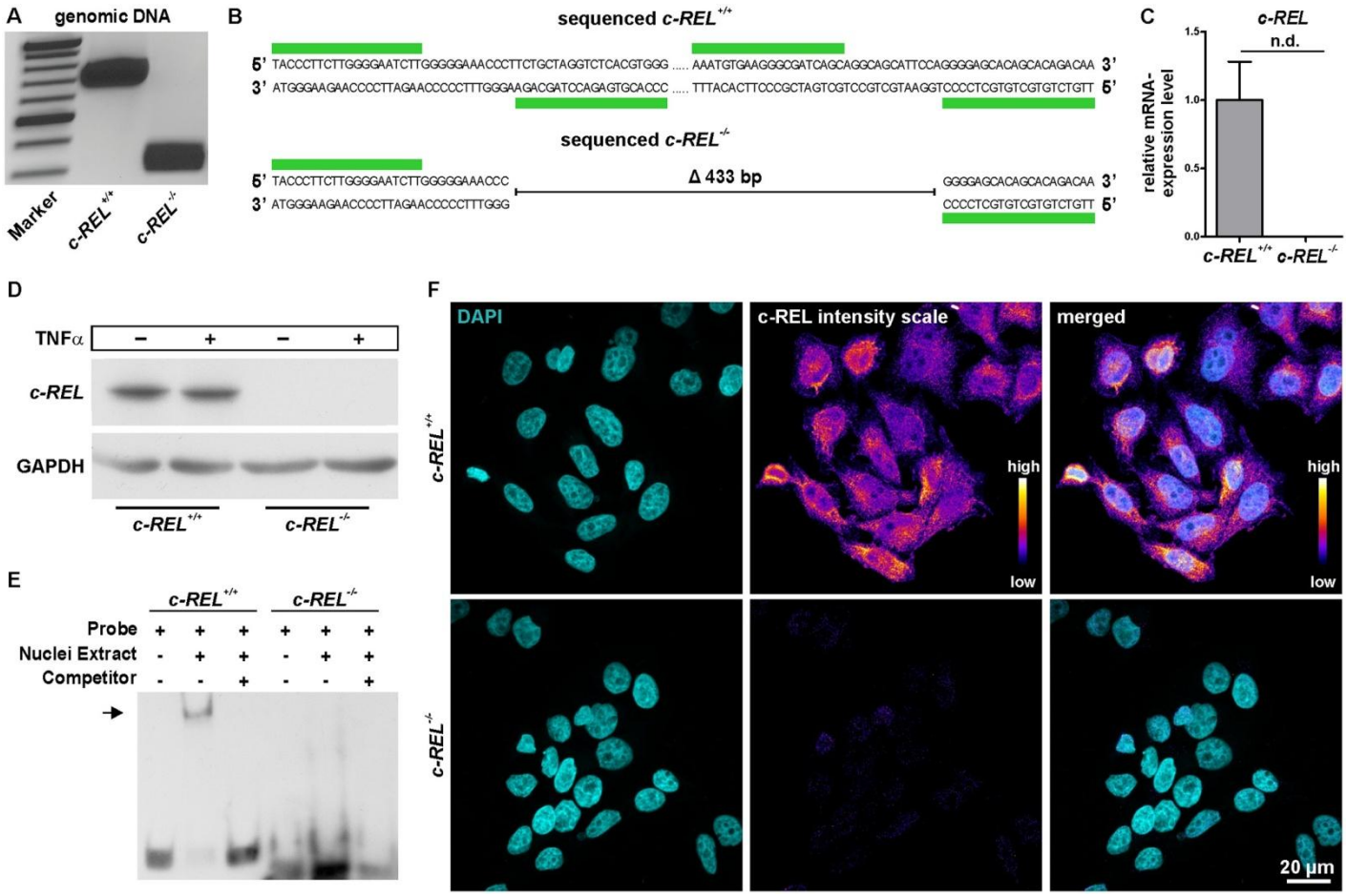

Fig 2. Successful validation of the *c-REL* knockout in HeLa Kyoto cells on DNA, mRNA and protein level. A: Genomic PCR depicting a profound deletion of the *c-REL* gene in the *c-REL* knockout clone (band at 300 bp) compared to the wt clone (band at 700 bp). **B:** Sequencing analysis confirmed the knockout in exon 2 of *c-REL*. **C:** qPCR with specific primers in targeted deletion of exon 2 showed no expression of *c-REL* on mRNA level in the *c-REL* knockout clone in comparison to wt. **D:** Western blot analysis validated the knockout of *c-REL* on protein level. **E:** Electrophoretic mobility shift assays (EMSA) showed DNA-binding of c-REL in HeLa Kyoto wt cells (arrow), which was not observable in the *c-REL* KO clone. **F:** Immunocytochemistry
depicted a nearly complete loss of c-REL-protein in *c-REL* knockout clone compared to HeLa Kyoto wt cells.

https://doi.org/10.1371/journal.pone.0182373.g002

a profound deletion of the *c-REL* gene in clonally grown HeLa Kyoto cells after transfection with the constructed CRISPR/Cas9 vector in comparison to untransfected HeLa Kyoto wt cells (Fig 2A). Sequenc- ing analysis confirmed the knockout of around 433 bp in exon 2 of *c-REL* within the trans- fected HeLa Kyoto clone.

CRISPR/Cas9n-mediated *c-REL* knockout can be validated on mRNA and protein level

After initial analysis of the *c-REL* knockout on DNA level, we assessed the expression level of *c-REL* in the HeLa Kyoto knockout clone by qPCR with primers in the targeted deletion. In contrast to HeLa Kyoto wt cells showing a robust expression of *c-REL* on mRNA level, no expression was detectable in the *c-REL* knockout clone (Fig 2C). Notably, we analysed the top three predicted exonic off-targets and detected no significant signs of off-target effects in the *c- REL* kockout clone (S1 Fig).

In contrast to HeLa Kyoto wt cells, no c-REL protein was detectable in knockout cells by western blot analysis even after TNFα-dependent stimulation, confirming the knockout of *c- REL* on protein level (Fig 2D). Assessing a potential loss in functionality of the c-REL protein, we investigated DNA binding activity of c-REL using electrophoretic mobility shift assay (EMSA). *c-REL*$^{-/-}$ cells showed no DNA-binding activity of c-REL (Fig 2E), whereas a clear shift was observable using HeLa Kyoto wt cells (Fig 2E, arrow). Immunocytochemistry further validated the *c-REL* knockout in the transfected HeLa Kyoto clone by showing a nearly com- plete loss of c-REL protein in comparison to HeLa Kyoto wt cells (Fig 2F).

CRISPR/Cas9n-mediated deletion of *c-REL* results in a decreased proliferation of HeLa Kyoto cells without affecting apoptosis

We next analyzed potential effects of the *c-REL* knockout on proliferation and apoptosis of HeLa Kyoto cells. Using Orangu Cell Proliferation Assay Kit (Cell Guidance Systems), prolif- eration of *c-REL* knockout and wt cells was assessed after 2 days. HeLa Kyoto *c-REL*$^{-/-}$ cells showed a strongly increased population doubling time of 26.54 h compared to wt HeLa Kyoto cells displaying a population doubling time of 15.68 h (Fig 3A). This robustly decreased prolif- erative behavior of *c-REL* knockout cells was accompanied by a 0.81 fold decrease in the amount of mitotic cells compared to wildtype, as shown by cell cycle analysis using flow cyto- metric DNA content measurements (Fig 3B). However, we observed only slightly increased levels of Annexin V-positive apoptotic cells in *c-REL*$^{-/-}$ cells compared to wt cells (Fig 3C), indicating the effect of the *c-REL* knockout on proliferation of HeLa Kyoto cells to be apopto- sis-independent.

c-REL$^{-/-}$ HeLa Kyoto cells reveal strongly reduced levels of histone H2B accompanied by a significantly delayed prometaphase or complete arrest of the cell cycle

Assessing the reduced proliferative behavior of *c-REL*$^{-/-}$ HeLa Kyoto cells in more detail, we analyzed the protein level of histone H2B, which is fused to mCherry in HeLa Kyoto cells [32]. Flow cytometric analysis of H2B-mCherry showed a strongly decreased amount of the H2B protein in 41.48% of *c-REL*$^{-/-}$ HeLa Kyoto cells. On the contrary, we observed a reduced H2B protein level in only 8.67% of HeLa Kyoto wt cells (Fig 3D). Taking advantage of the H2B- mCherry and alpha-tubulin-EGFP fusion in HeLa Kyoto cells, we further visualized the differ- ent stages of mitosis in fixed cell samples and living cells. Fluorescence imaging of fixed cells revealed a significantly increased amount of *c-REL*$^{-/-}$ HeLa Kyoto cells within the prometa- phase compared to wt cells (Fig 4E). We investigated this effect of the *c-REL* deletion in more detail by live cell imaging. Here, *c-REL*$^{-/-}$ cells showed a length of the prometaphase of 39.50 ± 9.96 min, which was significantly delayed in comparison to wt cells revealing a dura- tion of the prometaphase of 18.42 ± 1.58 min (Fig 4A–4C, S1 Movie). In addition, we observed only 5.4% of wt cells but 25.7% of *c-REL*$^{-/-}$ cells (n = 40) to arrest during mitosis without entry of the G2 phase of the cell cycle (Fig 4D, S2 Fig).

c-REL knockout leads to significantly decreased expression levels of NF-κB family members and cell cycle-associated *c-REL* target genes

Analyzing effects of the *c-REL* knockout in HeLa Kyoto cells on other NF-κB family members, we assessed respective gene expression levels by qPCR. *c-REL* knockout cells revealed signifi- cantly decreased mRNA levels of *RELA*, *NFKB1 (p50)*, *NFKB2* (*p52)*, IκB-Kinase ε (*IKBKE*)

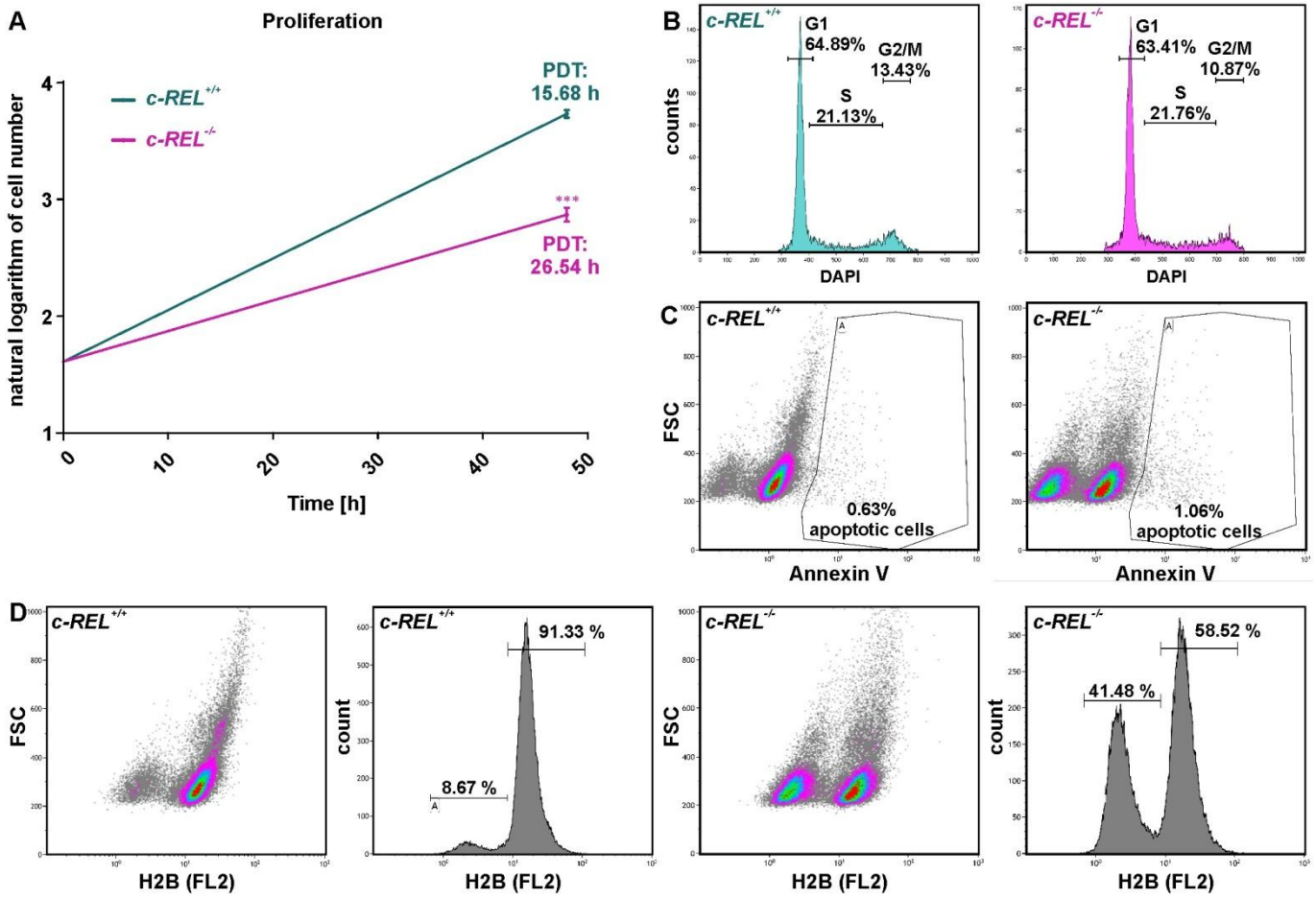

Fig 3. CRISPR/Cas9-mediated deletion of *c-REL* results in a decreased proliferation of HeLa Kyoto cell accompanied by strongly reduced amounts of histone H2B. A: Cell number assessed by Orangu Cell Proliferation Assay Kit (Cell Guidance Systems) set against cultivation time showed a strongly increased population doubling time of *c-REL* knockout cells compared to wt HeLa Kyoto cells. PDT: Population doubling time. **B:** Flow cytometric DNA content measurements of DAPI-stained *c-REL* knockout cells showed a decrease in the amount of mitotic cells in *c-REL* knockout cells compared to wildtype. **C:** Flow cytometric analysis of Annexin V-stained *c-REL*$^{-/-}$ and wt HeLa Kyoto cells revealed only slightly increased amounts of apoptotic cells upon *c*-REL deletion in comparison to wt. **D:** Flow cytometric analysis of histone H2B-mCherry showed a strongly decreased amount of the H2B protein in 41.48% of *c-REL*$^{-/-}$ HeLa Kyoto cells, which was observable in only 8.67% of HeLa Kyoto wt cells.

https://doi.org/10.1371/journal.pone.0182373.g003

and TANK-binding kinase 1 (*TBK1*) compared to wildtype cells (Fig 5A). On the contrary, expression levels of *RELB* were not significantly affected in the *c-REL* knockout clone (Fig 5A).

In accordance to the observed decrease in proliferation and in *c-REL* knockout cells, we fur- ther observed significantly decreased mRNA levels in cell cycle-related *c-REL* target genes. In particular, expression levels of A20 (*TNFAIP3*), B-cell lymphoma 2 (*BCL2*), B-cell lymphoma- extra large (*BCLXL*, *BCL2L1*) and transforming growth factor beta 1 (*TGFB1*) were found to be significantly decreased in comparison to HeLa Kyoto wildtype cells (Fig 5B). In addition, expression levels of the *c-REL* target genes *MYC* and Intercellular Adhesion Molecule 1 (*ICAM-1*) were likewise significantly decreased compared to wildtype HeLa Kyoto cells (Fig 5C).

Promoter analysis was further performed using the JASPAR Tool (jaspar.genereg.net) to validate the analyzed genes to be direct *c-REL* target genes. Binding sites for *c-REL* and *RELA* were analyzed in each promoter region and their presence confirmed IKBKE, TBK1, *A20, BCL2, BCL-XL, TGFB1, MYC* and *ICAM-1* to be direct *c-REL* target genes (S3 Fig).

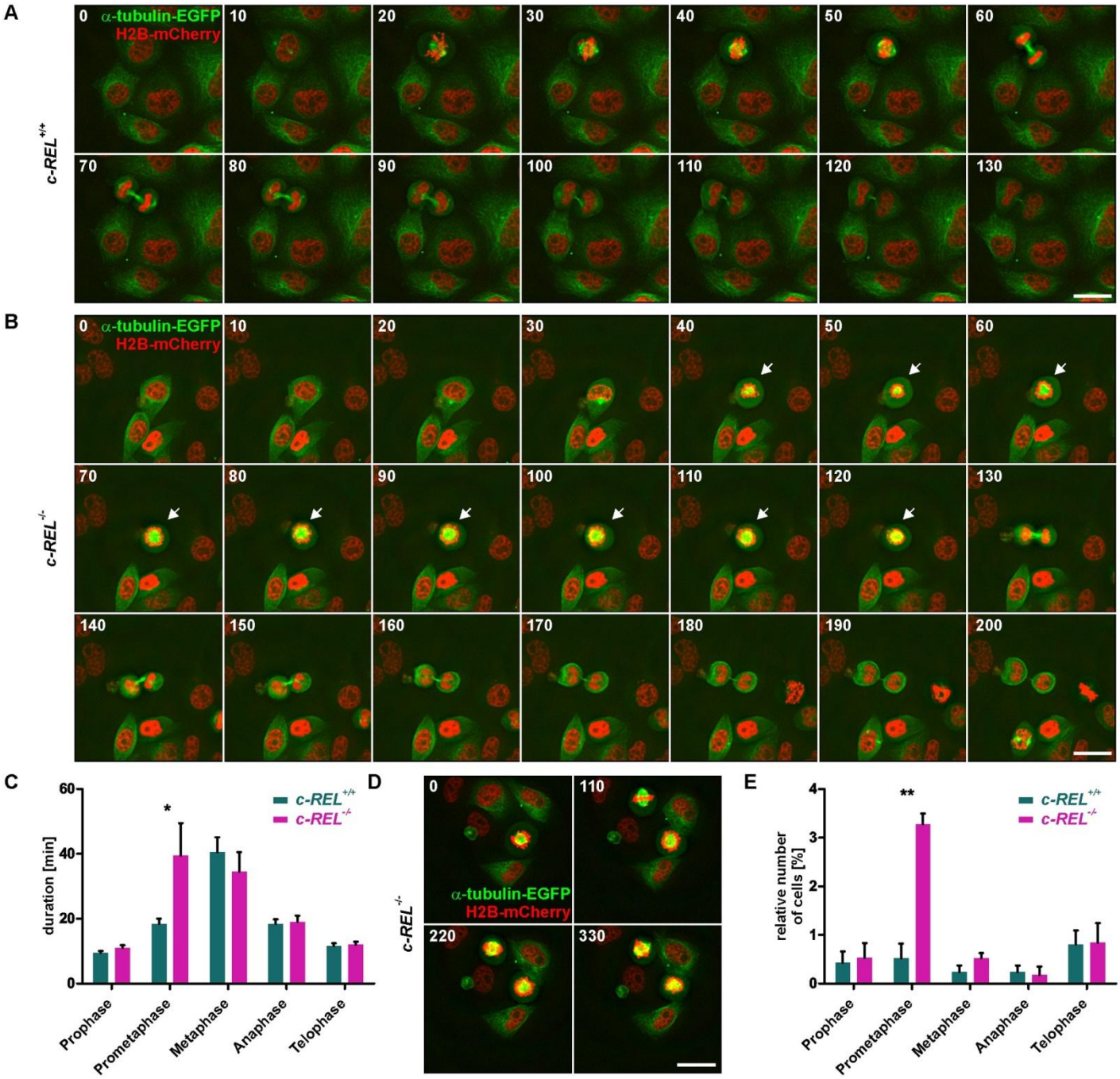

Fig 4. Knockout of *c-REL* leads to a significantly delayed prometaphase or even complete arrest of the cell cycle. A-B: Live cell imaging of *c- REL*$^{-/-}$ and *c-REL*$^{+/+}$ cells showed delayed duration of the prometaphase in *c-REL*$^{-/-}$ (arrows) in comparison to wildtype. Mitosis was visualized by H2B- mCherry and alpha-tubulin-EGFP. **C:** Quantification of life cell imaging validated the significant delay of *c-REL*$^{-/-}$ *in* length of the prometaphase
(39.50 ± 9.96 min) in comparison to wt (18.42 ± 1.58 min) (n = 20). **D:** Exemplary images of *c-REL*$^{-/-}$ cells arresting during mitosis without entry of the G2 phase of the cell cycle. **E:** Fluorescence imaging of H2B-mCherry in fixed cells displayed a significantly increased amount of *c-REL*$^{-/-}$ HeLa Kyoto cells
within the prometaphase compared to wt cells. (>1000 cells quantified per genotype, n = 3). Scale bar: 25 μm.

https://doi.org/10.1371/journal.pone.0182373.g004

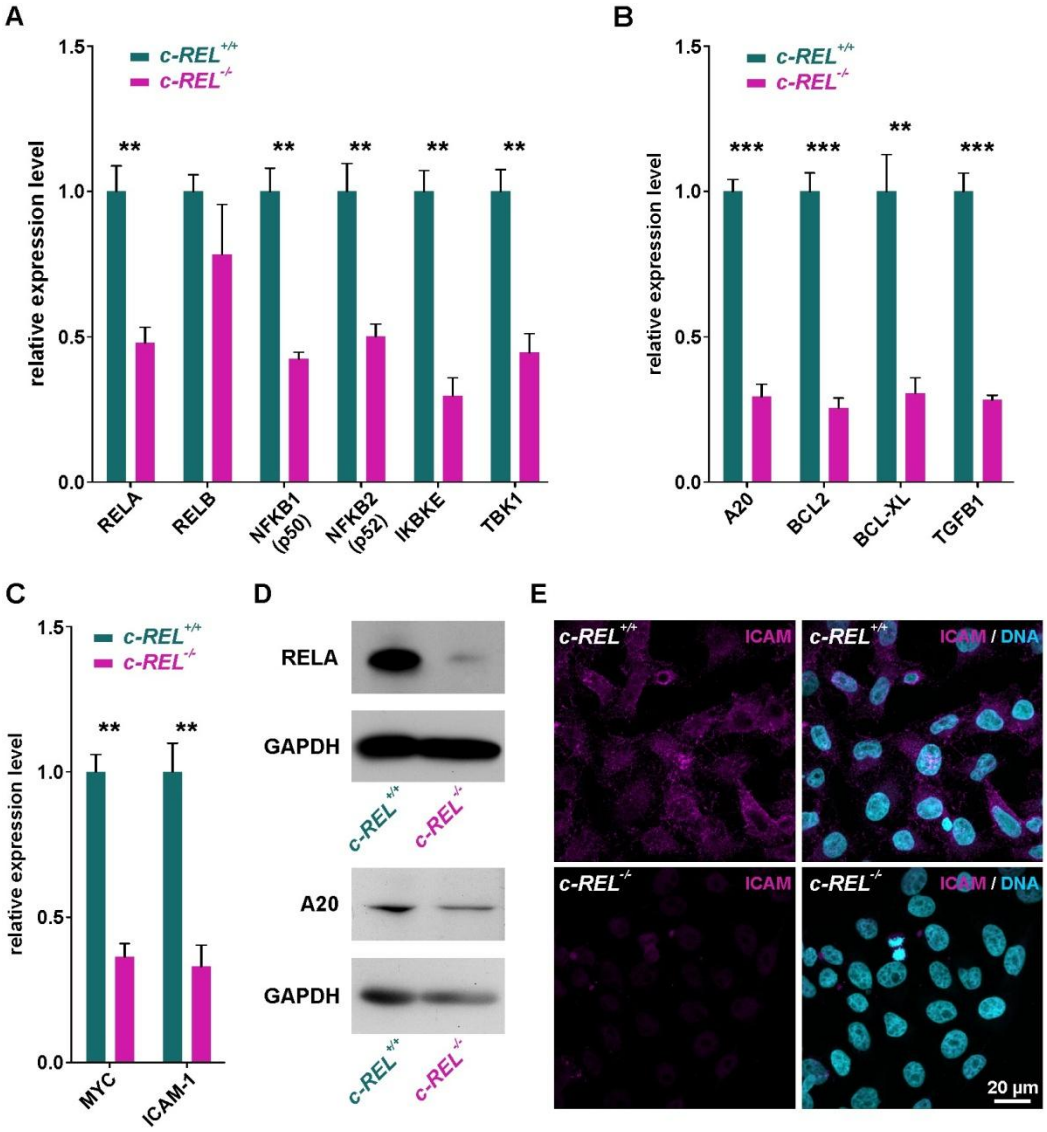

Fig 5. *c-REL* knockout leads to significantly decreased expression levels of NF-κB family member and cell cycle-associated genes. A: qPCR analysis showing significantly decreased mRNA levels of NF-κB family members *RELA*, *NFKB1 (p50)*, *NFKB2* (*p52)*, *IKBKE* and *TBK1* in *c-REL* knockout cells compared to wildtype cells. **B-C:** Expression levels of cell cycle-related *c-REL* target genes *A20*, *BCL2*, *BCL-XL* and *TGFB1* and *c-REL* target genes *MYC* and *ICAM-1* were significantly decreased in *c-REL* knockout cells in comparison to HeLa Kyoto wildtype cells. **D:** Western blot analysis validated the reduced expression levels of RELA and A20 in *c-REL*$^{-/-}$ cells in comparison to wt on protein level. WB were performed after TNFα-dependent stimulation of *c-REL*$^{-/-}$ and *c- REL*$^{+/+}$ cells. **E:** Immunocytochemistry revealed a strongly decreased protein amount of ICAM in *c-REL*$^{-/-}$ cells in comparison to wt.

https://doi.org/10.1371/journal.pone.0182373.g005

To validate the decreased expression levels of *c-REL* target genes in *c-REL*$^{-/-}$ HeLa Kyoto cells on protein level, we performed western blot analysis and immunocytochemistry. Western blot analysis revealed reduced amounts of RELA and A20 protein in *c-REL*$^{-/-}$ cells in compari- son to wt (Fig 5D). We further observed a nearly complete loss of ICAM protein in *c-REL*$^{-/-}$ cells by immunocytochemistry, while HeLa Kyoto wt cells showed an unchanged amount of ICAM protein (Fig 5E).

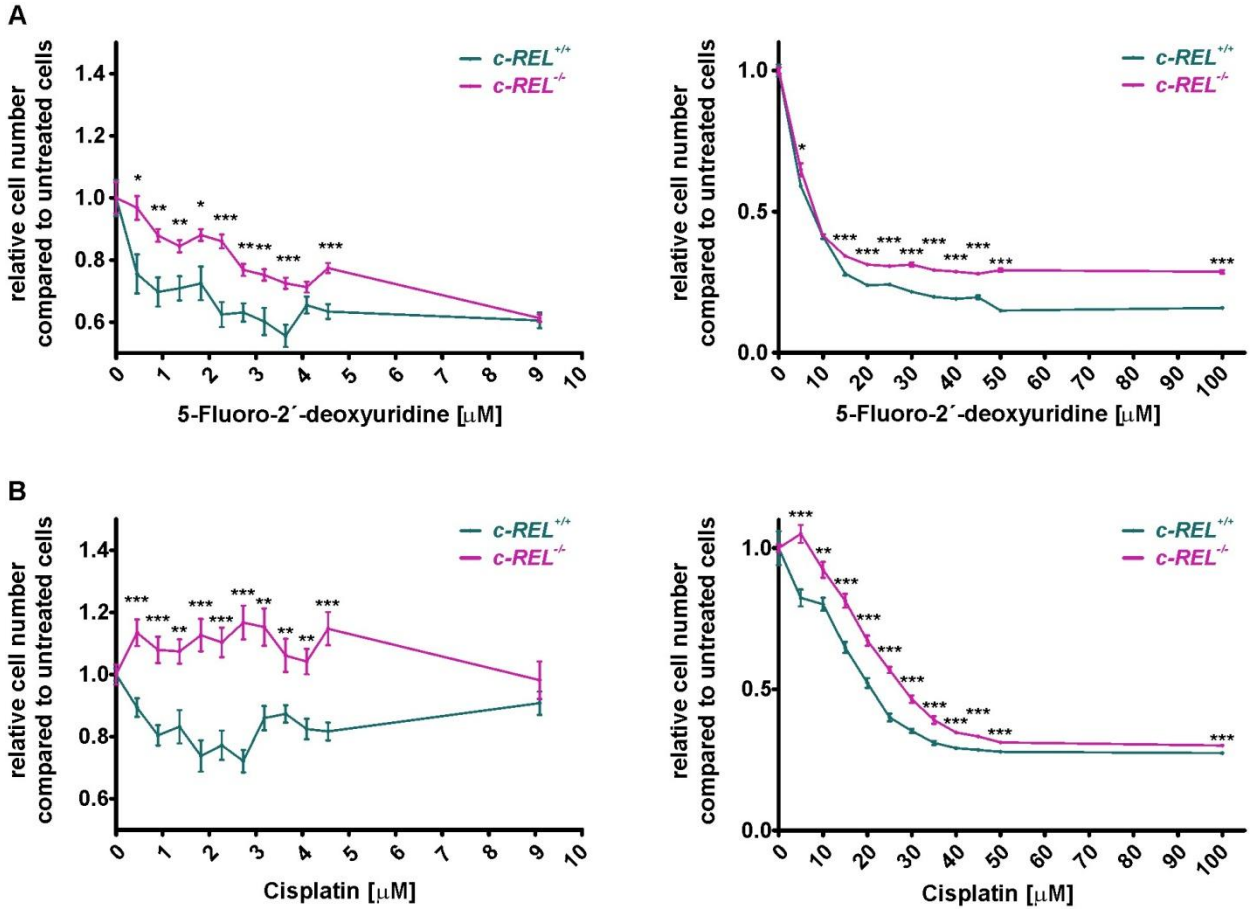

Fig 6. Significantly increased resistance against chemotherapeutic agents in HeLa Kyoto cells with *c-REL* deletion. A: Although both HeLa Kyoto wildtype and *c-REL* knockout cells showed cell death after treatment with 5-Fluoro-2'-deoxyuridine, the *c- REL* knockout clone showed significantly elevated cell numbers in comparison to wildtype cells. Cells were exposed to chemotherapeutic agents for 21 h, cell numbers were assessed using Orangu Cell Proliferation Assay Kit (Cell Guidance Systems) after
2 h of incubation. Cell number of untreated cells were set to 1 and used for comparison. **B:** Although cisplatin-treatment of 1–4 μM led to cell death of wildtype cells, survival of the *c-REL* knockout clone was significantly increased even in comparison to untreated control. Increasing concentrations of cisplatin (10–100 μM) affected survival of *c-REL* knockout cells, but cell numbers were still significantly elevated compared to wildtype. Cells were exposed to chemotherapeutic agents for 21 h, cell numbers were assessed using Orangu Cell Proliferation Assay Kit (Cell Guidance Systems) after 2 h of incubation. Cell number of untreated cells were set to 1 and used for comparison (n = 8).

https://doi.org/10.1371/journal.pone.0182373.g006

HeLa Kyoto cells with *c-REL* deletion show a significantly increased resistance against chemotherapeutic agents

With regards to the assessed overexpression of *c-REL* in human cancers (Fig 1A), potential clinical implications of the *c-REL* knockout were assessed by determining cell survival upon exposure to the chemotherapeutic agents 5-Fluoro-2'-deoxyuridine (5-FUDR) and cisplatin. Here, treatment with increasing concentration of 0.45–100 μM 5-FUDR for 21 h led to cell death of both *c-REL*$^{-/-}$ and wildtype cells (Fig 6A).

However, 5-FUDR-treated *c-REL* knockout clone showed significantly increased cell num- bers in comparison to wildtype cells, indicating a profoundly increased resistance against 5-FUDR (Fig 6A). We likewise observed this effect after treatment of HeLa Kyoto wildtype and knockout cells with cisplatin. While cisplatin-treatment of 0.45–4.5 μM led to cell death of wildtype cells, assessed cell numbers of the *c-REL* knockout clone were significantly increased

even in comparison to untreated control (Fig 6B). Although exposure to increasing concentra- tions of cisplatin (10–100 μM) also resulted in cell death of *c-REL* knockout cells, cell number were still found to be significantly increased compared to wildtype, validating a robust resis- tance against cisplatin (Fig 6B).

Discussion

The present study shows a successful CRISPR/Cas9n-mediated knockout of the NF-κB subunit *c-REL* in HeLa Kyoto cells. HeLa cells are one of the most frequently used model systems for epithelial and in particular cervical cancers [37–39]. Here, we observed a significantly decreased proliferation of *c-REL*$^{-/-}$ cells accompanied by a significant decline in expression levels of NF-κB target genes in comparison to wt cells. HeLa Kyoto cells with *c-REL* deletion further revealed a significantly increased resistance against the chemotherapeutic agents 5-Fluoro-2'-deoxyuridine (5-FUDR) and cisplatin. These are commonly used as the trade- marked chemotherapeutics Platinol$^{®}$ and FUDR$^{®}$ in the clinic.

With NF-κB being involved in many cellular processes [10, 11], a broad range of genes were described to be direct targets of NF-κB, including cytokines, chemokines, cell adhesion mole- cules, cell surface receptors, regulators of apoptosis and growth factors [40]. Interestingly, par- ticular subunits of NF-κB were only rarely directly linked to specific target genes. In the present study, *c-REL*$^{-/-}$ HeLa Kyoto cells showed significantly decreased expression levels of NF-κB fam- ily members *RELA*, *NFKB1*, *NFKB2* as well as *IKBKE* and *TBK1*. We also observed several *c-REL* binding sites in the promoter region of the *TBK1* and *IKBKE* gene, suggesting *TBK1* and *IKBKE* as direct *c-REL* target genes. In addition to their role in phosphorylating NF-κB p65 [41], TBK1 and IKBKE were in turn described to directly phosphorylate the C-terminal domain of the c-REL protein resulting in its nuclear accumulation [42]. Extending these promising findings, we suggest a positive feedback loop by *c-REL*-mediated expression of *TBK1* and IKBKE in turn leading to a pronounced activation of *c-REL*. Being also closely linked to the pathogenesis of breast cancer by promoting activation of NF-κB [43], targeting *IKBKE* may be an interesting future perspective for developing new treatment strategies against cervical cancer. Next to *TBK1* and *IKBKE*, *c-REL* knockout was observed to be sufficient to downregulate the expression of *MYC* in growing HeLa cells by more than 50% with the relative *MYC* expression being highly elevated in comparison to other target genes. Accordingly, Grumont and coworkers showed an impaired expression of *MYC* in stage III thymocytes with a *RELA*/*c-REL* double knockout [44]. We also demonstrated the presence of three *c-REL* binding sites in the downstream region of the *MYC* promoter, further validating *MYC* as a direct target gene of *c-REL*.

In comparison to wildtype, *c-REL*$^{-/-}$ HeLa Kyoto cells further revealed a significantly decreased expression of *BCL-2*, *BCL-XL* and *A20*, which are commonly known as anti-apoptotic genes [45, 46]. In accordance to our promoter analysis depicting *c-REL*-binding sites, *BCL-XL* and *BCL2* were described to be direct *c-REL* target genes [47, 48]. Expression of *TGFB1*, already known as direct target of *c-REL* [49] and a common inducer of cell prolifera- tion [50], was also significantly reduced in *c-REL*$^{-/-}$ HeLa Kyoto cells. On functional level, we observed the *c-REL* knockout to result in a significantly reduced proliferation, which we sug- gest to be at least in part mediated by the depicted decline in pro-proliferative target gene expression. In consistence with these findings, knockdown of the *c-REL* target gene *IKBKE* in HeLa cells was also shown to result in a suppression of proliferation [51]. In human keratinocytes, small interfering RNA-mediated knockdown of c-REL was reported to directly affect cell cycle progression by cell cycle delay of the G2/M phase [23]. The present study further extended these findings by showing the CRISPR-Cas9n-mediated knockout of *c-REL* to result in a robustly delayed prometaphase of mitosis accompanied by strongly reduced levels of

Table 1. Overexpression of *REL* in human cancers.

tissue type	% of *REL* overexpression	no. tested
Ovary	7.52	266
Lung	7.26	1019
Urinary tract	7.11	408
Endometrium	6.81	602
Pancreas	6.7	179
Haematopoietic and lymphoid	6.33	221
Soft tissue	6.08	263
Cervix	5.86	307
Upper aerodigestive tract	5.75	522
Kidney	5.5	600
Thyroid	5.46	513
Large intestine	4.92	610
Stomach	4.91	285
Liver	4.83	373
CNS	4.73	697
Prostate	4.62	498
Breast	3.71	1104
Skin	3.59	473
Oesophagus	3.2	125
Adrenal gland	2.53	79

https://doi.org/10.1371/journal.pone.0182373.t001

histone H2B protein. In addition, we observed a novel linkage between the decreased amount of histone H2B protein and the prolonged prometaphase in *c-REL*$^{-/-}$ cells. In mice, silencing of
c-Rel by siRNA was shown to lead to a reduction of mitosis in a B cell tumor cell line [52]. Gru- mont and coworkers likewise demonstrated a cell cycle arrest in B-cells of *c-Rel*$^{-/-}$ mice [53]. Our present findings for the first time transfer these promising data to the human cancerous systems and provide deeper insights into the biology of cervical cancers in relation to *c-REL*- signaling. In this regard, we were also able to observe significantly reduced expression levels of *ICAM1* in *c-REL*$^{-/-}$ HeLa Kyoto cells. Downregulation of this adhesion molecule was described to result in a suppression of human breast cancer cell invasion with the level of expression being directly correlated to their metastatic potential [54]. Accordingly, inhibition of MYC protein family members have been shown to induce regression of lung cancer in mice [55], suggesting the downregulation of *MYC* observed here likewise to be linked to the reduced pro- liferation of *c-REL*$^{-/-}$ cells.

The NF-κB subunit *c-REL* is also directly linked to cancer development and progression. In 1999, Krappmann and colleagues described a constitutive NF-κB-activity with NF-κB-complexes containing RELA and c-REL in malignant cells derived from Hodgkin's disease [56]. Whereas *c-REL* was currently discussed as being mutated in hematopoietic and lymphoid tumors [57], a high throughput database analysis performed in the present study including 3397 hematopoietic and lymphoid tumors detected mutations in only a few samples [35, 58]. In 2004, Futreal and coworkers described a 'census' of human cancers indicating mutations in >1% of genes of the human genome to contribute to cancer, although genes showing solely altered expression levels were not included in this initial 'census' [59]. Here, we applied database mining using the COSMIC database [35] and observed profound overexpression of *c-REL* in various human tumors (Table 1), which is in accordance to the observed amplification of *c-REL* in human B-cell lymphomas [20, 21]. Likewise in line with previous studies, *c-REL* can be

considered as one of the most oncogenic members of the NF-κB family, in fowl reticuloen- dotheliosis virus also contains mutated oncogenic *v-Rel* [18, 19, 52, 60].

In the present study, knockout of *c-REL* in a cellular model of cervical carcinoma resulted in a significantly increased resistance against the chemotherapeutic agents 5-FUDR and cis- platin. Due to direct interaction of cisplatin and 5-fluorouracil with the DNA, highly prolifer- ating cells are exposed to DNA damage resulting in cell-cycle arrest and cell death [61, 62]. Thus, we suggest the reduced proliferation of HeLa *c-REL*$^{-/-}$ cells to account for the observed increase in resistance against cisplatin and 5-FUDR. Although activation of NF-κB was also described to lead to a decreased sensitivity of cancer cells against chemotherapeutic treatment [63, 64], our present findings propose a subunit specificity of NF-κB in terms of chemoresis- tance. While a knockout of *c-REL* promoted survival of HeLa cells to chemotherapy, expres- sion of the *c-REL* homolog *Xenopus* Xrel3 in cervical cancer cells treated with 5 μM cisplatin was shown to result in increased apoptosis [24].

In summary, our findings emphasize the importance of *c-REL*-signaling in a cellular model of cervical cancer particularly in terms of proliferation and resistance to chemotherapeutic agents. Considering the proposed NF-κB-subunit specificity of chemoresistance, we provide deeper insights into cervical cancer biology with direct clinical implications for the development of new treatment strategies.

Supporting information

S1 Fig. PAGE-analysis of top three predicted exonic off-targets revealed no signs of off-tar- get effects in the *c-REL* knockout clone.
(TIF)

S2 Fig. Live cell imaging showing *c-REL*$^{-/-}$ cells, which arrested during mitosis without entry of the G2 phase of the cell cycle. Scale bar: 25 μm.
(TIF)

S3 Fig. Promoter analysis using the JASPAR Tool (jaspar.genereg.net) validated *IKBKE*, *TBK1*, *A20*, *BCL2*, *BCL-XL*, *TGFB1*, *MYC* and *ICAM*-1 to be direct *c-REL* target genes. *c- REL* binding site is shown in magenta, *RELA* binding site is depicted in cyan and common binding sites are shown in purple.
(TIF)

S1 Movie. Live cell imaging of *c-REL*$^{-/-}$ and *c-REL*$^{+/+}$ cells showed delayed duration of the prometaphase in *c-REL*$^{-/-}$ in comparison to wildtype. Mitosis was visualized by H2B- mCherry and alpha-tubulin-EGFP.
(MP4)

Acknowledgments

The excellent technical help of Angela Kralemann-Kühler is gratefully acknowledged.

Author Contributions

Conceptualization: Barbara Kaltschmidt, Christian Kaltschmidt.

Data curation: Barbara Kaltschmidt, Christian Kaltschmidt.

Formal analysis: Carsten Slotta, Thomas Schlüter, Johannes F. W. Greiner.

Funding acquisition: Barbara Kaltschmidt, Christian Kaltschmidt.

Investigation: Carsten Slotta, Thomas Schli¨ ter, Lucia M. Ruiz-Perera, Hussamadin M. Kad- him, Tobias Tertel, Elena Henkel, Wolfgang Hi¨ bner.

Methodology: Carsten Slotta, Thomas Schlu¨ ter, Barbara Kaltschmidt, Christian Kaltschmidt.

Project administration: Barbara Kaltschmidt, Christian Kaltschmidt.

Resources: Thomas Huser, Barbara Kaltschmidt, Christian Kaltschmidt. Supervision: Barbara Kaltschmidt, Christian Kaltschmidt.

Validation: Carsten Slotta, Johannes F. W. Greiner, Barbara Kaltschmidt, Christian Kaltschmidt.

Visualization: Carsten Slotta, Thomas Schli¨ ter, Johannes F. W. Greiner.

Writing – original draft: Carsten Slotta, Thomas Schli¨ ter, Johannes F. W. Greiner.

Writing – review & editing: Carsten Slotta, Lucia M. Ruiz-Perera, Hussamadin M. Kadhim, Tobias Tertel, Elena Henkel, Wolfgang Hi¨ bner, Johannes F. W. Greiner, Thomas Huser, Barbara Kaltschmidt, Christian Kaltschmidt.

References

1. Shehata MF. Rel/Nuclear factor-kappa B apoptosis pathways in human cervical cancer cells. Cancer cell international. 2005; 5(1):10. Epub 2005/04/29. https://doi.org/10.1186/1475-2867-5-10 PMID:15857509
2. Stewart BW, Wild CP, (Editors). World Cancer Report 2014. World Health Organization; 2014.
3. Schiffman M, Castle PE, Jeronimo J, Rodriguez AC, Wacholder S. Human papillomavirus and cervical cancer. Lancet. 2007; 370(9590):890–907. Epub 2007/09/11. https://doi.org/10.1016/S0140-6736(07)61416-0 PMID:17826171
4. Garland SM. Human papillomavirus update with a particular focus on cervical disease. Pathology. 2002; 34(3):213–24. Epub 2002/07/12. PMID: 12109780
5. Kang YJ, O'Connell DL, Tan J, Lew JB, Demers A, Lotocki R, et al. Optimal uptake rates for initial treat- ments for cervical cancer in concordance with guidelines in Australia and Canada: Results from two large cancer facilities. Cancer epidemiology. 2015; 39(4):600–11. Epub 2015/05/26. https://doi.org/10.1016/j.canep.2015.04.009 PMID: 26004990
6. Lorusso D, Petrelli F, Coinu A, Raspagliesi F, Barni S. A systematic review comparing cisplatin and car- boplatin plus paclitaxel-based chemotherapy for recurrent or metastatic cervical cancer. Gynecologic oncology. 2014; 133(1):117–23. Epub 2014/02/04. https://doi.org/10.1016/j.ygyno.2014.01.042 PMID:24486604
7. Nishiyama M, Yamamoto W, Park JS, Okamoto R, Hanaoka H, Takano H, et al. Low-dose cisplatin and 5-fluorouracil in combination can repress increased gene expression of cellular resistance determinants to themselves. Clinical cancer research: an official journal of the American Association for Cancer Research. 1999; 5(9):2620–8. Epub 1999/09/28.
8. Sen R, Baltimore D. Inducibility of kappa immunoglobulin enhancer-binding protein Nf-kappa B by a posttranslational mechanism. Cell. 1986; 47(6):921–8. Epub 1986/12/26. PMID: 3096580
9. Sen R, Baltimore D. Multiple nuclear factors interact with the immunoglobulin enhancer sequences. Cell. 1986; 46(5):705–16. Epub 1986/08/29. PMID: 3091258
10. Kaltschmidt B, Kaltschmidt C. NF-kappaB in the nervous system. Cold Spring Harbor perspectives in biology. 2009; 1(3):a001271. Epub 2010/01/13. https://doi.org/10.1101/cshperspect.a001271 PMID:20066105
11. Perkins ND. Integrating cell-signalling pathways with NF-kappaB and IKK function. Nature reviews Molecular cell biology. 2007; 8(1):49–62. Epub 2006/12/22. https://doi.org/10.1038/nrm2083 PMID: 1718 3360
12. Xia Y, Shen S, Verma IM. NF-kappaB, an active player in human cancers. Cancer immunology research. 2014; 2(9):823–30. Epub 2014/09/05. https://doi.org/10.1158/2326-6066.CIR-14-0112PMID:25187272

13. Li Q, Withoff S, Verma IM. Inflammation-associated cancer: NF-kappaB is the lynchpin. Trends in immunology. 2005; 26(6):318–25. Epub 2005/06/01. https://doi.org/10.1016/j.it.2005.04.003 PMID:15922948

14. Ben-Neriah Y, Karin M. Inflammation meets cancer, with NF-kappaB as the matchmaker. Nature immu- nology. 2011; 12(8):715–23. Epub 2011/07/21. https://doi.org/10.1038/ni.2060 PMID: 21772280

15. Sovak MA, Bellas RE, Kim DW, Zanieski GJ, Rogers AE, Traish AM, et al. Aberrant nuclear factor-kap- paB/Rel expression and the pathogenesis of breast cancer. The Journal of clinical investigation. 1997; 100(12):2952–60. Epub 1998/01/31. https://doi.org/10.1172/JCI119848 PMID: 9399940

16. Nair A, Venkatraman M, Maliekal TT, Nair B, Karunagaran D. NF-kappaB is constitutively activated in high-grade squamous intraepithelial lesions and squamous cell carcinomas of the human uterine cervix. Oncogene. 2003; 22(1):50–8. Epub 2003/01/16. https://doi.org/10.1038/sj.onc.1206043 PMID:12527907

17. Gilmore TD. Multiple mutations contribute to the oncogenicity of the retroviral oncoprotein v-Rel. Onco- gene. 1999; 18(49):6925–37. Epub 1999/12/22. https://doi.org/10.1038/sj.onc.1203222 PMID:10602467

18. Gilmore TD, Cormier C, Jean-Jacques J, Gapuzan ME. Malignant transformation of primary chicken spleen cells by human transcription factor c-Rel. Oncogene. 2001; 20(48):7098–103. Epub 2001/11/13. https://doi.org/10.1038/sj.onc.1204898 PMID: 11704834

19. Gilmore TD, Kalaitzidis D, Liang MC, Starczynowski DT. The c-Rel transcription factor and B-cell prolif- eration: a deal with the devil. Oncogene. 2004; 23(13):2275–86. Epub 2004/02/03. https://doi.org/10.1038/sj.onc.1207410 PMID: 14755244

20. Rosenwald A, Wright G, Chan WC, Connors JM, Campo E, Fisher RI, et al. The use of molecular profil- ing to predict survival after chemotherapy for diffuse large-B-cell lymphoma. The New England journal of medicine. 2002; 346(25):1937–47. Epub 2002/06/21. https://doi.org/10.1056/NEJMoa012914 PMID:12075054

21. Houldsworth J, Olshen AB, Cattoretti G, Donnelly GB, Teruya-Feldstein J, Qin J, et al. Relationship between REL amplification, REL function, and clinical and biologic features in diffuse large B-cell lym- phomas. Blood. 2004; 103(5):1862–8. Epub 2003/11/15. https://doi.org/10.1182/blood-2003-04-1359 PMID: 14615382

22. Shehata M, Shehata F, Pater A. Apoptosis effects of Xrel3 c-Rel/Nuclear Factor-kappa B homolog in human cervical cancer cells. Cell biology international. 2005; 29(6):429–40. Epub 2005/08/02. https:// doi.org/10.1016/j.cellbi.2004.12.014 PMID: 16054560

23. Lorenz VN, Schon MP, Seitz CS. c-Rel downregulation affects cell cycle progression of human keratino- cytes. The Journal of investigative dermatology. 2014; 134(2):415–22. Epub 2013/07/31. https://doi. org/10.1038/jid.2013.315 PMID: 23892589

24. Shehata M, Shehata F, Pater A. Dual apoptotic effect of Xrel3 c-Rel/NF-kappaB homolog in human cer- vical cancer cells. Cell biology international. 2004; 28(12):895–904. Epub 2004/11/30. https://doi.org/10.1016/j.cellbi.2004.09.002 PMID: 15566959

25. Horvath P, Barrangou R. CRISPR/Cas, the immune system of bacteria and archaea. Science. 2010;327(5962):167–70. Epub 2010/01/09. https://doi.org/10.1126/science.1179555 PMID: 20056882

26. Cong L, Ran FA, Cox D, Lin S, Barretto R, Habib N, et al. Multiplex genome engineering using CRISPR/ Cas systems. Science. 2013; 339(6121):819–23. Epub 2013/01/05. https://doi.org/10.1126/science.1231143 PMID: 23287718

27. Mali P, Yang L, Esvelt KM, Aach J, Guell M, DiCarlo JE, et al. RNA-guided human genome engineering via Cas9. Science. 2013; 339(6121):823–6. Epub 2013/01/05. https://doi.org/10.1126/science.1232033 PMID: 23287722

28. Matano M, Date S, Shimokawa M, Takano A, Fujii M, Ohta Y, et al. Modeling colorectal cancer using CRISPR-Cas9-mediated engineering of human intestinal organoids. Nature medicine. 2015; 21 (3):256–62. Epub 2015/02/24. https://doi.org/10.1038/nm.3802 PMID: 25706875

29. Jinek M, East A, Cheng A, Lin S, Ma E, Doudna J. RNA-programmed genome editing in human cells. eLife. 2013; 2:e00471. Epub 2013/02/07. https://doi.org/10.7554/eLife.00471 PMID: 23386978

30. Ran FA, Hsu PD, Lin CY, Gootenberg JS, Konermann S, Trevino AE, et al. Double nicking by RNA- guided CRISPR Cas9 for enhanced genome editing specificity. Cell. 2013; 154(6):1380–9. Epub 2013/ 09/03. https://doi.org/10.1016/j.cell.2013.08.021 PMID: 23992846

31. Sakuma T, Nishikawa A, Kume S, Chayama K, Yamamoto T. Multiplex genome engineering in human cells using all-in-one CRISPR/Cas9 vector system. Scientific reports. 2014; 4:5400. Epub 2014/06/24. https://doi.org/10.1038/srep05400 PMID: 24954249

32. Neumann B, Walter T, Heriche JK, Bulkescher J, Erfle H, Conrad C, et al. Phenotypic profiling of the human genome by time-lapse microscopy reveals cell division genes. Nature. 2010; 464(7289):721–7. Epub 2010/04/03. https://doi.org/10.1038/nature08869 PMID: 20360735

33. Tokunaga S, Stegeman JJ. Elimination of nonspecific bands in non-radioactive electrophoretic mobility shift assays using the digoxigenin system. Analytical biochemistry. 2014; 465:70–2. Epub 2014/07/09. https://doi.org/10.1016/j.ab.2014.06.020 PMID: 25004462

34. Kaltschmidt B, Kaltschmidt C, Hehner SP, Droge W, Schmitz ML. Repression of NF-kappaB impairs HeLa cell proliferation by functional interference with cell cycle checkpoint regulators. Oncogene. 1999;18(21):3213–25. Epub 1999/06/08. https://doi.org/10.1038/sj.onc.1202657 PMID: 10359527

35. Forbes SA, Beare D, Gunasekaran P, Leung K, Bindal N, Boutselakis H, et al. COSMIC: exploring the world's knowledge of somatic mutations in human cancer. Nucleic acids research. 2015; 43(Database issue):D805–11. Epub 2014/10/31. https://doi.org/10.1093/nar/gku1075 PMID: 25355519

36. Stemmer M, Thumberger T, Del Sol Keyer M, Wittbrodt J, Mateo JL. CCTop: An Intuitive, Flexible and Reliable CRISPR/Cas9 Target Prediction Tool. PloS one. 2015; 10(4):e0124633. Epub 2015/04/25. https://doi.org/10.1371/journal.pone.0124633 PMID: 25909470

37. Zhao Y, Yao R, Ouyang L, Ding H, Zhang T, Zhang K, et al. Three-dimensional printing of Hela cells for cervical tumor model in vitro. Biofabrication. 2014; 6(3):035001. Epub 2014/04/12. https://doi.org/10.1088/1758-5082/6/3/035001 PMID: 24722236

38. Vidya Priyadarsini R, Senthil Murugan R, Maitreyi S, Ramalingam K, Karunagaran D, Nagini S. The fla- vonoid quercetin induces cell cycle arrest and mitochondria-mediated apoptosis in human cervical can- cer (HeLa) cells through p53 induction and NF-kappaB inhibition. European journal of pharmacology.2010; 649(1–3):84–91. Epub 2010/09/23. https://doi.org/10.1016/j.ejphar.2010.09.020 PMID:20858478

39. Hamada K, Alemany R, Zhang WW, Hittelman WN, Lotan R, Roth JA, et al. Adenovirus-mediated trans- fer of a wild-type p53 gene and induction of apoptosis in cervical cancer. Cancer research. 1996; 56 (13):3047–54. Epub 1996/07/01. PMID: 8674061

40. Gilmore TD. NF-kB Target Genes. https://www.bu.edu/nf-kb/gene-resources/target-genes/: Boston University Biology; [cited 2017 13.02.].

41. Buss H, Dorrie A, Schmitz ML, Hoffmann E, Resch K, Kracht M. Constitutive and interleukin-1-inducible phosphorylation of p65 NF-{kappa}B at serine 536 is mediated by multiple protein kinases including I
{kappa}B kinase (IKK)-{alpha}, IKK{beta}, IKK{epsilon}, TRAF family member-associated (TANK)-bind- ing kinase 1 (TBK1), and an unknown kinase and couples p65 to TATA-binding protein-associated fac- tor II31-mediated interleukin-8 transcription. The Journal of biological chemistry. 2004; 279(53):55633– 43. Epub 2004/10/19. https://doi.org/10.1074/jbc.M409825200 PMID: 15489227

42. Harris J, Oliere S, Sharma S, Sun Q, Lin R, Hiscott J, et al. Nuclear accumulation of cRel following C-ter- minal phosphorylation by TBK1/IKK epsilon. J Immunol. 2006; 177(4):2527–35. Epub 2006/08/05. PMID: 16888014

43. Eddy SF, Guo S, Demicco EG, Romieu-Mourez R, Landesman-Bollag E, Seldin DC, et al. Inducible IkappaB kinase/IkappaB kinase epsilon expression is induced by CK2 and promotes aberrant nuclear factor-kappaB activation in breast cancer cells. Cancer research. 2005; 65(24):11375–83. Epub 2005/12/17. https://doi.org/10.1158/0008-5472.CAN-05-1602 PMID: 16357145

44. Grumont R, Lock P, Mollinari M, Shannon FM, Moore A, Gerondakis S. The mitogen-induced increase in T cell size involves PKC and NFAT activation of Rel/NF-kappaB-dependent c-myc expression. Immu- nity. 2004; 21(1):19–30. Epub 2004/09/04. https://doi.org/10.1016/j.immuni.2004.06.004 PMID:15345217

45. Grey ST, Arvelo MB, Hasenkamp W, Bach FH, Ferran C. A20 inhibits cytokine-induced apoptosis and nuclear factor kappaB-dependent gene activation in islets. The Journal of experimental medicine. 1999;190(8):1135–46. Epub 1999/10/19. PMID: 10523611

46. Boise LH, Gonzalez-Garcia M, Postema CE, Ding L, Lindsten T, Turka LA, et al. bcl-x, a bcl-2-related gene that functions as a dominant regulator of apoptotic cell death. Cell. 1993; 74(4):597–608. Epub1993/08/27. PMID: 8358789

47. Grossmann M, O'Reilly LA, Gugasyan R, Strasser A, Adams JM, Gerondakis S. The anti-apoptotic activities of Rel and RelA required during B-cell maturation involve the regulation of Bcl-2 expression. The EMBO journal. 2000; 19(23):6351–60. Epub 2000/12/02. https://doi.org/10.1093/emboj/19.23.6351 PMID: 11101508

48. Chen C, Edelstein LC, Gelinas C. The Rel/NF-kappaB family directly activates expression of the apo- ptosis inhibitor Bcl-x(L). Molecular and cellular biology. 2000; 20(8):2687–95. Epub 2000/03/25. PMID:10733571

49. De Siervi A, De Luca P, Moiola C, Gueron G, Tongbai R, Chandramouli GV, et al. Identification of new Rel/NFkappaB regulatory networks by focused genome location analysis. Cell Cycle. 2009; 8 (13):2093–100. Epub 2009/06/09. https://doi.org/10.4161/cc.8.13.8926 PMID: 19502793

50. Strutz F, Zeisberg M, Renziehausen A, Raschke B, Becker V, van Kooten C, et al. TGF-beta 1 induces proliferation in human renal fibroblasts via induction of basic fibroblast growth factor (FGF-2). Kidney international. 2001; 59(2):579–92. Epub 2001/02/13. https://doi.org/10.1046/j.1523-1755.2001.059002579.x PMID: 11168939

51. Adli M, Baldwin AS. IKK-i/IKKepsilon controls constitutive, cancer cell-associated NF-kappaB activity via regulation of Ser-536 p65/RelA phosphorylation. The Journal of biological chemistry. 2006; 281 (37):26976–84. Epub 2006/07/15. https://doi.org/10.1074/jbc.M603133200 PMID: 16840782

52. Tian W, Liou HC. RNAi-mediated c-Rel silencing leads to apoptosis of B cell tumor cells and suppresses antigenic immune response in vivo. PloS one. 2009; 4(4):e5028. Epub 2009/04/07. https://doi.org/10.1371/journal.pone.0005028 PMID: 19347041

53. Grumont RJ, Rourke IJ, O'Reilly LA, Strasser A, Miyake K, Sha W, et al. B lymphocytes differentially use the Rel and nuclear factor kappaB1 (NF-kappaB1) transcription factors to regulate cell cycle pro- gression and apoptosis in quiescent and mitogen-activated cells. The Journal of experimental medicine.1998; 187(5):663–74. Epub 1998/03/28. PMID: 9480976

54. Rosette C, Roth RB, Oeth P, Braun A, Kammerer S, Ekblom J, et al. Role of ICAM1 in invasion of human breast cancer cells. Carcinogenesis. 2005; 26(5):943–50. Epub 2005/03/19. https://doi.org/10.1093/carcin/bgi070 PMID: 15774488

55. Soucek L, Whitfield JR, Sodir NM, Masso-Valles D, Serrano E, Karnezis AN, et al. Inhibition of Myc fam- ily proteins eradicates KRas-driven lung cancer in mice. Genes & development. 2013; 27(5):504–13. Epub 2013/03/12.

56. Krappmann D, Emmerich F, Kordes U, Scharschmidt E, Dorken B, Scheidereit C. Molecular mecha- nisms of constitutive NF-kappaB/Rel activation in Hodgkin/Reed-Sternberg cells. Oncogene. 1999; 18 (4):943–53. Epub 1999/02/19. https://doi.org/10.1038/sj.onc.1202351 PMID: 10023670

57. Perkins ND, Gilmore TD. Good cop, bad cop: the different faces of NF-kappaB. Cell death and differen- tiation. 2006; 13(5):759–72. Epub 2006/01/18. https://doi.org/10.1038/sj.cdd.4401838 PMID:16410803

58. Forbes SA. cancer.sanger.ac.uk [cited 2017 14.02].

59. Futreal PA, Coin L, Marshall M, Down T, Hubbard T, Wooster R, et al. A census of human cancer genes. Nature reviews Cancer. 2004; 4(3):177–83. Epub 2004/03/03. https://doi.org/10.1038/nrc1299 PMID: 14993899

60. Wilhelmsen KC, Eggleton K, Temin HM. Nucleic acid sequences of the oncogene v-rel in reticuloen- dotheliosis virus strain T and its cellular homolog, the proto-oncogene c-rel. Journal of virology. 1984;52(1):172–82. Epub 1984/10/01. PMID: 6090694

61. Wang D, Lippard SJ. Cellular processing of platinum anticancer drugs. Nature reviews Drug discovery. 2005; 4(4):307–20. Epub 2005/03/25. https://doi.org/10.1038/nrd1691 PMID: 15789122

62. Peters GJ, Backus HH, Freemantle S, van Triest B, Codacci-Pisanelli G, van der Wilt CL, et al. Induc- tion of thymidylate synthase as a 5-fluorouracil resistance mechanism. Biochimica et biophysica acta. 2002; 1587(2–3):194–205. Epub 2002/06/27. PMID: 12084461

63. Wang CY, Cusack JC Jr., Liu R, Baldwin AS Jr.. Control of inducible chemoresistance: enhanced anti- tumor therapy through increased apoptosis by inhibition of NF-kappaB. Nature medicine. 1999; 5 (4):412–7. Epub 1999/04/15. https://doi.org/10.1038/7410 PMID: 10202930

64. Yang L, Zhou Y, Li Y, Zhou J, Wu Y, Cui Y, et al. Mutations of p53 and KRAS activate NF-kappaB to pro- mote chemoresistance and tumorigenesis via dysregulation of cell cycle and suppression of apoptosis in lung cancer cells. Cancer letters. 2015; 357(2):520–6. Epub 2014/12/17. https://doi.org/10.1016/j.canlet.2014.12.003 PMID: 25499080

BBA - Molecular Cell Research 1865 (2018) 1025–1033

Contents lists available at ScienceDirect

BBA - Molecular Cell Research

journal homepage: www.elsevier.com/locate/bbamcr

IKK1/2 protect human cells from TNF-mediated RIPK1-dependent apoptosis in an NF-κB-independent manner

Carsten Slotta[a,b], Jonathan Storm[a], Nina Pfisterer[a], Elena Henkel[a], Svenja Kleinwächter[a], Maren Pieper[a], Lucia M. Ruiz-Perera[b], Johannes F.W. Greiner[a], Barbara Kaltschmidt[a,b,1], Christian Kaltschmidt[a,*,1]

[a] Department of Cell Biology, University of Bielefeld, Universitaetsstr. 25, 33501 Bielefeld, Germany
[b] Molecular Neurobiology, University of Bielefeld, Universitaetsstr. 25, 33501 Bielefeld, Germany

ARTICLE INFO

Keywords:
NF-kappa-B
IKK
Cell death
Apoptosis
Tumor necrosis factor
RIPK1

ABSTRACT

TNF signaling is directly linked to cancer development and progression. A broad range of tumor cells is able to evade cell death induced by TNF impairing the potential anti-cancer value of TNF in therapy. Although sensitizing cells to TNF-induced death therefore has great clinical implications, detailed mechanistic insights into TNF-mediated human cell death still remain unknown. Here, we analyzed human cells by applying CRISPR/Cas9n to generate cells deficient of IKK1, IKK2, IKK1/2 and RELA. Despite stimulation with TNF resulted in impaired NF-κB activation in all genotypes compared to wildtype cells, increased cell death was observable only in IKK1/2-double-deficient cells. Cell death could be detected by Caspase-3 activation and binding of Annexin V. TNF-induced programmed cell death in IKK1/2$^{-/-}$ cells was further shown to be mediated via RIPK1 in a predominantly apoptotic manner. Our findings demonstrate the IKK complex to protect from TNF-induced cell death in human cells independently to NF-κB RelA suggesting IKK1/2 to be highly promising targets for cancer therapy.

1. Introduction

The tumor necrosis factor (TNF) is a well-characterized pro-inflammatory cytokine known to activate the canonical NF-κB signaling pathway. A particular important regulatory factor in NF-κB signaling is the IκB kinase (IKK) complex. It consists of the catalytic subunits IKKα (IKK1) and IKKβ (IKK2) and the regulatory subunit NF-kappa-B essential modulator (NEMO; IKKγ). The IKK complex is required for the activation of the transcription factor NF-κB, which ultimately results in the expression of NF-κB target genes involved in cell growth, survival, but also inflammation and cell death [1]. Deregulation of NF-κB signaling is strongly associated with diseases, in particular with tumor formation [2,3].

In the canonical NF-κB signaling pathway binding of TNF to the TNF receptor 1 (TNFR1) results in the formation of the so-called complex I consisting of the TNFR1 associated death domain protein (TRADD), TNF receptor associated factor 2 (TRAF2), cellular inhibitors of apoptosis 1 and 2 (cIAP1/2), linear ubiquitin assembly complex (LUBAC) and Receptor-interacting serine/threonine-protein kinase 1 (RIPK1) [4]. Ubiquitination of RIPK1 leads to the recruitment of the IKK complex by binding of NEMO to M1-linked ubiquitin chains on the one hand and of the TAK1/TAB2/3 complex via K63-linked chains on the other hand [5,6]. Being phosphorylated by TAK1, IKK2 in turn phosphorylates IκBα at Ser32/36. Phosphorylated IκBα will be polyubiquitinated by SCF$^{\beta\text{-TrCP}}$ E3 ubiquitin ligases leading to its proteasomal degradation [7]. This results in the unmasking of the nuclear localization sequence of NF-κB, in canonical signaling mostly comprised of a p65/p50 dimer, whereby p65 is the transactivating subunit [8]. Due to the unmasked NLS, NF-κB is no longer retained in the cytoplasm and can enter the nucleus leading to the expression of target genes [9]. Tight regulation of the specificity of this process is achieved by a broad range of post-translational modifications (PMTs) potentially resulting in conformational changes of NF-κB and by this specifying the subset of target genes being expressed [10,11].

Although TNFR1 belongs to the death receptor family [12], under physiological conditions TNF signaling will not induce cell death in a broad range of cell types, since TNF-mediated activation of NF-κB will result in the expression of anti-apoptotic genes such as c-FLIP, cIAP-1, cIAP-2 and Bcl-2 [13–16]. However, genetic or pharmacological inhibition of NF-κB is known to increase sensitivity to TNF-induced

* Corresponding author at: Christian Kaltschmidt, Department of Cell Biology, University of Bielefeld, Universitaetsstr. 25, 33501 Bielefeld, Germany.
E-mail address: c.kaltschmidt@uni-bielefeld.de (C. Kaltschmidt).
[1] These authors contributed equally to this work.

https://doi.org/10.1016/j.bbamcr.2018.04.003
Received 21 November 2017; Received in revised form 30 March 2018; Accepted 5 April 2018
Available online 07 April 2018
0167-4889/

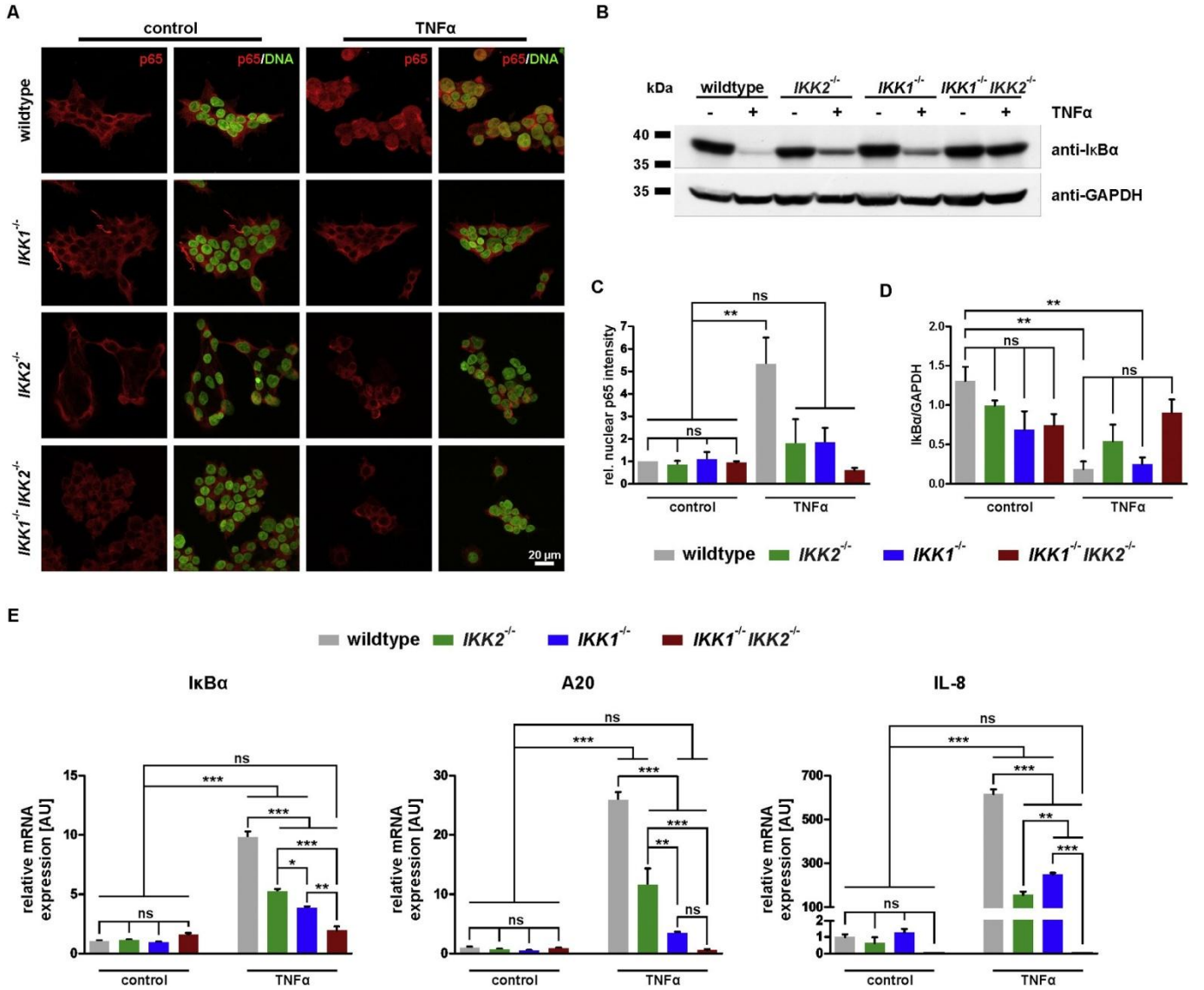

Fig. 1. Strongly impaired NF-κB activation in knockout cells. (A) Immunocytochemical stainings of cells stimulated for 20 min with 10 ng/mL TNFα. Only in wildtype cells a clear nuclear translocation of p65 after stimulation is observable. (B) Western blot analysis of IκBα after stimulation with 10 ng/mL TNFα for 20 min. (C) Quantification of the nuclear intensity of cells stained against p65 (One-way ANOVA, Bonferroni post-test, three independent replicates (n = 3), at least 40 cells per replicate, genotype and condition were analyzed).(D) Quantification of western blot analysis (B). No degradation of IκBα after TNFα stimulation was observed in double-deficient cells (One-way ANOVA, Bonferroni post-test, n = 3). (E) qPCR analysis of the NF-κB target genes IκBα, A20 and IL-8 revealed reduced expression in the knockout cells after 6 h of TNFα (10 ng/mL) treatment compared to wildtype cells (One-way ANOVA, Bonferroni post-test, n = 3).

apoptosis [17]. Here, cell death is mediated via the so-called complex IIa comprised of TRADD, Fas-associated protein with death domain (FADD) and caspase-8, which only assembles upon NF-κB inhibition [18,19]. However, programmed cell death induced by TNF signaling can also be mediated via an NF-κB-independent manner [20]. In this context, cell death occurs via the complex IIb [20]. In contrast to complex IIa, FADD and caspase-8 are recruited by RIPK1 in complex IIb. Upon inhibition of caspase-8, NF-κB-independent cell death via TNFR1 can also be necroptotic. Necroptosis is a more recently described way of programmed cell death, which is independent on caspase-8 activation and induced by RIPK3 and the pseudokinase mixed lineage kinase like (MLKL) [21–23]. In 2015, Dondelinger and colleagues described Ikk1 and Ikk2 to act directly on RIPK1 and thereby protect cells from TNF-induced cell death independently on NF-κB activation [24].

Most studies regarding TNF-induced cell death were performed using mouse models, in which members of the NF-κB signaling pathway were genetically depleted. Many of these genetic knockouts are resulting in lethality during embryonic development, e.g. in RelA- and Ikk2-deficient mice [25–27]. In both cases, embryonic lethality is caused by TNFα-induced death of hepatocytes and subsequent liver degeneration, which can be rescued by additional depletion of TNFR1 [26,28]. In contrast to this, a frameshift mutation within the human IKBKB gene, which was found in patients suffering from severe combined immunodeficiency (SCID), had no effect on embryonic survival or liver constitution [29]. These findings suggest the presence of potential differences in the regulation of TNFα-induced cell death between mouse and human. Since TNF signaling is highly elevated in a broad range of cancer cells, which are resistant to cell death induced by TNF [30], sensitizing these cells to TNF-induced cell death appears to be a promising approach for cancer therapy. Despite this clinical relevance, the detailed molecular mechanisms of TNF-induced cell death in human cells still remain unknown.

Facing this challenge, we made use of the CRISPR/Cas9 system to generate genomic knockouts of several members of the NF-κB signaling pathway in human cells. Originally discovered as part of the bacterial adaptive immune system [31,32], the clustered regularly interspaced

short palindromic repeats (CRISPR) system has become a state-of-the-art tool broadly applied for efficient genome editing [33,34]. In this study, a nickase mutant of the S. pyogenes Cas9 (D10A; Cas9n) has been used minimizing potential off-target effects and by this increasing the specificity of genome editing [35]. We successfully generated cells deficient for IKK1, IKK2, IKK1/2 and RelA and demonstrate that TNFα-induced cell death in human cells is mediated predominantly via RIPK1 and independently of NF-κB. Targeting the IKK complex in tumor cells genetically or pharmacologically therefore appears promising to increase sensitivity to TNF-induced cell death with direct implications for potential therapeutic approaches.

2. Results

2.1. Knockout of IKK1 and IKK2 leads to strongly impaired NF-κB activation

To assess clinical implications of IKK1 and IKK2 knockouts, we first analyzed levels of overexpression in human cancer with database mining using COSMIC [36]. Here, particularly IKBKB (IKK2) was found to be profoundly overexpressed in a variety of tissues including breast, endometrium, large intestine and skin (Fig. S1).

We now aimed to analyze the role of IKK1 and IKK2 in the context of TNF signaling and activation of NF-κB. For this, we utilized the CRISPR/Cas9n system to generate IKK1- and IKK2-deficient cells as well as an IKK1/IKK2 double knockout by inducing two double-strand breaks spanning an intron-exon border (Fig. S2A). Deletions within the IKBK1 and IKBK2 gene of clonally grown cells were validated by genomic PCR using primers flanking the deletion (Fig. S2B) and by RT-PCR using primer pairs with one primer set within the deletion (Fig. S2C). Absence of IKK1 and IKK2 protein was finally shown on western blot (Fig. S2D). Notably, we did not observe a strong reduction in the amount of the NF-κB subunit p65 in the knockout clones, which was described earlier for IKK2-deficient human fibroblast [29]. Only in IKK1-deficient cells, a slight reduction was detected (Fig. S3). Next, we examined NF-κB activation in all genotypes after stimulation with TNFα. Nuclear translocation of p65 was significantly impaired compared to wildtype cells (Fig. 1A, C). This effect was strongest in the double-deficient cells. In line with this, qPCR analysis of the NF-κB target genes IκBα, A20 and IL-8 after TNFα stimulation revealed a significantly reduced expression in all genotypes compared to wildtype cells (Fig. 1E). In IKK1/2-double-deficient cells, no increase in expression upon stimulation was detected at all (Fig. 1E). Moreover, we detected no signs of IκBα degradation upon TNFα treatment in these cells (Fig. 1B, D). We likewise observed no significant degradation of IκBα in IKK2 single knockout cells, although IKK1$^{-/-}$ cells showed sig- nificantly decreased protein levels of IκBα after TNFα-treatment in comparison to wildtype control (Fig. 1B, D).

2.2. IKK1 and IKK2 double-deficiency results in TNFα-induced cell death

We aimed to analyze TNFα-induced cell death in our newly generated knockout cells. After long-term exposure (24 h) to TNFα, a high number of dead cells was observable only in the double-deficient cells (Fig. 2A; Fig. S4), while there was hardly any difference detectable between the single knockouts and wildtype cells (Fig. 2A). Immunocytochemical staining of TNFα-treated cells also revealed 32.1% of the IKK1/IKK2$^{-/-}$ cells to be positive for activated Caspase-3. In comparison, only 3.0% Caspase-3-positive cells were found in wildtype cells (Fig. 2B). Without TNFα stimulation, in both genotypes $< 0.3\%$ cells were positive (Fig. 2B). We additionally detected the increased cell death in the IKK1/2 double-deficient cells using DNA content measurements (Fig. S5). In the IKK1 and IKK2 single knockout cells, no difference in the amount of apoptotic cells upon TNFα stimulation was observable compared to wildtype cells. However, in IKK1/2-double-deficient cells, this amount was increased from 4.2% (wildtype) to 34.7% (Fig. S5). Furthermore, increased cell death of the IKK1/2$^{-/-}$ cells within 24 h of TNFα stimulation could be demonstrated using an Annexin V-based apoptosis assay. Annexin V-based luminescent signal was strongly elevated in the double-deficient cells in relation to wildtype (Fig. 2C).

In the presence of Nescrostatin-1s (Nec-1s), a potent inhibitor of RIPK1, cell death was markedly reduced in IKK1/2-deficient cells (Fig. 3A). Stainings against activated caspase-3 revealed 12.8% caspase-3-positive cells (Fig. 3B), a strong reduction when compared to the 32.8% positive cells, which were stimulated only with TNFα (Fig. 2B). Using the Annexin V-based apoptosis assay, the protective effect of Nec-1s was further validated (Fig. 3C).

2.3. TNFα does not induce programmed cell death upon RelA deficiency

Since cells deficient for either IKK1 or IKK2 also showed strongly impaired NF-κB activation, we speculated an NF-κB-independent mechanism might lead the cell death observed. To further analyze this, we generated cells deficient for the NF-κB-subunit RelA (p65) (Fig. 4). Using the same approach, we generated a genomic deletion spanning the intron-exon boundary of exon 2 (Fig. 4A), which is present in all transcript variants listed at ENSEMBL.org. We validated the designed deletion using genomic PCR and qPCR (Fig. 4B, C) and lack of p65 protein by immunocytochemistry (Fig. 4D). Analysis of NF-κB activation in these cells was assessed by qPCR of the NF-κB target genes IκBα and A20 showing reduced expression in the RelA$^{-/-}$ cells after stimulation with TNFα compared to wildtype cells (Fig. 4E). This impairment was validated by usage of an NF-κB-driven luciferase reporter demonstrating reduced activation of NF-κB in the knockout cells (Fig. 4F).

Upon long-term exposure to TNFα we detected no increased amount of dead RelA-deficient cells compared to wildtype cells (Fig. 5A). In an immunocytochemical analysis, the amount of cells positive for the activated form of caspase-3 only very mildly increased (Fig. 5B), being even below the values for TNFα-stimulated wildtype cells (Fig. 2B). Signals for Annexin V were hardly elevated in the GloMax Annexin V Apoptosis Assay in RelA$^{-/-}$ cells within 24 h of TNFα treatment (Fig. 5C).

3. Discussion

In the present study, we successfully generated genomic knockouts for IKK1, IKK2, IKK1/2 and RelA in HEK293 cells to initially analyze the role of IKK1 and IKK2 in the context of TNF-induced cell death. HEK293 cells are a broadly used cellular model for TNF-signaling [18]. Upon stimulation with TNFα, a vast increase in cell death was observed only in cells deficient for both IKK1 and IKK2. We further partially rescued cell death in these cells using the RIPK1-specific inhibitor Necrostatin-1s indicating RIPK1 activity to be the predominant cause of the cell death observed.

Activation of the death receptor TNFR1 does not necessarily lead to death but often results in cell survival or even increased proliferation [37,38]. Downstream of TNFR1 two major pathways – an NF-κB – dependent and an – independent one – have been described to regulate and control cell death [39]. The first one is well characterized and demonstrates the activation of NF-κB by TNF-signaling resulting in the expression of anti-apoptotic NF-κB target genes such as cIAP-1, cIAP-2 or c-FLIP [13,14,17]. In contrast, signaling via TNFR1 independently of NF-κB activation is far less well understood and just gained attention in the last years [39,40]. In the present study, we carefully investigated NF-κB activation in response to TNFα in all genotypes we created. While differences between the different knockouts were observable, all cells showed significantly reduced activation when compared to wildtype cells. In contrast, experiments conducted in Ikk1-deficient mice showed no major impairments in canonical NF-κB signaling, although strong developmental aberrations and death shortly after birth were

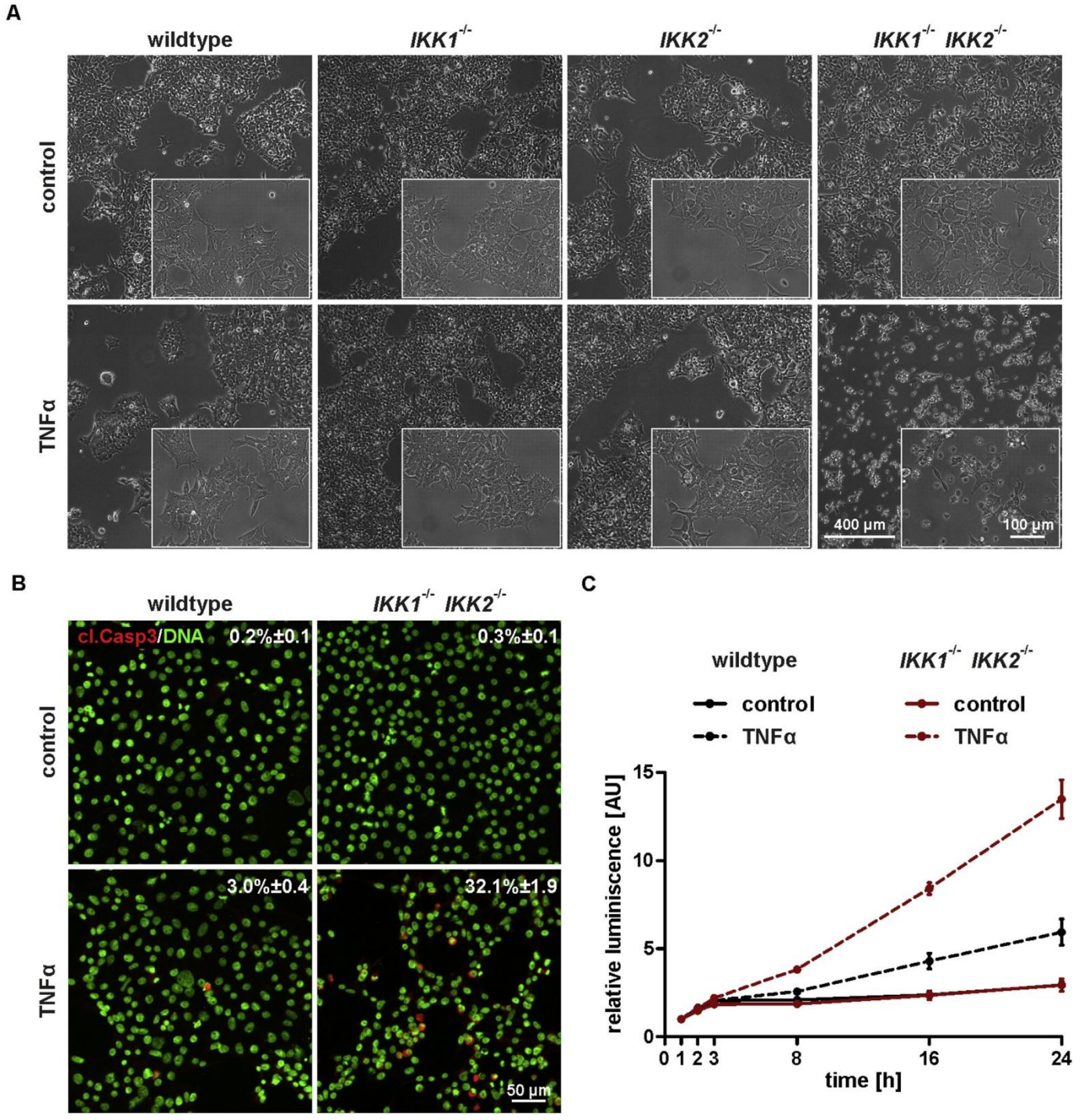

Fig. 2. IKK1/2-deficiency results in profound TNFα-induced cell death. (A) Light microscopic images demonstrate vastly increased cell death in IKK1/2-double deficient cells upon 24 h exposure to TNFα (20 ng/mL). (B) Immunocytochemical stainings of wildtype and IKK1/2$^{-/-}$ cells revealed a huge increase in caspase-3-positive cells in the double knockout after 24 h of TNFα stimulation (20 ng/mL) (n = 3; for each genotype and condition > 2500 cells were analyzed). (C) RealTime Glo Annexin V apoptosis assay of wildtype and IKK1/2-deficient cells. Compared to wildtype cells, a strong increase in apoptotic cells was observable.

observable [41]. Consequently, IKK2 is concluded to be the catalytic subunit needed for canonical NF-κB signaling by directly phosphorylating IκBα. However, in IKK1-deficient cells we observed severely affected NF-κB activation after TNFα stimulation. In fact, most experiments demonstrated impairments within the same range as in IKK2-deficient cells indicating that IKK2 cannot compensate loss of IKK1 in the cells we used. Interestingly, while no significant increase in nuclear localization of p65 after TNFα stimulation was observable in IKK1-deficient cells, IκBα was significantly degraded. These data are in accordance to Ikk1$^{-/-}$ mouse hepatocytes showing highly decreased amounts of IκBα accompanied by a decreased nuclear translocation of p65 in comparison to wt after treatment with TNFα. In line with Luedde and coworkers, we thus suggest IKK1 to control NF-κB nuclear translocation by a mechanism independent of IκB phosphorylation and degradation [42]. Remarkably, although activation of NF-κB via TNF is associated with cell growth, especially in the context of tumor formation and progression, we detected no signs of reduced proliferation in any of the genotypes created (data not shown). Recently, we generated

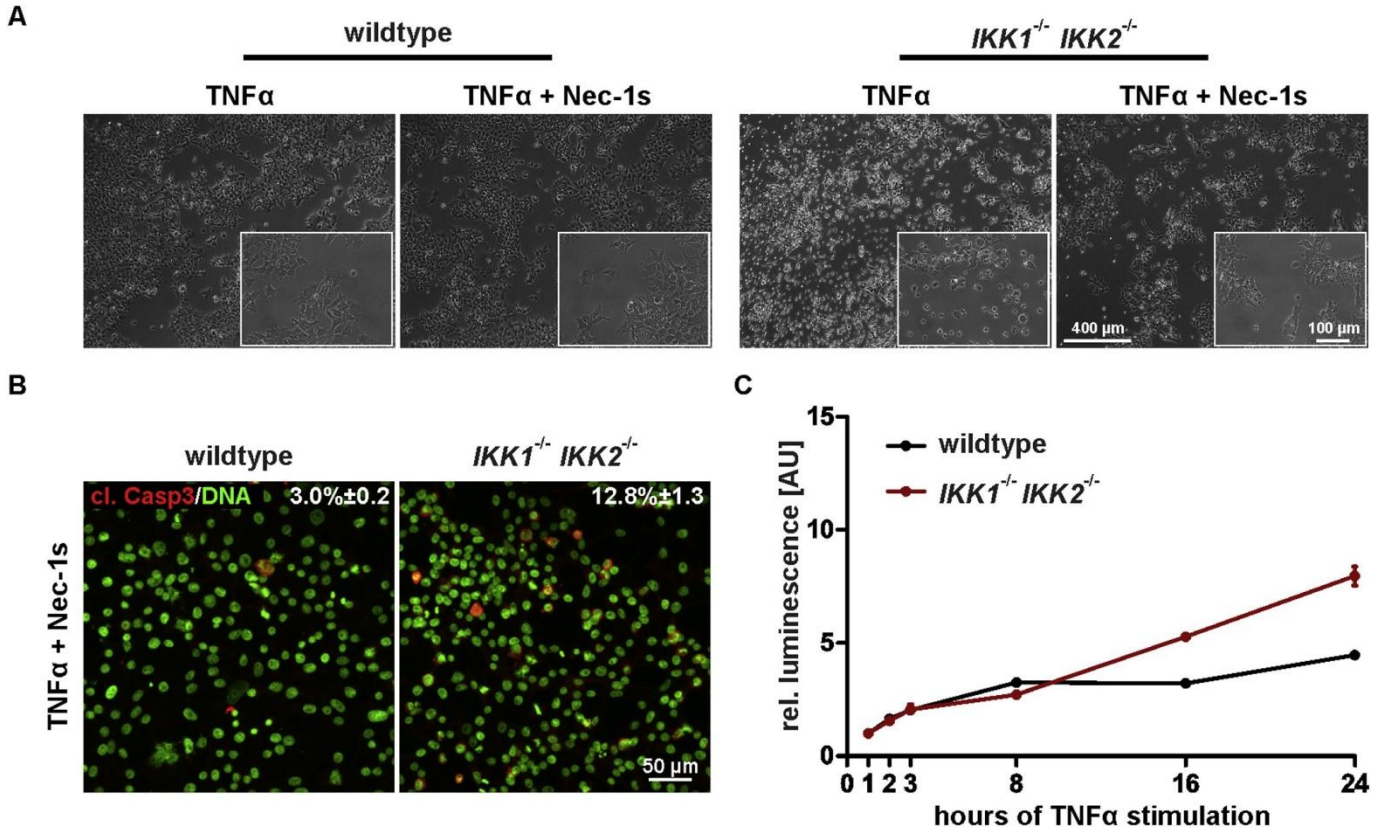

Fig. 3. TNFα-induced cell death is mediated via RIPK1. (A) Stimulation of IKK1/2-deficient cells with 20 ng/mL TNFα and the RIPK1 inhibitor Nec-1s (10 μM; middle panel) (1 μM; bottom panel) resulted in a profound protection from TNFα-induced cell death for Nec1s (B) Upon TNFα treatment immunocytochemistry revealed 12.8% caspase-3-positive cells in the presence of Nec-1s ($n = 3$; for each genotype and replicate > 2500 cells were analyzed). (C) RealTime Glo Annexin V apoptosis assay of TNFα-stimulated wildtype and IKK1/2-deficient cells in the presence of Nec-1s (C).

HeLa cells deficient for the NF-κB subunit c-Rel, which showed a significantly lowered proliferation rate [43]. However, although NF-κB activation was significantly impaired in these cells, no increase in cell death was observed after treatment with TNFα already suggesting the presence of an NF-κB-independent mechanism to prevent from TNF-induced cell death in human cells. Dondelinger and colleagues described a novel function of both Ikk1 and Ikk2 in mice by demonstrating RIPK1 to be a bona fide target of the Ikk complex [24]. By directly phosphorylating RIPK1, Ikk1/2 inactivate RIPK1 and prevent from TNF-induced cell death independently of NF-κB. In this NF-κB-independent pathway, RIPK1 will be required to recruit FADD into the so-called complex IIb resulting in apoptosis. Upon caspase-8 inhibition RIPK1 can also be incorporated into the necrosome, which will lead to the activation of RIPK3 and its substrate MLKL leading to necroptotic cell death [20]. Interestingly, deficiency of either Ikk1 or Ikk2 was not sufficient to induce cell death upon TNFα. However, in fibroblasts derived from Ikk1/2-double deficient mice, cell death was vastly increased when cells were exposed to TNFα [24]. Extending these findings, we observed no strong increase in cell death when either, IKK1 or IKK2 was genetically depleted. Only in cells deficient for both, IKK1 and IKK2, significant increase in cell death was detectable. We hypothesized that cell death predominantly occurred in an NF-κB-independent way mediated via RIPK1. Confirming this, application of the RIPK1-specific inhibitor Nec-1s partially rescued from TNF-induced cell death in the IKK1/2-double deficient cells. Previously, the IKK complex particularly was considered to be important in regard to anticancer therapy. In mice, Ikk1 and Ikk2 have been shown to control liver cancer by directly acting on RIPK1, extending the initial findings by Dondelinger to a tumor environment [44]. Similar results were obtained for NEMO, which controlled RIPK1-mediated hepatocyte death and by this formation of hepatocellular carcinoma [45]. Notably, most studies dealing with the causes of cell death induced by TNFα included the application of mouse models to gain their findings. However, differences between humans and mice have been reported in the past in terms of TNF and NF-κB signaling. Mice deficient for either, RelA, Ikk2 or NEMO were reported to die during embryonic development, in each case due to TNF-induced death of hepatocytes resulting in liver degeneration [25–27,46]. In 2013, Panicke and co-workers described a frameshift mutation in the human IKBKB gene to be the cause of severe combined immunodeficiency [29]. Patients carrying this loss-of-function mutation did not show any signs of liver degeneration indicating potential differences in TNF signaling between humans and mice. This elucidates the necessity to analyze TNF-mediated cell death in human cells, especially when considering that TNF signaling is closely connected to human diseases, in particular with cancer. Several reports describe TNF being involved in all parts of carcinogenesis, namely transformation of healthy cells, survival, proliferation, invasion, angiogenesis and metastasis of tumor cells (reviewed in [30]). In a broad range of tumorigenic tissues or tumor cells, TNF expression is strongly increased [47,48]. Consequently, many types of tumor cells are particularly resistant to TNF-induced cell death [30]. A better understanding of the mechanisms, on how tumor cells evade death therefore is a promising approach to increase the anti-cancer value of TNF. Supporting our findings of NF-κB-independent cell death in human cells, Legarda-Addison and co-workers demonstrated in Jurkat cells increased sensitivity to TNF-induced cell death upon NEMO deficiency, which was independent of NF-κB [49]. As was observed from Dondelinger, NEMO deficiency in mice also sensitized cells regarding TNF-induced cell death, in a similar manner as Ikk1/2 combined [24]. Studies in mice depicted differences in RIPK1-mediated cell death, depending on

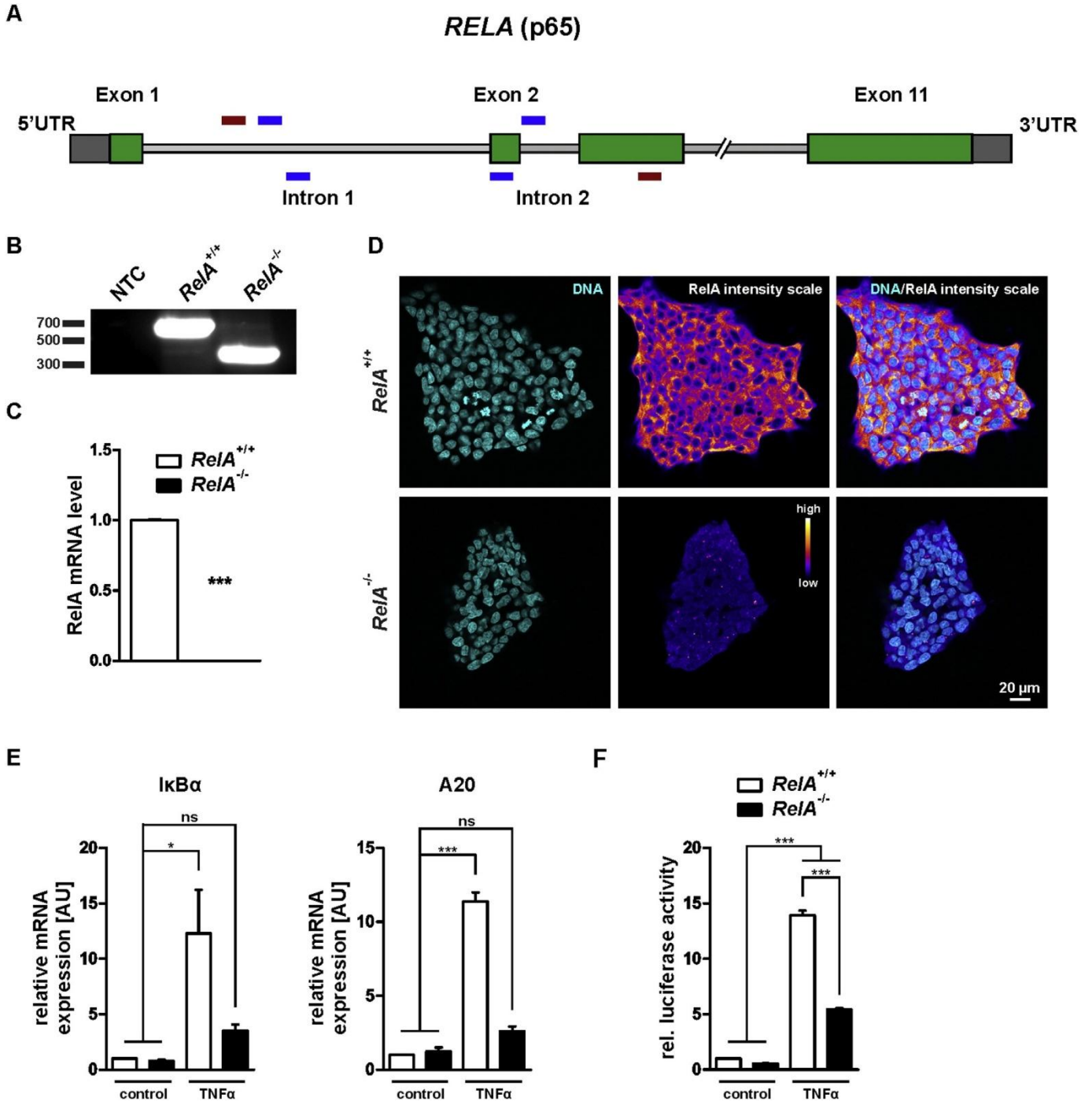

Fig. 4. Generation of RELA-deficient cells. (A) Target design for the CRISPR/Cas9-mediated knockout of RELA. Depicted in blue are the sgRNAs and depicted in red are the flanking primers used for genomic PCR. (B) Genomic PCR of clonally grown cells revealed genomic deletion within the RELA gene. (C) qPCR analysis using a primer set, where one primer is designed within the deletion showed a highly significant downregulation of RelA mRNA (t-test, two-tailed, n = 3). (D) Immunocytochemical stainings depicted almost complete loss of RelA protein in RelA-deficient cells. (E) Expression of the NF-κB target genes IκBα and A20 is markedly reduced in RelA$^{-/-}$ cells after 6 h of TNFα stimulation (10 ng/mL) compared to wildtype cells (One-way ANOVA, Bonferroni post-test, n = 3). (F) An NF-κB driven luciferase reporter assay revealed a significantly reduced NF-κB activation after 24 h TNFα stimulation in RelA-deficient cells (One-way ANOVA, Bonferroni post-test, n = 3).

the cellular environment. While a mostly NF-κB-independent regulation of RIPK1 was demonstrated in the liver [45], in the small intestine an NF-κB-mediated activation of RIPK1 was shown to result in the loss of Paneth cells [50]. Future studies on the role of human IKK1 and IKK2 therefore have to consider potential differences between different cell populations.

In summary, our findings demonstrate that in human cells IKK1 and IKK2 have an NF-κB-independent function in preventing from TNF-induced cell death. Targeting – genetically or pharmacologically – both catalytic IKKs therefore appears to be a promising approach in cancer therapy, especially for tumor cells resistant to TNF-induced cell death.

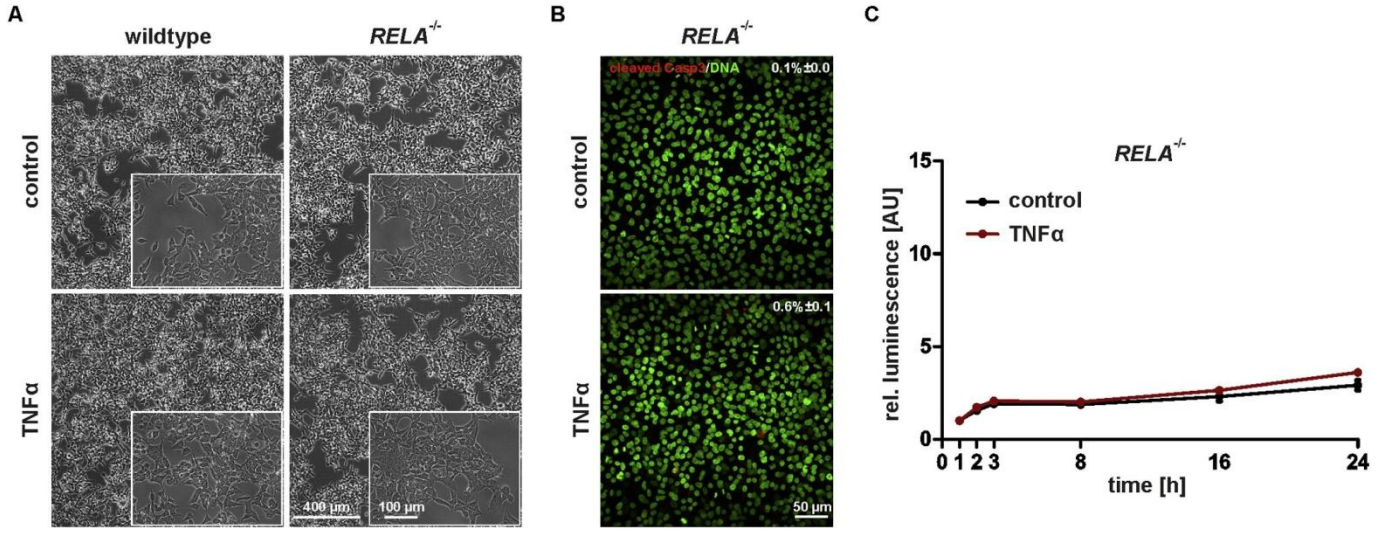

Fig. 5. No increase in TNFα-induced cell death upon RelA deficiency. (A) After 24 h of TNFα stimulation (20 ng/mL) no differences in the amount of dead cells between RelA-deficient and wildtype cells was observable. (B) Immunocytochemistry revealed only a small increase in Caspase-3-positive cells after TNFα treatment ($n = 3$; for each condition > 5000 cells were analyzed). (C) RealTime Glo Annexin V apoptosis assay of TNFα-treated RelA$^{-/-}$ cells showed no difference in the amount of apoptotic cells compared to untreated cells.

4. Materials and methods

4.1. Statistical analysis

All statistical tests were performed using GraphPad Prism 5 (GraphPad Software, La Jolla, USA). Data is presented as the mean of at least three biological replicas ± SEM if not stated otherwise. The statistical test used is mentioned in the respective figure legend. ns, not significant, *$p < 0.05$, **$p < 0.01$, ***$p < 0.001$.

4.2. Target design and cloning

Single guide RNAs (sgRNAs) were designed using the online prediction tool from the University of Heidelberg [51]. Nicking pairs were chosen as described by Ran and colleagues [35]. For efficient gene knockout we designed two nicking pairs creating a deletion spanning an intron-exon border within the respective gene. sgRNAs for IKK1 and IKK2 knockout were cloned into pSpCas9n(BB)-2A-Puro (PX462) V2.0 (Addgene plasmid #62987) essentially as described [52], while sgRNAs for knockout of RELA were cloned into pX335_G2P (modified Addgene plasmid #42335, kindly provided by Boris Greber).

4.3. Cell culture and transfection

HEK293 cells were cultivated in Dulbecco's Modified Eagle's Medium (DMEM) (Sigma Aldrich, Taufkirchen, Germany) containing 10% (v/v) heat-inactivated fetal calf serum (FCS) (VWR, Darmstadt, Germany), 2 mM L-glutamine (Sigma Aldrich) and 100 U/mL Penicillin/Streptomycin (P/S) (Sigma Aldrich) at 37 °C and 5% CO_2 at saturated humidity.

Transfection was performed either using standard calcium-phosphate precipitation or TurboFect transfection reagent (Thermo Fisher Scientific) according to manufacturer's guidelines.

4.4. Genomic PCR

Cells were harvested at 300 g for 5 min and resuspended in cell lysis buffer (0.1 µg/mL Gelatine, 50 mM KCl, 1.5 mM MgCl2, 0.45% NP40, 10 mM TRIS pH 8.3, 0.45% TWEEN 20, 200 µg/mL Protein kinase K). Lysate was incubated for 1 h at 55 °C and 5 min at 95 °C before being used as template for genomic PCR. The following primers were used: IKBKA-fwd 5′-GCCTTGGAACAACTGTGGAAC-3′, IKBKA-rev 5'-GGACGCACACATTCCCAAAG-3′, IKBKB-fwd 5′-CCACCTTGTTTGCCTGCTTG-3′, IKBKB-rev 5′-GTCTCCCCATCCCTCTTCCT-3′, RELA-fwd 5′-GGAGCAGAGGGAACCTTGAC-3′, RELA-rev 5′-GTATCTGTGCTCCTCTCGCC-3′.

4.5. RT-PCR and quantitative real-time PCR

Total RNA was isolated using TRI Reagent (Sigmal-Aldrich) according to the manufacturer's protocol. 1 µg of RNA was used for cDNA synthesis. For RT-PCR, 1 µL cDNA was used as template and for quantitative real-time PCR (qPCR), cDNA was diluted 1:100 and 2 µL/reaction were used. qPCR was carried out with SYBR Green Master Mix (Thermo Fisher Scientific). The following primers were used: IKK1-fwd 5′-CTTCGGGAACGTCTGTCTGTA-3′, IKK1-rev 5′-TTGGCATGGTTCAACTTCTTCAT-3′, IKK2-fwd 5′-GCTGACCCACCCCAATGTG-3′, IKK2-rev 5′-TAAGCGCAGAGGCAATGTCA-3′, RelA-fwd 5′-CTGTTCCCCCTCATCTTCCC-3′, RelA-rev 5′-GCCATTGATCTTGATGGTGGG-3′, IκBα-fwd 5′-CCCTACACCTTGCCTGTGAG-3′, IκBα-rev 5′-TAGACACGTGTGGCCATTGT-3′, A20-fwd 5′-CTGAAAACGAACGGTGACGG-3′, A20-rev 5′-TCCAGTTGCCAGCGGAATTT-3′, IL8-fwd 5′-TCTGTGTGAAGGTGCAGTTTTG-3′, IL8-rev 5′-TTTCTGTGTTGGCGCAGTGT-3′. Ct values obtained in qPCR were normalized to the reference genes GAPDH (fwd 5′-CATGAGAAGTATGACAACAGCCT-3′; rev 5′-AGTCCTTCCACGATACCAAAGT-3′), eEF2 (fwd 5′-AGGTCGGTTCTACGCCTTTG-3′; rev 5′-TTCCCACAAGGCACATCCTC-3′) and RPLP0 (fwd 5′-TGGGCAAGAACACCATGATG-3′; rev 5′-AGTTTCTCCAGAGCTGGGTTGT-3′).

4.6. Western blotting

Protein extracts were made using RIPA buffer (1 mM EGTA, 150 mM NaCl, 1 mM Na_2EDTA, 1 mM Na_3VO_4, 1% (w/v) NP-40, 1 µg/mL leupeptin, 1% (w/v) sodium deoxycholate, 2.5 mM sodium pyrophosphate, 20 mM Tris-HCl (pH 7,5), 1 mM β-glycerophosphate) and equal amounts of protein were separated by SDS-PAGE and transferred to a PVDF membrane. Membranes were blocked using PBS containing 0.05% Tween 20 and 5% milk powder, followed by probing with primary antibodies (rabbit anti-IKK1 (#7182; Santa-Cruz Biotechnology, Dallas, USA), rabbit anti-IKK2 (#2370; Cell Signaling, Danvers, USA), rabbit anti-p65 (#8242; Cell Signaling), mouse anti-IκBα (#4814; Cell Signaling) overnight at 4 °C. Horseradish peroxidase-conjugated

secondary antibodies were applied for 1 h at room temperature. Blots were developed using enhanced chemiluminescence. GAPDH (#32233; Santa-Cruz Biotechnology) served as loading control.

4.7. Immunocytochemistry

For immunocytochemical stainings cells were cultivated on coverslips. Fixation was done with 4% paraformaldehyde (PFA) for 10 min at RT. Prior to application of the primary antibodies (rabbit anti-p65 (#8242; Cell Signaling), rabbit anti-cleaved caspase-3 (#9661; Cell Signaling)) cells were permeabilized and blocked using PBS containing 0.02% Triton X-100 and 5% goat serum. After repetitive washing, secondary fluorochrome-conjugated antibodies (goat anti-rabbit/mouse Alexa Fluor 555, Thermo Fisher Scientific) were applied, followed by nuclear counterstaining with DAPI (1 μg/mL) and finally mounting using Mowiol/DABCO. Imaging was done by confocal laser scanning microscopy (LSM 780, Carl Zeiss, Oberkochen, Germany) and image processing was performed using Fiji [53] and Corel Draw (Corel Corporation, Ottawa, Canada).

4.8. Dual luciferase reporter assay

Cells were transiently transfected with TK (NF-κB)6 LUC vector [54] and pRL-CMV (Promega Cooperation) using TurboFect Transfection Reagent (Thermo Fisher Scientific) according to manufacturer's guidelines. 24 h after transfection, cells were stimulated with TNFα or left untreated. The next day, cells were lysed in 1 × Passive Lysis buffer (Promega Corporation) and Luciferase activity was measured using the Dual-Luciferase® Reporter Assay System (Promega Corporation). Signals were normalized as a ratio of Firefly luciferase activity to Renilla luciferase activity.

4.9. RealTime Glo Annexin V apoptosis assay

Apoptosis was analyzed using the RealTime-Glo™ Annexin V Apoptosis Assay (Promega Corporation) according to manufacturer's guidelines. One day prior to stimulation, 10.000 cells were seeded in white, tissue culture-treated 96-well multiwell plates (BRAND, Wertheim, Germany). Cells were stimulated as indicated and simultaneously detection reagent – prepared according to the manufacturer's protocol – was added. Annexin V-based luminescence was measured at the times indicated using a GloMax®-Multi Plus Detection System (Promega Corporation). No-cell controls were used for background subtraction.

4.10. Flow cytometric analysis

DNA content was measured essentially as described [55]. Briefly, 1×10^6 cells – treated as indicated – were harvested and fixed for 5 min using 70% (v/v) ethanol. After centrifugation at 300 g cells were stained with staining solution (PBS containing 1 mg/mL glucose (Roth), 50 mg/mL propidium iodide (Partec, Sysmex Deutschland GmbH, Bornbarch, Germany) and 100 Kunitz units RNaseA (Thermo Fisher Scientific) for 60 min under exclusion of light. PI-staining was analyzed using a Gallios™ 10/3 flow cytometer (Beckman Coulter, Brea, CA, USA). Data analysis was done using FlowJo Software (TreeStar, Olten, Switzerland), doublet discrimination was assured by gating FL3-A- versus FL3-W signals.

Transparency document

The http://dx.doi.org/10.1016/j.bbamcr.2018.04.003 associated this article can be found, in online version.

Acknowledgements

The excellent technical help of Angela Kralemann-Köhler is gratefully acknowledged. This research received no specific grant from any funding agency in the public, commercial, or not-for-profit sectors.

Author contributions

Conceptualization, C.S., B.K. & C.K.
Methodology, C.S., J.S. & L.R.P.
Validation, C.S., J.G., B.K. & C.K.
Formal analysis, C.S., N.P. & J.G.
Investigation, C.S., J.S., N.P., S.K, M.P., E.H. & J.G.
Data curation, B.K. & C.K.
Writing – Original Draft, C.S.
Writing – Review & Editing, C.S., J.S., N.P., S.K., M.P., L.R.P., E.H., J.G., B.K. & C.K.
Visualization, C.S.
Supervision, B.K. & C.K.
Project Administration, B.K. & C.K.
Funding Acquisition, C.K.

Conflict of interest

The authors declare no conflict of interest.

Appendix A. Supplementary data

Supplementary data to this article can be found online at https://doi.org/10.1016/j.bbamcr.2018.04.003.

References

[1] N.D. Perkins, Integrating cell-signalling pathways with NF-kappaB and IKK function, Nat. Rev. Mol. Cell Biol. 8 (2007) 49–62.
[2] Y. Xia, S. Shen, I.M. Verma, NF-kappaB, an active player in human cancers, Cancer immunology research 2 (2014) 823–830.
[3] Y. Ben-Neriah, M. Karin, Inflammation meets cancer, with NF-kappaB as the matchmaker, Nat. Immunol. 12 (2011) 715–723.
[4] H. Walczak, TNF and ubiquitin at the crossroads of gene activation, cell death, inflammation, and cancer, Immunol. Rev. 244 (2011) 9–28.
[5] E. Varfolomeev, D. Vucic, Intracellular regulation of TNF activity in health and disease, Cytokine 101 (2018) 26–32.
[6] N. Peltzer, M. Darding, H. Walczak, Holding RIPK1 on the ubiquitin leash in TNFR1 signaling, Trends Cell Biol. 26 (2016) 445–461.
[7] Y. Ben-Neriah, Regulatory functions of ubiquitination in the immune system, Nat. Immunol. 3 (2002) 20–26.
[8] M.L. Schmitz, P.A. Baeuerle, The p65 subunit is responsible for the strong transcription activating potential of NF-kappa B, EMBO J. 10 (1991) 3805–3817.
[9] M.S. Hayden, S. Ghosh, Shared principles in NF-kappaB signaling, Cell 132 (2008) 344–362.
[10] S.T. Smale, Dimer-specific regulatory mechanisms within the NF-kappaB family of transcription factors, Immunol. Rev. 246 (2012) 193–204.
[11] M. Milanovic, M. Kracht, M.L. Schmitz, The cytokine-induced conformational switch of nuclear factor kappaB p65 is mediated by p65 phosphorylation, The Biochemical journal 457 (2014) 401–413.
[12] K. Schulze-Osthoff, D. Ferrari, M. Los, S. Wesselborg, M.E. Peter, Apoptosis signaling by death receptors, Eur. J. Biochem. 254 (1998) 439–459.
[13] O. Micheau, S. Lens, O. Gaide, K. Alevizopoulos, J. Tschopp, NF-kappaB signals induce the expression of c-FLIP, Mol. Cell. Biol. 21 (2001) 5299–5305.
[14] C.Y. Wang, M.W. Mayo, R.G. Korneluk, D.V. Goeddel, A.S. Baldwin Jr., NF-kappaB antiapoptosis: induction of TRAF1 and TRAF2 and c-IAP1 and c-IAP2 to suppress caspase-8 activation, Science 281 (1998) 1680–1683.
[15] S.D. Catz, J.L. Johnson, Transcriptional regulation of bcl-2 by nuclear factor kappa B and its significance in prostate cancer, Oncogene 20 (2001) 7342–7351.
[16] P.T. Daniel, K. Schulze-Osthoff, C. Belka, D. Guner, Guardians of cell death: the Bcl-2 family proteins, Essays Biochem. 39 (2003) 73–88.
[17] D.J. Van Antwerp, S.J. Martin, T. Kafri, D.R. Green, I.M. Verma, Suppression of TNF-alpha-induced apoptosis by NF-kappaB, Science 274 (1996) 787–789.
[18] O. Micheau, J. Tschopp, Induction of TNF receptor I-mediated apoptosis via two sequential signaling complexes, Cell 114 (2003) 181–190.
[19] A.T. Ting, M.J. Bertrand, More to life than NF-kappaB in TNFR1 signaling, Trends Immunol. 37 (2016) 535–545.
[20] V. Kondylis, S. Kumari, K. Vlantis, M. Pasparakis, The interplay of IKK, NF-kappaB and RIPK1 signaling in the regulation of cell death, tissue homeostasis and

inflammation, Immunol. Rev. 277 (2017) 113–127.
[21] Y.S. Cho, S. Challa, D. Moquin, R. Genga, T.D. Ray, M. Guildford, F.K. Chan, Phosphorylation-driven assembly of the RIP1-RIP3 complex regulates programmed necrosis and virus-induced inflammation, Cell 137 (2009) 1112–1123.
[22] S. He, L. Wang, L. Miao, T. Wang, F. Du, L. Zhao, X. Wang, Receptor interacting protein kinase-3 determines cellular necrotic response to TNF-alpha, Cell 137 (2009) 1100–1111.
[23] L. Sun, H. Wang, Z. Wang, S. He, S. Chen, D. Liao, L. Wang, J. Yan, W. Liu, X. Lei, X. Wang, Mixed lineage kinase domain-like protein mediates necrosis signaling downstream of RIP3 kinase, Cell 148 (2012) 213–227.
[24] Y. Dondelinger, S. Jouan-Lanhouet, T. Divert, E. Theatre, J. Bertin, P.J. Gough, P. Giansanti, A.J. Heck, E. Dejardin, P. Vandenabeele, M.J. Bertrand, NF-kappaB- independent role of IKKalpha/IKKbeta in preventing RIPK1 kinase-dependent apoptotic and Necroptotic cell death during TNF signaling, Mol. Cell 60 (2015)
63–76.
[25] A.A. Beg, W.C. Sha, R.T. Bronson, S. Ghosh, D. Baltimore, Embryonic lethality and liver degeneration in mice lacking the RelA component of NF-kappa B, Nature 376 (1995) 167–170.
[26] Q. Li, D. Van Antwerp, F. Mercurio, K.F. Lee, I.M. Verma, Severe liver degeneration in mice lacking the IkappaB kinase 2 gene, Science 284 (1999) 321–325.
[27] M. Tanaka, M.E. Fuentes, K. Yamaguchi, M.H. Durnin, S.A. Dalrymple, K.L. Hardy,
D.V. Goeddel, Embryonic lethality, liver degeneration, and impaired NF-kappa B
activation in IKK-beta-deficient mice, Immunity 10 (1999) 421–429.
[28] E. Alcamo, J.P. Mizgerd, B.H. Horwitz, R. Bronson, A.A. Beg, M. Scott,
C.M. Doerschuk, R.O. Hynes, D. Baltimore, Targeted mutation of TNF receptor I rescues the RelA-deficient mouse and reveals a critical role for NF-kappa B in leukocyte recruitment, J. Immunol. 167 (2001) 1592–1600.
[29] U. Pannicke, B. Baumann, S. Fuchs, P. Henneke, A. Rensing-Ehl, M. Rizzi, A. Janda, K. Hese, M. Schlesier, K. Holzmann, S. Borte, C. Laux, E.M. Rump, A. Rosenberg, T. Zelinski, H. Schrezenmeier, T. Wirth, S. Ehl, M.L. Schroeder, K. Schwarz, Deficiency of innate and acquired immunity caused by an IKBKB mutation, N. Engl. J. Med. 369 (2013) 2504–2514.
[30] X. Wang, Y. Lin, Tumor necrosis factor and cancer, buddies or foes? Acta Pharmacol. Sin. 29 (2008) 1275–1288.
[31] P. Horvath, R. Barrangou, CRISPR/Cas, the immune system of bacteria and archaea, Science 327 (2010) 167–170.
[32] K.S. Makarova, D.H. Haft, R. Barrangou, S.J. Brouns, E. Charpentier, P. Horvath, S. Moineau, F.J. Mojica, Y.I. Wolf, A.F. Yakunin, J. van der Oost, E.V. Koonin, Evolution and classification of the CRISPR-Cas systems, Nat. Rev. Microbiol. 9 (2011) 467–477.
[33] L. Cong, F.A. Ran, D. Cox, S. Lin, R. Barretto, N. Habib, P.D. Hsu, X. Wu, W. Jiang, L.A. Marraffini, F. Zhang, Multiplex genome engineering using CRISPR/Cas sys- tems, Science 339 (2013) 819–823.
[34] P. Mali, L. Yang, K.M. Esvelt, J. Aach, M. Guell, J.E. DiCarlo, J.E. Norville, G.M. Church, RNA-guided human genome engineering via Cas9, Science 339 (2013) 823–826.
[35] F.A. Ran, P.D. Hsu, C.Y. Lin, J.S. Gootenberg, S. Konermann, A.E. Trevino, D.A. Scott, A. Inoue, S. Matoba, Y. Zhang, F. Zhang, Double nicking by RNA-guided
CRISPR Cas9 for enhanced genome editing specificity, Cell 154 (2013) 1380–1389. [36] S.A. Forbes, D. Beare, P. Gunasekaran, K. Leung, N. Bindal, H. Boutselakis, M. Ding, S. Bamford, C. Cole, S. Ward, C.Y. Kok, M. Jia, T. De, J.W. Teague, M.R. Stratton,
U. McDermott, P.J. Campbell, COSMIC: exploring the world's knowledge of somatic mutations in human cancer, Nucleic Acids Res. 43 (2015) D805–811.
[37] V.J. Palombella, J. Vilcek, Mitogenic and cytotoxic actions of tumor necrosis factor in BALB/c 3T3 cells. Role of phospholipase activation, J. Biol. Chem. 264 (1989)
18128–18136.
[38] B.B. Aggarwal, Signalling pathways of the TNF superfamily: a double-edged sword, Nat. Rev. Immunol. 3 (2003) 745–756.
[39] M.A. O'Donnell, A.T. Ting, RIP1 comes back to life as a cell death regulator in TNFR1 signaling, FEBS J. 278 (2011) 877–887.
[40] L. Wang, F. Du, X. Wang, TNF-alpha induces two distinct caspase-8 activation pathways, Cell 133 (2008) 693–703.
[41] Y. Hu, V. Baud, M. Delhase, P. Zhang, T. Deerinck, M. Ellisman, R. Johnson, M. Karin, Abnormal morphogenesis but intact IKK activation in mice lacking the IKKalpha subunit of IkappaB kinase, Science 284 (1999) 316–320.
[42] T. Luedde, J. Heinrichsdorff, R. de Lorenzi, R. De Vos, T. Roskams, M. Pasparakis, IKK1 and IKK2 cooperate to maintain bile duct integrity in the liver, Proc. Natl. Acad. Sci. U. S. A. 105 (2008) 9733–9738.
[43] C. Slotta, T. Schluter, L.M. Ruiz-Perera, H.M. Kadhim, T. Tertel, E. Henkel, W. Hubner, J.F.W. Greiner, T. Huser, B. Kaltschmidt, C. Kaltschmidt, CRISPR/Cas9- mediated knockout of c-REL in HeLa cells results in profound defects of the cell cycle, PLoS One 12 (2017) e0182373.
[44] C. Koppe, P. Verheugd, J. Gautheron, F. Reisinger, K. Kreggenwinkel, C. Roderburg,
L. Quagliata, L. Terracciano, N. Gassler, R.H. Tolba, Y. Boege, A. Weber, M. Karin, M. Luedde, U.P. Neumann, R. Weiskirchen, F. Tacke, M. Vucur, C. Trautwein,
B. Luscher, C. Preisinger, M. Heikenwalder, T. Luedde, IkappaB kinasealpha/beta control biliary homeostasis and hepatocarcinogenesis in mice by phosphorylating the cell-death mediator receptor-interacting protein kinase 1, Hepatology 64 (2016)
1217–1231.
[45] V. Kondylis, A. Polykratis, H. Ehlken, L. Ochoa-Callejero, B.K. Straub, S. Krishna- Subramanian, T.M. Van, H.M. Curth, N. Heise, F. Weih, U. Klein, P. Schirmacher, M. Kelliher, M. Pasparakis, NEMO prevents steatohepatitis and hepatocellular carcinoma by inhibiting RIPK1 kinase activity-mediated hepatocyte apoptosis, Cancer Cell 28 (2015) 830.
[46] D. Rudolph, W.C. Yeh, A. Wakeham, B. Rudolph, D. Nallainathan, J. Potter, A.J.
Elia, T.W. Mak, Severe liver degeneration and lack of NF-kappaB activation in NEMO/IKKgamma-deficient mice, Genes & development, 14 (2000) 854–862.
[47] A. Ferrajoli, M.J. Keating, T. Manshouri, F.J. Giles, A. Dey, Z. Estrov, C.A. Koller, R.
Kurzrock, D.A. Thomas, S. Faderl, S. Lerner, S. O'Brien, M. Albitar, The clinical significance of tumor necrosis factor-alpha plasma level in patients having chronic lymphocytic leukemia, Blood, 100 (2002) 1215–1219.
[48] P.W. Szlosarek, M.J. Grimshaw, H. Kulbe, J.L. Wilson, G.D. Wilbanks, F. Burke,
F.R. Balkwill, Expression and regulation of tumor necrosis factor alpha in normal and malignant ovarian epithelium, Mol. Cancer Ther. 5 (2006) 382–390.
[49] D. Legarda-Addison, H. Hase, M.A. O'Donnell, A.T. Ting, NEMO/IKKgamma reg- ulates an early NF-kappaB-independent cell-death checkpoint during TNF signaling, Cell Death Differ. 16 (2009) 1279–1288.
[50] K. Vlantis, A. Wullaert, A. Polykratis, V. Kondylis, M. Dannappel, R. Schwarzer, P. Welz, T. Corona, H. Walczak, F. Weih, U. Klein, M. Kelliher, M. Pasparakis, NEMO prevents RIP kinase 1-mediated epithelial cell death and chronic intestinal inflammation by NF-kappaB-dependent and -independent functions, Immunity 44 (2016) 553–567.
[51] M. Stemmer, T. Thumberger, M. Del Sol Keyer, J. Wittbrodt, J.L. Mateo, CCTop: an intuitive, flexible and reliable CRISPR/Cas9 target prediction tool, PLoS One 10 (2015) e0124633.
[52] F.A. Ran, P.D. Hsu, J. Wright, V. Agarwala, D.A. Scott, F. Zhang, Genome en- gineering using the CRISPR-Cas9 system, Nat. Protoc. 8 (2013) 2281–2308.
[53] J. Schindelin, I. Arganda-Carreras, E. Frise, V. Kaynig, M. Longair, T. Pietzsch, S. Preibisch, C. Rueden, S. Saalfeld, B. Schmid, J.Y. Tinevez, D.J. White,
V. Hartenstein, K. Eliceiri, P. Tomancak, A. Cardona, Fiji: an open-source platform for biological-image analysis, Nat. Methods 9 (2012) 676–682.
[54] F. Bachelerie, J. Alcami, F. Arenzana-Seisdedos, J.L. Virelizier, HIV enhancer ac- tivity perpetuated by NF-kappa B induction on infection of monocytes, Nature 350 (1991) 709–712.
[55] B. Kaltschmidt, C. Kaltschmidt, S.P. Hehner, W. Droge, M.L. Schmitz, Repression of NF-kappaB impairs HeLa cell proliferation by functional interference with cell cycle checkpoint regulators, Oncogene 18 (1999) 3213–3225.